VNiVERSiDAD Ð SALAMANCA

Ribosomal RNA methylation controls the cell cycle through protein synthesis

PhD Thesis

Judith López Luis

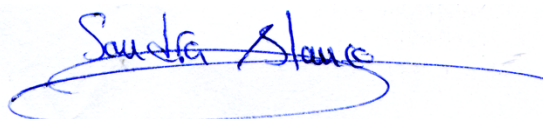*Supervisor: Sandra Blanco Benavente, PhD*

Centro de Investigación del Cáncer
IBMCC (University of Salaman-
ca-CSIC)
Miguel de Unamuno Campus
37007 Salamanca (Spain)
Tel.: (+34) 923 294720
www.cicancer.org

La **Doctora Sandra Blanco Benavente**, Científico Titular del Consejo superior de Investigaciones Científicas (CSIC),

CERTIFICA:

Que la Tesis Doctoral titulada **"Ribosomal RNA methylation controls the cell cycle through protein synthesis"** presentada por **Dª Judith López Luis** ha sido realizada bajo su dirección en el Instituto de Biología Molecular y Celular del Cáncer y reúne, a su juicio, la originalidad y contenidos suficientes para que sea presentada ante el tribunal correspondiente para optar al título de **Doctora por la Universidad de Salamanca**.

Y para que así conste a efectos oportunos, expide el presente certificado en Salamanca, a 13 de octubre de 2023.

Fdo.: Sandra Blanco Benavente

i

A mis abuelos, mis padres y mi hermana,

por su amor y aliento en este largo camino.

A todas las personas que alguna vez

han servido de inspiración en mi vida.

Este trabajo es un reflejo de mi deseo de seguir sus

pasos y contribuir al mundo de la misma manera.

Enjoy the little things in life,

for one day you will look back and

realize they were the big things.

– Robert Brault

Abstract

Cytosine-5 methylation (m^{5}C) is one of the most well-known post-transcriptional modifications in RNA. This mark is predominantly found in transfer RNAs (tRNAs) and ribosomal RNAs (rRNAs) and is mediated by DNMT2 and NSUN family members. Recently, m^{5}C modification on tRNAs has been shown to regulate stem cell function and stress response, and its inhibition specifically eliminates cancer initiating cells. This suggest that RNA methylation may regulate essential cellular and physiological processes and that its deregulation may lead to critical pathological consequences such as cancer.

In contrast to tRNAs, the functional significance of m^{5}C in other RNAs in which this mark is also prevalent, such as rRNAs, has not been deeply studied in mammals yet. NSUN5 is a m^{5}C methyltransferase that targets position C3782 of 28S rRNA, located at the interface between large and small ribosome subunits. Depletion of NSUN5 is known to alter global protein synthesis, translation fidelity and cell growth. However, how the loss of this methylation affects these key cellular processes is not well-understood yet.

Herein we show that NSUN5 loss-of-function in mammalian cells leads to reduced proliferation rates, primarily due to an impaired progression through the G2/M phases of the cell cycle. Mechanistically, reduced m^{5}C deposition at C3782 alters ribosomal structure and induces a translational shift, favoring the synthesis of ribosomal proteins and cell cycle regulators. Moreover, we have found that NSUN5 is post-translationally modified by CDK1 during mitosis, resulting in its destabilization. These findings suggest that NSUN5 expression is temporary modulated during the cell cycle to fine-tune translation and ensure proper progression through this critical cellular process.

Furthermore, our investigation reveals that NSUN5 is overexpressed in several cancers, particularly during advanced stages, correlating with increased risk of recurrence. While Nsun5 deficiency does not affect primary tumor growth *in vivo*, it significantly impairs tumor metastatic potential, indicating that NSUN5 may serve as therapeutic target to combat tumor metastasis.

Resumen

La metilación en citosina-5 (m^{5}C) es una de las modificaciones epitranscriptómicas más estudiadas en el ARN. Esta modificación se encuentra principalmente en el ARN de transferencia (ARNt) y en el ARN ribosómico (ARNr) y está mediada por DNMT2 y por los miembros de la familia de enzimas NSUN. Estudios recientes indican que la modificación m^{5}C en ARNt regula la función de las células madre y la respuesta a estrés, y que su inhibición contribuye a eliminar específicamente las células iniciadoras de tumor. Esto sugiere que la metilación de ARN podría regular procesos celulares y fisiológicos esenciales y que su desregulación puede tener consecuencias patológicas como el desarrollo de cáncer.

Al contrario que ocurre con los ARNt, las funciones de esta modificación en otros ARNs en los cuales es muy abundante, como el ARNr, no se han estudiado aún en profundidad. NSUN5 es una metiltransferasa que deposita la modificación m^{5}C en la posición C3782 del ARNr 28S, que se encuentra en la interfaz entre la subunidad grande y pequeña del ribosoma. La reducción en la expresión de esta enzima produce una alteración de la síntesis global de proteínas, la fidelidad de la traducción y del crecimiento celular. Sin embargo, aún no se conoce en profundidad cómo la pérdida de esta modificación afecta a estos procesos celulares esenciales.

En este estudio demostramos que la pérdida de expresión de NSUN5 produce una disminución del crecimiento celular, principalmente debido a una alteración en la progresión de las fases G2 y M del ciclo celular. A nivel molecular, encontramos que una bajada en la metilación del ribosoma en la posición C3782 produce una alteración en la estructura ribosomal e induce una alteración del programa traduccional de las células, favoreciendo la síntesis de proteínas ribosomales y reguladores del ciclo celular. Además de esto, describimos una modificación post-traduccional de NSUN5 mediada por CDK1 que ocurre durante mitosis y que conlleva la desestabilización de NSUN5. Nuestros datos sugieren que la expresión de NSUN5 está modulada a lo largo del ciclo celular para ajustar la síntesis de proteínas y asegurar la correcta progresión del ciclo celular.

Finalmente, nuestro estudio muestra que NSUN5 está altamente expresada en numerosos tipos de tumores, especialmente durante los estadios más avanzados, correlacionándose con un aumento en el riesgo de recaída. Nuestros estudios in vivo indican que la pérdida de expresión de NSUN5 no afecta a la formación del tumor primario, pero inhiben la capacidad de las células tumorales para metastatizar. Esto indica que NSUN5 podría ser usada como diana terapéutica para combatir el desarrollo de metástasis.

x

Table of contents

Introduction

Introduction

1. The epitranscriptome

In a manner analogous to how DNA and proteins can be modified without altering their original sequence, RNA has also been found to undergo dozens of post-transcriptional modifications, which are collectively known as the epitranscriptome. Despite the fact that all biological macromolecules can be subjected to covalent modifications, most research efforts have been focused on protein and DNA modifications. In contrast, RNA research has been left behind, likely due to the inherent complexities associated with its study, such as rapid turnover, instability, and a lack of tools for its investigation. These technical limitations significantly hindered the progression of RNA research until 1960s. Thus, while DNA methylation was first described in 1925 [1], it was not until 1960 that RNA modifications were discovered [2]. These post-transcriptional RNA modifications have been shown to be conserved and essential for numerous biological processes including development, cell homeostasis, and gene expression [3-6], among others. In recent years, the realization that RNA functions extend beyond serving as a mere intermediate between DNA and proteins, but rather act as a critical regulator of gene expression, combined with advancements in analytical chemistry and high-throughput sequencing, has exponentially expanded our understanding of the epitranscriptome [7].

1.1. The epitranscriptome composition and function

The epitranscriptome encompasses a variety of modifications, ranging from 5' cap and poly(A) tail addition to messenger RNAs (mRNAs), to RNA editing and chemical modifications in all RNA species.

The 5' cap, which is present in most eukaryotic mRNAs, consist of an inverted N7-methylguanosine (m^7G) linked by a 5'-5' triphosphate bridge to the first transcribed residue [8]. This 5' cap plays crucial roles in mRNA maturation, translation, and stability [8-10]. On the other hand, poly(A) tails are non-templated additions of adenosines placed at the 3' ends of most eukaryotic mRNAs. These 3' end additions are known to facilitate nuclear export, translation initiation, and recycling [10, 11]. Both poly(A) tails and 5' caps play pivotal roles in translation, as the interaction between these two structures is crucial during initiation [12-14].

RNA editing involves the modification of RNA sequences at one or more positions. It encompasses three distinct events: A-to-I substitution editing, C-to-U substitution editing and U/C/G insertion/deletion editing. These events can result in gene products with modified sequence and structure, thereby altering their function. A-to-I substitution editing is carried out by ADAR and

1

ADAT enzymes and occurs in coding and non-coding double-stranded RNA [15]. During this process, adenosine is deaminated to inosine, which preferentially pairs with cytosine, thereby modifying the genetic code. Thus, A-to-I editing affects various RNA features and biological processes including translation, structure, and splicing [16-19]. For example, it has been shown to alter RNA structure leading to the stabilization of a subset of mRNAs by reducing their interaction with RNA destabilizing proteins [16]. Moreover, editing in critical mRNA residues can result in alternative splicing through exon skipping or intron retention [17].

Another well-studied type of RNA editing is C-to-U substitution. This modification is mediated by AID/APOBEC family and can occur in various RNA species such as transfer RNAs (tRNAs), mRNAs or microRNAs (miRNAs) [20]. Interestingly, this modification can be tissue-specific. For instance, the mRNA of hepatic apolipoprotein B-100 undergoes C-to-U editing specifically in enterocytes, enabling the production of the intestinal apolipoprotein B-48 [21].

The highest diversity in the epitranscriptomics field can be found on RNA chemical modifications. More than 170 different chemical modifications have been described to date across all types of RNA and in almost all species [7]. These chemical modifications can occur on RNA bases or in the ribose ring and harbor the potential of fine-tuning and regulating the function and properties of RNA. Among all types of RNA, tRNAs are the most extensively modified, with an average of 17% of their nucleotides being modified. tRNA modification involves wide range of modifying enzymes and a high diversity of modifications. In fact, even 25 different chemical modifications have been identified in these molecules [22, 23].

Following tRNAs, ribosomal RNAs (rRNAs) are the second most heavily modified RNA specie, with a total of 201 modified nucleotides. The most common modification in rRNAs are 2'-OH ribose methylation (2'-O-me) and the isomerization of uridine to pseudouridine (Ψ) [24, 25]. Within mRNAs, the most prevalent internal modification is N6-methyladenosine (m^{6}A), which accounts for approximately 0.1-0.4% of all adenines in mRNA molecules [26].

1.2. Epitranscriptomic regulators

RNA modifications are introduced by a group of enzymes collectively known as "writers". These writers exhibit as much diversity as the RNA modifications themselves, and belong to different families such as NSUN family, that catalyzes the formation of 5-methylcytosine (m^{5}C) in various RNA molecules; METTL family, which has dozens of members that deposit a wide variety of modifications in RNA, DNA and proteins; or TRMT family, which methylate tRNAs; among many others [6, 27-29]. While some modifications as m^{6}A occur in a sequence-specific manner, many of these RNA modifying enzymes recognize specific positions in RNA secondary or tertiary structure,

independent of the nucleotide sequence [30]. However, the writers responsible for a significant number of modifications remain still unknown.

Notably, the discovery in 2011 of the activity of fat mass and obesity-associated protein (FTO) as m^6A demethylase shed light on the reversible nature of this modification [31]. Following FTO, the discovery of another two m^6A demethylases or "erasers" (ALKBH3 and ALKBH5) supported this observation [32, 33]. Intriguingly, a recent study has unveiled that, rather than m^6A, FTO preferentially displays demethylase activity towards N6, 2′-O-dimethyladenosine (m^6Am) at the 5' cap, which alters mRNA stability, integrity, and resistance to decapping enzyme [34]. This suggest that FTO could work on multiple substrates and underlies the necessity for further studies to understand the functional relevance of different FTO substrates.

Another group of proteins known as "readers" can recognize and selectively bind RNA modifications to carry out different functions such as facilitating the degradation of the modified RNA [35, 36], enhancing translation [36, 37] or regulating mRNA splicing [38], among other functions. The most well-known family of RNA modifications "readers" is the YTH domain-containing proteins, which bind m^6A-modified RNA. This family includes YTHDF1/2/3 and YTHDC1/2, each one carrying out different roles in different cell compartments [39]. For instance, YTHDF1 binds m^6A-modified mRNAs in the cytoplasm increasing their translation [37], while YTHDC1 binds methylated mRNAs in the nucleus and participate in their splicing [38]. Together with YTH proteins, other m^6A readers include the heterogeneous nuclear ribonucleoproteins (including hnRNPC, hnRNPG and hnRNPA2B1) [40-42], insulin-like growth factor 2A (IGF2BP1/2/3) [43], proline-rich and coiled-coil-containing protein 2A (PRRC2A) [44] and fragile X mental retardation 1 (FMR1) [45]. Moreover, ALYREF has been described as a "reader" of m^5C modification in mRNAs participating in nuclear export [46].

In contrast to DNA modifications, which are primarily known to regulate gene expression [47], RNA modifications have been found to play diverse roles. These include controlling RNA stability, transcription, location, splicing, degradation, or translation efficiency [38, 48-52]. Furthermore, the functions of many RNA modifications are still being uncovered.

2. The ribosome

Ribosomes are macromolecular complexes found in all living cells that catalyze protein synthesis during a complex and highly regulated process called translation. Ribosomes possess a strong degree of conservation and consist in two subunits in all species: the large ribosome subunit (LSU) or 60S subunit and the small ribosome subunit (SSU) or 40S subunit (Figure 1). In eukaryotes, the LSU is composed of three ribosomal RNA (28S/25S, 5.8S and 5S) and 47 ribosomal proteins (RPs) (Figure 1A), while the SSU carries the 18S rRNA and 33 RPs (Figure 1B) [53].
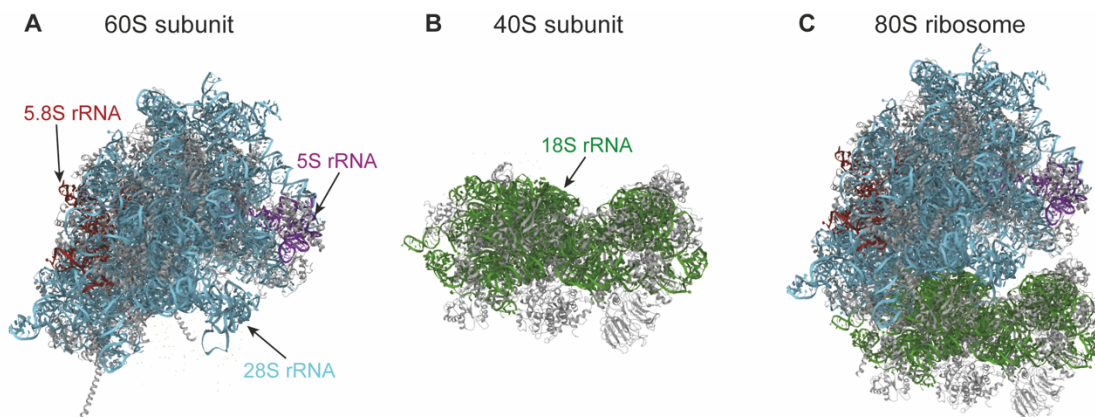
Figure 1. Structure of the human ribosome. A Structure of the human large ribosomal subunit or 60S subunit containing the 28S rRNA (blue), 5.8S rRNA (red) and 5S rRNA (purple). B Structure of the small ribosomal subunit or 40S subunit containing the 18S rRNA (green). C Structure of the assembled ribosome or 80S ribosome. In all panels, ribosomal proteins are represented in grey. Adapted from Protein Data Bank (PDB) file 4UG0.

Although ribosomes are highly conserved across all life forms, they have undergone significant evolutionary changes from prokaryotes to mammals (Figure 2). All ribosomes are built upon the same basal structure, known as the "universal core of the ribosome" (Figure 2A-C). Both genetic data and structural studies have confirmed that this universal core comprises 34 proteins and approximately 4400 RNA bases that are conserved from bacteria to humans and contain the key functional parts of the ribosome (Figure 2D) [54]. The conserved core in the LSU encompasses the peptidyl transferase center (PTC), where peptide bonds occur resulting in the formation of the polypeptide chain; and the exit tunnel, that serves as a passage for nascent peptides to exit the ribosome and where protein folding begins. Within the SSU, the conserved core includes the decoding center (DCC), where the anticodon of the aminoacylated tRNA interacts with the mRNA codon. The conserved core at both subunits also contains the transfer RNA (tRNA) binding sites designated as the aminoacyl (A) site, where the incoming aminoacylated tRNA binds; the peptidyl (P) site, which holds the tRNA carrying the nascent peptide chain; and the exit (E) site, where the deacylated tRNA resides before leaving the ribosome. Lastly, the conserved core also comprises the subunit interface, which plays critical roles in the function of the ribosome [54, 55].

4
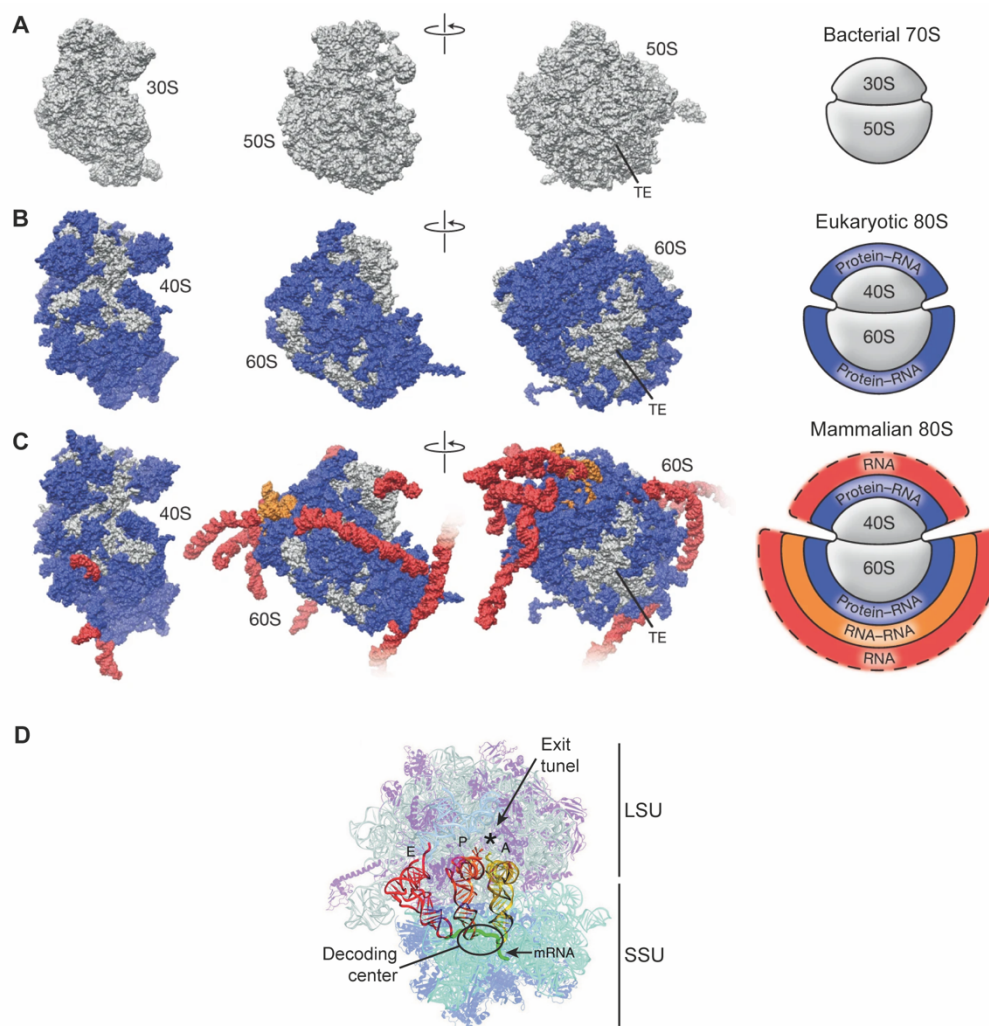
Figure 2. Structure in surface representation (left panel) and schematic representation (right panel) of the Thermus thermofilus (A), Saccharomyces cerevisiae (B) and Homo sapiens (C) ribosomal subunits. TE indicates the tunnel exit. Conserved core is represented in grey, eukaryotic additions are represented in blue and mammalian-specific additions are represented in orange and red. Figure adapted from [56]. D Functional important sites within the conserved core of the ribosome. tRNA binding sites are indicated with A, P and E letters. The peptidyl transferase center is indicated with an asterisk. Decoding center is circled in black and mRNA and exit tunel are indicated with an arrow. Figure adapted from [57].

2.1. Ribosome structural features

Throughout evolution, ribosomes have diverged in both structure and function. Notably, the process of translation initiation, termination and the regulation of translation have gained complexity from bacteria to humans [58, 59]. Due to the increased complexity, eukaryotic ribosomes are around 40% larger than their prokaryotic counterparts (Figure 2A-C). The major differences lie in the expansion segments (ESs), which are rRNA helixes that extend beyond the universal core, in the presence of extra protein moieties (including domain-specific proteins and extensions of conserved proteins), and in extra rRNA modifications [60, 61]. The eukaryotic-specific ESs and protein additions are primarily located on the solvent-exposed surfaces of both subunits, while the subunit interface remains conserved (Figure 2B), except for a few eukaryotic-specific bridges [62]. In human

ribosomes, ESs are remarkably long and compose an extra layer of rRNA that surround the ribosome in a tentacle-like manner (Figure 2C) [54, 63]. This location in the solvent surface makes these eukaryotic-specific additions accessible for interaction with other molecules such as chaperones and translation factors [63]. Interestingly, growing evidence suggest that specific ESs and RPs may play a role in selecting specific mRNAs and in determining specific cellular locations, thereby adding a new regulatory layer to translation [64-67]. By incorporating these structural variations and additional components, ribosomes have gained versatility and the ability to carry out more sophisticated regulatory functions, greatly contributing to the intricate control of gene expression in eukaryotes.

Crystal structures of ribosomes have provided valuable insight into their complex architecture derived from the interactions between RPs and rRNAs. Among these interactions, intersubunit bridges are particularly important for the formation of functional 80S ribosomes and for the conformational changes necessary for protein synthesis such as intersubunit rotation and swiveling of the head domain of the SSU [68]. Interestingly, the interaction surface between subunits has nearly doubled from bacteria to eukaryotes due to the formation of new bridges. In contrast to bacteria bridges which are mainly composed by RNA-RNA interactions, proteins play a central role in eukaryotic bridges formation [61]. These proteins, despite being non-essential in many cases, become highly important in the context of translation and may play a key role in the evolutionary success of the eukaryotic translation machinery [61, 69]. However, further research is needed to fully understand the specific functions and regulatory roles of these eukaryotic-specific bridge proteins.

2.2. Ribosome biogenesis

Ribosome biogenesis is a tightly regulated process that involves the coordinated function of all three RNA polymerases, over 200 assembly factors and several small nucleolar ribonucleoprotein complexes (snoRNPs) (Figure 3) [70, 71]. This intricated process begins in the nucleolus. The human nucleolus contains three layers termed fibrillar center (FC), dense fibrillar center (DFC), and granular component (GC) [53, 71, 72]. The inner part of the nucleolus, the FC, contains around 400 ribosomal DNA (rDNA) gene repeats that gather to form the nucleolar organizer regions (NORs) [73-75]. rDNA repeats are located in the acrocentric chromosomes (chromosomes 13, 14, 15, 21, and 22). Each rDNA gene codes for a transcriptional unit of 47S pre-rRNA. The 47S pre-rRNA contains the 28S, 5.8S and 18S rRNAs separated by the 5' and 3' external transcribed spacers (5' ETS and 3' ETS) and the internal transcribed spacer 1 and 2 (ITS1 and ITS2), harboring promoters, enhancers and other regulatory sequences [76]. The 47S pre-rRNA is transcribed at the boundary between FC and DFC by RNA polymerase I (pol I) [77], while RNA polymerase III (pol

III) transcribes the 5S rRNA from the 5S rDNA, that is found in the nucleoplasm in nucleolar proximity [70, 78]. Lastly, the activity of RNA polymerase II (pol II) is also essential to produce the RPs and trans-acting ribosome biogenesis factors (RBFs) that are then imported to the nucleus [71].

47S pre-rRNA processing to produce mature rRNAs requires the elimination of internal and external spacers by a combination of endonucleolytic and exonucleolytic processing [79, 80]. Pre-rRNA processing occurs concomitantly to the rRNA folding, the assembly of pre-ribosomal particles (which contain different RPs and RBFs depending on the maturation step) and the rRNA modification [79, 81]. Thus, while polycistronic pre-rRNA is emerging from pol I, a subset of SSU RPs and around 40 RBFs rapidly bind to it forming a large ribosomal pre-particle known as 90S pre-ribosome or SSU processome in the DFC [82, 83]. This is followed by the removal of 5' ETS and the cleavage of ITS1 at site 2, leading to the formation of pre-40S and pre-60S, that further mature independently [72, 79]. Then, 5S rRNA is incorporated to pre-60S particle as part of the 5S RNP complex [84]. While maturation continues, pre-ribosomal particles advance from nucleolus to nucleoplasm and are finally exported to the cytoplasm, where they undergo the final maturation steps and become functional ribosomal subunits.
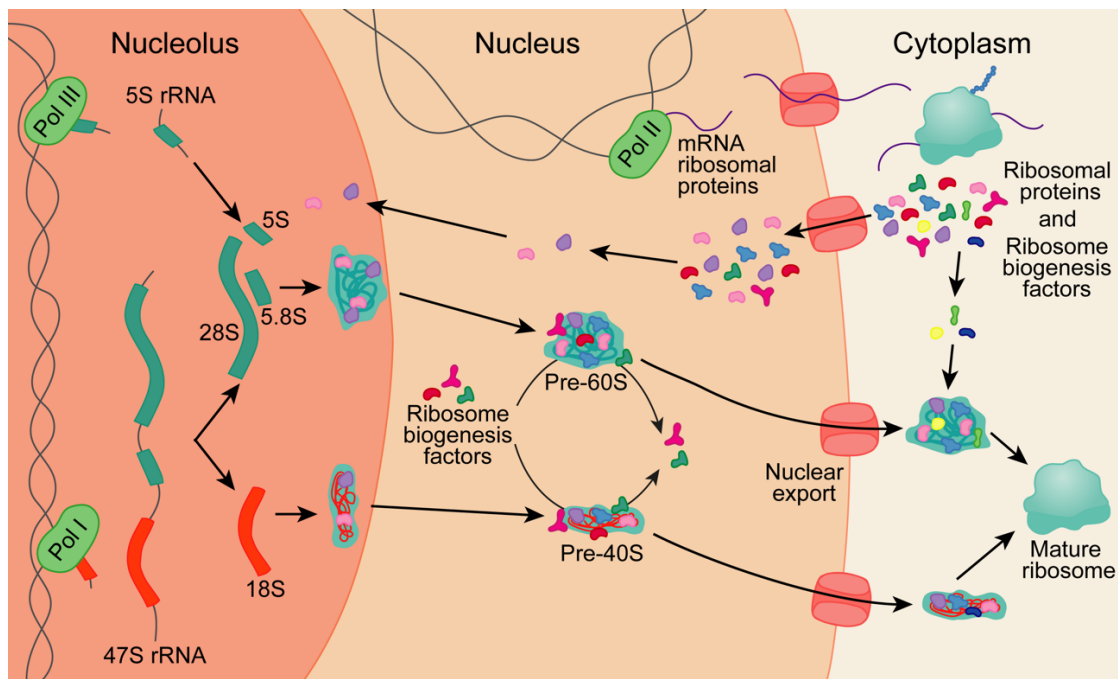
Figure 3. *Schematic representation of human ribosome biogenesis. Ribosome biogenesis starts in the nucleolus where 28S, 18S and 5.8S rRNAs are transcribed as the polycistronic 47S rRNA by Pol I. 5S is independently transcribed by Pol III. 47S is processed, folded, and complexed with RPs to form the pre-60S and pre-40S particles in the nucleolus. RPs are transcribed by Pol II in the nucleus, translated in the cytoplasm and then imported into the nucleus and nucleolus to bind the nascent ribosome. The pre-ribosomal particles suffer further processing in the nucleoplasm and cytoplasm to constitute the mature 60S and 40S ribosomal subunits, that can join to form the mature 80S ribosome. During the process of ribosome biogenesis, hundreds of ribosome biogenesis factors transiently bind the nascent ribosome and are liberated once their function is completed.*

Along all the maturation steps, several RBFs transitorily bind to the pre-ribosomes and are liberated once their function is complete in a well-orchestrated manner. The RBFs that participate during these processes are a very heterogeneous group of proteins that include the enzymes that cleavage the rRNA (endonucleases and exonucleases), chaperones, remodeling factors (helicases, ATPases and GTPases), structural proteins (needed to recruit other factors and to protect sensitive regions) and RNA modifying proteins (snoRNPs and stand-alone RNA modifying enzymes) [53, 71, 72, 79].

2.2.1. Role of RNA modifications during ribosome biogenesis

A crucial step that occurs co-transcriptionally and post-transcriptionally is the deposition of rRNA modifications by RNA modifying enzymes. rRNA modifications are not only necessary for optimal mRNA translation, but are also important for processing, folding and compaction of rRNAs [29, 71]. These rRNA modifications are introduced at different stages of rRNA maturation. The vast majority rRNA modifications are 2'-O-me and Ψ, which are guided by small nucleolar RNA (snoRNA), and likely occur on early stages of ribosome biogenesis (90S complexes), when the pre-ribosomal particles have a more open structure, fitting with the base-pairing mechanism of snoRNAs [71, 79, 85]. However, few snoRNAs such as SNORD68 or SNORD56 have been shown to associate with more mature pre-40S complexes [86]. rRNAs are also decorated by base modifications such as m^5C, N1-methyladenosine (m^1A), N6, N6-dimethyladenosine (m^6_2A) or N7-methylguanosine (m^7G), but in a lesser extent. In contrast to 2'-O-me and Ψ, these base modifications are thought to occur in later maturation steps, but precise timing of most of them has not been determined yet [85].

Numerous rRNA modifications have been identified as essential for ribosome biogenesis. For instance, the absence of a single 2'-O-me at position G2922 on yeast ribosomes completely halts the assembly and nuclear export of pre-60S subunits [87]. 2'-O-me at position G2922 is essential for the recognition of pre-60S subunits by the GTPase Nog2, which drives the recruitment of the Rix1–Rea1 complex allowing the maturation of the central protuberance. Moreover, binding of Nog2 is also essential for the export of 60S pre-rRNA particles to the cytoplasm [87]. Similarly, Nop2-mediated m^5C methylation is essential for pre-60S biogenesis in yeast [88], although this is not the case in humans [89]. In yeast, Nop2 depletion leads to impaired 32S pre-rRNA and 27S rRNA processing resulting in significantly lower levels of 25S and 5.8S rRNAs. Additionally, the absence of the hypermodification of $\Psi1248$ at SSU, which occurs in the cytoplasm during final steps of ribosome biogenesis, delays the final cleavage of 20S pre-rRNA, severely impairing 18S rRNA maturation. While this phenomenon is well-described in yeast, the role of this modification in humans remains unexplored [90]. Importantly, a recent study suggests that 13 out of 53 2'-O-me

found in yeast ribosomes are essential for ribosome biogenesis, underscoring the importance of RNA modifications in this process [91]. To date, no similar studies have been conducted in humans, but the higher abundance of 2'-O-me found in human ribosomes suggest that more essential 2'-O-me may exist in this organism [91].

In certain cases, it is not just the modification itself but also the enzyme responsible for the modification that plays a crucial role in ribosome biogenesis [29]. Examples of this phenomenon include DIMT1L, which methylates two adjacent adenosines on LSU [29], and WBSCR22, that deposits an m^{7}G on LSU [92]. These enzymes likely have catalytic-independent functions during ribosome biogenesis. For instance, DIMTL1 only methylates SSU in the nucleoplasm at late stages of its processing pathway [29], even though it already binds to early pre-ribosomal complexes in the nucleolus. It is proposed that DIMTL1 binding is required at early steps to act as a surveillance mechanism to prevent premature subunit joining [93, 94]. Similarly, human NOP2 regulates ribosome biogenesis in a non-catalytic manner by binding to the 5'-ETS region, where it recruits U3 and U8 snoRNAs and facilitate their assembly into snoRNP complexes, thereby promoting 47S rRNA processing [89]. Thus, reduced NOP2 expression results in a significant accumulation of the 47S primary transcript, demonstrating its importance in regulating very early steps of ribosome biogenesis [89].

Taken together, some rRNA modifications seem to play a key role in rRNA processing and folding, and thus are essential during ribosome biogenesis. However, while the functions of certain modifications in ribosome biogenesis, particularly in yeast, have been elucidated, further research is necessary to unravel the specific roles of individual modifications and modification clusters in human rRNA processing. In addition, it is especially important to distinguish the roles of the modifications themselves from those of the modifying enzymes, that may also have potential structural functions during this intricate process.

2.3. Ribosome function and the role of RNA modifications

Ribosomes were first identified in the mid-1950s and were officially named in 1958. At that time, the prevailing theory was "one gene-one ribosome-one protein" [95]. However, a few years later, ribosomes were characterized as non-specialized structures that simply translate mRNA templates into proteins, without contributing to gene expression regulation [96]. It took several decades to realize that ribosomes are highly complex and can exist as heterogeneous entities [97]. It then also became evident that alterations in ribosome function, regulation and composition are involved in several pathologies, including cancer.

A plethora of studies have demonstrated that ribosomes can differ in their protein composition [98, 99], the post-translational modifications of those proteins [100, 101], and more importantly, in the post-transcriptional modifications of their rRNAs. Approximately 2% of rRNA nucleotides have been found to carry modifications (Figure 4), which can be deposited by snoRNA-guided enzymes or by conventional stand-alone enzymes [24].
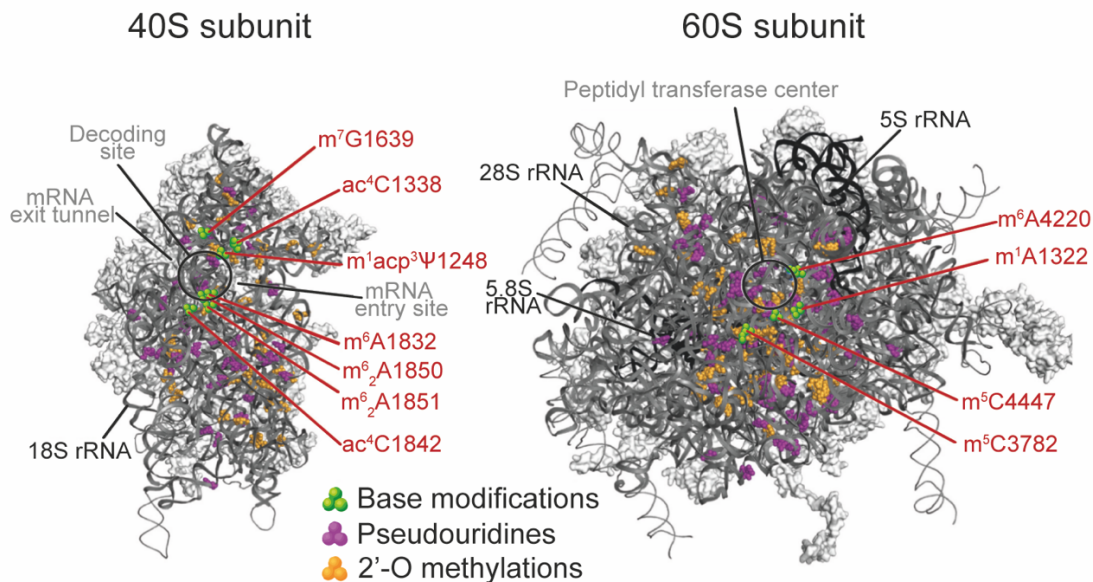
Figure 4. Chemical modifications found on the human ribosome. Structure of the 40S (left) and 60S (right) ribosome subunits is shown (PDB 4V6X). Proteins are presented in surface representation while rRNAs are shown as ribbons. Chemical modifications are represented by dots (base modifications in green, pseudouridines in purple and 2'-O-me in yellow). All base modifications present in human ribosomes are named in red and indicated by red lines. rRNAs are indicated with black lines and letters. Functionally important areas of the ribosome are indicated with black lines and named in grey. Adapted from [102].

2.3.1. rRNA modifications guided by snoRNAs

95% percent of all rRNA modifications are 2'-O-me and Ψ. These two modifications are deposited by the methyltransferase Fibrillarin (FBL) [103, 104] and the pseudouridine synthase Diskerin (DKC1) [105, 106], respectively. These enzymes are guided by two classes of snoRNAs that work as antisense guides and are termed box C/D and box H/ACA snoRNAs, respectively [103-107].

2'-O-me involves the addition of a methyl group at 2'-OH position of the ribose. This modification can occur on all four ribonucleosides of RNA and encompasses a total of 110 sites in human rRNA (41 sites in 18S rRNA, 67 sites in 28S rRNA and 2 sites in 5.8S rRNA; (Figure 4, yellow dots)). The presence of a methyl group on position 2'-OH alters the physicochemical properties of the nucleotides, leading to an increased stability [108], impaired protein binding [109-111] and reduced RNA:DNA duplex formation [112]. Heterogeneity in 2'-O-me methylation patterns was first described by Erales *et al.* after the complete mapping of 2'-O-me on rRNAs [113]. This study

demonstrated that 15% of the 2'-O-me sites are not stoichiometric. Interestingly, when *FBL* was knocked down, cells exhibited decreased 2'-O-me methylation specifically at functionally important sites such as the A and P-sites, the intersubunit bridges and the peptide exit tunnel. This was accompanied by changes in translation initiation, favoring IRES (internal ribosomal entry sites)-mediated initiation [113]. Following this study, several groups have demonstrated that 2'-O-me is a variable modification that provides certain grade of functional specificity to the ribosome [91, 114, 115].

Ψ can be found in all rRNAs, with a total of 95 reported sites (Figure 4, purple dots) [116-118]. This modification involves a 180º rotation of the pyrimidine ring [117]. Due to this rotation, Ψ provides greater rigidity to the phosphodiester backbone of RNA and stabilizes Ψ-A base pairs (compared to A-U), thereby affecting RNA structure, conformation and function [119]. Ψ has also been reported to have functional importance in the ribosome. For instance, impaired pseudouridylation derived from mutations on *DKC1* gene leads to defective translation of IRES-containing mRNAs such as p27(Kip1), Bcl-xL, XIAP [120] and p53[121].

In addition to 2'-O-me and Ψ, a third snoRNA-guided modification can be found on rRNA: N4-acetylcytosine (ac^4C). Two ac^4C are present in 18S rRNA, located on helix 34 (ac^4C1337) and helix 45 (ac^4C1842) [122-124]. The formation of this highly conserved modification is catalyzed by N-acetyltransferase 10 (NAT10) and guided by the C/D snoRNA U13 [122, 123, 125]. ac^4C has been shown to increase the stability of C-G base pair, thus playing a role in structural stabilization [126]. These acetylations are essential for pre-rRNA processing and biogenesis of SSU [122]. Importantly, ac^4C1337 has been found to be crucial for maintaining translation accuracy [123]. Moreover, ac^4C1842 is also thought to play additional roles in translation due to its location close to the DCC [123]. ac^4C has shown to change in a temperature-dependent manner in hyperthermophile archaea and to be essential for growing under extreme temperature conditions [127], showing the adaptive role of this modification. However, the function of this modification in conferring plasticity to eukaryotic ribosomes requires further investigation.

2.3.2. rRNA modifications deposited by stand-alone enzymes

The remaining 5% of all rRNA modifications comprise base methylations and aminocarboxypropylation (Figure 4, green dots). All four bases can undergo methylation at both nitrogen and carbon atoms, while aminocarboxypropylation occurs in uridine and Ψ residues. Eukaryotic rRNAs are decorated with 8 different base modifications, distributed across the small and large subunits. In human ribosomes, the SSU carries one m^7G residue (m^7G1639) deposited by WBSCR22, two m^6_2A residues (m^6_2A1850 and m^6_2A1851) deposited by DIMTL1, one m^6A

(m^{6}A1832) deposited by METTL5 and one N1-methyl-N3-aminocarboxypropylpseudouridine hypermodification (m^{1}acp^{3}Ψ1248). This hypermodification is formed by sequential action of three enzymes: the H/ACA snoRNP snR35, EMG1 and an enzyme yet to be identified. On the other hand, LSU 28S rRNA contains one m^{1}A residue (m^{1}A1322) deposited by NML; two m^{5}C residues (m^{5}C3782 and m^{5}C4447) deposited by NSUN5 and NOP2, respectively; one m^{6}A residue (m^{6}A4220) deposited by ZCCHC4 and one N3-methyluridine residue (m^{3}U4500) for which the responsible enzyme remains unknown. Interestingly, most of these base modifications are conserved from yeast to humans except for the two m^{6}A residues found in position A1832 of the 18S rRNA and A4220 of 28S rRNA, which are not present in yeast [128]. In addition, yeast ribosomes possess two m^{3}Us in their 25S rRNA (m^{3}U2634 and m^{3}U2843), neither of which homologous to the single m^{3}U residue found in human 28S rRNA [128-130]. The high degree of conservation from yeasts to humans indicates potentially important functions for these base modifications. In fact, these rRNA modifications are not randomly distributed, they tend to cluster mainly at functionally critical areas of the ribosome: the DCC, the PTC and the subunit interface, further suggesting key functions for these modifications (Figure 4) [24, 25, 85].

Several base modifications have been demonstrated to impact ribosome function. For instance, the absence of m^{1}A methylation on 28S rRNA, which is deposited by NML [131, 132], results in an altered translational program that favors the translation of key metabolic enzymes and ribosome biogenesis factors such as PGK1, ENO1 or RPS5 [132]. m^{1}A is believed to stabilize RNA secondary and tertiary structures due to its positive charge [52]. Thus, the lack of this modification on rRNA leads to a structural alteration in the LSU which in turn affects protein translation [132]. Furthermore, loss of the m^{6}A methyltransferase METTL5 leads to a translational reprogramming in which translation of transcription factors is largely favored, leading to a massive alteration of the transcription of, specially, pluripotency genes, thus impacting mouse embryonic stem cell differentiation [133]. Similarly, the loss of METTL5-mediated methylation in human cells also resulted in translational reprogramming, favoring the translation of mRNAs related with mitochondrial biogenesis and mitochondrial function regulation [134]. Moreover, loss of ZCCHC4, responsible for depositing m^{6}A4220 in 28S rRNA, has been shown to alter codon-specific translation dynamics and favor the translation of transcripts related to RNA metabolism and the nucleosome [135]. Another example is the m^{5}C methylation of rRNA which has also been reported to alter ribosome function. For instance, loss of m^{5}C4447, which is deposited by NOP2 and located near the PTC [88], has shown to strongly affect ribosome biogenesis and to induce translation of specific transcripts [88, 136]. In fact, depletion of Nsun-1, the NOP2 homolog in *C. elegans*, leads to methylation-dependent translational rewiring in which translation of collagens and factors related with embryo development is repressed [136].

Importantly, several studies have demonstrated that RNA modifications frequently act in a cumulative manner and significant phenotypes can only be observed after deletion of clusters of modifications [90, 137-139], such as the cluster composed by Cm1639, $m^1acp^3\Psi1191$ and Gm1428 found near the DCC [90, 139] or the cluster composed by $\Psi2264$, $\Psi2266$, Am2256, $\Psi2258$ and $\Psi2260$ on helix 69, which is a component of the intersubunit bridge B2a [137, 139]. Therefore, further investigation is needed to study the combined role of modification clusters located in important regions of the ribosome.

2.4. Ribosome alterations in disease

A growing number of genetic diseases have been associated with ribosome dysfunction. Due to their ethiology, these diseases are collectively known as ribosomopathies and are characterized by a wide range of symptoms [140, 141]. Interestingly, some alterations in RPs or ribosome biogenesis factors have been linked to tissue-specific phenotypes, which was unexpected considering the fundamental role of ribosomes in all tissues. This observation suggests a potential mechanism of cell type-specific translation regulation that is not well understood yet.

Two well-known examples of ribosomopathies are Diamond-Blackfan anemia and the 5q-syndrome, which are caused by mutations in RPs [141]. Diamond-Blackfan anemia (DBA) primarily manifest as red cell aplasia [142]. While the first mutation described in DBA was found in eS19 [143], subsequent research has revealed mutations in 10-15 different RPs, including eS26, uL5 and uL18, among others [142]. On the other hand, 5q- syndrome, currently considered a subtype of myelodysplastic syndrome, is characterized by a macrocytic anemia [144]. In this case, disease is driven by haploinsufficiency of the ribosomal protein uS11 [145, 146].

2.4.1. Ribosomal RNA modifications in disease

Importantly, not only RPs but also enzymes responsible for rRNA modifications have been associated with ribosomopathies. For instance, the *DCK1* gene, which encodes for the pseudouridine synthase Diskerin, is mutated in X-linked diskeratosis congenita [147, 148]. This disease is characterized by mucocutaneous abnormalities, bone marrow failure, and pulmonary fibrosis. Mutations in *DKC1* found in patients with X-linked diskeratosis congenita have been shown to impair ribosome biogenesis and the translation of IRES-containing mRNAs such as those encoding for p53, p27 or the anti-apoptotic factors XIAP and BCL2L1 [120, 149]. Moreover, mutations in another pseudouridine synthase, EMG1, have been linked to Bowen-Conradi syndrome, characterized by severe growth retardation. EMG1 mutations also lead to impaired ribosome biogenesis causing cell growth defects [150, 151].

Except for the case of 5q- syndrome, which has shown a positive response to lenalidomide, current treatments of ribosomopathies are primarily focused on managing the symptoms [140, 141]. Advances in our understanding of the molecular mechanisms that control ribosome biogenesis, translation regulation and genetic mutations leading to ribosomopathies are essential to identify new vulnerabilities potentially leading to the development of new target therapies to treat these complex diseases.

2.4.2. Ribosomal RNA modifications in cancer

Ribosomal RNA modifications have also been widely associated with cancer. In fact, several ribosomopathies are linked to an increased susceptibility to cancer, such as diskeratosis congenita [148]. It is important to note that not only mutations in the *DKC1* gene, but also alterations in the expression of this enzyme are associated to cancer [141]. Initially, it was believed that lower levels of Ψ were a common feature in cancer and that DKC1 acted as a tumor suppressor [152]. However, further studies have also found upregulation of DKC1 in various tumor types, indicating that this enzyme may also act as an oncogene. Thus, increased expression of DKC1 has been found in prostate cancer, liver cancer, cholangiocarcinoma or breast cancer, among others [153-157]. Although DKC1 plays an important role in maintaining telomere activity, it has been shown that its tumorigenic capacities are independent of this role but associated to its role in translation regulation [158].

2'-O-me in rRNA has also been linked to cancer. The first analysis of 2'-O-me sites in rRNA using ribomethylation sequencing (RiboMethSeq) in two patient cohorts (breast cancer and B-cell lymphoma) revealed a subset of 2'-O-me sites with substoichiometric modification. Importantly, these sites were differentially and distinctively modified between patient samples and could discriminate between different grades of the disease [159, 160]. Moreover, these studies have revealed a significant overlap of 2'-O-me altered sites between the two cancer types, but also cancer-specific subsets of alterations, suggesting the existence of tissue-specific ribomethylation signatures, and supporting the existence of ribosome heterogeneity [159, 160]. How these 2'-O-me sites are differentially modified is still not fully understood, however differential box C/D snoRNA expression and enzyme catalytic activity may be involved. In fact, FBL has been shown to be directly controlled by p53. Thus, the loss of p53 in tumors leads to increased FBL expression, resulting in aminoacid misincorporation and increased IRES-dependent translation [161].

Recently, the loss of the hypermodified residue $m^1acp^3\Psi1248$ has been identified as a major alteration in cancer [162]. This alteration has been observed in more than 22 types of cancer, with colorectal cancer standing out, as nearly 46% of the patients exhibit hypomodified $m^1acp^3\Psi1248$.

Interestingly, patients with this alteration share a common translational signature characterized by the increased expression of RPs. These studies support the contribution of rRNA modifications to ribosome heterogeneity.

Enzymes related with base methylations have also been found to be altered in several cancer types. One well-known example is the m^5C methyltransferase NOP2, also known as nucleolar antigen p120, which is upregulated in several cancer types while almost undetectable in normal tissues [163]. Another rRNA methyltransferase often upregulated in many cancer types is METTL5 [164-166]. This modification has been shown to enhance the binding of mRNAs to the 40S rRNA, thereby increasing translation rates [166]. Moreover, the upregulation of METTL5 in cancer has been shown to increase *c-MYC* translation, resulting in increased proliferation [164].

Although alterations in rRNA modifications, such as methylations, have been shown to be associated with cancer and play a tumorigenic role, no specific inhibitor for any rRNA methyltransferase has been developed to date. Nonetheless, it worth mentioning that small molecule inhibitors have been designed against the mRNA m^6A methyltransferase METTL3. One recently developed effective inhibitor, STM2457, has shown very promising results in reducing the tumoral growth in a preclinical model of acute myeloid leukemia (AML) [167]. Moreover, an optimized version of this compound, STC-15, recently started a phase 1 clinical trial for advance tumors (clinical trial NCT05584111). This achievement shows that the epitranscriptome is druggable and opens the door to new therapeutic strategies targeting RNA modifying enzymes to treat cancer or other epitranscriptome-associated diseases.

3. 5-methylcytosine

5-methylcytosine is a well-characterized modification in DNA, but its role in RNA remains largely unexplored. This modification can be found across all domains of life and in a wide range of RNAs, with higher abundance in tRNAs and rRNAs [168]. Less frequently, m^5C has also been found in mRNAs, long non-coding RNAs (lncRNAs), vault RNAs (vtRNAs), and snoRNAs [26, 168-170].

3.1. Cytosine-5 methyltransferases and demethylases

The deposition of m^5C on RNA is catalyzed by a group of methyltransferases that belong to the superfamily of Rossman fold-containing enzymes that use S-adenosyl-L-methionine (SAM) as a methyl donor. In eukaryotes, this modification is catalyzed by the DNA methyltransferase family member 2 (DNMT2) and the NOL1/NOP2/Sun Domain (NSUN) family (Figure 5) [171].

DNMT2, also known as tRNA Aspartic Acid Methyltransferase 1 (TRDMT1), belongs to the family of DNA methyltransferases (DNMT family). Due to its homology with other members of

the family, DNMT2 was originally considered a DNA methyltransferase. However, in 2006 Bestor Lab demonstrated that DNMT2 actually methylates position 38 in tRNA$^{Asp-GUC}$ [171, 172]. Subsequent studies confirmed that DNMT2 can also methylate tRNA$^{Asp-GUC}$, tRNA$^{Gly-GCC}$ and tRNA$^{Val-AAC}$ [173].

The NSUN family consists of seven members: NOP2 and NSUN2-7, each one with specificity for a different RNA specie or position (Figure 5). NSUN2 and NSUN6 methylate cytoplasmic tRNAs with distinct specificities. NSUN2 methylates most of tRNAs at the variable loop as well as the wobble position of leucine tRNA [3, 174], while NSUN6 catalyzes the methylation of the acceptor stem in cysteine and threonine tRNAs [175]. NSUN2 is also responsible for m^{5}C methylation in mRNAs, lncRNAs and vtRNAs [46, 176-178] and recently NSUN6 has been reported to also methylate mRNAs [179]. NSUN3 targets mitochondrial tRNAs (mt-tRNAs) at the wobble position [180]. NOP2 and NSUN5 methylate cytoplasmic rRNA at two highly conserved positions (position C3782 and C4447 of 28S rRNA, respectively) [6, 24, 181]. Additionally, NSUN4 methylates mitochondrial rRNA (mt-rRNA) at position C841 of the 12S rRNA [182]. Lastly, NSUN7 has shown to interact with enhancer RNAs (eRNAs), which are short non-coding RNAs that regulate transcription, and to methylate mRNAs [183, 184]. Notably, NOP2, NSUN2 and NSUN5 are the most conserved m^{5}C RNA methyltransferases, as they are found in yeast as Nop2, Trm4 and Rcm1, respectively, suggesting highly conserved and important functional roles [88, 185].

Importantly, m^{5}C is also targeted by "erasers". It is well-known that m^{5}C in DNA can be hydoxylated by the ten-eleven translocation (TET) family of proteins, including TET1, TET2 and TET3, to produce cytosine-5-hydroxymethylation (hm^{5}C). However, in 2014, TET proteins were reported to act also on RNA [186]. Few years later, the AlkB homolog 1, Histone H2A dioxygenase (ALKBH1) was also reported to hydroxylate m^{5}C on RNA [180].

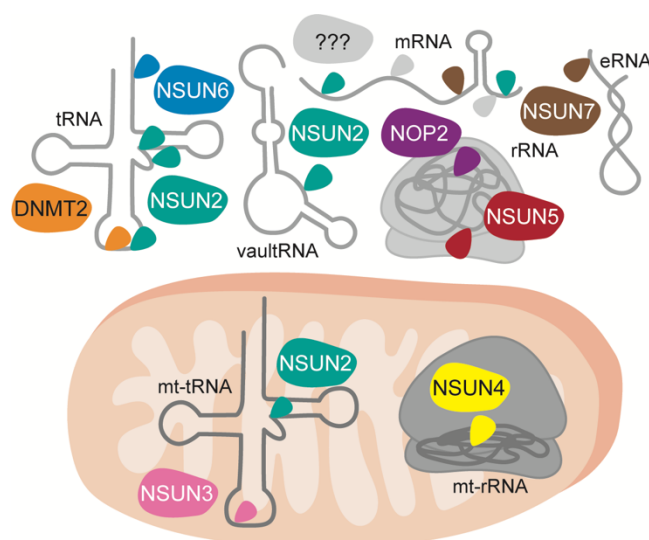*Figure 5. Cytosine-5 methyltransferases and their substrate RNAs. Cytosolic tRNAs are methylated by DNMT2, NSUN2 and NSUN6. mRNAs are methylated by NSUN2 and NSUN7 and may be methylated by an unknown methyltransferase. Cytosolic rRNAs are methylated by NOP2 and NSUN5. vtRNAs are methylated by NSUN2 and eRNAs are targeted by NSUN7. In the mitochondria, tRNAs are methylated by NSUN2 and NSUN3 while rRNA is targeted by NSUN4.*

3.2. Physiological functions of cytosine-5 methyltransferases and demethylases

Among the extensive variety of m^5C RNA modifications, the most studied in mammals are those occurring on tRNAs. NSUN2 is responsible for methylating the variable loop of 80% of the tRNAs, as well as the anticodon loop of leucine tRNA. NSUN2-mediated methylation has been found to play a pivotal role in regulating protein synthesis rates during tissue homeostasis, development, and cancer [3, 4, 168, 174]. These changes in the translational program mediated by NSUN2 promote the synthesis of proteins associated with stress response, cell motility and morphogenesis [3, 48, 187]. Mechanistically, NSUN2 protects tRNAs from angiogenin-mediated cleavage. Consequently, in the absence of NSUN2, cells accumulate 5' tRNA-derived small RNA fragments (5'tRFs), that are able to repress global protein synthesis but activate translation of specific transcripts [3, 4].

Similarly, DNMT2 methylates tRNAs on the anticodon loop, contributing to tRNA processing, translational accuracy and amino acid charging [171, 174]. Importantly, this methylation deposited by DNMT2 is also essential to protect tRNAs from fragmentation and to maintain normal protein synthesis [4, 174, 188].

On the other hand, NSUN6 is known to methylate mature tRNAs in the acceptor stem, although the precise role of this methylation remains elusive. Due to its proximity to the amino acid charging position, this methylation is thought to play a role in amino acid discrimination [169]. Recently, NSUN6 has been reported to also methylate mRNAs at 3'UTR, contributing to accurate protein translation termination [179].

Mitochondrial tRNAs are methylated at the wobble position by NSUN3. This modification has been shown to be crucial to maintain mitochondrial translation and mitochondrial metabolic plasticity [189]. Moreover, NSUN3 catalytic activity is also essential for the differentiation of mouse embryonic stem cells (mECS), although the molecular mechanism for this process remains unknown [190].

RNA methyltransferases that methylate the rRNA have also been found to play important roles in cell function. NOP2 plays a significant role in the LSU biogenesis in humans and yeast [88, 89]. Moreover, NOP2 methylates position C4447 of human 28S rRNA, which is located in the A-loop of the peptidyl transferase center, suggesting that this methylation may play a role in protein synthesis [88]. Studies in *C. elegans* indicate that loss of the homolog of NOP2 leads to the translation of specific transcripts [136], although this has not been explored in humans yet. On the other hand, NSUN5 loss does not affect ribosome biogenesis but strongly impacts protein synthesis [6, 88, 181, 191].

The mitochondrial rRNA methyltransferase NSUN4 is required for the methylation of the 12S rRNA in the SSU but also facilitates the assembly of the LSU by interacting with MTERF4 [182]. Moreover, NSUN4 has also been reported as essential for mouse embryonic development [182].

Lastly, the function of NSUN7 is still largely unknown, although it has been shown to interact with several eRNAs of genes targeted by the transcriptional co-activator PGC1-α, regulating their stability [183]. Interestingly, NSUN7 expression and eRNA methylation has been reported to increase during starvation, suggesting that NSUN7 may contribute to the regulation of gene expression during stress responses [183]. Furthermore, recent studies have demonstrated that NSUN7 methylates several mRNAs, including *CCDC9B*, thereby modulating their stability and contributing to the MYC signaling pathway [184].

m^{5}C RNA demethylases have also been shown to play important physiological roles. For instance, TET2 mediates the production of hm^{5}C on mRNA, thereby inhibiting the function of m^{5}C on double-stranded RNA formation. TET2-mediated hydroxylation of m^{5}C on mRNAs has also been shown to increase ADAR1 binding, promoting the editing of hydroxymethylated mRNAs [192]. These findings suggest an intricated regulatory mechanism that combines various post-transcriptional modifications that regulate important processes such as immune responses.

hm^{5}C has also been identified in tRNAs. In these molecules, ALKBH1 first hydroxylates m^{5}C to form hm^{5}C and subsequently oxidizes hm^{5}C to 5-formylcytosine (f^{5}C) in the anticodon loop of mitochondrial tRNA^{Met} and cytoplasmic tRNA^{Leu}. This modification plays important roles in regulating mitochondrial translation and oxygen consumption [180]. Moreover, TET1 can mediate the oxidation of f^{5}C to 5-carboxylcytosine (ca^{5}C) in RNA *in vitro* [193]. While m^{5}C oxidation appears to be a highly dynamic process much more research is needed to fully understand the biological relevance of these low-abundant modifications.

3.3. Pathological implications of altered m^{5}C deposition

m^{5}C RNA methyltransferases play crucial roles in in cell function, controlling protein synthesis, cell metabolism, proliferation, cell cycle progression or differentiation. Therefore, it is not surprising that alterations in these enzymes can lead to pathological consequences. All m^{5}C RNA methyltransferases have been linked to various diseases, especially to cancer, although their precise role in the etiology of these diseases is not always fully understood (Table 1).

3.3.1. Pathological implications of altered m^{5}C deposition on tRNAs

NSUN2 mutations have been linked to several neurodevelopmental disorders. For instance, homozygous missense mutation of *NSUN2* has been linked to autosomal-recessive intellectual

disability. This mutation impedes NSUN2 localization to the nucleus, where it carries out its function [194]. Additionally, Noonan-like syndrome has also been associated to *NSUN2* mutations. In this case, a homozygous 1-bp frameshift deletion results in an early termination codon, causing the degradation of the mRNA by nonsense-mediated decay [195]. Moreover, homozygous mutations at the canonical splice acceptor of exon 6 generate a new splice variant, leading to mRNA instability. This mutation, which is linked to Dubowitz-like syndrome, results in reduced protein expression and tRNA methylation [196]. The accumulation of tRNA fragments in the absence of Nsun2 has been reported to impair neuron differentiation and migration in mice, which might be the cause of these neurodevelopmental disorders in humans caused by impaired NSUN2 function [197].

NSUN2 is also widely associated to cancer. Increased NSUN2 expression has been reported in gastric cancer (GC), esophageal squamous cell carcinoma (ESCC), hepatocellular carcinoma (LIHC), prostate cancer (PRAD), nasopharyngeal carcinoma (NPC) and melanoma, among others [198-202]. Importantly, loss of NSUN2-mediated m^5C methylation, which results in tRNA cleavage and stress-related translational program, leads to an increased proliferation of tumor-initiating cells. However, NSUN2-deficient cells also exhibit increase sensitivity to 5-fluorouracil (5-FU), suggesting that the combination of NSUN2 inhibition and classical chemotherapeutic agents could be used to specifically eliminate tumor-initiating cells [4].

NSUN3 has also been shown to be upregulated in tumors. Interestingly, m^5C and f^5C in mt-tRNA can act as sensors of cellular energy requirements, allowing the adaptation of mitochondrial functions. In fact, high methylation levels in mt-tRNAs are essential to allow the metabolic switch of tumors from glycolysis to OXPHOS, a requirement for cells metastasis [189]. *NSUN3* mutations affecting splicing, frameshifting or introducing premature stop codons have been found in patients with early-onset mitochondrial encephalomyopathy and seizures and other mitochondrial disorders. Moreover, mutations in mt-tRNA^{Met} (C39U) also leads to mitochondrial disorders. In both cases, mutations result in a lack of NSUN3-mediated methylation, impairing mitochondrial translation and, consequently, mitochondrial function.

NSUN6 is frequently downregulated in cancers such as pancreatic ductal adenocarcinoma (PDAC), clear cell renal cell carcinoma (ccRCC) and glioblastoma (GBM). Interestingly, loss of *NSUN6* in GBM has been reported to increase the resistance to temozolomide, the first-choice chemotherapeutic agent in GBM, due to global downregulation of m^5C methylation [203]. Mechanistically, low m^5C levels lead to the accumulation of negative elongation factor B (NELFB) and ribosomal protein S6 kinase B2 (RPS6KB2), resulting in a transcriptional pausing and temozolomide resistance [203].

3.3.2. Pathological implications of altered m^{5}C deposition on rRNAs

NOP2 has been largely considered as a predictive marker in diverse cancer types including PRAD, LIHC, breast cancer (BRCA), and colorectal cancer (CRC) [204-208]. NOP2 is cell cycle-regulated and essential for progression to the S phase, with its upregulation increasing the cell cycle rates and promoting cell proliferation [204, 209]. However, whether NOP2-mediated methylation is responsible of the increased cell proliferation it is still unknown.

The mitochondrial rRNA methyltransferase NSUN4 has also been linked to cancer, specially to LIHC. NSUN4 expression is upregulated in LIHC and can be used as an independent prognostic marker, correlating with poor prognosis [210]. However, the contribution of NSUN4 to the malignant phenotype remains to be elucidated. Similarly, other *in silico* studies have reported that NSUN4 can be used as prognostic marker in combination with other m^{5}C regulators in ccRCC, together with NOP2, NSUN6 and TET2, [208] and lung squamous cell carcinoma (LUSC), together with NSUN3 [211].

3.3.3. Pathological implications of altered m^{5}C deposition on other RNA species

Although tRNAs and rRNAs are the most heavily modified RNA species, m^{5}C methylation in other RNAs has also shown to have significant biological functions and to be associated with human diseases. For instance, nonsense and missense mutations in exon 4 and 7 of NSUN7, respectively, have been found in asthenospermic men [212]. However, it remains unclear whether the methyltransferase activity of NSUN7 or its RNA binding capacity is hampered by these mutations or whether its mRNA or eRNA targets are associated with this disease.

mRNA methylation has also been widely associated to cancer progression. For instance, NSUN2-mediated methylation of *HDGF* mRNA 3'UTR increases its half-life and impacts protein abundance, supporting tumor growth [200]. Similarly, NSUN2-mediated methylation of *FOXC2* mRNA increases its stability in gastric cancer favoring its oncogenic role [213]. Interestingly, NSUN2 involvement in cancer is not limited to the aberrant methylation of tRNAs and mRNAs, it also includes lncRNAs. For instance, NSUN2 has been shown to methylate lncRNA H19, a well-known cancer-related lncRNA. Aberrant NSUN2-mediated methylation increases the stability of lncRNA H19, which, in turn, binds G3BP1, leading to MYC accumulation and promoting tumor development in LIHC [178]. In addition, TET2 is usually mutated in AML, leading to TET2 deficiency. This reduction resulted in the accumulation of m^{5}C modification in mRNAs such as *TSPAN12* mRNA, increasing its stability and driving leukemogenesis [214].

20

Altogether, m⁵C methylation is widely deregulated in cancer. Further study of these alterations and their mechanism of action could contribute to our understanding of tumor cell function, and more importantly, could provide new targets for cancer therapy.

Table 1. *Diseases associated to m⁵C methylation. The methyltransferase responsible of the methylation, RNA specie affected, alteration produced, physiological function and related disease are indicated. PRAD: prostate adenocarcinoma, LIHC: liver hepatocellular carcinoma, BRCA: breast cancer, CRC: colorectal cancer, NPC: nasopharyngeal carcinoma, ESCC: esophageal squamous cell carcinoma, GC: gastric cancer, LUSC: lung squamous cell carcinoma, HNSCC: head and neck squamous cell carcinoma, LUAD: lung adenocarcinoma, ccRCC: clear cell renal cell carcninoma, GBM: glioblastoma, PDAC: pancreatic ductal adenocarcinoma.*

Enzyme	RNA specie	Alteration	Pathological function	Desease	Ref
NOP2	rRNA	Upregulation	Increases proliferation rates	Cancer (PRAD, LIHC, BRCA and CRC, among others)	[206, 208, 215]
NSUN2	tRNA	Splicing variant	Splicing variation causes NSUN2 instability leading to reduced methylation of target tRNAs and tRNA fragmentation	Dubowitz-like syndrome and intellectual disability	[196, 197]
		1-bp deletion	Deletion alters reading frame and promotes the degradation of *NSUN2* mRNA	Noonan-like syndrome	[195]
		Homozygous missense mutation	Mutated produces NSUN2 relocalization within the cell	Autosomal-recessive intellectual disability	[194]
		Upregulation	Promotes tRNA stability, increases translation efficiency and regulates stress response	Cancer (LIHC, NPC ESCC, PRAD, among others)	[200-202, 216]
	mRNA	Upregulation	Enhances stability of several oncogenes as FOXC2 or HDGF and repress expression of tumor suppressors such as p57kip2 promoting tumor growth and metastasis	Cancer (LIHC, GC)	[199, 213, 217]
NSUN3	mt-tRNA	Upregulation	NSUN3-mediated methylation regulates mitochondrial function and enhances metastasis	Cancer (LUSC and HNSCC)	[189, 211]
		Biallelic mutation	Missense and nonsense mutations lead to mitochondrial disease due to oxidative phosphorylation deficiency	Early-onset Mitochondrial Encephalomyopathy and Seizures and other combined mitochondrial disorders	[180, 218, 219]
NSUN4	mt-rRNA	Upregulation	Unknown	Cancer (LUAD, LIHC and ccRCC)	[208, 210, 211]
NSUN5	rRNA	Deletion	Nsun5 deletion in mice produced impaired proliferation of oligodendrocyte precursor cells and hypomyelination leading to cognitive deficits	Williams-Beuren syndrome	[220-223]
		Promoter methylation	NSUN5 regulated proliferation of tumor cells and protein synthesis	Cancer (GBM)	[6]
		Upregulation	NSUN5 regulated proliferation of tumor cells and cell cycle progression	Cancer (LIHC, CRC and ccRCC)	[224-226]

Table 1 (cont.). *Diseases associated to m⁵C methylation. The methyltransferase responsible of the methylation, RNA specie affected, alteration produced, physiological function and related disease are indicated. LIHC: liver hepatocellular carcinoma, NPC: nasopharyngeal carcinoma, ESCC: esophageal squamous cell carcinoma, PRAD: prostate adenocarcinoma, GC: gastric cancer, LUSC: lung squamous cell carcinoma, HNSCC: head and neck squamous cell carcinoma, LUAD: lung adenocarcinoma, ccRCC: clear cell renal cell carcinoma, GBM: glioblastoma, CRC: colorectal cancer, PDAC: pancreatic ductal adenocarcinoma.*

Enzyme	RNA specie	Alteration	Pathological implication	Desease	Ref
NSUN6	tRNA	Downregulation	Regulates cell cycle and G2/M checkpoints	Cancer (PDAC, ccRCC, GBM)	[208, 227]
NSUN7	-	Mutation	Mutation produces missfolding of NSUN7 protein and affects sperm motility	Asthenospermia	[212]
DNMT2	tRNA	Somatic mutations	Altered enzymatic activity	Cancer	[228, 229]
		Upregulation	Unknown	Cancer	[228, 230]
TET2	mRNA	Mutation	TET2 deficiency leads to m⁵C accumulation on several mRNAs resulting in mRNA stabilization and disease progression	Cancer (AML)	[214]

3.4. Targeting altered m⁵C RNA deposition

The abundance of alterations in m⁵C RNA methylation makes it an intriguing target for cancer treatment. m⁵C modification in RNA is targetable by already developed cytosine analogs. These analogs, such as azacytidine, were initially developed to interfere with DNA methylation [231, 232] but have also demonstrated complete inhibition of DNMT2-mediated tRNA methylation [233, 234]. However, the use of these compounds has not yet been explored for inhibiting other m⁵C methylations, such as those occurring in rRNA or mRNA.

Moreover, in the recent years, several TET inhibitors have been developed to inhibit hm⁵C formation in DNA. For instance, TET1/2/3 inhibitor, TETi76, has been tested *in vivo* with promising results in restricting clonal evolution of TET2-mutant cells without affecting normal hematopoietic precursor cells [235]. A cytosine-based inhibitor of TET enzymes, Bobcat339, has also been developed with strong inhibitory capacities, although it has not been tested *in vivo* yet [236]. More recently, Itaconate have been reported as a TET2-specific inhibitor. Interestingly, use of Itaconate reduced TET2 catalytic activity *in vivo* and exhibited an immunomodulatory function, suppressing acute inflammatory responses [237]. Unfortunately, the activity of these inhibitors on TET-mediated RNA modification has not been evaluated yet.

However, in any case, it is important to note that the widespread abundance of m⁵C modification in RNA and DNA, together with the lack of selectivity of most of these drugs, could lead to off-target effects with potential harmful consequences [168].

3.5. Role of the ribosomal RNA methyltransferase NSUN5

NSUN5 is a highly conserved methyltransferase that methylates human rRNA at position C3782 [6, 181]. This modification is located within the helix 70, domain IV of 28S rRNA in humans, which constitutes part of the subunit interface of the ribosome (Figure 6) [24, 61]. m^5C3782 is one of the most conserved methylation marks across all organisms, suggesting an important role on ribosome function [168].
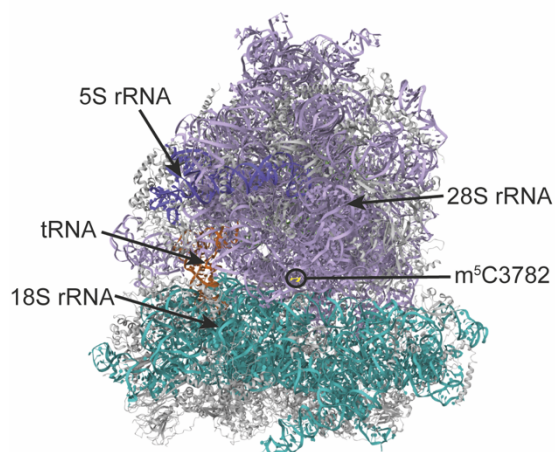
Although many of the functional and structural studies conducted to understand the role of NSUN5 have focused on the yeast homolog, the high degree of conservation suggests similar

Figure 6. *Location of m^5C3782 on human 80S rRNA. rRNA and proteins are presented as ribbons. 28S rRNA is represented in light purple, 5S rRNA in dark purple and 18S rRNA in blue. Initiator tRNAMet is depicted in orange and proteins in grey. m^5C3782 is represented in yellow and indicated with a circle.*

roles in human ribosomes [25]. In yeast, the NSUN5 homolog, known as Rcm1, methylates position C2278 of 25S rRNA [88]. This modification is part of a highly conserved cluster of methylated nucleotides in helixes 70 and 71, along with the 2'-O-me located on G2288. Combined loss of these methylations in yeast has been shown to alter ribosome stability due to a dramatic alteration of rRNA structure [238]. Interestingly, Rcm1-mediated m^5C methylation contacts the ribosomal protein eL41, that constitutes the centrally located eukaryotic-specific bridge eB14 [24, 61]. This bridge acts as a motion center for 40S subunit rotation during translation [239]. Moreover, other three modifications in the SSU (ac^4C1773, m^6_2A1781 and m^6_2A1782) interact with the other side of this bridge [24, 61]. Although the role of these modifications on the function of eB14 bridge has not been explored yet, it is proposed that these modifications may play regulatory roles on translation efficiency by the transmission of allosteric information [25, 85]. Interestingly, NSUN5-mediated methylation has been largely considered to occur stoichiometrically. However, methylation studies in adult mouse liver suggest that this site is incompletely modified [181], suggesting that both m^5C-methylated and non-methylated ribosomes can coexist in cells in physiological conditions.

The loss of Rcm1-mediated methylation alone has no effect in ribosome biogenesis or polysome assembly but increased the sensitivity of the cells to the antibiotic anisomycin due to changes in 25S rRNA structure [88, 191]. Moreover, the loss of Rcm1 also resulted in an increased chronological lifespan of yeasts but a decreased replicative lifespan [191]. Similarly, studies in *Caenorhabditis elegans* and *Drosophila melanogaster* have shown that the silencing of their NSUN5 homolog leads to an increased lifespan and resistance to heat and oxidative stress [191].

Mechanistically, the loss of Rcm1 results in a more efficient translation of stress response mRNAs even under control conditions. This is proposed to promote a faster response and an improved modulation of translation upon stress initiation, which may contribute to the increased stress resistance [191].

In humans, *NSUN5* loss produces a reduction of bulk protein synthesis [6, 181, 240]. Importantly, despite the global decrease in protein synthesis, an activation of a stress-related translational program was observed [6], consistent with findings from yeast lacking Rcm1 [191], and suggesting that NSUN5 might regulate survival under stress conditions in a conserved manner.

3.5.1. Pathological implications of NSUN5

In humans, *NSUN5* is located at 7q11.23, the chromosomal region deleted in Williams-Beuren syndrome (WBS) [221, 241]. WBS is a multisystemic developmental disorder characterized by a recognizable pattern of malformations, cognitive disabilities, mild to moderate mental retardation and characteristic behavior patterns [221, 241, 242]. The typical WBS deletion cluster spans approximately 1.5 Mb and affects around 25 genes [221, 242]. Thus, determining the contribution of each deleted gene to a specific WBS symptom appears to be intricate. *NSUN5* is deleted in 95% of WBS patients [220]. Recent findings in *Nsun5*-knocked out mice showed that the loss of this enzyme leads to cognitive impairments [220, 222, 223] and reduced body mass [181], suggesting that reduced m^{5}C methylation plays a role in this complex disease.

Further studies in humans have linked NSUN5 to cancer development. NSUN5 has been identified as an oncogene in CRC [226], LIHC [225], ccRCC [224] and in HeLa cells [181]. The loss of *NSUN5* in these tumors correlated with lower proliferation rates and decreased tumor size [181, 224-226]. Mechanistically, *NSUN5* loss has been shown to increase p53 levels in ccRCC [224], and to alter cell cycle progression in CRC [226], leading to proliferation inhibition in both cases. NSUN5 has also been found altered in glioblastoma (GBM). However, the role of NSUN5 in this cancer remains controversial, as it has been shown to behave as either a tumor suppressor [6] or an oncogene [240]. In one hand, Janin and colleagues demonstrated that *NSUN5* loss is associated with increased tumor growth and cell proliferation, while NSUN5 overexpression hinders this increased proliferation [6]. Conversely, Zhou *et al.* found that *NSUN5* silencing decreases the growth, sphere formation and migration of GBM cells and reduces tumor growth [240]. Interestingly, an activation of a stress-related translational program has been reported in GBM and HeLa cells after *NSUN5* loss, which might help cancer cells to survive the stressful conditions encountered during tumor progression, such as hypoxia or nutrient deprivation [6, 181].

Considering the current limited understanding of the role of NSUN5 in cell physiology and its controversial implications in tumor development, it is evident that further research efforts are necessary to comprehensively elucidate the role of NSUN5 in healthy tissues and its involvement in tumor initiation and progression.

3.6. Upstream regulation of cytosine-5 RNA methyltransferases

While function of many methyltransferases and their dependent methylation is starting to be elucidated, a key missing piece of the puzzle is the upstream regulation of these methyltransferases. One of the most common mechanisms for the regulation of protein activity is protein post-translational modification, which is a highly dynamic and reversible process. Post-translational modifications are diverse, including phosphorylation, acetylation or ubiquitination, among others, and can alter the structure or properties of the proteins, thereby allowing the cells to integrate signals and modulate their physiological state [243]. To date, NSUN2 is the only m^5C methyltransferase that has been shown to be post-translationally regulated [244]. NSUN2 is phosphorylated at serine 139 by Aurora kinase B (Aurora-B), a key regulator of chromosome segregation (Figure 7). This phosphorylation represses NSUN2 activity and avoids the association with its nucleolar binding protein NPM1 [244]. It is proposed that this phosphorylation allows the release of NSUN2 from NPM1 during mitosis to associate with the mitotic spindle, thereby allowing normal spindle formation [245]. The high conservation of NSUN family suggest that other members may be also regulated in a similar fashion. However, further research is needed to find the regulatory pathways of m^5C methyltransferases.
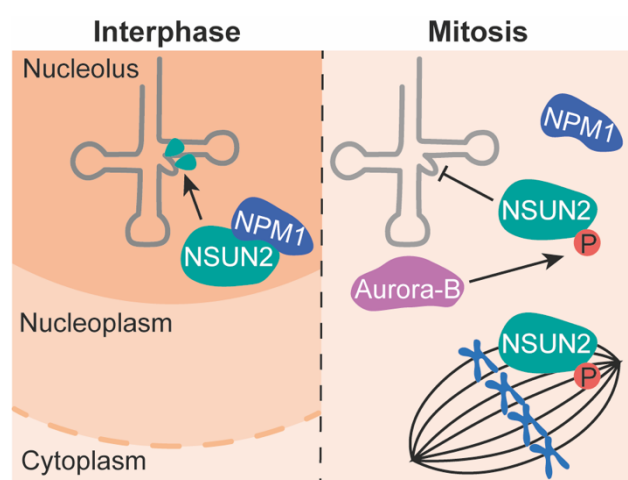
Figure 7. *Upstream regulation of NSUN2 by Aurora-B. During Interphase, NSUN2 is located in the nucleolus and interacts with NPM1. At the onset of mitosis, NSUN2 is phosphorylated by Aurora-B, which inhibits its catalytic activity. This phosphorylation of NSUN2 also avoids the interaction with NPM1 and might act as a signal for translocation of NSUN2 to the mitotic spindle.*

Interestingly, DNMT2 activity has been found to be enhanced by the micronutrient queuosine [246, 247]. Queuosine is an hypermodified 7-deaza-guanosine that replaces the guanosine typically found at the wobble position of tRNAs presenting a GUN anticodon. In the presence of queuosine, the methylation at tRNA$^{Asp-GUC}$ increased from 14% to 100%, indicating that DNMT2 activity is

directly activated by the queuosinylated targets [246]. Importantly, this incorporation of queuosine has been reported to increase the translation speed. Thus, depletion of queuosine leads to a strong deregulation of translation, resulting in the activation of the unfolded protein response. Although the precise mechanism of queuosine regulation is still not fully understood, the fact that eukaryotes cannot synthesize queuosine and must obtain it from the environment suggest that it may serve as a mechanism coupling translation regulation with nutritional status [247].

In addition to these two regulatory mechanisms, which occur in physiological conditions, m^5C RNA methyltransferases often undergo genetic alterations that modulate their expression in pathological conditions, especially in cancer. Pancancer studies have revealed that *NSUN2* is highly amplified in several cancer types, with amplification percentages reaching as high as 12.11%. *NSUN2* also exhibit the highest mutation rate among the m^5C RNA methyltransferases in a wide range of tumors [248]. Importantly, the expression of these methyltransferases in cancer is not only regulated by genetic alterations but also by epigenetic changes. For instance, *NSUN5* and *NSUN7* suffer hypermethylation of the CpG islands near their respective promoters, resulting in transcriptional silencing of their expression in glioblastoma and liver cancer, respectively [6, 184].

4. Cell cycle

Cell cycle is a series of events that leads to the accurate duplication and segregation of cellular components, ultimately leading to the formation of two genetically identical daughter cells. It typically consists of four phases: Gap 1 (G1), S phase, Gap 2 (G2) and mitosis (M) (Figure 8). Phases G1, S and G2 are collectively known as interphase [249]. Additionally, cells can also exit the cell cycle and enter a state of quiescence known as G0. G0 is sometimes reversible, allowing cells to re-enter G1 phase [250].

G1 is a growth phase in which cells increase in size, synthesize proteins, and enlarge and amplify organelles, such as mitochondria. During this phase, cells integrate all environmental signals, stress and metabolic cues to determine whether to divide, differentiate or undergo cell death [250]. The G1 phase is followed by the S phase, during which cells replicate their DNA, resulting in chromosomes consisting of two identical sister chromatids. Upon successful completion of DNA replication, cells enter G2 phase, where they prepare for mitosis. This phase is characterized by significant protein synthesis and cell growth [251]. G2 culminates in mitosis, which comprises 5 stages: prophase, metaphase, anaphase, telophase and cytokinesis. During prophase, chromosomes condensate and the nuclear envelope is disrupted. Then, during metaphase, chromosomes attach to mitotic spindle microtubules to form the metaphase plate at the equator of the cell. Anaphase involves the shortening of mitotic spindle microtubules, causing the migration of each sister chromatid towards opposite poles. Then, telophase is characterized by chromosome decondensation

26

and the formation of a new nuclear envelope. Finally, mitosis concludes with cytokinesis, which separates the cytoplasm of the parental cell into two daughter cells, that re-enter the G1 phase. Each phase of the cell cycle relies on the proper completion of the preceding phase, highlighting the required strict regulation of this process [249].

4.1. Cell cycle control

The cell cycle is closely monitored by cyclin-dependent kinases (CDKs), which are serine/threonine kinases that target a wide range of substrates. Each CDK is activated by their associated regulator cyclin [234, 251, 252]. The expression of cyclins is tightly controlled throughout the cell cycle, with their levels increasing and decreasing to temporary activate CDKs, thus facilitating progression through different phases (Figure 8) [253]. Cyclins also confer substrate specificity to CDKs, determining the targets that they can phosphorylate during each phase of the cell cycle [249, 251, 252].
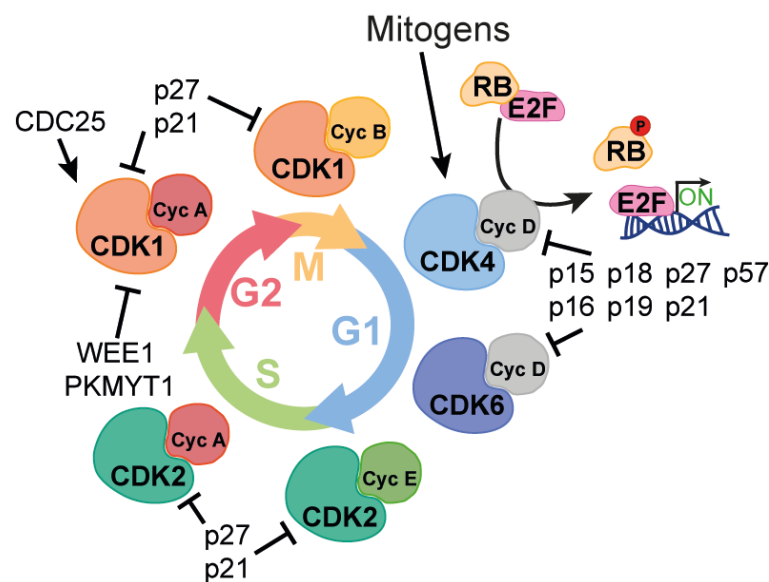
Figure 8. *Schematic representation of cell cycle progression and its main regulatory elements. Cyclin-dependent kinases, cyclins and the main regulators of CDK-cyclin complexes inhibitors and activators are represented.*

During the G1 phase, CDK4 and/or CDK6 are activated by D-type cyclins, enabling them to phosphorylate the Retinoblastoma protein (Rb), leading to its inactivation (Figure 8). This inactivation promotes the release of E2F transcription factor, a crucial event that triggers the transcription of several genes required for cell cycle progression [254]. Among these genes, A- and E-type cyclins start to be transcribed during this phase. This leads to a significant accumulation of cyclin E, that binds and activates CDK2. This key event allows the cell to pass the restriction point at the boundary between G1 and S phase successfully [251, 255]. Subsequently, cyclin A begins to accumulate and complex with CDK2, facilitating the phosphorylation of proteins involved in DNA

replication [255, 256]. During late S phase, cyclin A also associates with CDK1, driving the transition to the G2 phase. As G2 phase progresses, cyclin B expression increases and binds to CDK1. The levels of the CDK1/Cyclin B complex peak in late G2, leading to transition to the M phase. Finally, the levels of this complex decrease, allowing the completion of mitosis [251, 253]. Importantly, while different CDKs are known to drive different phases of the cell cycle, it has been demonstrated that the only essential CDK is CDK1, since in absence of other CDKs, CDK1 can bind to all cyclins and promote cell division [257].

Importantly, cell cycle is extensively regulated by several CDK inhibitors that prevent CDKs from phosphorylating their substrates. These inhibitors can be categorized into two classes: first-class inhibitors and second-class inhibitors. First-class inhibitors comprise mainly CDK4 and CDK6 inhibitors and include $p15^{INK4B}$, $p16^{INK4A}$, $p18^{INK4C}$ and $p19^{INK4D}$ [258, 259]. Second-class inhibitors, which includes $p21^{CIP1}$, $p27^{KIP1}$ and $p57^{KIP2}$, were initially described as inhibitors of CDK/Cyclin E and CDK/Cyclin A complexes but have been demonstrated to inhibit all CDKs [260]. CDK-cyclins complexes are further regulated by WEE1 and PKMYT1, which phosphorylate them, thereby inhibiting their activity. In contrast, CDC25C phosphatases dephosphorylate these residues, activating their function and allowing cell cycle progression [261].

Moreover, the cell cycle also contains several checkpoints to ensure the proper completion of key processes. There are two primary checkpoints: the DNA damage checkpoint, which can be activated during G1, S phase and G2/M transition, and the spindle assembly checkpoint (SAC), which occurs during M phase [262-264]. The DNA damage checkpoint is activated in response to double strand breaks, stalled replication forks, or nucleotide excision/repair processes. Additionally, during the DNA damage checkpoint at G2/M transition, DNA is proofread to ensure the accuracy of the replicative process. These checkpoints involve the sensor kinases ATM and ATR, the checkpoint kinases CHK1 and CHK2, as well as p53, which plays a critical role in the G1 checkpoint. Activation of these pathways leads to increased levels of p21 and inhibition of CDC25, preventing G1-to-S or G2-to-M transitions (Figure 6) [262, 264]. On the other hand, the SAC ensures the proper segregation of sister chromatids by inhibiting anaphase-metaphase transition until proper chromosome attachment is achieved. This mechanism involves the inhibition of anaphase-promoting complex/cyclosome (APC/C), which mediates chromosome segregation, and recruitment of the Mitotic Checkpoint Complex (MCC) to unattached or tensionless kinetochores [263].

4.2. Role of RNA modifying enzymes and RNA modifications in cell cycle control

Several epitranscriptomics regulators have been linked to cell cycle progression. For instance, METTL3, which deposits m[6]A on mRNAs, has shown to methylate *CDC25B* mRNA, favoring its translation in a YTHDF1-dependent manner [265]. METTL3 has also been reported to regulate the alternative splicing of cell cycle-regulated genes, such as *MDM2* or *CTNNB1*, by modulating the expression of the splicing factor SFPQ [266]. It is not only methyltransferases but also demethylases that are involved with cell cycle. For instance, the m[6]A demethylase FTO exhibits cell cycle-regulated localization. During G1, FTO is located in the nucleus, allowing the demethylation of *Cyclin D* mRNAs, thereby promoting their stabilization. On the contrary, during S, G2 and M phases, FTO is exported to the cytoplasm preventing *Cyclin D* mRNA demethylation, leading to its degradation and contributing to the regulation of Cyclin D expression along the cell cycle [267].

The tRNA methyltransferases NSUN2 and DNMT2 also play a role in cell division. NSUN2 has been found to bind to the mitotic spindle during mitosis promoting spindle stability (Figure 7) [245]. Similarly, DNMT2 has also been shown to relocate to the mitotic spindle during cell division in *Drosophila* [268]. DNMT2 is localized in the cytoplasm and nuclei during interphase, but rapidly relocalizes to the nuclei and condenses around mitotic chromosomes at the onset of mitosis, where is thought to access DNA, contributing to the control of chromatin compaction. Then, during telophase, DNMT2 localizes to microtubules structures such as the midbody, where it might provide structural support for the mitotic spindle [268].

Particularly, ribosomal RNA modifiers seem to play an important role in cell cycle regulation. For instance, the expression of the m[5]C rRNA methyltransferase NOP2 is well-known to peak between G1 and S phase and has been found to be essential for entering S phase [209, 269]. This is likely because NOP2 is required for cell cycle-associated ribosomal biogenesis, which is needed for G1 to S phase transition [269]. Importantly, improper ribosome biogenesis is known to trigger p53-dependent cell cycle arrest. Thus, alterations in ribosome biogenesis lead to the release of the ribosomal proteins uL5 and uL18, which can sequester and inactivate MDM2. This results in the stabilization and accumulation of p53, leading to cell cycle arrest [270-272]. This mechanism is known to be activated upon loss of the m[1]A methyltransferase NML, leading to growth arrest, further linking rRNA methylation to cell cycle control [131].

Thus, these observations indicate that RNA modifying enzymes could provide an additional regulatory layer to the tightly controlled regulation of the cell cycle, either by transcriptionally controlling gene expression, as in the case of the mRNA modifiers; by interacting with the mitotic machinery through non-canonical mechanisms; or by interfering with ribosome biogenesis, as is

the case of rRNA modifiers. However, whether rRNA modifiers can contribute to this cell cycle control by inducing translational reprogramming is still unknown.

4.3. Protein synthesis along cell cycle

Protein synthesis is a highly regulated process catalyzed by ribosomes in which mRNA templates are translated into proteins. The continuous synthesis and degradation of proteins allow the cells to alter their composition and dynamically respond to internal and external signals. Precise control of all individual steps involved in protein synthesis are crucial for maintaining cell and organism homeostasis, as their alteration can lead to various diseases [273].

Thus, protein synthesis is strongly regulated along cell cycle, since different phases require specific sets of proteins (Figure 9). Quiescent cells are known to maintain relatively constant levels of the majority of proteins. In contrast, dividing cells need to precisely modulate protein synthesis to support cell cycle progression [274]. However, the mechanism underlying this control of translation is not fully understood yet.

The canonical pathway of protein synthesis begins with the recognition of the m^{7}G cap located at the 5'-end of the mRNA by the eukaryotic initiation factor 4F (eIF4F) [9, 10]. This complex consists of the cap binding protein eIF4E, the DEAD-box RNA helicase eIF4A, the scaffolding protein eIF4G and the poly(A)-binding protein (PABP). PABP plays a crucial role in the circularization of the mRNA by interacting with the poly(A) tail [14]. Circularized mRNA can then bind to the 43S preinitiation complex, which is composed by the 40S ribosome subunit, the initiator tRNA (tRNA-Met), and the initiation factors eIF1, eIF1a, eIF3 and eIF5. The 43S preinitiation complex scans the mRNA in order to align the initiator tRNA with the first AUG codon, which serves as start codon. Once a suitable start codon is identified, the 60S subunit joins the complex and elongation process begins [59]. Although most eukaryotic mRNAs follow this mechanism for translation, there are few exceptions. One well-known case is the initiation mediated by internal ribosome entry sites (IRES), which are highly-structured sequences that are able to recruit ribosomes internally without relying on cap-binding factors [275].

During the cell cycle, in G1 phase, cells exhibit high biosynthetic activity, including a high rate of protein synthesis. However, during S phase, protein synthesis is mostly repressed, except for histones, which are predominantly produced during this phase to support DNA replication. After completion of S phase, protein synthesis rate is highly increased again during G2 phase (Figure 9) [249, 273]. Notably, translation during mitosis was traditionally believed to be globally repressed [276, 277]. Although this global repression was already described decades ago, its biological significance remained unclear. Subsequent studies suggested that, while cap-dependent translation

30

is globally repressed, a few transcripts can still be translated through non-canonical translation initiation mediated by IRES [277-280]. However, a recent study showed that CDK1 phosphorylates the eukaryotic initiation factor 4E-binding protein (4E-BP1), releasing eIF4E and sustaining cap-dependent translation during mitosis [281, 282]. This observation together with others indicating that commonly used mitotic synchronization compounds like nocodazole strongly repress protein synthesis [283], has created controversy regarding whether a switch between cap-dependent and cap-independent translation initiation actually occurs during mitosis. Ribosome profiling studies, using less aggressive synchronization methods, suggest that global repression of translation is lower than previously thought, estimated to be around 30%. In addition, approximately 200 mRNAs appear to undergo mitosis-specific regulation of their translation [284]. Importantly, recent single-cell translation analysis showed that protein synthesis is slightly increased during early mitosis and only decreases during late mitosis (Figure 9), a process controlled by CDK1-mediated phosphorylation of 4E-BP1 [285]. Altogether, these findings demonstrate that cap-dependent translation is maintained, at least partially, during mitosis. However, further research efforts are needed to fully comprehend the regulation of translation during mitosis.
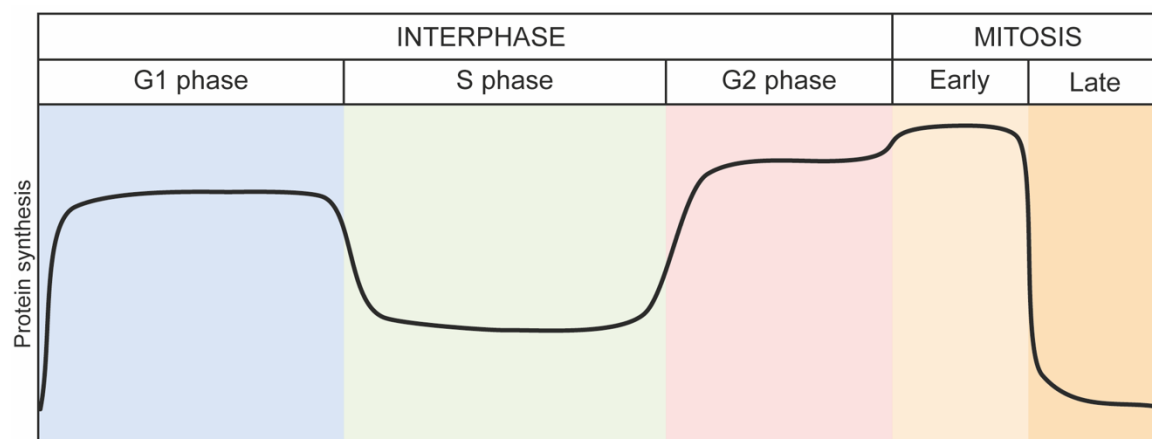
Figure 9. *Regulation of protein synthesis rates along cell cycle. Protein synthesis is high during G1, but decrease during S phase. Then, protein synthesis rates increase again during G2. Recent studies indicate that protein synthesis rates increase even more during early mitosis, but are strongly repressed during late stages of mitotic cell division.*

CDK1 has emerged as a key regulator of protein synthesis, further confirming the connection between protein synthesis regulation and cell cycle progression. In addition to 4E-BP1, CDK1 has been found to phosphorylate other regulators of protein synthesis during mitosis including S6 kinase 1(S6K1) [286], the protein elongation factor-1 (EF-1) [287], eEF2K [288], eIF4GI [289] and the non-canonical translation initiation factor DENR [290]. Interestingly, CDK1 has recently been implicated in the regulation of translation through the phosphorylation of the 5' terminal oligopyrimidine tract (5'TOP) binding protein LARP1 in a cell cycle-independent manner. This suggests that CDK1 adjust the protein synthesis to the overall proliferation rates rather than to a

specific phase of the cell cycle [291]. The phosphorylation of LARP1 by CDK1 significantly enhances the translation of 5'TOP mRNAs, which includes most RPs, potentially influencing in protein synthesis by promoting ribosome biogenesis [291]. Moreover, CDK1 has also been shown to phosphorylate the ribosomal protein uL11, which modulates the translation of specific transcripts [292]. Therefore, CDK1 represents one of the mechanisms by which cells coordinate cell cycle progression and protein synthesis. However, further research is required to fully comprehend how CDK1 precisely controls mitotic and extra-mitotic protein synthesis.

Cell cycle regulation is not limited to protein synthesis; it also involves protein degradation, as specific proteins need to be expressed during each phase of the cell cycle and then either degraded or inhibited. In mammals, the ubiquitination and proteasomal degradation of cell cycle regulators is mainly driven by two families of E3 ubiquitin ligases: anaphase-promoting complex/cyclosome and Skp1-Cul1-F-box protein complex (extensively reviewed in [293, 294].

4.4. Key role of cell cycle alterations on cancer progression

Cancer is characterized by abnormal cell proliferation caused by uncontrolled progression of the cell cycle. Molecular analysis of tumors has revealed frequent alterations of the cell cycle regulators (Table 2). These alterations often allow cancer cells to enter cell cycle without mitogenic signals and to ignore anti-mitogenic signals [295]. Tumorigenic alterations can occur at different levels, including mutations and amplifications in mitogenic signaling pathway ligands and receptors, such as HER2; alterations in downstream signaling pathways, such as RAS-RAF-MAPK or PI3K-AKT pathways; as well as in cell cycle regulators themselves, such as gene amplification of cyclin D or CDK4, and inactivation of CDK inhibitors, such as p16 or p27 [295-300]. Aberrant signaling resulting from these alterations frequently deregulate CDK/cyclin complexes, leading to continuous proliferation or unscheduled re-entry into the cell cycle. Moreover, the cell cycle is surveilled by checkpoints that detect potential errors in DNA replication or chromosome segregation. Identification of these alterations triggers different signaling cascades that ultimately results in CDK inhibition and cell cycle arrest [262]. Defective checkpoints contribute to genomic and chromosomal instability which, if not repaired, lead to the accumulation of mutations and drives tumor evolution [262, 296].

Increased expression of cyclin D1 is one of the most common alterations observed in human cancer, occurring in 60% of breast cancers, 40% of colorectal cancers and 20% of prostate cancers, among others [301].This suggests that CDK4 and CDK6 kinases are hyperactive in many human tumors [259, 301]. Apart from cyclin D, deregulation of CDK4 and CDK6 themselves has also been implicated in several cancers. These CDKs are overexpressed in tumors such as sarcoma, glioma,

breast, lymphoma, and melanoma [254, 259]. Moreover, a mutation of CDK4 that prevents binding of INK4 CDK inhibitors can be found in a significant amount of melanoma patients [302].

The S phase kinase, CDK2, is not frequently found mutated or amplified in cancer. On the contrary, its associated cyclin, cyclin E is often overexpressed in human tumors including breast, colon, bladder, liver, prostate, skin, among others, and is associated with a poor prognosis [300, 303]. Interestingly, several tumors express a proteolytically cleavage cyclin E, which has a low molecular weight (LMW) [304]. This LMW-cyclin E binds with increased affinity to CDK2, hyperactivating the complex and making it resistant to p21 and p27 inhibition [305, 306].

Table 2. Main alterations of cell cycle regulators in cancer. The type of alterations, the pathological implication and the type of cancers primarily affected are indicated. UCS: uterine carcinosarcoma, CHOL: cholangiocarcinoma, PDAC: pancreatic ductal adenocarcinoma, GC: gastric cancer, CRC: colorectal cancer, BRCA: breast cancer, GBM: glioblastoma, T-LBL/ALL: T-cell lymphoblastic lymphoma and T-cell acute lymphoblastic leukemia, NK/TL: natural killer T-cell lymphoma, SMZL: splenic marginal zone lymphoma, LIHC: liver hepatocellular carcinoma, LUAD: lung adenocarcinoma, PRAD: prostate adenocarcinoma, OC: ovarian cancer, EAC: esophageal adenocarcinoma , CC-EC: clear cell endometrial carcinoma, BLCA: bladder cancer, AML: acute myeloid leukemia, DLBCL: Diffuse large B-cell lymphoma, ESCA: esophageal carcinoma, HNSCC: head and neck squamous cell carcinoma, SCLC: small cell lung cancer, OS: osteosarcoma.

Cell cycle regulator	Alteration	Pathological implication	Main cancer types affected and frequency	Ref
CDK1	Amplification	Hyperactivation of CDK1	UCS (6%), CHOL (2%), PDAC (1%)	[307]
CDK2	Amplification	Hyperactivation of CDK2-cyclin E complex	GC (0.48%), CRC (0.22), BRCA (0.11%)	[308]
CDK4	Amplification	Hyperactivation of CDK4/6-cyclin D complex	GBM (50%), UCS (26%), BRCA (16%)	[259]
CDK6	Overexpression	Hyperactivation of CDK4/6-cyclin D complex	T-LBL/ALL (100%), NK/TL (90%), SMZL (13%)	[259]
Cyclin A	Overexpression	Hyperactivation of CDK1-cyclin A complex	T-ALL (84%), melanoma (47-74%), LIHC (78%), LUAD (80%)	[309]
Cyclin B1	Copy number alteration	Hyperactivation of CDK1-cyclin B complex	LUAD (30%), BRCA (21%), LIHC (9%)	[310]
Cyclin D	Amplification	Hyperactivation of CDK4/6-cyclin D complex	BRCA (50%), CRC (40%), PRAD (20%)	[311]
Cyclin E	Amplification	Hyperactivation of CDK2-cyclin E complex	OC (22%), EAC (18%), CC-EC (14%)	[312-314]
	Proteolytical cleavage	Expression of a proteolytically cleaved, low molecular weight cyclin E that binds with increased affinity to CDK2 and are resistant to p21 and p27	BRCA (50% ER+, 75% HER2+, 80% TNBC), GC (8-35%), CRC (58%)	[304-306, 315]
p15	Promoter hypermethylation	Reduced p15 expression leading to hyperactivation of CDK4/6-cyclin D complex	T-LBL/ALL (100%), Lymphoma (55%), GBM (35%)	[259]
p16	Deletion	Hyperactivation of CDK4/6-cyclin D complex	T-LBL/ALL (58%), BLCA (50%), GBM (35%)	[259]

Table 2 (Cont.). Main alterations of cell cycle regulators in cancer. The type of alterations, the pathological implication and the type of cancers primarily affected are indicated. UCS: uterine carcinosarcoma, CHOL: cholangiocarcinoma, PDAC: pancreatic ductal adenocarcinoma, GC: gastric cancer, CRC: colorectal cancer, BRCA: breast cancer, GBM: glioblastoma, T-LBL/ALL: T-cell lymphoblastic lymphoma and T-cell acute lymphoblastic leukemia, NK/TL: natural killer T-cell lymphoma, SMZL: splenic marginal zone lymphoma, LIHC: liver hepatocellular carcinoma, LUAD: lung adenocarcinoma, PRAD: prostate adenocarcinoma, OC: ovarian cancer, EAC: esophageal adenocarcinoma , CC-EC: clear cell endometrial carcinoma, BLCA: bladder cancer, AML: acute myeloid leukemia, DLBCL: Diffuse large B-cell lymphoma, ESCA: esophageal carcinoma, HNSCC: head and neck squamous cell carcinoma, SCLC: small cell lung cancer, OS: osteosarcoma.

Cell cycle regulator	Alteration	Pathological implication	Main cancer types affected and frequency	Ref
p16	Deletion	Hyperactivation of CDK4/6-cyclin D complex	T-LBL/ALL (58%), BLCA (50%), GBM (35%)	[259]
p21	Mutation	Uncontrolled cell cycle progression and increased metastasis	BLCA (14%),	[316]
	Overexpression	Overexpression correlates with worse prognosis	Glioma (50%), AML (17%)	[317, 318]
p27	Deletion	Hyperactivation of CDK/cyclin complexes	PRAD (3.85%), DLBCL (2.1%), LUAD (1.4%)	[319, 320]
	Mutation	Hyperactivation of CDK/cyclin complexes	BRCA (60%)	[321]
p53	Mutation	Uncontrolled cell cycle progression, increased proliferation, cell survival and invasion	OC (47.8%), CRC (43.2%), ESCA (43.1%), HNSCC (40.6%)	[322]
RB1	Deletion	Uncontrolled cell cycle progression and increased proliferation	SCLC (90%), OS (20-40%), PRAD (30%)	[311, 323]

In addition, expression of p21 and p27, which inhibit CDK2, is frequently downregulated during tumorigenesis [297, 300]. All this data suggests that CDK2 activity might play an important role in cancer. However, experimental data has shown no role of CDK2 in driving tumorigenesis in those tumors lacking p21 and p27 [297]. Since these two CDK inhibitors can also act on CDK1, it is possible that CDK1 might be responsible for tumor development in these malignancies. CDK1 has been found to be overexpressed in various cancer types including ovarian cancer, gastric cancer, colorectal cancer or liver cancer, among others [324-326]. Its regulatory cyclin, cyclin B1, has been found to be constitutively expressed in tumor cells rather than cell cycle-regulated [327]. Thus, this cyclin is also overexpressed in several cancers and associated with a poor prognosis [296, 327].

Another central step in cancer development is *RB1* loss or inactivation, which usually occurs due to chromosome alterations causing deletions or epigenetic inactivation [328]. This alterations are particularly common in small-cell lung cancer, glioma, esophageal cancer and liver tumors [329]. Moreover, inherited mutations in *RB1* are well-known to predispose for retinoblastoma and osteosarcoma [330].

Taken together, the cell cycle is extensively deregulated in cancer. The crucial role of CDKs as well as other kinases such as checkpoint kinases or CDK regulatory kinases in controlling the cell cycle

provides a broad range of possibilities for the development of therapeutic strategies based on the druggability of this kind of molecules.

4.5. Targeting the cell cycle as cancer treatment

Due to the crucial role of cell cycle alterations in driving cancer progression, significant research efforts have been devoted to finding therapeutic options capable of inhibiting cancer cell division. The reliance of cancer cells on cell cycle regulatory pathways provides an opportunity to target processes that are essential for cancer cells but not healthy cells.

Since the main drivers of cell cycle progression are CDKs, these kinases have become attractive targets for new therapeutic strategies. Various CDK inhibitors have been developed, and few have reached clinical trials with satisfactory results. CDK4/6 inhibitors such as ribociclib, abemaciclib and palbociclib are the best example of this phenomenon. These drugs have demonstrated significant clinical benefit for hormone-receptor positive metastatic breast cancer, leading to FDA approval for this disease [331, 332]. Clinical trials testing these inhibitors in multiple solid tumors are currently underway [254, 259, 333]. However, a major challenge faced by CDK4/6 inhibitors is the development of resistance in a significant percentage of patients [334]. Therefore, one of the main objectives now is to discover the mechanisms that lead to this resistance. This knowledge could facilitate the improvement of inhibitor designs and the development of combination therapies that may delay or overcome resistance [254].

In addition to CDK4/6 inhibitors, CDK7 inhibitors have shown promising results in several studies. CDK7 is a CDK-activating kinase able to phosphorylate CDK1, CDK2, CDK4 and CDK6. Importantly, while cancer cells have shown to be sensitive to CDK7, healthy cells remain insensitive, suggesting that CDK7 inhibitors might be well tolerated by patients [335, 336].

Other strategies have been explored for drug discovery, including preventing the interaction between CDK and cyclins using peptidomimetics or restoring the function of CDK inhibitors by gene therapy, peptidomimetics, and by preventing their degradation [337, 338]. In addition, in cases where the expression of CDK inhibitors is epigenetically silenced, the use of demethylating agents such as 5'-deoxyazacytidine (5'-dAZA) could prevent promoter methylation. This drug has already demonstrated antitumor activity in leukemia and other neoplasias [231, 232]. Further strategies involve preventing the degradation of CDK inhibitors by blocking their phosphorylation (which triggers degradation) or by using proteasomal inhibitors, although use of the latter entails an obvious lack of specificity. Lastly, techniques such as downregulation of cyclin expression by antisense oligos and stimulation of their phosphorylation to trigger degradation have also been explored but have not reached the clinic [339, 340].

Importantly, identifying the specific requirements of cell cycle regulators in both cancer and healthy cells is essential for the development of new drugs. Focusing on crucial aspects, such as the regulatory mechanisms of synthesis and proteolysis of essential cell cycle proteins, as well as their post-translational regulation, could be particularly intriguing.

5. Alterations in RNA modifications and cell cycle regulators in liver cancer

Liver cancer is a significant health concern, ranking as the third leading cause of cancer-related deaths in Spain and showing incidence rates that rise globally each year (SEOM, 2023). Hepatocellular carcinoma (LIHC) is the most prevalent form of liver cancer, accounting for approximately 90% of the cases, while other types such as cholangiocarcinoma (~10%) and angiosarcoma (~1%) are less common [341, 342].

LIHC is a highly complex disease influenced by numerous risk factors. Mayor risk factors include hepatitis B (HBV) and hepatitis C (HCV) virus infection, diabetes, obesity, alcoholic fatty liver disease (AFLD) and non-alcoholic fatty liver disease (NAFLD), smoking and various dietary exposures [341, 343]. Treatment options for LIHC include surgical resection, local ablation with radiofrequency, transcatheter arterial chemoembolization (TACE) or radioembolization. Notably, the tyrosine kinase inhibitor (TKI) Sorafenib was approved in 2007 as the first systemic treatment against LIHC, marking a significant turning point in the treatment of this disease [344]. However, only a small percentage of patients are eligible for surgical removal and almost all of the patients treated with Sorafenib or other single agents develop drug resistance within a few months [341, 343]. Consequently, both surgical interventions and systemic treatments have limited effectiveness in significantly enhancing patient outcomes, underscoring the critical need to identify new targets and strategies for liver cancer treatment.

LIHC is normally initiated as a hepatic injury involving inflammation that leads to necrosis and subsequent regeneration. Then, this chronic liver disease typically progresses through stages of fibrosis, cirrhosis and, eventually, results in hepatocellular carcinoma [341, 345]. Sequential accumulation of genetic and epigenetic alterations has been shown to drive the malignant transformation of hepatocytes in LIHC. The most common alterations include: overexpression of telomerase reverse transcriptase gene (*TERT*) [346, 347]; *CTNNB1*, which encodes for ß-catenin, a critical effector of the Wnt pathway [348]; the hypermethylation of *TSPYL5* and the chr.8q loss [347, 349]. Moreover, mutations in *TP53*, *AXIN1* and other epigenetic regulators such as *BAP1*, *ARID1A/B* and *ARID2* also play key roles in LIHC carcinogenesis [346]. In fact, epigenetic factors have emerged as key contributors to the transition from normal liver to cirrhotic tissues and ultimately LIHC [349, 350].

While the role of genetic and epigenetic alterations is well-studied, the role of epitranscriptomic marks in LIHC pathogenesis is much less understood. It has been reported that total m^{6}A levels are lower in LIHC compared to adjacent tissues, and increasing evidence suggest that m^{6}A writers, erasers and reader can regulate LIHC development, progression and metastasis [351]. Moreover, *in silico* studies indicate that m^{5}C regulators are frequently altered in LIHC and correlated with patient prognosis and stage [210]. m^{5}C levels have been found to be upregulated in tumor tissues compared to normal tissues [200]. Accordingly, NSUN2 has been reported to be upregulated in LIHC, influencing the sensitivity to Sorafenib [200], and promoting tumor progression by increasing the expression of the lncRNA H19 and stabilizing *FZR1* mRNA and other mRNAs related to the Ras signaling pathway [178, 200].

Alterations in rRNA methylation have been less explored in LIHC, and most studies have been focused on the role of Ψ. Loss of snoRNA H/ACA box 24 (SNORA24)-guided Ψ has been associated to increased translation errors and stop codon read-through, correlating with poor prognosis [352]. On the other hand, upregulation of DCK1 has been used as a marker of increased proliferative potential of LIHC and unfavorable patient outcomes [155], suggesting that Ψ and its regulators could serve as diagnostic markers and therapeutic targets. In fact, Ψ levels have been found upregulated in serum from LIHC patients, suggesting its potential use as an accessible diagnostic method [353, 354].

Direct alterations in the cell cycle are also prevalent in LIHC, especially in the Rb pathway, which is altered in more than two thirds of LIHC [355]. Loss of *RB* expression is found in around 50% of LIHC tumors, but this protein is also frequently found mutated or truncated [355, 356]. Moreover, LIHC often exhibits loss of expression of p16 and p14 due to hypermethylation of the CpG islands around their shared promoter [357, 358]. Interestingly, a correlation between HBV infection and DNMT1 and DNMT3A upregulation has been identified, leading to hypermethylation of p16 promoter [359]. This might contribute to the promoter hypermethylation observed in early stages of liver dysplasia and chronic hepatitis associated with HBV infection [360-362]. *CCDN1*, which encodes for Cyclin D1, is also amplified in 11-20% of LIHC cases [363] and correlates with poor differentiation and aggressiveness [364].

These cell cycle alterations, along with many others, suggest that cell cycle-based therapies could be considered for LIHC treatment. Mouse models have shown that Cdk1 expression loss prevents liver cancer development by halting cell division without affecting liver function [365]. However, treatments with CDK1 inhibitors would need to be administrated specifically to the liver due to their high toxicity to highly proliferative cells. Normal hepatocytes in adult liver, however, remain in a quiescent state, where CDK1 is not expressed [366]. Other CDK inhibitors, such as CDK4/6 inhibitors, have demonstrated to halt tumor proliferation in mouse models [367, 368], and are being

tested in phase 2 clinical trials in patients with Sorafenib intolerance (Clinical trial NCT01356628). Although cell cycle-based therapies hold promise for LIHC treatment, the potential of hepatocytes to enter quiescence and not divide could lead to the creation of a dormant pool of cancer cells, that can later lead to relapses [366]. The use of combination therapies may help to overcome this challenge and enhance the efficacy of LIHC treatments. Therefore, the discovery of new targets remains essential to advance on LIHC treatment strategies.

6. Alterations in RNA modifications and cell cycle regulators in prostate cancer

Prostate adnocarcinoma (PRAD) is the second most diagnosed cancer in men globally and a leading cause of male cancer-associated deaths (GLOBOCAN 2020). Age represents the primary risk factor for the development of PRAD development, as higher incidence and mortality are observed in elderly men above 65 years old [369, 370]. Other risk factors include African ancestry, a positive family history, obesity, and Lynch disease [369-371].

The main treatments for patients showing low-grade, localized disease include active monitoring, total or partial prostatectomy, cryotherapy and radiotherapy, while androgen deprivation therapy (ADT) is the first option for patients with advanced localized disease [370, 372]. ADT relies in the strong dependency of PRAD on testosterone and usually produces an initial favorable response [373]. However, prolonged exposures to ADT often results in the development of resistance due to genomic mutations in androgen receptor (*AR*) gene, leading to castration-resistant prostate cancer (CRPC) [374, 375]. Moreover, CRPC can further progress to metastatic CRCP (mCRPC), characterized by seminal vesicle invasion followed by metastasis, especially to the bones [374, 376, 377]. mCRPC is characterized by its poor prognosis and limited therapeutic options, with Docetaxel being the standard treatment for years. However, improvements in patient survival following Docetaxel treatment remain very limited [378]. Recently, two second-generation ADT, enzalutamide and abiraterone, have been developed with promising results in mCRPC [379-381]. Nevertheless, more research efforts are still needed to improve the survival of patients with advanced prostate cancer.

Prostate tumors originate from abnormal luminal cell proliferation within the prostate gland ducts. This abnormal proliferation leads to the formation of a prostate intraepithelial neoplasia (PIN) which can progress to *in situ* adenocarcinoma, further evolving into invasive prostate cancer and eventually metastatic prostate cancer [382, 383]. Although PRAD is considered a tumor with low mutational burden, several genetic alterations have been associated to its development over the last decades. Genomic studies have revealed the increased tendency of prostate tumors to present genomic rearrangements, copy number variations and gene fusions [384, 385]. One of the most common genomic rearrangements found in PRAD is the fusion of the androgen-responsible

TMPRSS2 gene with members of the ETS transcription factor family such as *ERG*, *ETV1* and *ETV4* [385, 386]. Mutations and copy number alterations affecting *TP53*, *AR*, *RB1*, *BRCA2*, *ATM* and *PTEN/PIK3CA* pathway are also very common [371, 385, 387, 388]. While AR pathway alterations are usually low in untreated primary tumors, they dramatically increase in hormone-refractory PRAD, reaching a prevalence of over 50% of cases [385, 386]. Moreover, the key tumor suppressor *TP53* is found to be mutated or deleted also in approximately 50% of the PRAD patients [386]. The PTEN/PIK3CA/AKT/mTOR pathway plays a central role in prostate carcinogenesis and progression [388-390]. In fact, *PTEN* loss, which leads to the upregulation of AKT/mTOR signaling pathway supporting tumor growth [385, 391, 392], has been reported as an early event in PRAD tumorigenesis and correlates with progression to aggressive, castration resistant disease [384, 386]. Furthermore, alterations in cell cycle are also pivotal events during prostate carcinogenesis. In this regard, deletion or mutation of *RB1*, observed in 14% and 23% of PRAD, respectively, leads to activation of the E2F transcription factor, leading to uncontrolled cell cycle progression [385, 386]. Moreover, loss-of-function alterations in cell cycle related genes, especially in *CDKN1B* (p27) and *CDKN2A* (p16) genes are also frequently found in PRAD, further contributing to abnormal cell cycle progression [386, 393, 394].

Importantly, advances in high-throughput next-generation sequencing have unveiled a complex scenario in PRAD, wherein not only genetic alterations but also epigenetic changes, such as DNA methylation, play crucial roles in driving disease progression [395]. CpG island hypermethylation near the promoters of *GSTP1*, *PTEN*, *AR* or *CDKN2A* rank among the most common epigenetic alterations in PRAD, and lead to increased tumor proliferation, significantly contributing to carcinogenesis [396-398]. Intriguingly, studies indicate that epigenetic alterations are particularly enriched in mCRPC and hormone-refractory tumors, suggesting a crucial role for epigenetic regulation in malignant progression of PRAD [395].

Similarly, RNA methylation is also frequently altered in prostate cancer. In fact, increased expression of the rRNA methyltransferase NOP2 is considered a marker of poor prognosis in clinical practice, correlating with Gleason score, PSA levels and recurrence after radical prostatectomy [399, 400]. NOP2 is cell cycle-regulated and has been shown to play a role in nuclear activation associated with proliferation [399]. *DCK1* is also overexpressed in PRAD [157] and elevated rRNA Ψ levels have been found in prostate tumors compared to adjacent tissues as well as in prostate cancer cell lines compared to prostate epithelial cells [401]. DCK1 upregulation has been linked to proliferation and modulation of telomerase activity [402]. Furthermore, Ψ levels have been found increased in urine of PRAD patients, suggesting its potential as a novel predictive biomarker together with PSA levels in serum [403]. Moreover, a recent study has uncovered a methyltransferase-independent role of EZH2, a histone lysine methyltransferase, that relies in its

direct interaction with fibrillarin. This novel interaction results in increased 2'-O-me levels in rRNA and enhanced protein translation [404]. These findings indicate a role for rRNA modifications in PRAD development and progression. However, further research is needed to explore the function of other modifications to gain a comprehensive understanding of the role of rRNA modifications and ribosomal function in this type of cancer. Importantly, not only rRNA modifications but also other modifications such as those occurring in tRNAs or mRNAs have been found altered in prostate cancer and are extensively reviewed in [405]. Altogether, the epitranscriptome emerges as a novel and crucial layer of regulation in PRAD development, offering potential new diagnostic biomarkers and therapeutic targets.

Aim of the study

Aim of the study

Cytosine-5 methylation is a widespread epitranscriptomic mark primarily found in tRNAs and rRNAs, with less frequent occurrences in mRNAs, lncRNAs and vtRNAs. Extensive research has elucidated the critical roles of m^5C methylation on tRNAs, including its impact on tRNA stability, stem cell functions and stress response. However, our understanding of the roles of m^5C modification in rRNAs remain limited.

Ribosomes contain two m^5C residues decorating their 28S rRNA, in the large subunit. One of these residues is deposited by NOP2 at the peptidyl transferase center of the ribosome. NOP2 is a cell cycle-regulated methyltransferase that plays crucial roles in ribosome biogenesis and translation regulation. Moreover, NOP2 is highly overexpressed in many tumors, being considered a well-known marker of poor prognosis in clinical practice. The other m^5C residue in the 28S rRNA is deposited by the highly conserved enzyme NSUN5 at the subunit interface, and is known to impact protein synthesis and stress resistance in various model organisms. Furthermore, NSUN5 has recently been associated with several cancers and implicated in the regulation tumor cell proliferation. However, the mechanism underlaying its contribution to tumorigenesis remain largely unexplored.

Given the high degree of conservation and the functionally crucial location of NSUN5-mediated m^5C modification, we hypothesize that it contributes to the regulation of key cellular processes, such as the cell cycle and proliferation, by modulating ribosomal function. To test this hypothesis, we propose the following specific objectives:

1. Investigate the impact of NSUN5-mediated m^5C rRNA methylation on ribosome biogenesis and the control of protein synthesis.
2. Explore the upstream factors that modulate dynamic RNA m^5C methylation changes.
3. Assess NSUN5 expression patterns across various cancer types.
4. Determine the tumorigenic potential of NSUN5 in tumor cells both *in vivo* and *in vitro*.

Results

Results

Generation of constitutive NSUN5-silenced cells

Ribosomal RNA m^{5}C methylation is the most conserved form of m^{5}C methylation across species [168]. While extensive research has been conducted on the m^{5}C methylation deposited by NOP2 in the peptidyl transferase center [89, 163, 204, 205, 209, 215, 269], there is considerably less knowledge regarding the function of the m^{5}C deposited by NSUN5 at the subunit interface. To investigate the role of NSUN5, we silenced *NSUN5* in a human prostate cancer cell line. With that aim, lentiviral constructs (pLKO.1) were used to generate cells stably and constitutively expressing shRNAs targeting *NSUN5* (*NSUN5*-knocked down or *NSUN5*-KD cells). These shRNAs (herein referred to as sh1 and sh2) targeting the coding region of *NSUN5* were selected from Sigma MISSION shRNA library, as well as a scramble shRNA (scr), that does not target any coding or untranslated region, which was used as control.
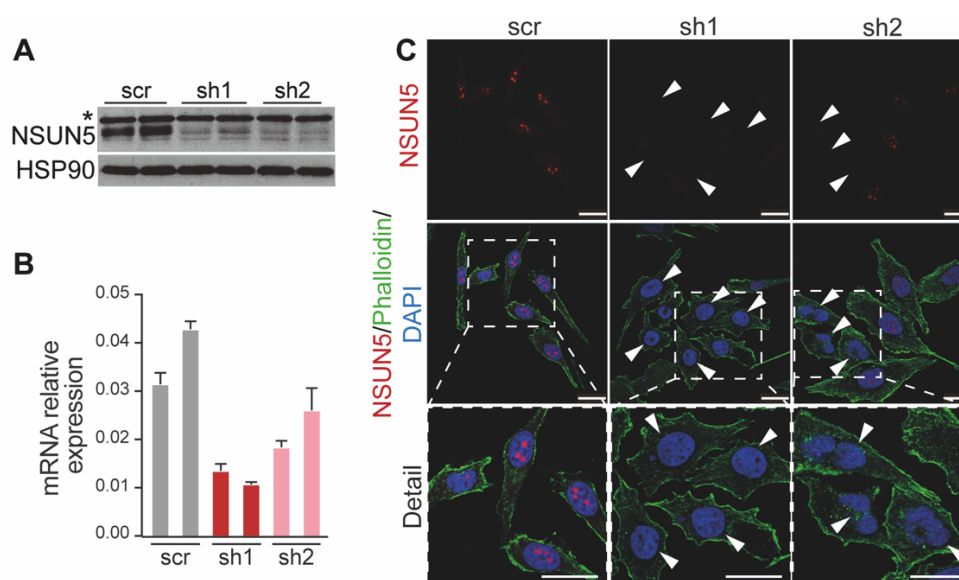
Figure 10. *Generation of cell lines stably and constitutively expressing shRNAs against NSUN5.* ***A*** *Western blot analysis of NSUN5 protein expression levels in NSUN5-KD (sh1 and sh2) and control (scr) cells. * Indicates an unspecific band.* ***B*** *Quantification of NSUN5 mRNA levels by RT-qPCR, normalized to the expression of GAPDH mRNA. Data shown as means ± SD, n = 2 replicates.* ***C*** *Immunofluorescence of NSUN5 (red) in NSUN5-KD and control cells. F-actin is stained in green using Alexa Fluor 488 Phalloidin and nuclei are counterstained with DAPI (blue). Arrowheads indicate loss of NSUN5 expression. Scale bar represents 25 μm.*

The expression of *NSUN5* in *NSUN5*-knocked down cells was assessed through RT-qPCR and Western blot analysis and compared to cell lines stably and constitutively expressing a scr shRNA (Figure 10A, B). Western blot analysis clearly demonstrated a significant reduction in NSUN5 protein expression in both shRNAs-expressing cell lines (Figure 10A). At the mRNA level, *NSUN5* expression was also notably depleted in both *NSUN5*-KD cell lines, with sh1 yielding more substantial results (Figure 10B). Cell immunofluorescence using an antibody against NSUN5

confirmed the previously reported location of NSUN5 in the nucleolus [181] and verified the successful silencing of NSUN5 protein, especially in the cells silenced with sh1 (Figure 10C).

NSUN5 is a known ribosomal RNA methyltransferase that specifically targets position C3782 of 28S rRNA [6, 181]. To further validate that NSUN5 depletion led to reduced levels of m^{5}C3782 methylation, the m^{5}C methylation status of rRNA was examined using bisulfite-PCR. Originally designed for the detection of m^{5}C methylation in DNA, this technique has been adapted for RNA studies [406]. This method relies on the distinct chemical reactivity of cytosine and 5-methylcytosine to sodium bisulfite treatment. Thus, through a series of chemical reactions, cytosine (C) is deaminated into uracil (U) (Figure 11A), resulting in a thymine (T) after reverse transcription and PCR amplification (Figure 11C). In contrast, m^{5}C is protected from this deamination (Figure 11B), maintaining its identity as cytosine after reverse transcription and PCR amplification (Figure 11C). These differences can subsequently be detected through sequencing.

Bisulfite-PCR analysis of *NSUN5*-KD cells using Methylamp RNA bisulfite conversion kit (Epigenetek) revealed only a mild reduction of approximately 20% in the methylation of position C3782 in cells silenced with sh1 (Figure 11D, E). Conversely, cells silenced using sh2 showed no discernible differences in methylation at position C3782 compared to the scramble control (Figure 11E), possibly due to the lower silencing efficiency of sh2 in silencing *NSUN5*, to the limited resolution of bisulfite-PCR or to technical limitations of the detection method used.

Bisulfite-PCR presents several limitations that could influence on the resolution of the analysis. The analysis of cytosine methylation using this method require high C-to-U conversion rates (>95%). Moreover, bisulfite conversion only affects single-stranded RNA [407]. Thus, conversion of highly structured RNA molecules, such as rRNA, is only achieved after prolonged incubations with sodium bisulfite at high temperatures. These harsh conditions promote the degradation of the RNA molecules, limiting the resolution of the analysis. Furthermore, C3782 is located in a highly structured area, the helix H70 of the domain IV of 28S rRNA [6, 181]. This area is constituted by multiple stem loops, which could protect from the deamination by sodium bisulfite treatment even under aggressive denaturation conditions. In fact, several cytosines are observed after deamination, especially in samples from cell silenced with sh2, indicating uncomplete deamination of the sequences. m^{5}C methylation detection on rRNA is known to be intricate, as, for instance, position m^{5}C2982 in *C. elegans* has been reported to be refractory to sodium bisulfite treatment, possibly due to the rRNA secondary structure [136]. Moreover, the querying of a reduced number of clones also limits the resolution of bisulfite-PCR and the conclusions that can be drawn from the analysis. All these limitations might explain why *NSUN5*-KD cells exhibit high levels of methylation despite presenting low levels of NSUN5 protein. Other approaches such as quantitative HPLC could allow a better analysis of the real changes upon *NSUN5* depletion.
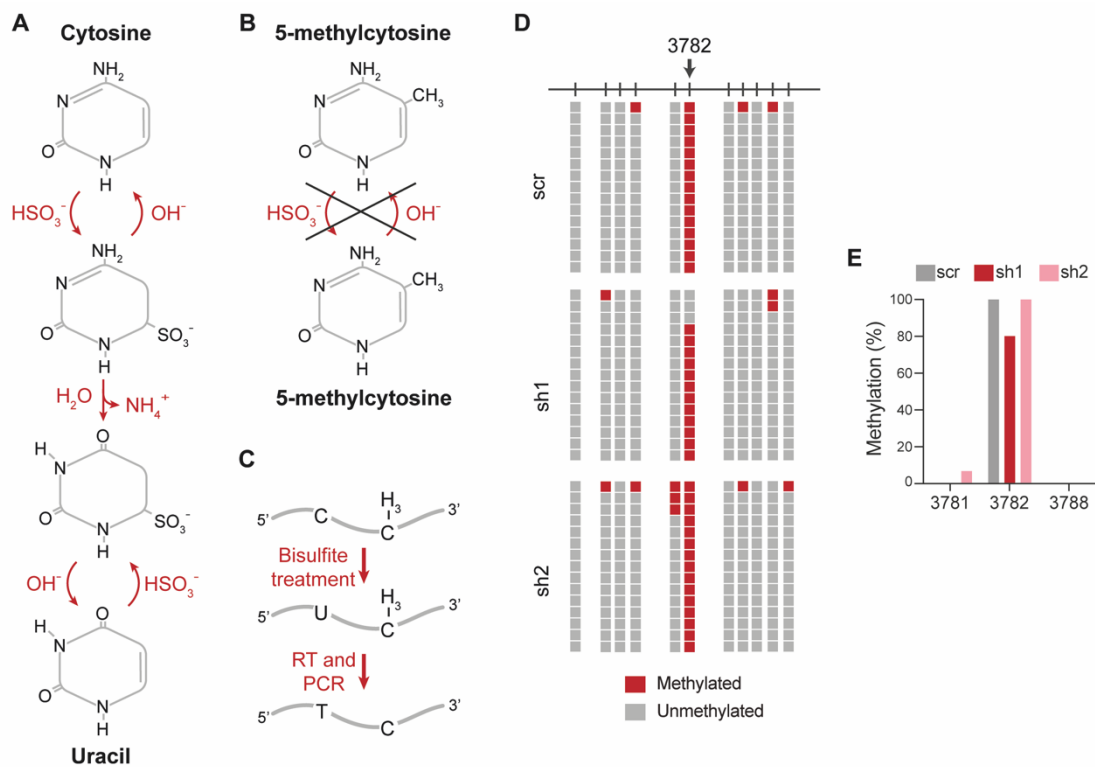
Figure 11. m^5C3782 *methylation status analysis after NSUN5 depletion.* ***A, B*** *Schematic representation of the bisulfite-induced chemical deamination of cytosines. Cytosine is sulfonated into cytosinesulfonate, deaminated into uracilsulfonate and desulfonated into uracil (**A**), while 5-methylcytosine is protected from the initial sulfonation (**B**). **C** Schematic representation of the bisulfite-PCR workflow. After bisulfite treatment, C is converted into U, while m^5C remains as a C. After reverse transcription (RT) and PCR amplification, C is detected as a T by sequencing while m^5C is detected as C. **D** Result of the bisulfite-PCR of the 28S rRNA near C3782 position in NSUN5-silenced and control cells. Each row represents a single RNA molecule, while columns represent cytosines. C3782 is marked with an arrow. Methylated and unmethylated cytosines are represented as red and grey squares, respectively. **E** Percentage of methylation in C3782 and neighboring cytosines.*

Generation of NSUN5-knocked out cells using CRISPR-Cas9

To further validate the function of NSUN5, we employed the CRISPR-Cas9 technology to generate *NSUN5*-knocked out (*NSUN5*-KO) cells. With this aim, 11 different single guide RNAs (sgRNAs) and more than 250 single-cell clones were generated and tested using different CRISPR-Cas9 systems and transfection/infection methods.

In a first approach, 7 sgRNAs targeting exons 2-4 of NSUN5 were designed using CRISPOR (http://crispor.tefor.net). These exons were selected as they are included in all transcript variants. Moreover, targeting of early exons is recommended to increase the chances of generating and early termination codon and the elimination of the mRNA by nonsense-mediated decay [408]. These guides were cloned into pLentiCRISPR-v2 plasmid and delivered to the cells by lentiviral infection. Cell population after selection of the infected cells showed almost no reduction of NSUN5 expression by RT-qPCR or Western blot analysis (data not shown). Despite not seeing significative

differences in NSUN5 expression in the whole cell population, single-cell clones were seeded and tested, but any *NSUN5*-KO clone was observed (data not shown).

In a second approach, NSUN5 was targeted using a commercial plasmid containing a Cas9 nickase mutant (D10A) and two sgRNAs specifically targeting *NSUN5* (sc-407812-NIC, Santa Cruz Biotechnology). Use of this system produces a specific double nicking of the *NSUN5* gene, which simulates a double-strand break, obtaining high cleavage specificity while lowering the number of off-targets [409]. However, while this method yielded clones with very low expression of NSUN5, no changes in rRNA methylations were observed, suggesting that active NSUN5 protein was still present in the cell (data not shown).

Finally, we opted for direct electroporation of the CRISPR-Cas9 ribonucleoprotein (RNP) complex [410]. As targeting early exons of NSUN5 gene had been unsuccessful in previous approached, in this case be targeted exon 7 and 8, which constitute the catalytic pocket of NSUN5, in order to obtain, at least, cells expressing a catalytic-incompetent NSUN5. For that, two sgRNAs, denoted in this work as sg1 and sg2, which target exon 7 and exon 8 of *NSUN5* gene, respectively, were designed using CRISPOR (Figure 12A). sgRNAs were 2'-O-methyl-3'-phosphorothioate-modified at the 5' and 3' ends to prevent degradation by cellular RNases. sgRNAs were incubated *in vitro* with a high-fidelity Cas9 mutant protein (Alt-R S.p. HiFi Cas9 v3 nuclease, IDT) to constitute the RNP complex. RNP complex was then electroporated into the cells.
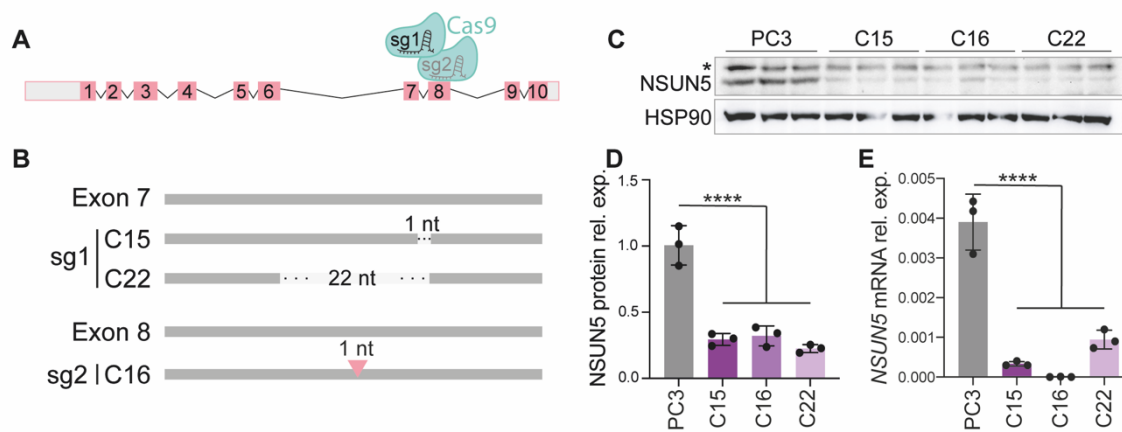

*Figure 12. Generation of NSUN5-KO cell lines using CRISPR-Cas9 technology. A Schematic representation of NSUN5 gene, illustrating the exons (boxes) and introns (lines). sgRNAs targeting their corresponding exons are indicated. B Schematic representation of the genetic alterations identified in the NSUN5-KO clones. DNA is depicted as grey lines, deletions as light grey lines with dots and insertions as pink triangles. Number of nucleotides deleted and inserted is indicated. C Western blot analysis of the NSUN5-KO clones and PC3 parental cell line assessing NSUN5 expression. * Indicates an unspecific band. D Western blot densitometry quantification. Densitometry values of the NSUN5 band were normalized to the densitometry of HSP90. E Quantification of NSUN5 mRNA expression by qPCR. NSUN5 mRNA expression was normalized to the expression of GAPDH mRNA. Data is represented as means ± SD, n = 3 replicates. Statistical analysis was performed using one-way ANOVA (**** p < 0.0001).*

After single-cell seeding, clones with genomic alterations in the targeted sequence were selected by PCR amplification followed by digestion with restriction enzymes, as sgRNAs were designed to disrupt the recognition site of different restriction enzymes to facilitate screening. Finally, only three positive clones were observed, two of which were generated using sg1, and one employing sg2. The genomic alterations in these clones were assessed by Sanger sequencing of genomic DNA sequences spanning the sgRNA-targeted regions. Clone 15 (C15) exhibited a deletion of 1 nucleotide in exon 7, leading to a disruption of the reading frame and the appearance of an early termination codon in exon 8 (Figure 12B). Meanwhile, clone 22 (C22) suffered a 22 nt-long deletion in exon 7, which similarly resulted in the alteration of the reading frame (Figure 12B). On the other hand, clone 16 (C16) presented an insertion of a single nucleotide, also producing an early termination codon in the following exon (Figure 12B).

NSUN5 expression in these three clones was evaluated by Western blot analysis and RT-qPCR (Figure 12C-E). The Western blot analysis was performed using a polyclonal antibody that recognizes amino acids 133-210 of human NSUN5, while the amino acids targeted by our CRISPR approach were located between position 308 and 359. Thus, this antibody could allow the recognition of truncated NSUN5 proteins generated by the early termination codons. The Western blot results showed a significant reduction of NSUN5 protein expression across all clones, with clone 22 demonstrating the most substantial reduction when compared to the parental cell line (PC3) (Figure 12C, D). However, all clones retained some protein expression, possibly due to the targeting of exon 7 and 8, which reduces the knockout efficiency by diminishing the chances of the mRNA to suffer nonsense-mediated decay, thus allowing some expression of the protein. Similarly, mRNA expression levels were assessed by using primers that align before the targeted region in the CRISPR/Cas9 approach. In the RT-qPCR results, all clones exhibited a significant decrease in *NSUN5* mRNA levels compared to the control (Figure 12E). In this context, C16 displayed the most significant reduction among all clones, whereas C22 retained the highest levels of mRNA (approximately 25% of the levels observed in the parental cell line) (Figure 12E). This suggests that, as hypothesized previously, some mRNA is scaping from the nonsense-mediated mRNA decay.

Subsequently, a methylation analysis was performed to confirm total loss of the methylation in position C3782 upon *NSUN5* loss. Given the apparent low efficiency of the bisulfite-PCR method used in the case of the *NSUN5*-KD cells, in this case be decided to use other bisulfite kit (Epitect Bisulfite kit, Qiagen), that showed increased deamination efficiency, and to increase the time of the sodium bisulfite treatment. Surprisingly, we found that parental cell line exhibited lower levels of methylation when using this kit compared to those observed with Epigentek kit. Although this position has been largely thought to be 100% methylated, recent studies in mouse tissues suggest

that this modification can be substoichiometric [181]. Thus, the methylation results obtained in this case could represent a more physiological situation. However, the use of other methods such as HPLC or Oxford Nanopore Technology (ONT) sequencing could shed light into the real methylation levels bypassing the limitations inherent to the use of sodium bisulfite. In any case, bisulfite-PCR analysis revealed a complete loss of the methylation in C22 (Figure 13A, B). On the other hand, C16 retained a 10% of methylation. However, analysis of the surrounding cytosines suggested that this is a false positive caused by an uncomplete deamination of the RNA molecule (Figure 13A). Conversely, C15 exhibited no significant reduction of the m^{5}C methylation at C3782 compared to the parental cell line, suggesting that these cells still possess active NSUN5 protein (Figure 13A, B). It is possible that the insertion of single nucleotide occurring in C15 was insufficient to eliminate the catalytic activity of the enzyme, allowing the methylation of 28S rRNA.

Taken together, this data suggested that C16 and C22 would be suitable for further characterization of NSUN5 function.

Figure 13. *Methylation analysis of 28S rRNA of CRISPR clones and PC3 parental cell line. **A** Each row represents a single clone, while columns represent cytosines. C3782 is marked with an arrow. Methylated and unmethylated cytosines are represented as red and grey squares, respectively. **B** Percentage of methylation in C3782 and neighboring cytosines.*

NSUN5 loss does not alter ribosome biogenesis

It has been shown that rRNA modifications, along with the enzymes responsible of their deposition, play important roles in ribosome biogenesis [25, 85]. Ribosome biogenesis is initiated in the nucleolus, that is comprised of three distinct layers in which different steps of ribosome biogenesis take place. (Figure 14A, B). rRNA transcription initiates at fibrillar centers (FC), characterized by containing RNA pol I subunits such as RPA194. Then, ribosome biogenesis continues in dense fibrillar component (DFC), characterized by the presence of fibrillarin (FBL) as primary marker. The third layer, referred to as the granular component (GC), is characterized by the presence of Pes1 and nucleophosmin (NPM1), among other proteins. Importantly, when rRNA transcription is inhibited, for instance through actinomycin D treatment, the nucleolus undergoes a deep reorganization, leading to the formation on nucleolar caps, that are constituted by the FC and the DFC (Figure 14B). In order to visualize NSUN5 location and to further infer in which step of ribosome biogenesis it carries out its functions, PC3 cells were treated with actinomycin D. This treatment produced the characteristic reorganization of the nucleolus, resulting in the migration of FBL to nucleolar caps due to its location in the DFC (Figure 14C). In contrast, NSUN5 did not localize in the nucleolar caps, indicating its presence in the GC (Figure 14C). This location suggested that NSUN5 may be involved in later stages of ribosome biogenesis.

To further investigate the potential role of NSUN5 in ribosome biogenesis, a Northern blot analysis of total RNA from *NSUN5*-KD and control cells was performed (Figure 14D-F). The 28S/18S ratio remained consistently between 1.1 and 1.3 in all cases, indicating no significant alterations in the abundance of mature rRNAs (Figure 14E). rRNA processing intermediates were detected using a radiolabeled probes targeting ITS1 and ITS2 (Figure 14D and 14E, left panel). The ITS1 probe (blue line in Figure 14D and 14E) detected processing intermediates of SSU, including 34S, 30S, 21S and 18S-E, along with the polycistronic transcripts (47S/45S) (Figure 14D). The ITS2 probe (pink line in Figure 14D and 5E) was employed to detect intermediates of LSU, namely 32S and 12S, along with the polycistronic transcripts (Figure 14E). Quantification of these intermediates of both LSU and SSU revealed no significant accumulation or reduction of any species (Figure 14F). In summary, this data strongly suggested that NSUN5 does not play an essential role in ribosome biogenesis.
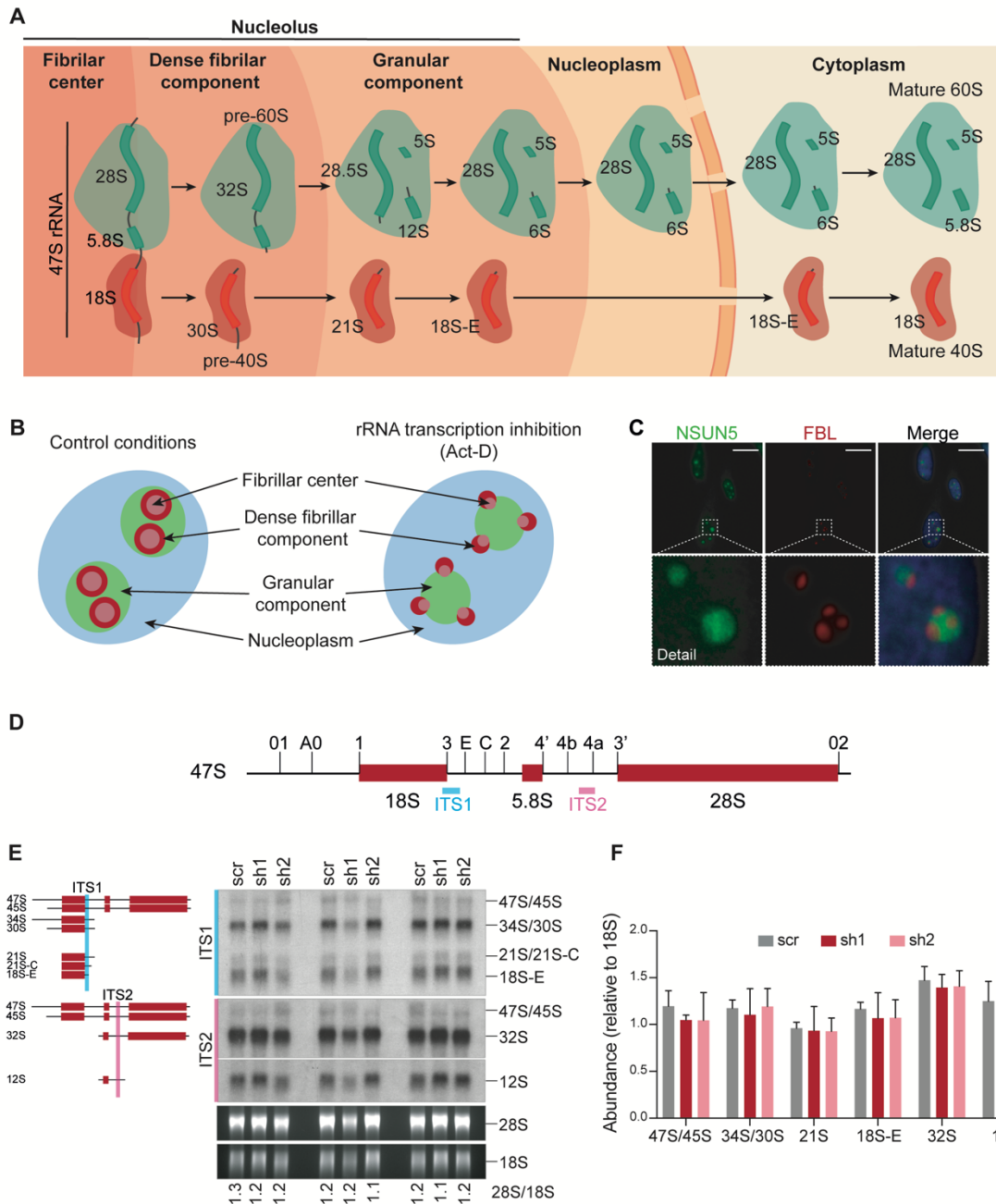
Figure 14. *Ribosome biogenesis is not affected in NSUN5-KD cells. **A** Schematic representation of the human ribosome biogenesis pathway. The names of the pre-rRNA species in each maturation step of the 60S (blue) and 40S (red) are indicated. Ribosome biogenesis starts with the transcription of the 47S pre-rRNA at the interface between the fibrillar center and the dense fibrillar component and continues as the pre-ribosomes travel to the granular component, the nucleoplasm and, eventually, the cytoplasm. Adapted from [411] **B** Schematic representation of the nucleolar structure of human cells under control conditions (left panel) and after rRNA transcription inhibition (right panel). In response to rRNA transcription inhibition, nucleolus suffer reorganization in which components of the fibrillar center and the dense fibrillar component aggregate forming the nucleolar caps. Nucleoplasm is represented in blue, granular component in green, dense fibrillar component in red and fibrillar centers in pink. **C** Immunofluorescence staining showing the location of NSUN5 (green) and FBL (red) upon rRNA transcription inhibition with actinomycin-D. DNA is counterstained with DAPI (blue). **D** Schematic representation of the 47S polycistronic transcript containing the sequence of the mature 18S, 5.8S and 28S, separated by the internal and external transcribed spacers. Vertical lines indicate the cleavage sites of 47S rRNA. Hybridization zones of the radiolabeled probes used for Northern blot analysis targeting the ITS1 (blue) and the ITS2 (pink) are indicated. **E** Northern blot analysis of NSUN5-KD and control cells. Left panel illustrates the rRNA processing intermediates detected. The upper part of the right panel shows the autoradiography using TIS1 and ITS2 probes, while the lower panel shows the mature rRNAs on an ethidium bromide-stained membrane. **F** Quantification of the pre-rRNA species detected in the Northern blot in (**E**). Data is represented as means ± SD, n = 3 replicates. Statistical analysis was performed using one-way ANOVA.*

54

To further confirm this observation, Northern blot analysis was also conducted using total RNA from *NSUN5*-KO clones (Figure 15). Similar to *NSUN5*-KD cells, rRNA processing intermediates were detected using ITS1 and ITS2 radiolabeled probes (indicated as blue and pink lines, respectively in Figure 15A). Quantification of the rRNA processing intermediates from both LSU and SSU showed no significant alteration of their abundance in C15 and C16 compared to PC3 parental cell line. However, minor differences were observed in the case of C22, which displayed lower levels of 21S, 18S-E and 12S than the control PC3 cells. Nevertheless, the 28S/18S ratio remained unchanged between *NSUN5*-KO clones and PC3 parental cell line, indicating that the loss of NSUN5 did not affect the abundance of mature rRNAs (Figure 15A).
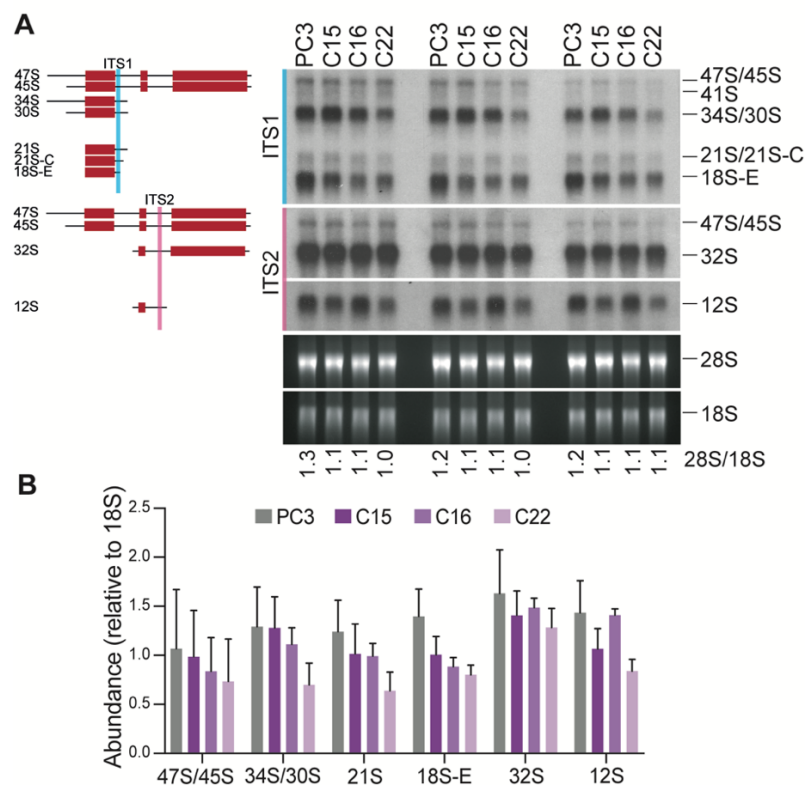
Figure 15. *Ribosome biogenesis in NSUN5-KO clones. **A** Northern blot analysis of NSUN5-KD and control cells. Left panel illustrates the rRNA processing intermediates detected. The upper part of the right panel shows the autoradiography using TIS1 and ITS2 probes, while the lower panel shows the mature rRNAs on an ethidium bromide-stained membrane. **B** Quantification of the pre-rRNA species detected in the Northern blot in (**A**). Data is represented as means ± SD, n = 3 replicates. Statistical analysis was performed using one-way ANOVA.*

Previous studies have suggested that *NSUN5* silencing might lead to a decrease in the abundance of 47S and 45S rRNA species in Northern blot analysis, indicating a potential defect in transcription of the primary transcript [412]. However, our Northern blot analysis did not reveal any alteration in the abundance of these species (Figure 14E, F and 15A, B). To rule out any potential impact of *NSUN5* depletion on the transcription of 47S rRNA, we quantified the number of transcription foci in *NSUN5*-KD and control cells, which served as a readout of active rDNA transcription (Figure 16A, B). Transcription foci were visualized through FBL immunofluorescence staining. Moreover,

co-staining using an NSUN5 antibody allowed to assess the correlation between NSUN5 expression and the number of transcription foci (Figure 16A). Although significance was achieved after the quantification of transcription foci, the low r value indicates no correlation, suggesting that NSUN5 depletion does not affect the capacity of cells to synthesize the 47S primary transcript (Figure 16B).

Moreover, the number of mature ribosomes was estimated through immunofluorescence using an antibody against 5.8S rRNA in *NSUN5*-KD and control cells (Figure 16C). Corrected total cell fluorescence (CTCF) of 5.8S rRNA in each individual cell was quantified using Fiji. CTCF is a metric that adjust the total fluorescence based on the cell size and background fluorescence levels in each cell [413]. The quantification results indicated a reduction in 5.8S rRNA staining in *NSUN5*-KD cells, suggesting that these cells might have lower number of mature ribosomes (Figure 16D).
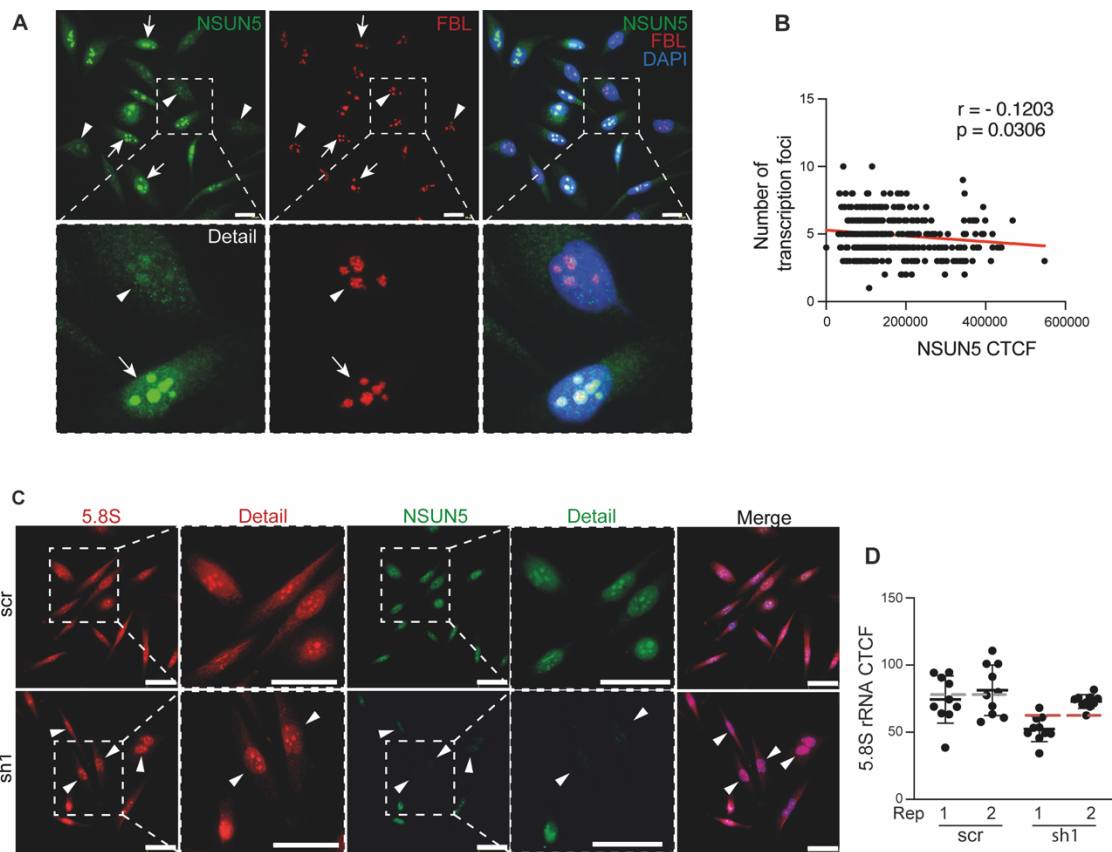

Figure 16. A *Immunofluorescence staining of NSUN5 (green) and FBL (red) in NSUN5-KD and control cells. Arrows indicate cells with high NSUN5 expression, while arrowheads mark cells with low NSUN5 expression. **B** Correlation analysis between NSUN5 expression and number of FBL foci. Statistical analysis was preformed using the Spearman correlation test. **C** Immunofluorescence staining of 5.8S rRNA (red) and NSUN5 (green) in NSUN5-KD and control cells. Nuclei are counterstained with DAPI (blue). Arrowheads indicate cell with low NSUN5 expression. **D** CTCF of 5.8S rRNA was measured using Fiji. The mean 5.8S rRNA CTCF of cells in 10 pictures from two independent replicates is represented. The mean of both replicates was calculated, and statistical analysis was performed using Student's t-test (*** p < 0.001).*

Loss of cytosine-5 methylation impacts ribosome structure

RNA modifications are well-known to participate in the folding and compaction of rRNA during ribosome biogenesis and in the maintenance of rRNA structure in mature ribosomes [29, 71]. Loss of Rcm1-mediated modification is suspected to impact the structure of yeast ribosomes, as it sensibilizes the cells to the antibiotic anisomycin [88]. Moreover, *in silico* simulations of the loss of m^{5}C3782 in human ribosomes predicted a conformational change affecting the P-site of the ribosome [6]. However, the structure of the ribosome upon loss of this methylation has not been experimentally evaluated yet.
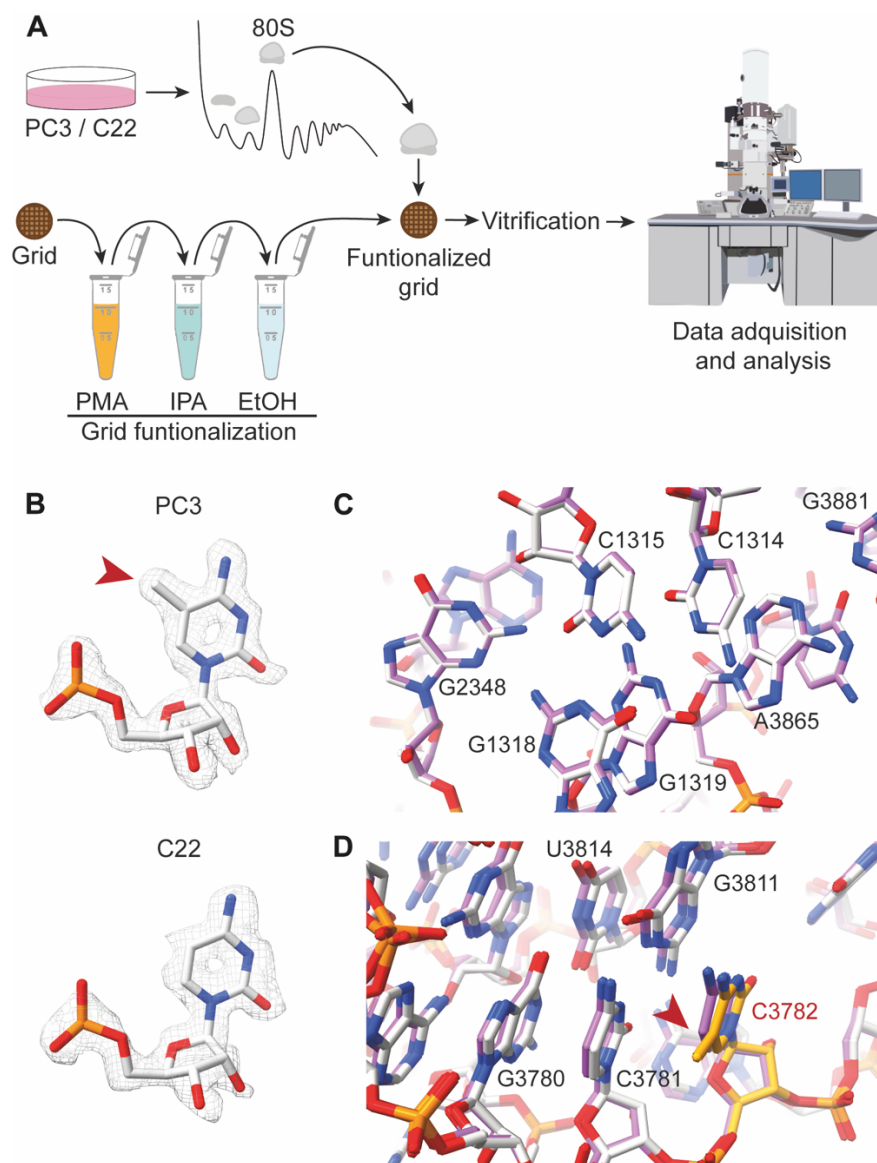
Figure 17. High-resolution structural analysis of human 80s ribosomes. A Schematic representation of the experimental workflow. PMA: 1-pyrenemethylamine, IPA: isopropanol, EtOH: Ethanol. B Visualization of cytosine 3782 of parental PC3 cells (upper panel) and NSUN5-KO C22 (lower panel). Grey mesh depicts the experimental map. Arrowhead indicates methyl residue. C Alignment of parental (white backbone) and NSUN5-KO (purple backbone) structures in the core of the 60S subunit. D Alignment of parental (white backbone) and NSUN5-KO (purple backbone) structures around residue C3782 (orange). Structures were refined in experimental cryo-EM maps of 60S subunits derived either from parental cells (2.3 Å resolution) or NSUN5-KO cells (2.2 Å resolution).

To determine whether the complete loss of m^5C3782 affects the ribosome structure, 80S ribosomes from *NSUN5*-KO C22 and parental PC3 cells were isolated using sucrose gradients and blotted into PMA-functionalized grids (Figure 17A). Micrographs were acquired by electron cryo-microscopy (Cryo-EM) at the Department of Biochemistry of Cambridge University (Cambridge, United Kingdom). Analysis of the collected datasets revealed very low number of 80S ribosomes in the *NSUN5*-KO samples (~10% of the particles) while in the parental cell line 80S represented most of the particles in the grids (~70% of the particles). This suggest that ribosomes lacking m^5C3782 are less stable under these experimental conditions. Given the low percentage of 80S ribosomes in the *NSUN5*-KO sample, the models in this study were generated from the 60S particles to increase resolution. Finally, experimental maps of 2.3 Å and 2.2 Å were obtained from parental and *NSUN5*-KO cell lines, respectively.

Close up images of the cytosine at position C3782 clearly showed a methyl group on carbon 5 of the cytosine in parental cell lines (Figure 17B, upper panel). Conversely, methyl group was not detected in *NSUN5*-KO cells (Figure 17B, lower panel), confirming the results obtained in the bisulfite analysis and demonstrating that these cells completely lack active NSUN5. Overlap of the refined structural models of parental and *NSUN5*-KO cells showed a good alignment of the models (Figure 17C). Interestingly, loss of the methylation produced a shift in the alignment in the area surrounding C3782 (Figure 17D). Although average mean square deviation remains to be calculated, this shift indicated that lack of NSUN5-mediated m^5C methylation leads to a structural alteration of the ribosome in the subunit interface, which could explain the decreased stability of non-methylated ribosomes.

In summary, our structural analysis suggested that loss of NSUN5-mediated m^5C methylation led to a structural rearrangement of the subunit interface potentially altering 80S stability. Whether this alteration can impact protein synthesis remains to be evaluated.

NSUN5 loss impairs global protein synthesis

Ribosomes play a pivotal role in protein synthesis, and any alterations in ribosome components or factors involved in ribosome biogenesis can lead to the formation of defective ribosomes, thereby impacting protein synthesis negatively. Accordingly, recent studies have shown reduced rates of protein synthesis following *NSUN5* loss [6, 181].

To investigate potential defects in protein synthesis rates upon *NSUN5* silencing in our model, we performed polysome profiling of *NSUN5*-KD and control cells. To capture a snapshot of the translation process, ribosome translocation was inhibited using cycloheximide. Cell lysates were resolved on 7-50% sucrose gradients, allowing the separation of free RNA and proteins, 40S and 60S subunits, 80S ribosomes or monosomes, and polysomes, which represent the actively
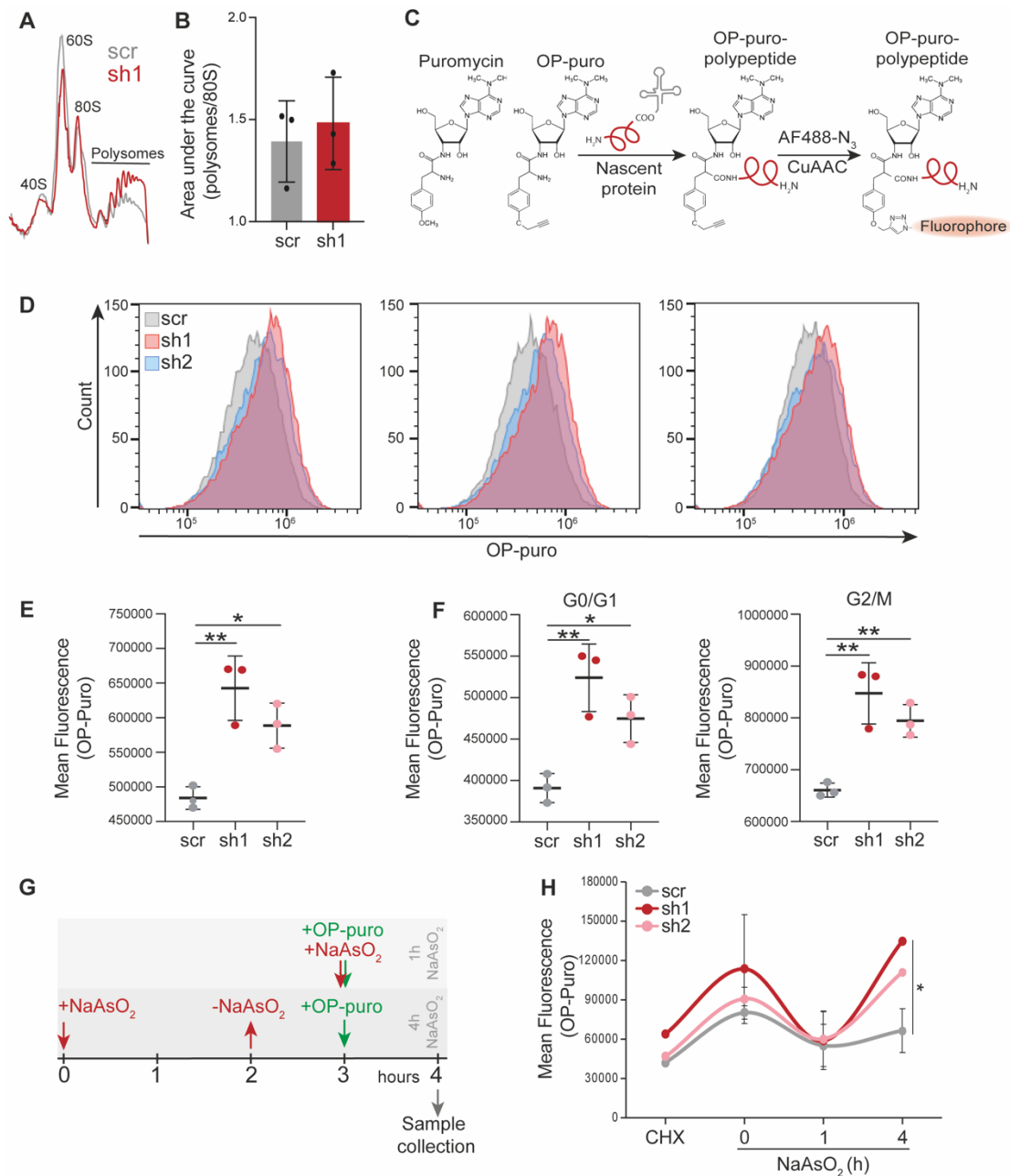
Figure 18. *Global protein synthesis in NSUN5-KD cells. **A** Polysome profiling analysis of NSUN5-KD cells (red) and scr cells (grey). Peaks corresponding to 40S and 60S subunit, monosomes (80S) and polysomes are indicated. **B** Quantification of the area under the curve of polysome fraction normalized to 80S peak. **C** Chemical structure of puromycin and its alkyne analog, O-propargyl puromycin (OP-puro), and schematic representation of Cu(I)-catalyzed azide-alkyne cycloaddition reaction. Op-puro is incorporated in nascent peptides due to its resemblance to the 3' end of aminoacylated tRNAs, resulting in irreversible premature termination of translation. The alkyne group of op-puro allows the binding of fluorescent groups or biotin groups via Cu(I)-catalyzed click chemistry. **D** OP-puro incorporation measured by flow cytometry. Cells debris were excluded using FSC-A/SSC-A representation, and single cells were selected using FSC-A/FSC-H representation. OP-puro fluorescence in single cells was represented as histogram. **E** Mean OP-puro fluorescence in single cells. Data is represented as means ± SD. n = 3. Statistical analysis was performed using Student's t-test (* p < 0.05, ** p < 0.01). **F** Mean fluorescence of OP-puro in each cell cycle phase. DNA content of cells was counterstained with propidium iodide, and cell cycle phases were manually gated. Statistical analysis was performed using Student's t-test (* p < 0.05, ** p < 0.01). **G** Schematic representation of the experimental workflow. Protein synthesis was measured under oxidative stress conditions. Oxidative stress was induced by exposing the cells to 200 μM of NaAsO$_2$ for up to 4 hours. For the 4-hour experimental point, NaAsO2 was applied for 2 hours and then washed out from the cells. Cells were allowed to incorporate OP-puro for 1 hour before collection. **H** Mean OP-puro fluorescence of single cells at each time point. Cycloheximide (CHX)-treated cells were used as a control of minimal OP-puro incorporation. Data is represented as means ± SD, n = 3 replicates. Statistical analysis was performed using one-way ANOVA (* p < 0.05).*

translating entities consisting of two or more ribosomes bound to an mRNA. Polysome profiles revealed a slight increase in the polysomal fraction in *NSUN5*-KD cells (Figure 18A). Quantification of the area under the curve of polysomes, normalized to the area of 80S peak, confirmed this slight increase, although it did not reach statistical significance (Figure 18B). This result suggest that silenced cells may unexpectedly have higher protein synthesis rates.

To further investigate this alteration in protein synthesis rates, the incorporation of O-propargyl-puromycin (OP-puro) was quantified in *NSUN5*-KD and control cells. OP-puro is an alkyne analog of puromycin, and similar to puromycin, it gets incorporated into the nascent polypeptide chain, leading to the premature termination of translation [414]. Additionally, its alkyne group allows the covalent binding of azide-containing molecules as fluorophores, facilitating its detection by microscopy or flow cytometry. Thus, its incorporation serves as a readout of protein synthesis rates (Figure 18C). Analysis of the OP-puro-fluorophore conjugate incorporation by flow cytometry showed increased fluorescence intensity in *NSUN5*-KD cells (Figure 18D). Quantification of the mean fluorescence confirmed that *NSUN5*-KD silencing significantly enhanced the protein synthesis rates (Figure 18E).

Given that protein synthesis rates are known to be regulated throughout the cell cycle, increasing during G1 and G2 phases, we next analyzed OP-puro incorporation in different cell cycle phases. To ensure that the observed differences in protein synthesis rates were not due to differential cell cycle progression between *NSUN5*-KD and control cells, in addition to OP-puro incorporation, DNA was counterstained using propidium iodide to gate cell cycle phases. Quantification of the mean fluorescence of OP-puro-fluorophore conjugate in each phase of the cell cycle indicated that *NSUN5* silencing significantly increases protein synthesis rates independent of the cell cycle phase (Figure 18F).

These results contradicted previous studies that have reported that *NSUN5* loss or silencing induces arrest of global protein synthesis in various model organisms [6, 191]. However, changes in protein synthesis in these studies are especially significant under stress conditions, such as oxidative stress. Since global protein synthesis rates are usually arrested upon oxidative stress induction, we investigated whether *NSUN5* loss in our model led too to reduced protein synthesis upon stress induction. For this purpose, OP-puro incorporation was measured after exposure to the oxidative stress-inducing agent, sodium arsenite ($NaAsO_2$) (Figure 18G). The results showed that upon $NaAsO_2$ treatment, protein synthesis rates decrease to a minimum in control cells after 1 hour of treatment and low levels were maintained after 4 hours of induction. By contrast, *NSUN5*-KD cells exhibited a remarkable recovery of protein synthesis rates after 2 hours of recovery from the treatment, surpassing even the levels observed under control conditions (Figure 18H). These findings confirm previous observations indicating that the loss of NSUN5 increases resistance to

stress and suggest that lower levels of NSUN5 contribute to an enhanced recovery of the translation machinery after stress-induced translation inhibition in human cancer cell lines.
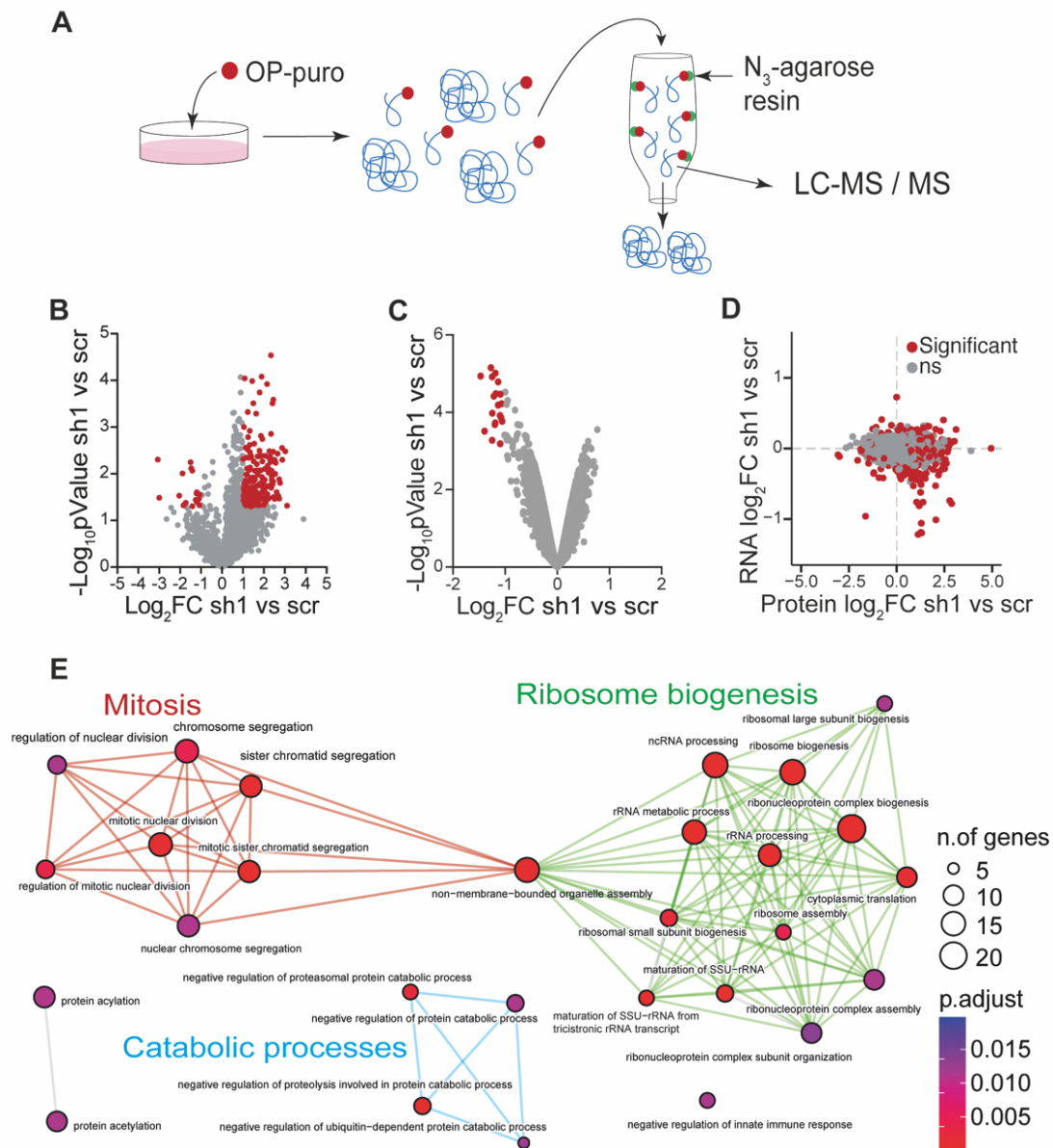
*Figure 19. Evaluation of the nascent proteome after NSUN5 depletion. **A** Schematic representation of the experimental workflow. Cells were allowed to incorporate OP-puro for 1 hour before collection. OP-puro labelled proteins were subsequently captured using an azide-agarose resin and analyzed by mass spectrometry. **B** Volcano plot depicting the differential protein expression between NSUN5-KD cells (sh1) and control cells (scr). Proteins showing statistically significant differences are highlighted in red. n = 4 replicates. **C** mRNA expression was measured using Clariom S Assay Human microarray. Differential mRNA expression between sh1 and scr cells was represented as a volcano plot, and significantly differentially expressed transcripts were highlighted in red. n = 3 replicates. **D** Correlation between RNA and protein differential expression. Proteins showing significant differences in the nascent proteome analysis are highlighted in red. **E** Gene ontology analysis of the differentially expressed proteins in the nascent proteome. The analysis was performed using the "enrichplot" package of R. Circle size represents the gene enrichment, color of the circle represents the adjusted p-value, color of the lines indicates the enriched pathway.*

NSUN5 depletion alters the translational program of the cells

Considering the unexpected finding that *NSUN5* loss led to increased protein synthesis rates in our model, we decided to deeper investigate whether NSUN5 could play a role in favoring or increasing the synthesis of particular proteins. To explore this, we took advantage of the properties of OP-puro to purify nascent peptides using an azide-agarose resin, followed by tandem mass spectrometry analysis (Figure 19A). The mass spectrometry analysis revealed that the majority of significantly differentially expressed peptides, corresponding to 197 proteins, were found to be upregulated in *NSUN5*-KD cells (Figure 19B), corroborating our previous findings (Figure 18A, E).

Subsequently, we aimed to determine whether this differential expression was driven by an upregulation of the mRNAs coding for those proteins. To explore this possibility, mRNA levels were quantified using Affymetrix expression microarrays. Interestingly, the results indicated minimal differences in mRNA levels between *NSUN5*-KD and control cells (Figure 19C). In fact, only 19 mRNAs were found to be differentially expressed in *NSUN5*-KD cells, and in all cases, the levels were lower than in control cells (Figure 19C). This strongly suggested that the upregulation in protein synthesis was not controlled at the transcriptional level. To further support this observation, the protein and mRNA levels were compared, and no significant correlation was found, providing additional evidence that induced protein synthesis changes were translationally regulated in *NSUN5*-KD cells (Figure 19D).

Next, we sought to identify which proteins were actively synthesized in *NSUN5*-KD cells. To identify affected pathways, Gene Ontology (GO) Enrichment Analysis was performed using the "enrichplot" package of R (Figure 19E). The enrichment analysis retrieved numerous GO terms related to ribosome biogenesis, which could be expected given the role of NSUN5 as an rRNA modifying enzyme (Figure 19E). Additionally, terms associated with mitotic regulation were also enriched in *NSUN5*-KD cells compared to control cells. Intriguingly, both cell cycle progression inducers and repressors were found to be upregulated in *NSUN5*-KD cells.

Numerous cell cycle-related proteins displayed differential expression in *NSUN5*-KD cells compared to control cells. For instance, significantly increased expression of Tubulin Gamma Complex Component 2 (GCP2), Proteasome 20S Subunit Beta 7 (PSMB7) and Zinc Finger Protein 207 (ZNF207) was detected by mass spectrometry. GCP2 is necessary for microtubule nucleation at the centrosome and mitotic spindle assembly and its deregulation might indicate alterations in mitotic spindle formation [415]. Similarly, ZNF207, also known as BuGZ, also plays a role in the kinetochore. ZNF207 presents several splicing variants with diverse functions. The longer isoform (isoform C) has been reported as dominant in stem cells, where it interacts with master transcription factors to control the transcription of key genes necessary to maintain self-renewal. In contrast, the

shorter isoform (isoform B) is present in more terminally differentiated cells, where it interacts with Bub3 [416] and facilitates its loading into the kinetochore to regulate proper chromosome alignment [417]. Moreover, PSMB7 is part of the 20S proteasome, whose function is essential for cell cycle progression as it is necessary to maintain the cyclic expression of cell cycle regulators [274, 294]. Thus, abnormal functioning of this crucial process might also contribute to a deregulated cell cycle progression.

To validate the results obtained in the proteomic analysis, the expression of these proteins was assessed by Western blot analysis (Figure 20A). Results showed higher expression of PSMB7 in both *NSUN5*-KD cell lines compared to control cells (Figure 20B, left panel). In contrast, increased expression of GCP2 was only observed in cell silenced using sh1, but not in those silenced using sh2 (Figure 20B, middle panel), possibly due to the lower silencing efficiency demonstrated by sh2. Interestingly, ZNF207 exhibited two bands corresponding to its different splicing variants. Western blot results showed that isoform B tends to be more expressed in *NSUN5*-KD cells while isoform C predominates in control cells (Figure 20A and 20B, right panel).

This alteration in the expression of several mitotic regulators, coupled with the alterations in protein catabolic processes, which are essential during cell cycle progression to ensure the proper cyclic expression of cell cycle regulators, suggest that *NSUN5*-KD cells may exhibit cell cycle alterations.
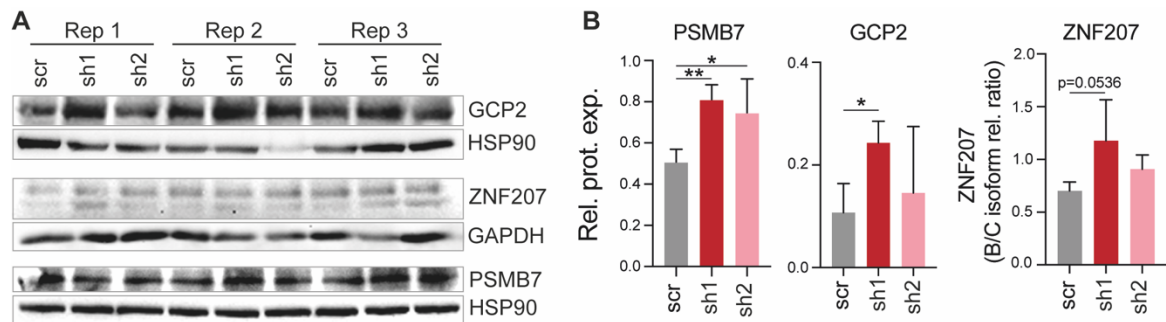
Figure 20. *Upregulation of cell cycle regulators. **A** Protein expression analysis using Western blot of proteins overexpressed in NSUN5-KD cells in proteomic analysis. **B** Quantification of the Western blot in (**A**). Densitometry of GCP2, ZNF207 and PSMB7 bands was normalized to that HSP90. Data is represented as means ± SD, n = 3 replicates. Statistical analysis was performed using one-way ANOVA (* p < 0.05, ** p < 0.01).*

NSUN5 loss impairs cell proliferation

Protein synthesis rate is a critical process closely associated with cell proliferation and cell cycle progression. Consequently, any changes in protein synthesis capacity often result in alterations in cell proliferation [291]. Given our results indicating that *NSUN5* depletion leads to increased global protein synthesis and an altered translational program, favoring the synthesis of mitotic regulators and ribosome biogenesis factors, we hypothesized that *NSUN5*-KD cells might exhibit alterations in their proliferation capacity. To test this hypothesis, anchorage-dependent and -independent growth of *NSUN5*-deficient cells was analyzed (Figure 21A-E).

Cell proliferation in anchorage-dependent conditions measured by growth curves showed that *NSUN5*-KD (Figure 21A) and *NSUN5*-KO (Figure 21B) cells proliferate significantly slower than their control counterparts. Next, the anchorage-independent growth, which is an indicator on cell transformation, was evaluated using the soft agar colony formation assay. In this assay, cells are kept in suspension and prevented from attaching to the plate surface using agar (Figure 21C). Thus, cells grow forming colonies that are then stained with crystal violet for visualization and quantification (Figure 21C, D). The quantification of the colonies confirmed that *NSUN5*-KD cells formed fewer colonies, although statistical significance was reached only in those cells silenced using sh1 (Figure 21D), likely due to the higher silencing efficiency (Figure 10).

This data strongly indicates that *NSUN5*-deficient cells displayed lower tumorigenic and proliferating capacities.

To explore whether the reduced proliferation capacity was a consequence of an increased cell death, cell death was measured by Annexin V assay. This assay relies on the detection of phosphatidylserine residues, which translocate to the cell surface during apoptosis, using annexin V. Additionally, the use of propidium iodide allows the detection of the increased membrane permeability that occurs during later stages of cell death. Quantification of Annexin V$^+$ and propidium iodide$^+$ cells showed no significant difference in cell death between *NSUN5*-KD and control cells (Figure 21F). In the case of the *NSUN5*-KO cells, increased cell death was observed only in C22 (Figure 21G). However, the percentage of cell death in C22 was lower than 8%, while cell proliferation was reduced to half compared to control, indicating that cell death is not the sole reason for the impaired proliferation of C22. These findings suggest an alternative mechanism leading to lower proliferation rates upon *NSUN5* depletion or deletion.
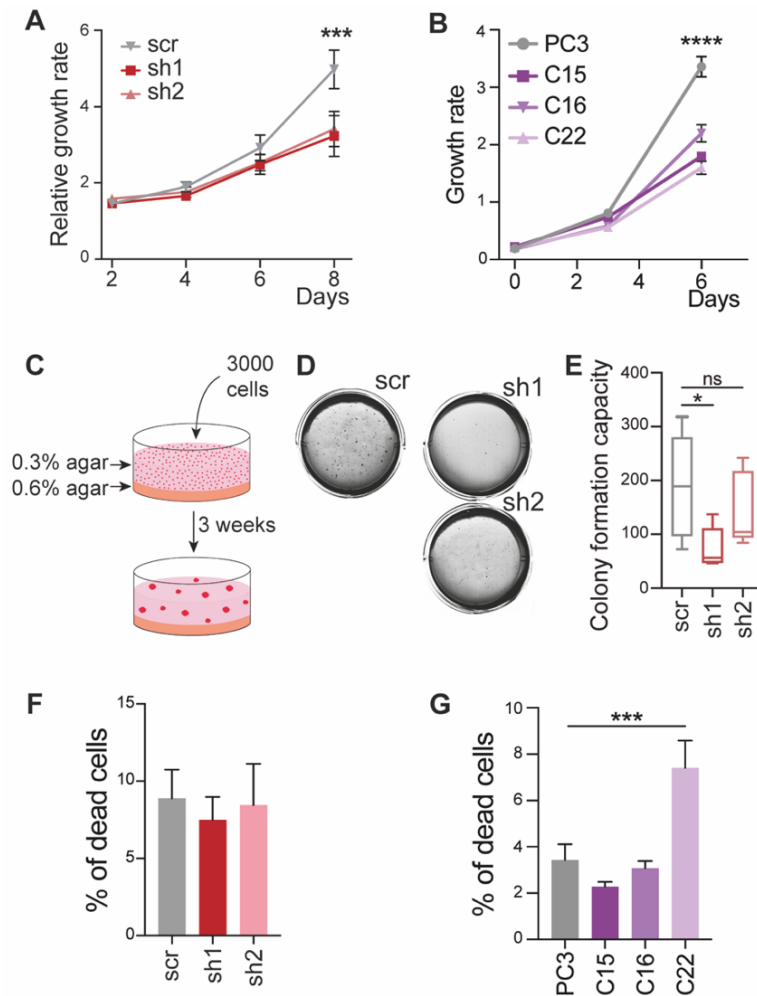
Figure 21. *NSUN5 loss impairs cell proliferation.* ***A, B*** *Growth curve of NSUN5-KD (**A**) and NSUN5-KO (**B**) cells in anchorage-dependent conditions. n = 6 replicates.* ***C-E*** *Anchorage independent growth.* ***C*** *Experimental workflow of the soft agar colony formation assay. Cells are seeded suspension conditions and prevented to attach to plate surface using agar. After 3 weeks, transformed cells are able to growth in suspension forming colonies.* ***D*** *Representative pictures of soft-agar colony formation assay wells after 3 weeks of cell growth. Cells were stained with crystal violet for visualization.* ***E*** *Quantification of the number of colonies. Data is represented as means ± SD, n = 4 replicates. Statistical analysis was performed using one-way ANOVA (* p < 0.05).* ***F, G*** *Analysis of the number of apoptotic cells using Annexin V staining in NSUN5-KD (**F**) and NSUN5-KO (**G**) cells. Total number of Annexin V+ cells is represented. Data is represented as means ± SD, n = 3 replicates. Statistical analysis was performed using one-way ANOVA (*** p < 0.001).*

NSUN5 loss impairs cell cycle progression

Given the increased translation of cell cycle regulators and the reduced cell proliferation, which was not associated to cell death, we hypothesized that cell cycle might be altered in *NSUN5*-deficient cells. To validate this hypothesis, cell cycle was analyzed by flow cytometry in asynchronous cultures of *NSUN5*-KD and *NSUN5*-KO cells (Figure 22A, B).

NSUN5 partial depletion using shRNAs resulted in accumulation of cells in G0/G1 and S phase and a reduction of cells in G2/M in asynchronous culture consistently using both shRNAs (Figure 22A). However, complete loss of *NSUN5* using CRISPR, resulted in different cell cycle profiles (Figure

22B). In one hand, C16 showed no differences in cell cycle distribution compared to control cells. On the other hand, C15 and C22 presented altered cell cycle profiles compared to parental PC3 cells, but differed from each other. While C15 presented an accumulation of cells in S phase, C22 demonstrated a strong arrest in G2/M phase, with nearly half of the cell population in this phase of the cell cycle (Figure 22B).

To gain further insight into the effect of *NSUN5* depletion on cell cycle progression, the expression of several cyclins was analyzed by RT-qPCR in *NSUN5*-KD cells. The expression of cyclins is known to oscillate along cell cycle due to their periodic synthesis and degradation. Thus, each cyclin is expressed during a specific phase of the cell cycle, forming complexes with specific CDKs, activating them, and providing them with substrate specificity. Then, after fulfilling their role, cyclins are degraded, allowing the progression to the subsequent cell cycle phase (Figure 22C). RT-qPCR analysis showed that the expression of all cyclins tended to be lower in *NSUN5*-KD cells compared to control cells, although only *cyclin A1* and *B1* reached statistical significance (Figure 22D).

This suggested that progression into the S and G2/M phases might be impaired in *NSUN5*-deficient cells.
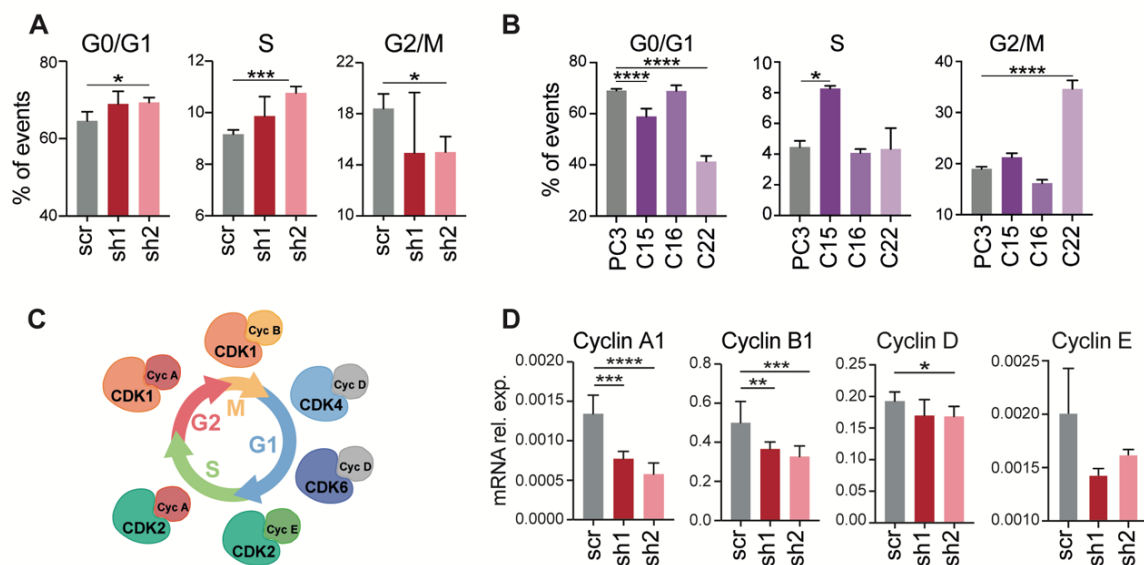

Figure 22. *NSUN5 loss alters cell cycle progression. **A, B** Cell cycle distribution of NSUN5-KD (**A**) and NSUN5-KO (**B**) cells. DNA was stained using propidium iodide and measured by flow cytometry. Data is represented as means ± SD, n = 3 replicates. **C** Schematic representation of the cell cycle phases and the cyclins and CDKs implicated in the progression of each phase. **D** Relative mRNA expression of cyclin A1, B1, D and E in asynchronous cultures of NSUN5-KD and control cells. Data is represented as means ± SD, n = 3 replicates. Statistical analysis was performed one-way ANOVA (* p < 0.05, ** p < 0.01, *** p < 0.001, **** p < 0.0001).*
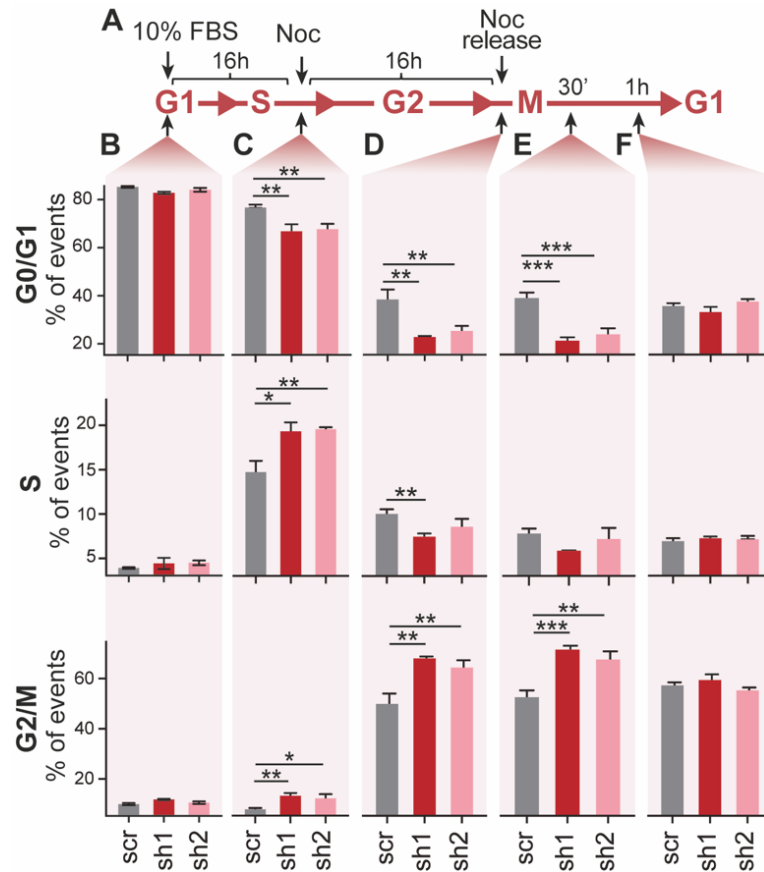
Figure 23. *NSUN5-KD and controls cells were synchronized in G0/G1 and G2/M phases and then released to analyze the progression to the following phase. **A** Schematic representation of the experimental set up. G0/G1 synchronization was achieved by serum starvation for 48 hours. Then, serum was added to the medium and cells were allowed to complete G1 and progress to S phase for 16 hours. Once this period of time had passed, nocodazole was added to the medium for 16 hours to synchronize cells at early M phase. Finally, nocodazole was washed out of the medium to allow cells to perform mitosis. **B-F** During the different stages of synchronization and release, cells were collected, stained, and acquired by flow cytometry to determine their cell cycle profile. Cell cycle profiles of cells in G0/G1 (**B**), S phase (**C**), G2/M (**D**) and 30 min (**E**) and 1 hour (**F**) after G2/M blockade release are shown. Data is represented as means ± SD, n = 3 replicates. Statistical analysis was performed one-way ANOVA (* p < 0.05, ** p < 0.01, *** p < 0.001).*

To deeper analyze the progression through S and G2/M phases, as well as the mitotic process, *NSUN5*-KD cells were synchronized at different phases and then released, and the cell cycle profiles were assessed by flow cytometry (Figure 23). First, cells were synchronized at the G0/G1 phase through 48 hours of serum starvation. Using this synchronization method, over 80% of the cell population was gated in G0/G1 phases in both *NSUN5*-KD and control cells, while the percentage of cells in S phase and G2/M was below 5% and 10%, respectively (Figure 23B). Subsequently, 10% of serum was added to the cells to allow the entry in the S phase. After 16 hours, increase in the percentage of cells in S phase could be observed, while the percentage of cells in G0/G1 decreased (Figure 23C). Then, nocodazole, which is a microtubule inhibitor that arrest the cell cycle in G2/M, was added to the cells for 16 hours to re-synchronize the culture at this point. Finally, nocodazole was carefully removed from the medium to allow the progression of the mitotic process. Interestingly, results showed that control cells rapidly perform mitosis and enter G1 phase again,

as evidenced by the significative increase in the percentage of cells in G0/G1 phase. However, *NSUN5*-KD cells accumulate longer for a longer time in G2/M phase, suggesting that mitotic process is impaired (Figure 23D, E). Eventually, after 1 hour, percentage of cells in G2/M in *NSUN5*-KD cells reached the values showed by the control cells.

All this data suggested that *NSUN5* depletion reduces the proliferation of cancer cells by altering the progression of the cell cycle, especially through G2/M phase transition.

NSUN5 depletion does not activate p53 response

Defective ribosome biogenesis activates cell cycle checkpoints and induces cell cycle arrest [270, 271]. Mechanistically, impaired ribosome biogenesis leads to the release of ribosomal proteins such as uL5 and uL18, which can interact with the E3 ubiquitin ligase MDM2, inhibiting its activity [270, 271]. Consequently, interaction of MDM2 with p53 is impaired resulting in the stabilization of p53. p53 is then able to transcriptionally activate a multitude of genes that, in turn, lead to cell cycle arrest, senescence, and apoptosis (Figure 24A).

Although no significant alterations in ribosome biogenesis were detected in our PC3 *NSUN5*-KD cells and only mild effects were observed in PC3 *NSUN5*-KO cells, we aimed to investigate whether *NSUN5* depletion could activate p53, potentially impairing cell cycle progression. To do that, we selected two cell lines with either p53 loss or mutated p53 (PC3 and DU145, respectively) and two cell lines with functional p53 (BPH-1 and A549) [418-420].

As previously mentioned, depletion of *NSUN5* in PC3 cell line using constitutively expressed shRNAs resulted in an increase in the percentage of cells in G0/G1 and S phase in asynchronous culture conditions, and therefore cell cycle arrest was p53-independent in PC3 cells (Figure 22A). *NSUN5* was further silenced in DU145, BPH-1 and A549 cell lines using transient transfection of siRNAs. *NSUN5* mRNA expression analysis confirmed successfully silencing of *NSUN5* in all cell lines, although silencing efficiency was significantly higher in BPH-1 and A549 cell lines (Figure 24B, first column). The cell cycle analysis showed that acute depletion of NSUN5 leads to an alteration of the cell cycle profiles in all cell lines tested. Similarly to PC3 *NSUN5*-KD cells (Figure 22A), DU145, BPH-1 and A549 cells silenced with siRNAs exhibited an increase in the number of cells in G0/G1 phase (Figure 24B, second and third columns). In addition, a decrease in the number of cells in G2/M phase was observed in these cell lines. Notably, the effect was significantly stronger in BPH-1 and A549 cells, in which the silencing of NSUN5 was more efficient, suggesting either a dose-dependent effect of NSUN5 in the cell cycle progression or a slight contribution of p53 in NSUN5-mediated cell cycle arrest (Figure 24B).

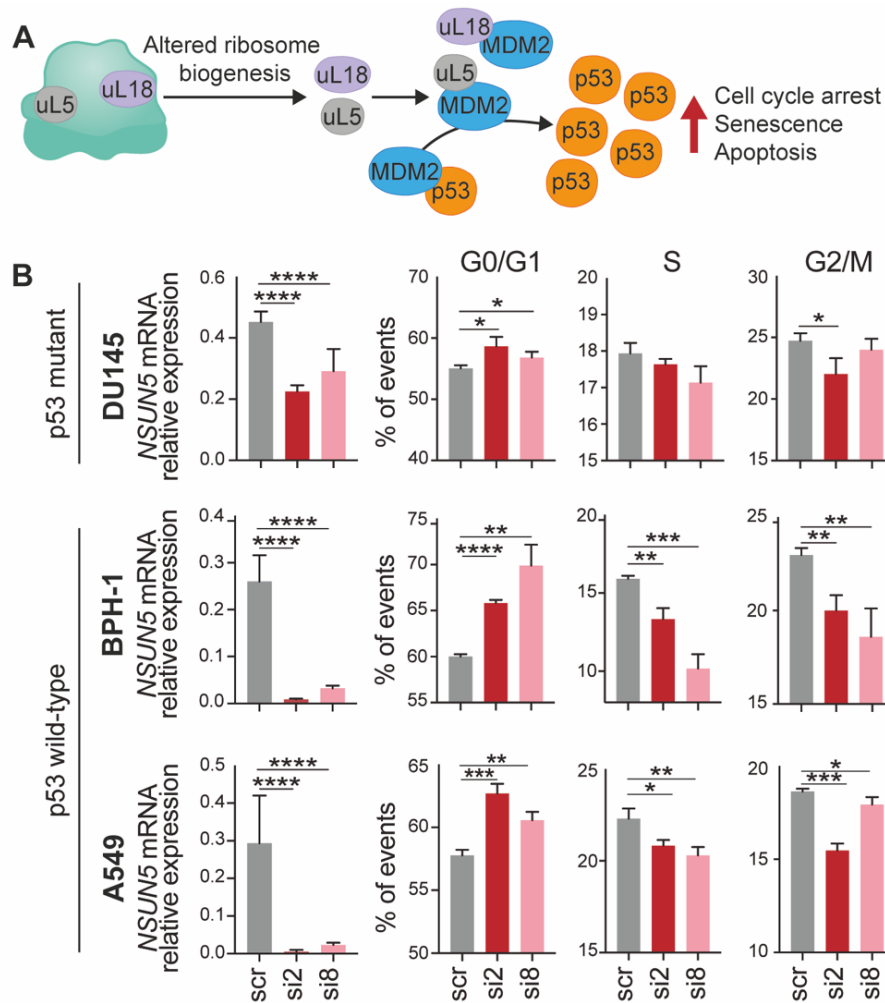*Figure 24. Altered ribosome biogenesis activates p53. A When ribosome biogenesis is altered, uL5 is accumulated and can sequester MDM2. This produces the stabilization of p53 resulting in cell cycle arrest, senescence and apoptosis. B Effect of acute depletion of NSUN5 in p53-mutant (DU145) and p53-WT (BPH-1 and A549) cell lines. First column shows the relative expression of NSUN5 mRNA measured by RT-qPCR. Second to fourth columns show the quantification of the cell cycle profiles in NSUN5-depleted and control cells. Data is represented as means ± SD, n = 3 replicates. Statistical analysis was performed using one-way ANOVA (* p < 0.05, ** p < 0.01, *** p < 0.001, **** p < 0.0001).*

To investigate whether the cell cycle arrest observed upon *NSUN5* depletion is associated to a p53 activation, the expression of p53 and the ribosomal protein uL5, which is often released and upregulated when ribosome biogenesis is altered leading to p53 activation [270, 271], was assessed by Western blot analysis. Western blot results showed no accumulation of uL5 in PC3 *NSUN5*-KD cells (Figure 25A, B). Similarly, no consistent p53 or uL5 accumulation was observed in the DU145, BPH-1 and A549 cells silenced using siRNAs against *NSUN5* (Figure 25C, D).

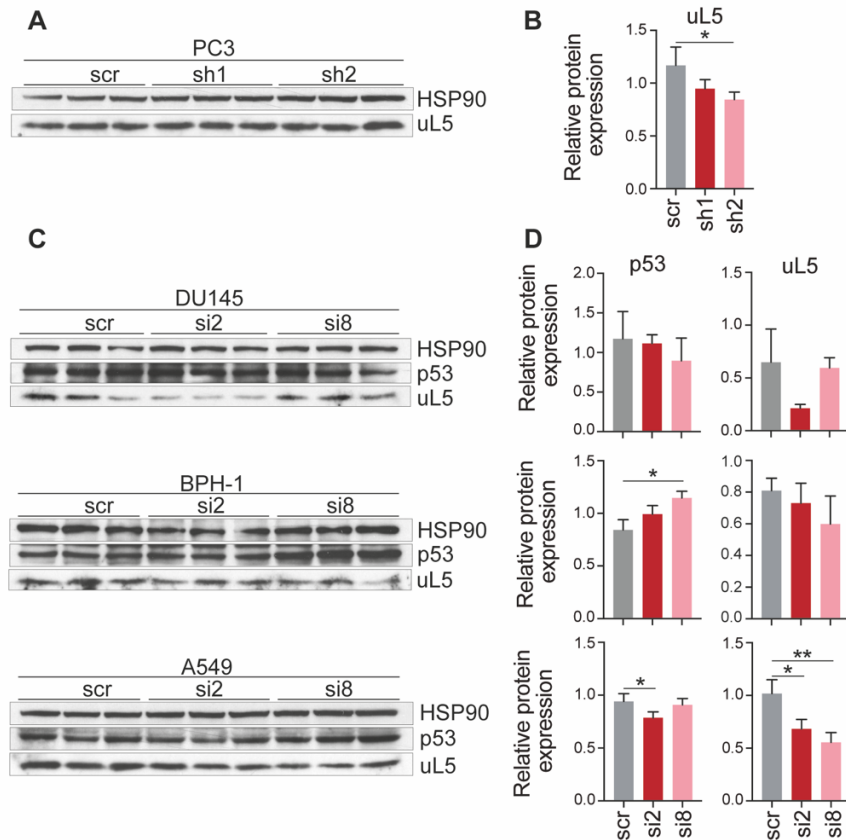Altogether, this data suggested that NSUN5 likely regulates the cell cycle in a p53-independent manner.

Figure 25. *p53 is not accumulated upon NSUN5 depletion.* ***A*** *Expression of uL5 in PC3 cells expressing constitutive shRNAs against NSUN5 analyzed by Western blot.* ***B*** *Densitometry quantification of uL5 band in* ***A****. densitometry of uL5 was normalized to the densitometry of HSP90.* ***C*** *Expression of uL5 and p53 in DU145, BPH-1 and A549 upon NSUN5 depletion using siRNAs analyzed by Western blot.* ***D*** *Quantification of the Western blots in* ***C****. Data is represented as means ± SD, n = 3 replicates. Statistical analysis was performed using one-way ANOVA (* p < 0.05, ** p < 0.01).*

NSUN5 is phosphorylated along cell cycle by CDK1

Our findings suggest that NSUN5, through post-transcriptional control of rRNA processing, plays a role in cell cycle regulation. Therefore, to further position NSUN5 function within the cell cycle event, we analyzed whether and how NSUN5 activity or expression could be dynamically regulated throughout the cell cycle as other key cell cycle regulators.

Analysis of the mRNA expression levels by RT-qPCR showed a slight increase in *NSUN5* mRNA levels in G0/G1 and S phase compared to asynchronous cultures, while no significant changes were observed during G2/M phase (Figure 26A). At the protein level, NSUN5 levels exhibited an increase during S phase (Figure 26B, top panel). More intriguingly, a shift in the electrophoretic mobility of NSUN5 was observed during G2/M phase (Figure 26B, top panel). Quantification of the ratio of the upper to lower NSUN5 band showed almost a 1:1 ratio during G2/M, while during G0/G1 and S phases this ratio was closer to 1:2 (Figure 26B, bottom panel). We hypothesized that this electrophoretic mobility shift could be attributed to a post-translational modification (PTM) of NSUN5 occurring during G2/M.
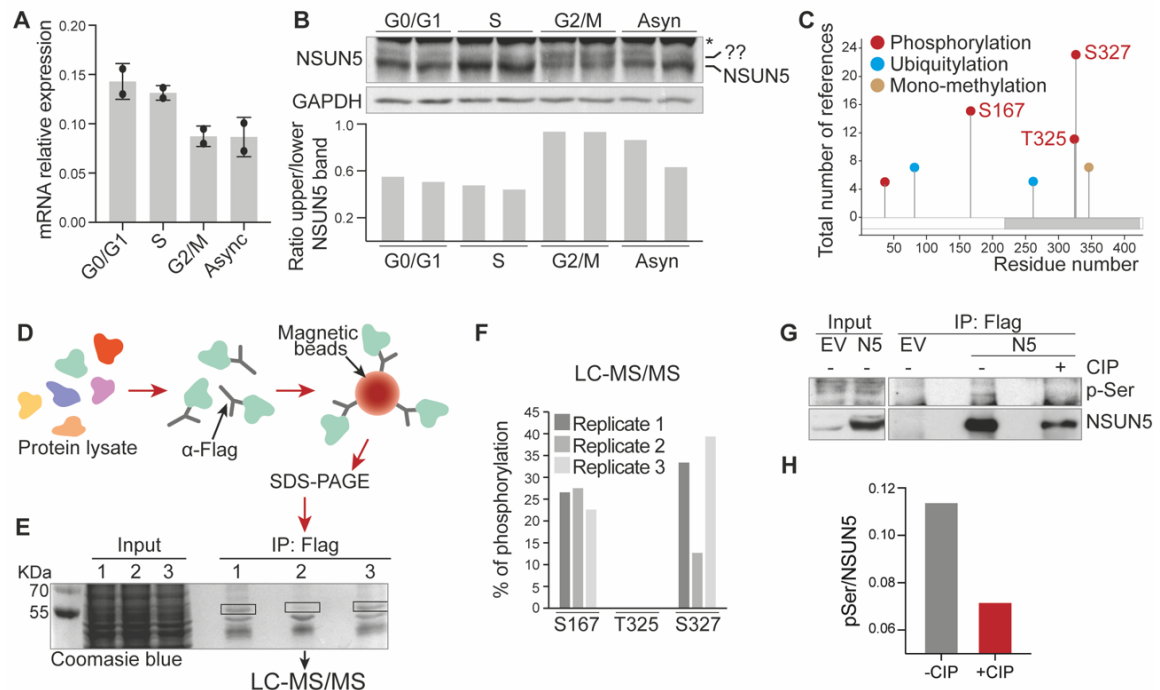
Figure 26. *NSUN5 is phosphorylated in G2/M phase. **A** Cells were synchronized in G0/G1, S phase and G2/M. NSUN5 mRNA levels were analyzed by RT-qPCR and compared to asynchronous cultures (Async). n = 2 replicates. **B** NSUN5 expression in asynchronous and synchronized cultures was assessed by Western blot (upper panel). * Indicates an unspecific band. Densitometry of NSUN5 band (NSUN5) and an upper unidentified band (??) was independently quantified and the upper/lower ratio was calculated (lower panel). n = 2 replicates. **C** Identification of potential post-translational modifications of NSUN5 using PhosphoSitePlus (http://www.phosphosite.org). The X-axis represents NSUN5 protein sequence. Dots depict the modifications reported in the indicated residue. The Y-axis represent the number of references supporting each modification. Only modifications with more than 5 references are shown. **D** Schematic representation of the workflow followed for NSUN5 gel purification for LC-MS/MS analysis. Cells expressing a flag-tagged version of NSUN5 (NSUN5-Flag) were lysed and NSUN5-Flag was immunoprecipitated using an anti-Flag antibody and magnetic beads. Immunoprecipitated NSUN5 was resolved by regular SDS-PAGE and the NSUN5-Flag band excised for further analysis. **E** Coomassie blue-stained gel of the NSUN5-Flag immunoprecipitation. Squares indicate the bands cut for the LC-MS/MS analysis. **F** Percentage of phosphorylated peptides detected using LC-MS/MS in cells synchronized in G2/M phase. Peptides were extracted from the bands showed in **E**. Percentage of phosphorylation in the three main residues found in the literature is shown. n = 3 replicates. **G** NSUN5-Flag was immunoprecipitated as previously described. As control, cells expressing the empty vector (EV) were used. Half of the NSUN5-Flag lysate was treated with calf intestinal alkaline phosphatase (CIP). Immunoprecipitates were submitted to Western blot analysis using anti-phosphoserine and anti-NSUN5 antibodies. **H** Quantification of phosphoserine (p-Ser) normalized to NSUN5 expression of the Western blot in **G**. n = 1 replicate.*

To explore this possibility, we analyzed reported post-translational modifications of NSUN5 using PhosphoSitePlus, a bioinformatic tool that compiles experimentally observed PTMs (https://www.phosphosite.org) [421]. According to this tool, four phosphorylations, two ubiquitylations and one mono-methylation of NSUN5 protein had been identified in more than five high-throughput analysis (Figure 26C). Phosphorylation in serine 167 (S167), threonine 325 (T325) and serine 327 (S327) were the most frequently observed, with more than 12 references supporting their presence in different models (Figure 26C). Importantly, phosphorylation of S327 and T325 had been identified in phosphorylation screenings following nocodazole treatment, which mimics a G2/M phase-like state.

To experimentally validate the presence of PTMs in NSUN5 during G2/M phase in our model, we synchronized cells expressing an inducible Flag-tagged version of NSUN5 (NSUN5-Flag) in G2/M using nocodazole. Then, NSUN5-Flag was immunoprecipitated using an anti-flag antibody and resolved on a polyacrylamide gel (Figure 26D, E). Bands corresponding to NSUN5-Flag (approximately 55 KDa) were excised, subjected to protease digestion and the resulting peptides were then analyzed by mass spectrometry (Figure 26E). The mass spectrometry analysis confirmed the presence of phosphorylated S167 and S327 of NSUN5 in the cell lines used in our study, while no phosphorylation of T325 was found (Figure 26F). Phosphorylation of S167 was detected in approximately 25% of all the NSUN5 peptides, while percentage of phosphorylation in S327 ranged from 12% to 40%. Worth noting that, lowest levels of phosphorylation in S327 corresponded to replicate 2, for which the immunoprecipitation efficiency was very low (Figure 26E). This low immunoprecipitation efficiency led to the detection of a reduced number of peptides (15) compared to replicates 1 and 3 (41 and 57 peptides detected, respectively), which could explain the variability of the phosphorylation observed between replicates (Figure 26F).

The presence of phosphorylated serine was further validated by Western blot analysis. With that aim, NSUN5-Flag expressing cells were synchronized in G2/M using nocodazole, and NSUN5-Flag was immunoprecipitated using an anti-Flag antibody. Phosphorylated NSUN5 was detected using an anti-phosphoserine antibody (Figure 26G), providing additional evidence for the presence of this PTM. Furthermore, phosphorylated NSUN5 was not detected in lysates treated with calf intestinal alkaline phosphatase (CIP), confirming the specificity of the signal obtained with the anti-phosphoserine antibody (Figure 26G, H).

Collectively, these results supported the notion that NSUN5 undergoes dynamic regulation during cell cycle progression at both transcriptional and post-transcriptional levels. The presence of phosphorylatable serine residues in NSUN5, susceptible to modification only during the G2/M phase, suggested that NSUN5 may play a role in cell cycle control and that its activity is cell cycle-dependent. This finding is not unique to this NSUN family member. Another clear example of a PTM-regulated methyltransferase is NSUN2, which is phosphorylated by Aurora-B during mitosis [244]. Thus, these findings, together with previous studies, underscored a cell cycle-dependent upstream regulation of the NSUN family members and suggested that cytosine-5 RNA methylation may fluctuate throughout the cell cycle.

To determine the kinase responsible of NSUN5 phosphorylation during G2/M phase, an analysis of the sequence surrounding S167 and S327 was performed. Notably, the sequence surrounding S327 matched the consensus motif for CDK1 phosphorylation (Figure 27A). CDK1 is a proline-directed serine/threonine kinase known to phosphorylate substrates with the minimal consensus motif S/T-P, being the optimal sequence S/T-P-X-R/K [422-424]. Thus, NSUN5 sequence (SPVR)

possessed the optimal motif for CDK1 phosphorylation (Figure 27A). Moreover, CDK1 is active during G2/M phase, further suggesting that it could be driving NSUN5 phosphorylation.

To test whether CDK1 can phosphorylate NSUN5 during G2/M, cells expressing inducible NSUN5-Flag, were synchronized with nocodazole, and then treated with the CDK1-specific inhibitor RO-3306 [425]. NSUN5 was subsequently immunoprecipitated and its phosphorylation was detected using an anti-phosphoserine antibody. The results revealed a reduction in NSUN5-Flag phosphorylation after treatment with the CDK1 inhibitor RO-3306 compared to the vehicle control, suggesting that CDK1 is indeed responsible for NSUN5 phosphorylation (Figure 27B, C). This result was further validated by mass spectrometry analysis, which showed that NSUN5 phosphorylation was significantly reduced upon CDK1 inhibition with RO-3306, while phosphorylation of S167 was not affected (Figure 27D).
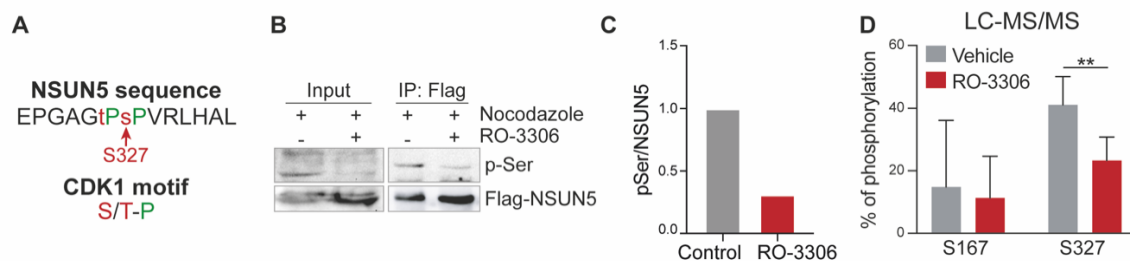
Figure 27. NSUN5 is phosphorylated by CDK1. *A Comparison between NSUN5 protein sequence surrounding serine at position 327 (S327) and the CDK1 minimal consensus motif [422, 423]. B NSUN5-Flag-expressing cells synchronized in G2/M using nocodazole were treated with the CDK1-specific inhibitor RO-3306. NSUN5-Flag was immunoprecipitated and immunodetected using anti-phosphoserine and anti-NSUN5 antibodies. C Quantification of p-Ser normalized to the expression of NSUN5 in the Western blot in B. n = 1 replicate. D Flag-NSUN5-expressing cells were treated with RO-3306 or the vehicle. NSUN5-Flag was immunoprecipitated as previously explained and resolved in an SDS-PAGE. Band corresponding to NSUN5-Flag was cut and analyzed by LC-MS/MS. Data is represented as means ± SD, n = 5 replicates. Statistical analysis was performed using Student's t-test (** p < 0.01).*

Moreover, the phosphorylation of NSUN5 by CDK1 was further validated by *in vitro* kinase assays. With this aim, a recombinant GST- and His-tagged NSUN5 protein was incubated with a recombinant CDK1/Cyclin B complex in the presence of γ^{32}P-ATP for 30 min at 30ºC. *In vitro* kinase assays rely on the capacity of kinases to transfer radioactively labeled phosphates from a donor substrate (γ^{32}P-ATP) to an acceptor substrate. Subsequently, samples are resolved in an SDS-PAGE and phosphorylation is detected by autoradiography.

The efficacy of this CDK1 *in vitro* kinase assay was verified using one of the canonical substrates of CDK1, Histone H1 (Figure 28A). The results showed that in the presence of CDK1/Cyclin B complex, Histone H1 exhibited a strong autoradiography signal, indicating a robust phosphorylation by CDK1 (Figure 28A, lane 13). Moreover, the addition of the CDK1-specific inhibitor RO-3306 substantially reduced Histone H1 phosphorylation (Figure 28A, lane 14), indicating the high specificity of this reaction. Importantly, no autoradiography signal was detected

when CDK1 or Histone H1 were not added to the reaction mix (Figure 28A, lanes 2, 5 and 6), further confirming the specificity of our kinase assay.

Similarly, autoradiography revealed that NSUN5 (approximately 68 KDa due to the addition of GST and His tags) was phosphorylated in the presence of CDK1 and γ^{32}P-ATP (Figure 28A, lanes 7-9). Conversely, no signal was observed when CDK1 or NSUN5 were not added to the mix (Figure 28A lane 4 and 6, respectively). Furthermore, the addition of RO-3306 in the mixture significantly reduced NSUN5 phosphorylation (Figure 28A, lanes 10-12; Figure 28B), confirming the specificity of CDK1 phosphorylation.

Taken together, these results strongly indicate that NSUN5 is phosphorylated by CDK1 during G2/M phase.
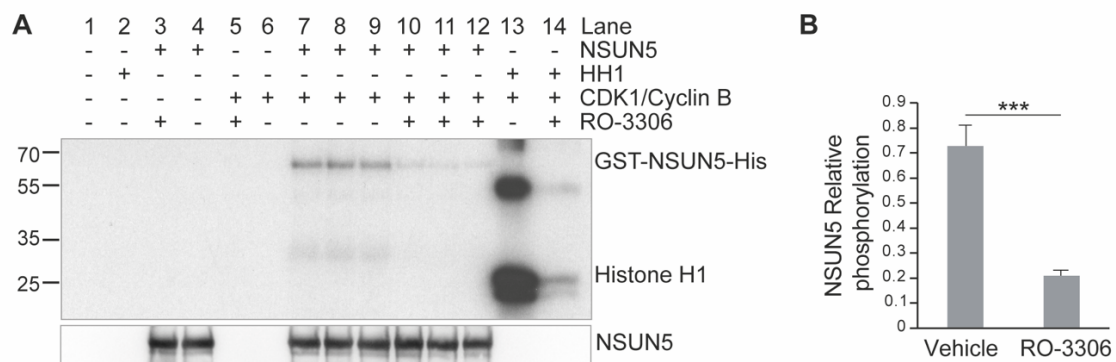

Figure 28. NSUN5 is phosphorylated by CDK1 in vitro. A In vitro kinase assay using recombinant GST-NSUN5-His and recombinant CDK1/Cyclin B. The well-known CDK1 substrate Histone H1 was used as positive control. CDK1 inhibition with RO-3306 was used as negative control. B Quantification of NSUN5 autoradiography normalized to total NSUN5 protein loaded in A. Data is represented as means ± SD, n = 3 replicates. Statistical analysis was performed using Student's t-test (*** p < 0.001).

CDK1 phosphorylation reduces NSUN5 stability

Protein phosphorylation serves as a dynamic and highly sensitive mechanism to regulate protein activity, stability, sub-cellular localization, and interaction [426]. To uncover the role of CDK1-mediated phosphorylation of NSUN5, an analysis of NSUN5 structure was performed. To date, NSUN5 structure has not been experimentally validated; however, it can be predicted through its amino acid sequence. AlphaFold is an Artificial Intelligence-driven system able to computationally predict protein structures with high accuracy [427]. Visualization of the NSUN5 structure predicted by AlphaFold indicated that S327 is not located within the catalytic pocket of NSUN5 and that it does not interact with the two catalytic cysteines of NSUN5 (C308 and C359) (Figure 29A). Moreover, although function cannot be directly deduced from the structural analysis, the location of the phosphorylated residue suggested that it is unlikely that phosphorylation of S327 participates in regulating NSUN5 catalytic function, and rather suggest an involvement in protein stability.

To investigate whether the phosphorylation of residue S327 affects NSUN5 protein stability, a CHX chase assay was performed. Subsequently, NSUN5 protein expression was analyzed in cells that were either untreated or treated with RO-3306 by Western blot (Figure 29B). The Western blot analysis revealed that NSUN5 was more stable in those cells treated with the CDK1 inhibitor (Figure 29B, C), suggesting that phosphorylation of S327 mediated by CDK1 leads to NSUN5 degradation.
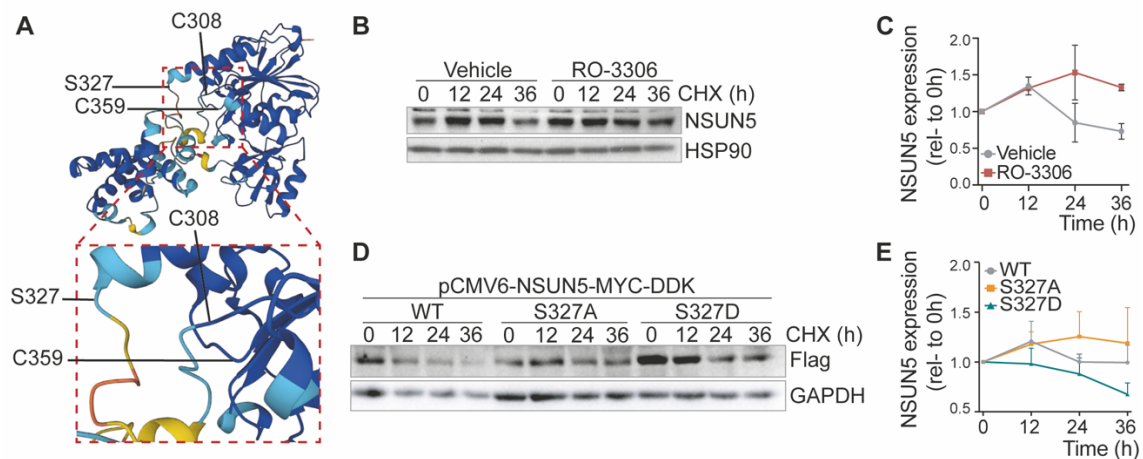

Figure 29. *NSUN5 phosphorylation by CDK1 reduces its stability.* ***A*** *AlphaFold structure prediction of NSUN5. Colors depict model confidence (dark blue: very high; light blue: condifent; yellow: low; orange: very low). NSUN5 catalytic cysteines (C308 and C359) and phosphorylated residue (S327) are indicated.* ***B*** *Protein synthesis was inhibited with CHX and stability of NSUN5 was assessed in CDK1-inhibited and control cells by Western blot.* ***C*** *Quantification of the Western blot in* ***B***. ***D*** *An NSUN5-Myc-DDK-containing plasmid was mutated to obtain a phosphonull (S327A) and a phosphomimetic (S327D) version of the NSUN5 using site-directed mutagenesis. Cells were transfected with each plasmid and 48h later, protein synthesis was inhibited using CHX. Stability of WT and mutant NSUN5 was assessed by Western Blot.* ***E*** *Quantification of the Western blot in* ***D***. *Data is represented as means ± SE, n = 3 replicates. Statistical analysis was performed using one-way ANOVA.*

To further characterize the role of NSUN5 phosphorylation, residue S327 was mutated using site-directed mutagenesis in plasmids containing *NSUN5* cDNA. On one hand, serine was mutated to alanine (S327A) to generate a non-phosphorylatable version of NSUN5 (phosphonull). On the other hand, serine was mutated to aspartic acid (S327D), which mimics a phosphorylated serine, resulting in a NSUN5 protein that is always in phosphorylated state (phosphomimetic). Moreover, these proteins were tagged with a Myc-DDK tag to facilitate specific detection of ectopically expressed proteins. Finally, plasmids containing NSUN5 mutants, as well as a Myc-DDK-tagged wild-type (WT) version of NSUN5, were transfected into PC3 cells and CHX chase assay was performed for up to 36 hours (Figure 29D). Western blot results indicated that the phosphomimetic version of NSUN5 is significantly less stable than the WT NSUN5, while the phosphonull version tends to be exhibit greater stability (Figure 29D, E). This result further validates that NSUN5 phosphorylation at residue S327 promotes NSUN5 degradation.

Phosphorylation is also known to regulate protein localization. To investigate whether CDK1-mediated phosphorylation alters NSUN5 localization, immunofluorescence staining of NSUN5 was performed in untreated cells and cells treated with RO-3306 (Figure 30A). The nuclei of individual cells were then selected using the "analyze particles" plugin of Fiji and the CTCF of NSUN5 was calculated in each individual nucleus. The quantification revealed a slight but significant increase in fluoresce intensity in cells treated with RO-3306 compared to the untreated cells (vehicle) (Figure 30B). This result validates our previous observations (Figure 29), demonstrating that NSUN5 phosphorylation mediated by CDK1 reduces its stability.

Furthermore, NSUN5 fluorescence within nucleoli was quantified using the "analyze particles" plugin of Fiji and subtracted from NSUN5 fluorescence within each nucleus to calculate NSUN5 intensity within the nucleoplasm. Then, nucleoli/nucleoplasm ratio was calculated to detect variations in NSUN5 localization. Thus, a ratio greater than 1 indicates higher expression of the enzyme within the nucleoli, while a ratio lower than 1 indicates translocation to the nucleoplasm. The results showed no significant differences in the percentage of cells with ratio greater or lower than 1 between control and treated cells, although a slight increase in the percentage of cells with a ratio > 1 can be observed in the RO-3306-treated cells (Figure 30C). This result could suggest a modest stabilization of NSUN5 within the nucleoli when the protein is not phosphorylated.

In summary, our findings indicate that the phosphorylation of NSUN5 at S327 by CDK1 leads to the destabilization of the enzyme with no substantial alteration of its subcellular localization.
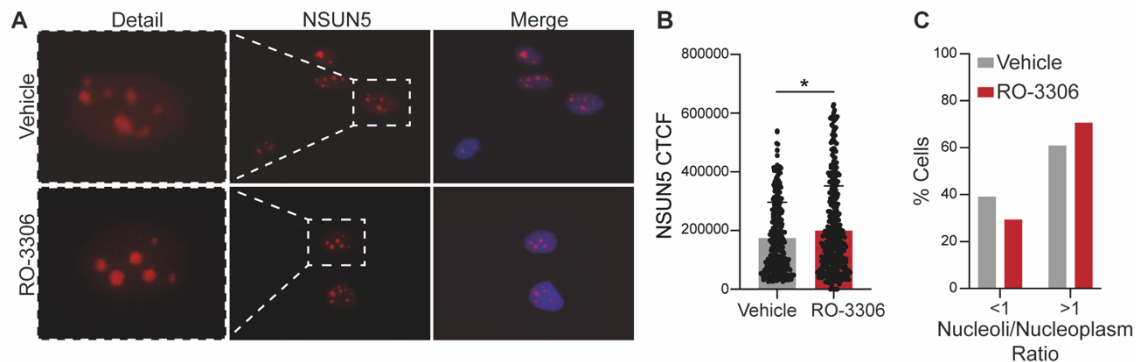

*Figure 30. Inhibition of CDK1 increases NSUN5 stability. **A** Representative images of NSUN5 immunofluorescence (red) in untreated cells (vehicle) and cells treated with RO-3306. Nuclei are counterstained with DAPI (blue). **B** Quantification of corrected total cell fluorescence (CTCF) of NSUN5 in the nuclei of untreated cells and cells treated with RO-3306. Data is represented as means ± SD, n = 3 replicates. A total of 15 images per replicate were analyzed. Statistical analysis was performed using Student's t-test (* p < 0.05). **C** NSUN5 fluorescence was quantified in the nucleolus and in the nucleoplasm of untreated cells and cells treated with RO-3306 and the ratio of NSUN5 fluorescence between nucleoli and nucleoplasm was calculated for each individual cell. The percentage of cells with ratio greater and lower than 1 is represented. n = 3 replicates, 15 images per replicate.*
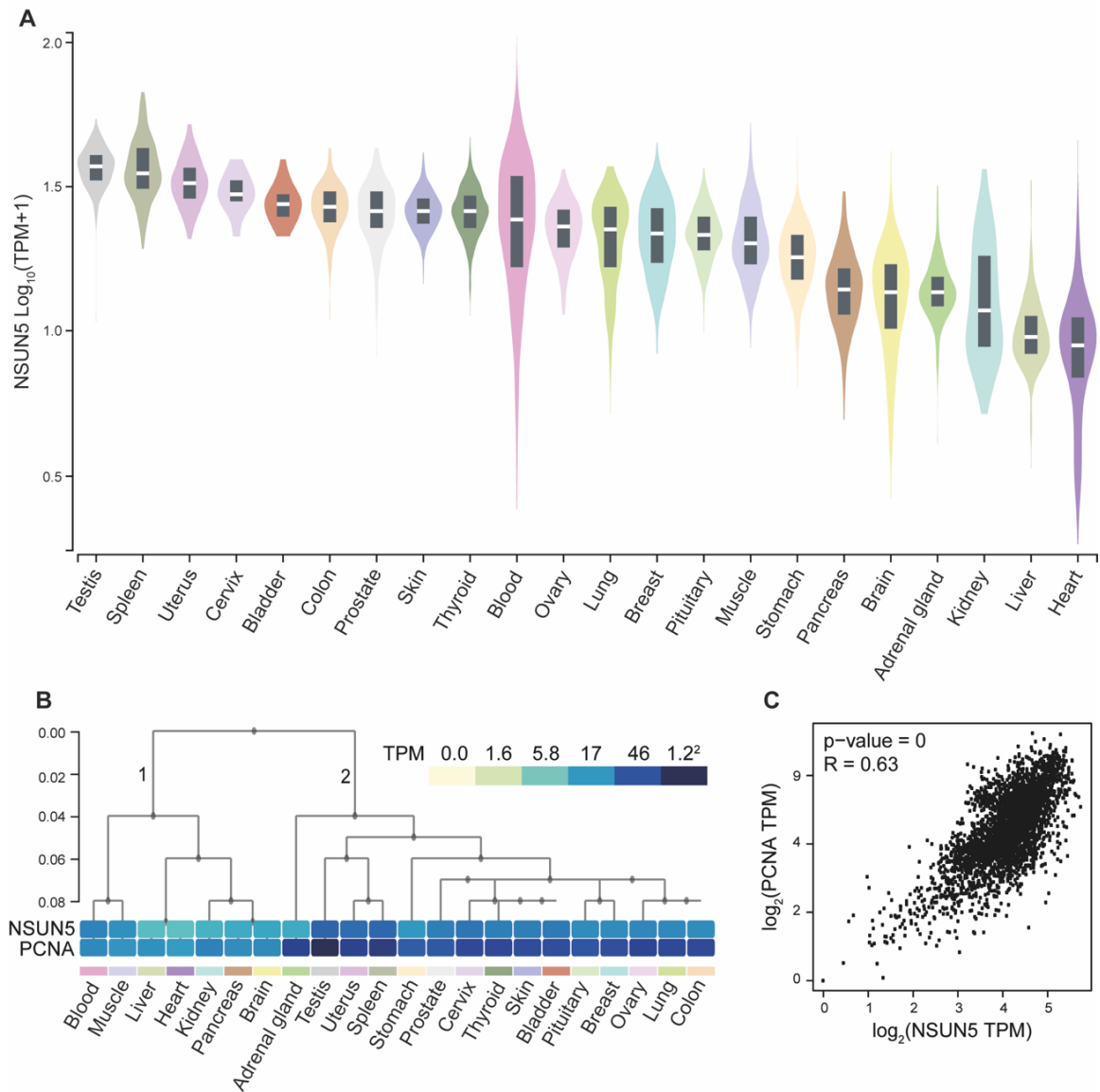
Figure 31. *NSUN5 expression in healthy tissues.* ***A*** *NSUN5 mRNA expression in various healthy adult tissues analyzed using GTEx portal (https://www.gtexportal.org/home/).* ***B*** *NSUN5 and PCNA mRNA expression in healthy adult tissues analyzed using GTEx portal. Tissues were grouped based on the correlation between these two genes.* ***C*** *Pearson correlation analysis of NSUN5 and PCNA mRNA expression in healthy adult tissues.*

NSUN5 is highly expressed in proliferative tissues

Silencing and knock-out of *NSUN5* resulted in a reduction of cell proliferation *in vitro* due to alterations in cell cycle progression, which suggest a therapeutic potential for this enzyme in cancer. To determine if NSUN5 could serve as a therapeutic target or diagnostic marker in cancer, the *NSUN5* mRNA expression was analyzed using the Genotype-Tissue Expression (GTEx) database (Figure 31A). *NSUN5* was ubiquitously expressed in all healthy adult tissues, with the highest expression levels observed in testis and spleen and the lowest levels in liver and heart (Figure 31A). Next, we interrogated whether NSUN5 correlates with the proliferative potential of the tissues. To address this, the expression of the proliferating cell nuclear antigen (PCNA), a well-known marker

of cell proliferation, was analyzed in the GTEx database. Correlation analysis grouped samples in two main clusters (Figure 31B). Cluster 1 represented tissues with lower *PCNA* expression, indicating lower proliferation rates, while cluster 2 encompasses tissues which higher *PCNA* expression. Interestingly, *NSUN5* expression in cluster 2 was higher than in cluster 1, suggesting a direct correlation between *NSUN5* expression and the proliferative potential of the tissue (Figure 31B). To validate this correlation, Pearson correlation analysis between *NSUN5* and *PCNA* mRNA expression was performed in all tissues, resulting in a significant positive correlation (Figure 31C).

This finding confirms that tissues with higher proliferation rates express higher levels of *NSUN5*, supporting the role of NSUN5 in maintaining cell proliferation.

Given the positive correlation between NSUN5 expression and the proliferative capacity of various tissues, coupled with the fact that cancers are characterized by aberrant cell proliferation, we hypothesized that NSUN5 may be overexpressed in human tumors. To test this hypothesis, we analyzed the expression of *NSUN5* in different publicly available databases of tumors derived from highly proliferative tissues (cluster 2), such as prostate adenocarcinoma (PRAD), as well as non-proliferative tissues (cluster 1), such as cholangiocarcinoma (CHOL) and liver hepatocellular carcinoma (LIHC).
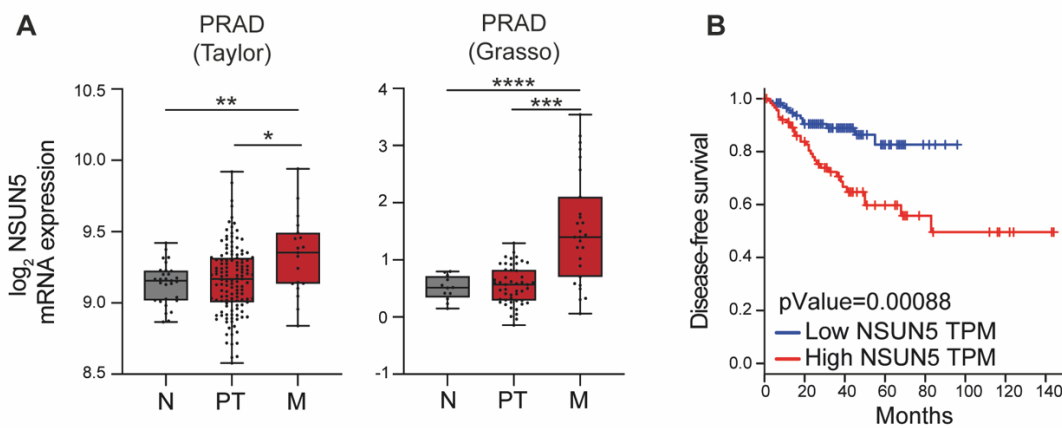

Figure 32. *NSUN5 expression in prostate cancer. **A** NSUN5 mRNA expression in healthy prostate tissue (N), primary prostate tumors (PT) and metastatic tumors (M) using data from two publicly available databases [377, 386]. Statistical analysis was performed using Mann-Whitney test (* p < 0.05, ** p < 0.01, *** p < 0.001, **** p < 0.0001). **B** Association between NSUN5 expression and disease-free survival of prostate cancer patients. NSUN5 expression was divided in quartiles and Q1 (low NSUN5 TPM) and Q4 (high NSUN5 TPM) were used for the Kaplan-Meier plot. Data was obtained from The Cancer Genome Atlas (TCGA) and GTEx. n = 123 patients per quartile.*

NSUN5 is overexpressed in prostate cancer

NSUN5 mRNA expression was analyzed in two publicly available databases [377, 386] using the bioinformatic tool CANCERTOOL [428]. *NSUN5* mRNA expression analysis showed no differences in terms of expression between normal prostate (N) and primary tumors (PT) (Figure 32A). However, a significative increase in *NSUN5* expression was observed between normal prostate or primary tumors and metastatic tumors. This observation suggests a potential role of NSUN5 in the metastatic phase of prostate cancer progression. Notably, the analysis of the disease-free survival (DFS) using the online tool GEPIA (Gene Expression Profiling Interactive Analysis), which integrates the data from The Cancer Genome Atlas (TCGA) and GTEx projects, revealed a correlation between increased *NSUN5* mRNA expression and higher rates of disease recurrence (Figure 32B).

Given the increased expression of *NSUN5* mRNA observed in expression databases, we decided to analyze NSUN5 expression at the protein level in prostate cancer using a tumor microarray (TMA). This TMA encompassed 31 prostate cancer tissues and 9 non-tumoral adjacent tissues in which NSUN5 expression was evaluated through immunohistochemistry (IHC). IHC results from non-tumoral tissues showed that NSUN5 is expressed in cell nucleus, with intensified staining observed in the nucleolus (Figure 33A, left panels), corroborating the localization of NSUN5 observed in cultured cell lines (Figure 10C). In the case of the tumor samples, NSUN5 staining exhibited much greater intensity and was more homogenously distributed through the nucleus (Figure 33A, right panels). Quantification of the DAB intensity using the "Colour Deconvolution 2" plugin of Fiji corroborated the significant increased expression of NSUN5 in tumor tissues compared to non-tumoral controls (Figure 33B).

Moreover, NSUN5 higher expression in prostate cancer was further validated by Western blot analysis in a small cohort of patients of benign hyperplasia (BH) and prostate cancer (PRAD) from Basurto Hospital (Basque Country, Spain) in collaboration with Professor Arkaitz Carracedo (CIC bioGUNE, Basque Country, Spain). Western blot results indicated that BH patients, who present a non-cancerous enlargement of the prostate, showed significant lower levels of NSUN5 protein than the PRAD patients (Figure 33C, D), thereby supporting the *in silico* analysis of prostate cancer mRNA expression databases.

In summary, this data demonstrated that NSUN5 is overexpressed in PRAD both at mRNA and protein levels and that it can serve as a marker for increased risk of recurrence in prostate cancer.
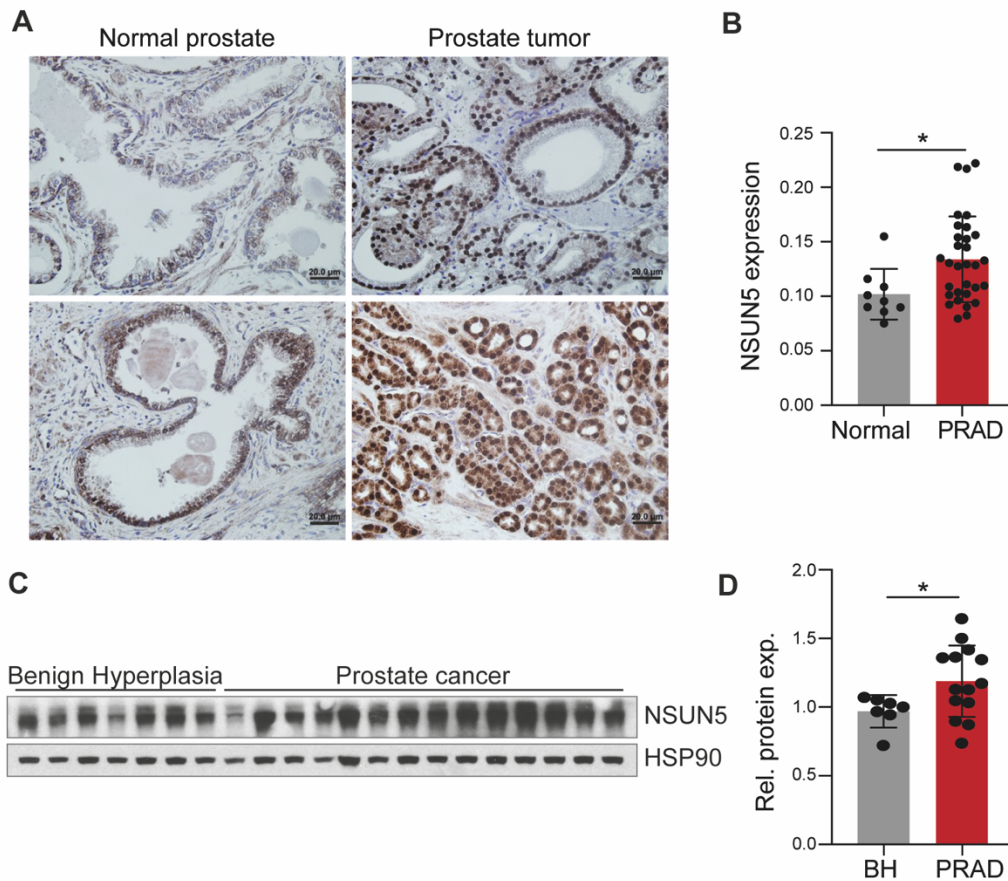
Figure 33. *NSUN5 expression in prostate cancer.* **A** *Immunostaining of NSUN5 in a prostate cancer tissue microarray (TMA). Cell nuclei are counterstained with hematoxylin (purple). Scale bars correspond to 20 µm.* **B** *Quantification of NSUN5 expression in* **A**. *n = 9 normal prostate and 31 prostate cancer tissues. Statistical analysis was performed using Mann-Whitney test (* p < 0.05).* **C** *NSUN5 protein expression in a local cohort of prostate cancer (PRAD) and benign hyperplasia (BH) patients of Basurto Hospital (Basque Country, Spain) analyzed by Western blot.* **D** *Quantification of NSUN5 protein expression in the Western blot in* **C**. *NSUN5 band intensity was normalized by the intensity of the corresponding HSP90 band. n = 7 benign hyperplasia and 14 prostate cancer patients. Statistical analysis was performed using Mann-Whitney test (* p < 0.05).*
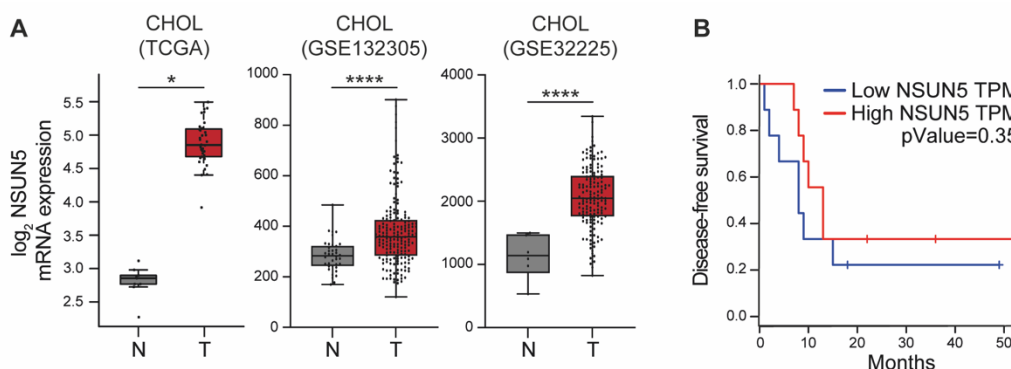

Figure 34. *NSUN5 expression in cholangiocarcinoma.* **A** *NSUN5 mRNA expression in healthy bile duct (N) and tumors (M) using data from TCGA data and two publicly available databases [429, 430]. Statistical analysis was performed using Mann-Whitney test (* p < 0.05, **** p < 0.0001).* **B** *Association between NSUN5 expression and disease-free survival of cholangiocarcinoma patients. NSUN5 expression was divided in quartiles and Q1 (low NSUN5 TPM) and Q4 (high NSUN5 TPM) were used for the Kaplan-Meier plot. Data was obtained from TCGA. n = 9 patients per quartile.*

NSUN5 is overexpressed in cholangiocarcinoma and hepatocellular carcinoma

Given that NSUN5 was overexpressed in prostate cancer, we next aimed to evaluate whether NSUN5 is also upregulated in tumors developed from non-proliferative tissues. Analysis of *NSUN5* mRNA expression in TCGA and two publicly available databases [429, 430] showed higher *NSUN5* expression in cholangiocarcinoma compared to healthy bile duct tissues (Figure 34A). However, no correlation between increased *NSUN5* expression and worse prognosis was observed in cholangiocarcinoma, possibly due to the limited number of patients available for the analysis in the TCGA and GTEx databases (Figure 34B).

Next, we interrogated the expression levels of NSUN5 in LIHC in TCGA and seven publicly available databases [431-437]. mRNA expression analysis showed consistent and significant increased *NSUN5* expression in liver cancer compared to healthy liver tissues in all databases (Figure 35A). Importantly, proteomic analysis of liver tumors and healthy tissues also detected increased NSUN5 protein expression in tumors (Figure 35B), suggesting that *NSUN5* overexpression at mRNA levels is translated into increased protein levels. Interestingly, *NSUN5* mRNA expression was found to be increased in liver tumors with adrenal metastasis (AM) compared to non-metastatic (NM), although no expression differences were observed in patients with lung metastasis (LM) (Figure 35C). This higher expression in tumors with adrenal metastasis further supports the results observed in metastatic prostate cancer (Figure 32A) and suggested that NSUN5 might play a role in disease progression by conferring increased metastatic potential to tumor cells. Lastly, a correlation between higher *NSUN5* mRNA expression and increased recurrence was observed in LIHC patients (Figure 35D), further supporting our observations in prostate cancer.

These findings were validated in a liver cancer patient cohort from Reina Sofía University Hospital (Córdoba, Spain) in collaboration with Dr Manuel Gahete (Instituto Maimónides de Investigación Biomédica de Córdoba, Spain). RT-qPCR results showed a significant upregulation of *NSUN5* expression in tumor tissue (LIHC) compared with non-tumoral adjacent tissue (N) (Figure 36A). Importantly, NSUN5 expression was further increased in those tumors presenting microinvasions in other tissues (Figure 36B). Similarly, the analysis of expression databases indicated elevated *NSUN5* mRNA expression in cholangiocarcinoma. Although this data could not be validated in a patient cohort, NSUN5 expression was analyzed in normal immortalized cholangiocites (N) and in several cholangiocarcinoma cell lines kindly provided by Dr Javier Vaquero (Centro de Investigación del Cáncer, Salamanca, Spain) (Figure 37). Tumoral cell lines were derived from four types of cholangiocarcinoma: intrahepatic cholangiocarcinoma (iCCA), distal cholangiocarcinoma (dCCA), gallbladder cholangiocarcinoma (gCCA) and intrahepatic cholangiocarcinoma and

hepatocellular carcinoma (HCC-iCCA), with the latter exhibiting a more mesenchymal phenotype, and thus a higher metastatic potential. *NSUN5* mRNA expression analysis by RT-qPCR revealed higher *NSUN5* expression in almost all tumoral cell lines compared to immortalized cholangiocites (MMNK1). Interestingly, NSUN5 expression was particularly high in those cell lines displaying a more mesenchymal phenotype and thus increased migratory capacity (Figure 37).
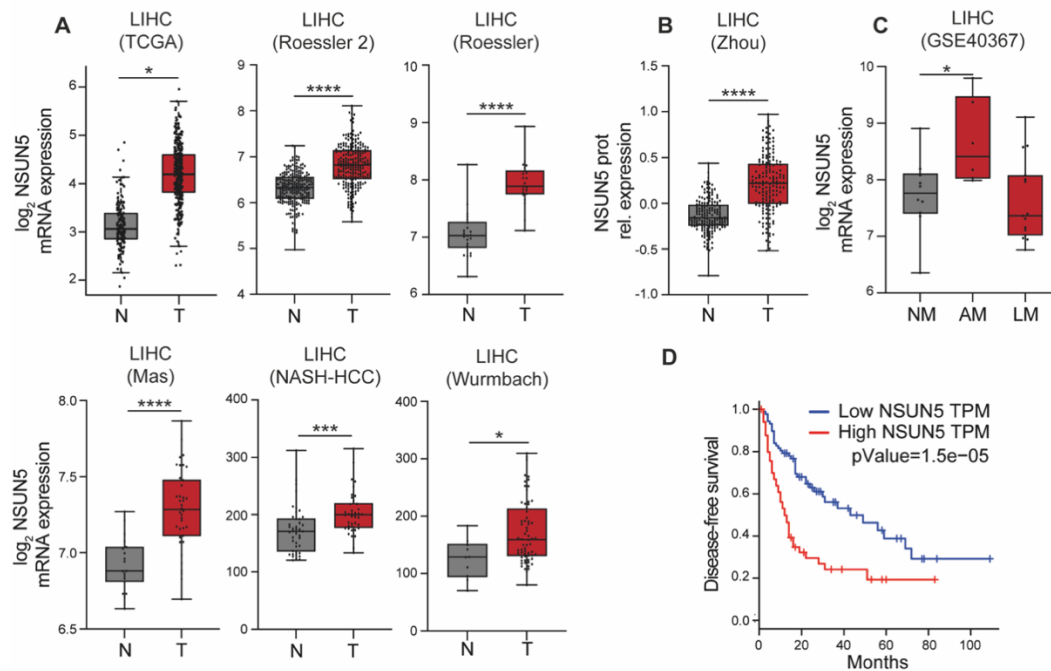

***Figure 35.** NSUN5 expression in liver cancer. **A** NSUN5 mRNA expression in healthy liver (N) and tumors (M) using data from TCGA data and seven publicly available databases [431-435]. **B** NSUN5 protein expression in healthy liver (N) and tumors (M) in a publicly available database [436]. **C** NSUN5 mRNA expression in non-metastatic tumors (NM) and tumors with adrenal (AM) and lung (LM) metastasis in a publicly available database [437]. Statistical analysis was performed using Mann-Whitney test (* p < 0.05, *** p < 0.001, **** p < 0.0001). **D** Association between NSUN5 expression and disease-free survival of liver patients. NSUN5 expression was divided in quartiles and Q1 (low NSUN5 TPM) and Q4 (high NSUN5 TPM) were used for the Kaplan-Meier plot. Data was obtained from TCGA and GTEx. n = 91 patients per quartile.*
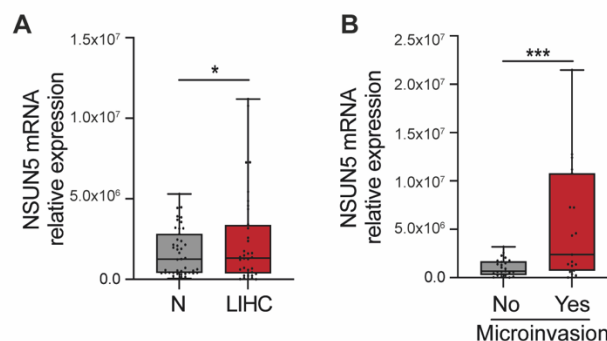

***Figure 36.** NSUN5 expression in liver cancer patients and cholangiocarcinoma cells. **A** NSUN5 mRNA quantification in non-tumoral adjacent tissue (N) and liver cancer (LIHC) in a local cohort of liver cancer patients from Reina Sofía University Hospital (Cordoba, Spain). n = 45. Statistical analysis was performed using Mann-Whitney test (* p < 0.05). **B** NSUN5 mRNA expression analyzed by RT-qPCR in tumors showing microinvasions or not in a local cohort of liver cancer patients from Reina Sofía University Hospital (Cordoba, Spain). n = 61. Statistical analysis was performed using Mann-Whitney test (* p < 0.05).*

Altogether, our data indicates that NSUN5 is highly expressed in proliferative tissues and is further overexpressed in tumors derived from both proliferative tissues, such as prostate cancer, and non-proliferative tissues, such as cholangiocarcinoma and hepatocellular carcinoma, especially during advanced phases of the disease. Our experimental data obtained from prostate and liver cancer patient cohorts, as well as cholangiocarcinoma cell lines, confirm the *in silico* results and demonstrate that NSUN5 is overexpressed in prostate cancer, hepatocellular carcinoma and cholangiocarcinoma. Notably, our observations *in silico* in prostate cancer and hepatocellular carcinoma and *in vitro* in cholangiocarcinoma suggest that NSUN5 expression increases even further as cancer progress to a metastatic state. This upregulation of NSUN5 expression suggests that this enzyme could be explored as a therapeutic target in cancer. Furthermore, high NSUN5 expression correlates with poor prognosis in prostate and liver cancer, suggesting that NSUN5 could serve as a diagnostic marker to identify patients at higher risk of recurrence.
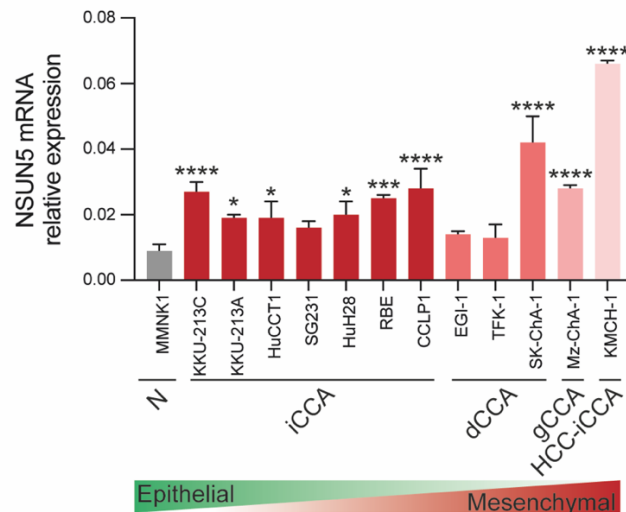
Figure 37. NSUN5 mRNA expression analyzed by RT-qPCR in a non-transformed bile duct cell line (N) and in cell lines derived from various cholangiocarcinoma subtypes including: intrahepatic cholangiocarcinoma (iCCA), distal cholangiocarcinoma (dCCA), gallbladder cholangiocarcinoma (gCCA) and intrahepatic cholangiocarcinoma and hepatocellular carcinoma (HCC-iCCA).

NSUN5 is upregulated in murine prostate cancer

To further validate whether NSUN5 overexpression in tumors in a conserved feature, we analyzed the expression of NSUN5 in murine prostate tumors. Prostate cancer has been successfully modeled in mice [438]. Although several mice models of prostate cancer have been developed, one of the most extended is the one developed by Prof Pier Paolo Pandolfi (Harvard Medical School, USA). In this model, prostate cancer is induced by promoting the prostate-specific deletion of Pten [390]. To achieve this, exons 4 and 5 of Pten are flanked by LoxP sites, while Cre recombinase is expressed under the control of the *rat Probasin* (*PB*) gene promoter. This gene is androgen-

responsible and is expressed post-puberty in the prostatic epithelium at high levels, leading to the deletion of Pten in these cells. These mice (hereafter referred to as *Pten^flox/flox^; PB-Cre^+/-^* or simply *Pten*-KO) develop high-grade prostate intraepithelial neoplasia (PIN) at 3 months and adenocarcinoma at 6 months (Figure 38A).

Nsun5 mRNA expression analysis by RT-qPCR in *Pten*-WT and *Pten*-KO mouse prostates demonstrated that *Nsun5* expression is significantly higher in *Pten*-KO mice (Figure 38B). The upregulation of *Nsun5* expression was evident at 3 months of age and even higher at 6 months, when tumors had already progressed to invasive adenocarcinoma. Importantly, this increased expression was not age-dependent, since *Pten*-WT mice showed no *Nsun5* upregulation over time, but was rather dependent on tumor progression (Figure 38B).

The prostate is a gland arranged in acini and ducts formed by a glandular epithelium that encompasses three different cell types: luminal cells, which are specialized cells that secrete different products that contribute to the seminal fluid; basal cells, locates between luminal cells and the basal membrane; and neuroendocrine cells, which are usually small in number (Figure 38C) [439]. The identification of the cell of origin of prostate cancer is still controversial, as tumors exhibit both luminal and basal phenotypes and both types of cells have been demonstrated to have tumorigenic potential. However, luminal cells are considered the of origin since they exhibit increased susceptibility to oncogenic transformation.

To analyze whether Nsun5 is differentially expressed in the cells that comprise the mouse prostatic epithelium, prostates from healthy mice were dissected, digested and analyzed by fluorescence-activated cell sorting (FACS). To achieve a proper cell sorting, viable cells were first separated as those negative for DAPI staining (Figure 38D, left panel). Then, epithelial, and stromal cells were separated from endothelial and blood cells using the linage markers CD31, CD45 and Ter119, which are exclusive to the latter (Figure 38D, center panel). Finally, using Sca1 and CD49f staining, cells were sorted into stromal (Sca1^high^, CD49f^-^), luminal (Sca1^low^, CD49f^low^) and basal (Sca1^high^, CD49f^high^) cell populations (Figure 38D, right panel). RNA was isolated from these sorted cells, and the expression of *Nsun5*, *CD49f*, *Sca1*, the basal marker *Krt5* and the luminal marker *Krt8* were analyzed by RT-qPCR (Figure 38E). *CD49f* and *Sca1* RT-qPCR results confirmed the sorting efficiency, as *CD49f* was only amplified in basal cells and *Sca1* showed the highest levels in stromal cells and lowest levels in luminal cells, as expected. The efficiency of our sorting strategy was further evidenced by the amplification of the basal marker *Krt5* exclusively in the basal compartment. Regarding the luminal marker *Krt8*, as anticipated, the highest levels were found in the luminal compartment, although *Krt8* mRNA was also detected in the basal compartment, suggesting a minor contamination with luminal cells. Although *Nsun5* was expressed nearly

uniformly in basal, luminal and stromal cells, a slight but not significant increase in the expression was observed in the luminal compartment (Figure 38E).

In summary, *Nsun5* was expressed in basal, luminal and stromal cells within the murine prostate, indicating that it may be crucial for the maintenance of all three cell types. Nonetheless, a slight increase in *Nsun5* expression was observed in luminal cells, considered cell of origin of prostate cancer, which may confer increased proliferative potential to these cells during tumorigenesis.
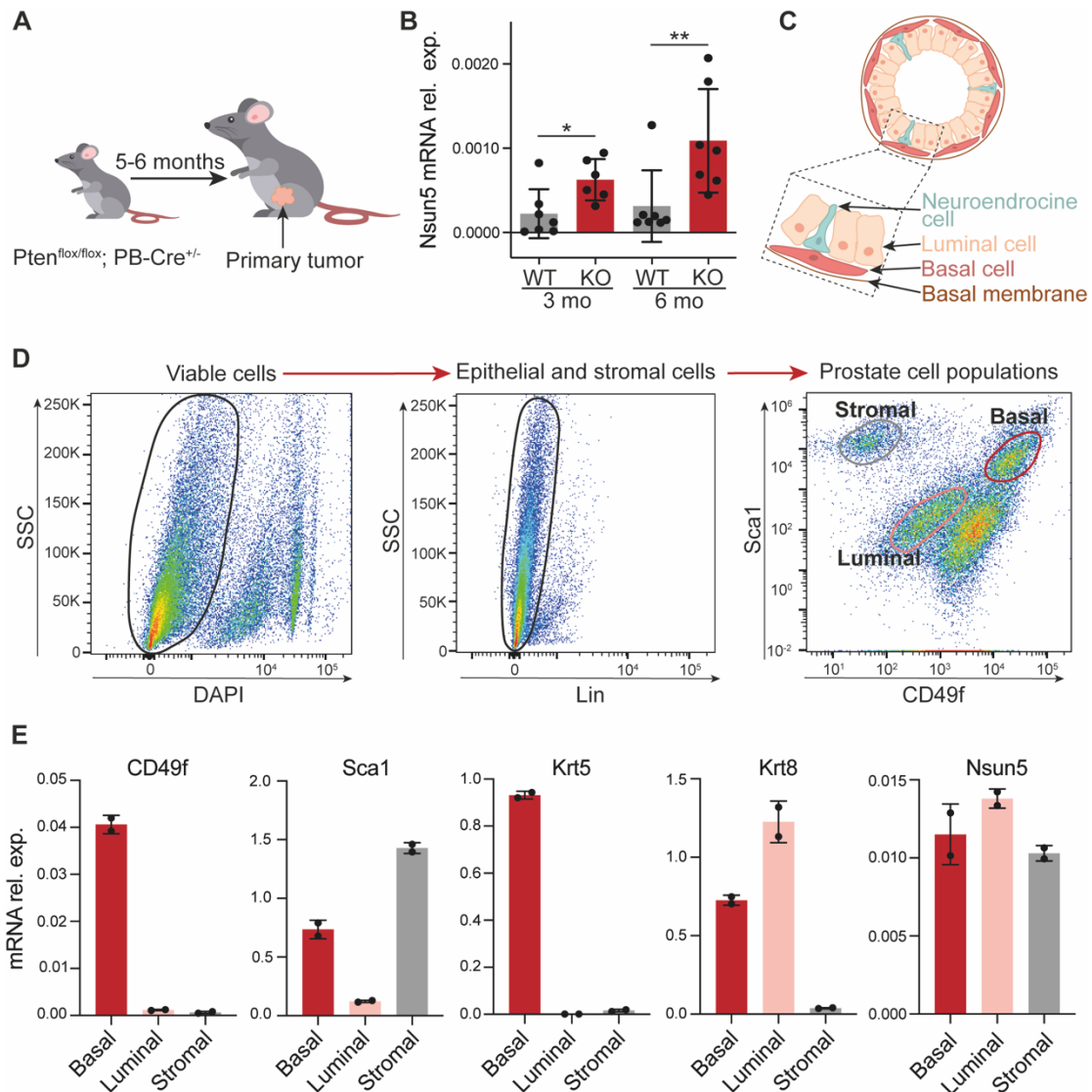
Figure 38. *NSUN5 expression in a prostate cancer mouse model.* ***A*** *Pten^(flox/flox); Pb-Cre4 mouse model developed by Prof Pandolfi [390]. This mouse model carries both Pten alleles floxed and Cre recombinase expressed under the prostate-specific probasine promoter. Thus, Cre recombinase is expressed specifically in prostate epithelium after puberty leading to prostate intraepithelial neoplasia at 3 months of age and adenocarcinoma at 6 months of age with a 100% of penetrance.* ***B*** *NSUN5 mRNA expression analyzed by RT-qPCR in Pten^(flox/flox); PB-Cre^(+/-) mice and Pten^(flox/flox); PB-Cre^(+/+) mice at 3 and 6 months of age. n = 6 mice. Statistical analysis was performed using one-way ANOVA test (* p < 0.05, ** p < 0.01).* ***C*** *Schematic representation of a cross-section of a murine prostate duct. Basal, luminal and neuroendocrine cells are indicated.* ***D*** *Gating strategy for isolation of cell populations within Pten^(flox/flox); Pb-Cre^(+/-) mice prostates by fluorescence activated cell sorting (FACS). Viable cells are separated by selecting DAPI^- cells. Then, epithelial and stromal cells are separated from endothelial and blood cells, which are positive for linage markers (CD31, CD45 and TERT). Finally, luminal (Sca1^(low), CD49f ^(low)), basal (Sca1^(high), CD49f ^(high)) and stromal (Sca1^(high), CD49f ^-) cells were separated depending on their expression of Sca1 and CD49f.* ***E*** *mRNA expression of CD49f, Sca1, Krt5, Krt8 and Nsun5 in basal, luminal and stromal cells extracted from the prostate of Pten^(flox/flox); Pb-Cre^(+/-) mice as explained in* ***D***.

Characterization of *Nsun5* knocked-out mice

Nsun5 has been knocked-out by the Knockout Mouse Phenotyping Program (KOMP2) [440]. This mouse model, named Nsun5[tm2b(EUCOMM)Wtsi], was generated by the addition of loxP sites flanking the critical exons 3 and 4. Consequently, crossing with a Cre recombinase-expressing mouse resulted in a conditional *Nsun5* knockout mouse (Figure 39A). To validate that this model resulted in a successful Nsun5 knockout, *Nsun5* mRNA expression was analyzed. Expression analysis by RT-qPCR in RNA extracted from limbs of *Nsun5*^{+/+}, *Nsun5*^{+/-} and *Nsun5*^{-/-} mice showed no *Nsun5* expression in *Nsun5*^{-/-} mice, confirming the efficiency of the knock-out (Figure 39B). On the other hand, *Nsun5*^{+/-} presented half of the expression of Nsun5 mRNA than the control *Nsun5*^{+/+} mice, as expected. Interestingly, although *Nsun5*^{-/-} mice were viable and did not show evident weight alteration or developmental delays, some degree of embryonic lethality was detected (Figure 39C). Consequently, lower number of *Nsun5*^{-/-} and *Nsun5*^{+/-} mice than expected were obtained in each litter, with embryonic lethality ratios reaching up to 50% in the case of *Nsun5*^{-/-} mice (Figure 39C, upper panel).

Next, we analyzed the 28S rRNA methylation in *Nsun5*^{+/+} and *Nsun5*^{-/-} mice. NSUN5 has been reported to methylate position C3438 in mouse 28S rRNA, which corresponds to the homologous human position C3781 [181]. The methylation of position C3438 was assessed by bisulfite-PCR as previously explained. The results showed no methylation of C3438 in *Nsun5*^{-/-}, while the 28S rRNA of *Nsun5*^{+/+} mice was 100% methylated, further supporting the efficiency of the *Nsun5* knock-out in this model (Figure 39D). However, it is worth mentioning that bisulfite-PCR technique presents certain limitations that could result in altered results. Consequently, our methylation analysis was validated using Oxford nanopore technology (ONT) sequencing in collaboration with Dr Eva Novoa (Centre for Genomic Regulation, Barcelona, Spain). ONT sequencing relies in the use of membrane-embedded nanopores through which RNA is driven, producing current changes that are then translated into nucleotide sequences (Figure 39E). ONT sequencing results were analyzed using the NanoConsensus algorithm (developed by Dr Eva Novoa Laboratory), which detects differences in methylation between two samples. Thus, a high NanoConsensus Score in a nucleotide position indicates a significant difference in the methylation of that position between the two samples. ONT sequencing results of 28S rRNA of *Nsun5*^{-/-} and *Nsun5*^{+/-} mice revealed significant differences in methylation at several positions, located between 3429 to 3431 (which would correspond to position C3438) showing the highest score and thus being the most likely to be differentially modified. This data supports the results obtained by bisulfite-PCR and confirms that 28S rRNA from *Nsun5*^{-/-} mice is not methylated. Consequently, these mice are suitable for their use in further experiments aimed to elucidate the role of NSUN5 *in vivo*.
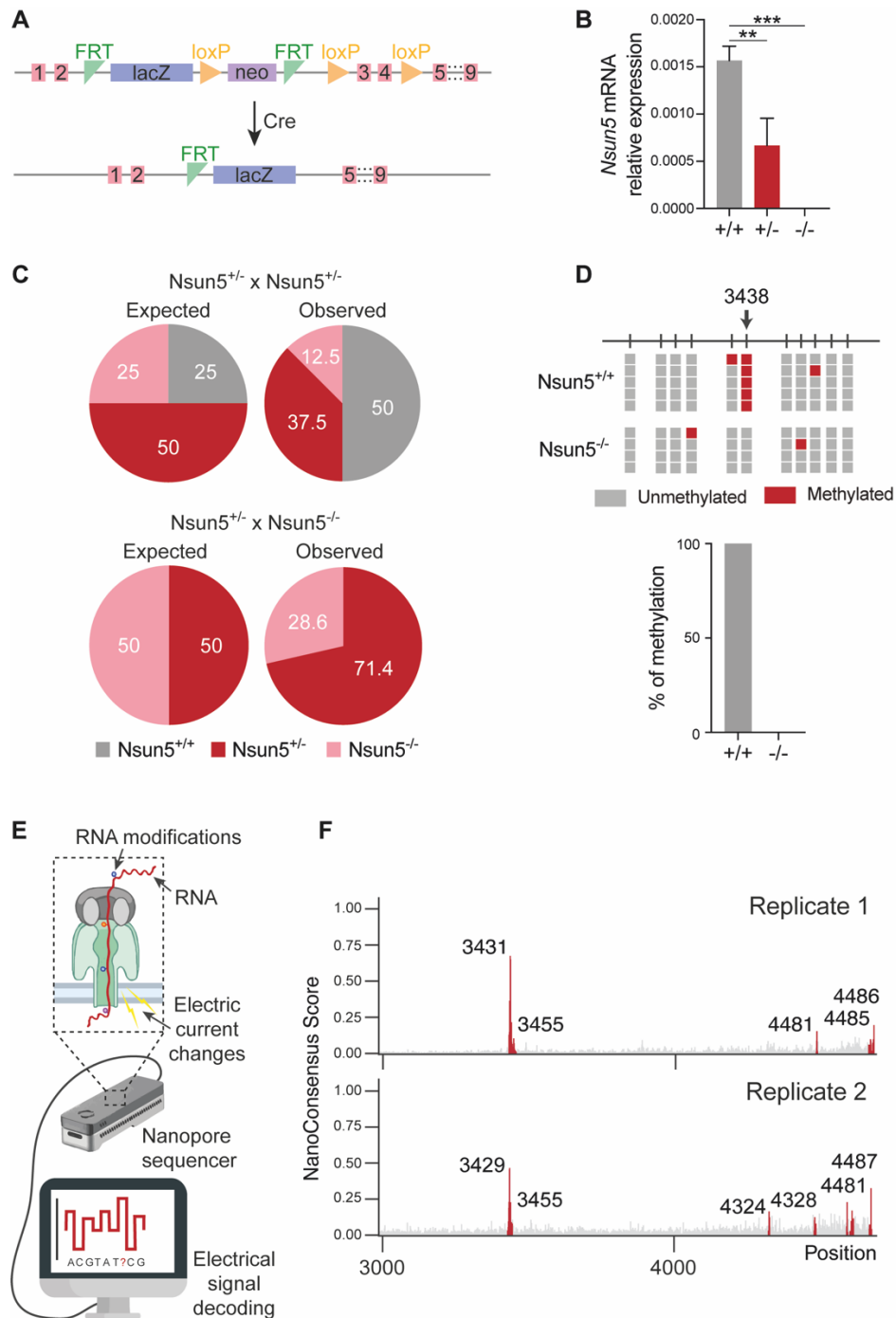
Figure 39. *Characterization of an Nsun5 knockout mouse model.* **A** *Schematic view of the Nsun5[tm2b(EUCOMM)Wtsi] cassette and strategy followed to generate conditional Nsun5 knockout mice.* **B** *Nsun5 mRNA expression analyzed by RT-qPCR in Nsun5^{+/+}, Nsun5^{+/-} and Nsun5^{-/-} mice. n = mice. n = 6 mice. Statistical analysis was performed using one-way ANOVA test (** p < 0.01, *** p < 0.001).* **C** *Percentage of expected (left) and observed (right) born pups from each genotype after crossing two heterozygous mice (upper panel) or heterozygous and knock-out mice (lower panel).* **D** *Methylation analysis of 28s rRNA by bisulfite-PCR. In the upper panel, each row represents a single clone, while columns represent cytosines. C3438 is marked with an arrow. Methylated and unmethylated cytosines are represented as red and grey squares, respectively. In the lower panel, the percentage of methylation in C3438 in Nsun5^{+/+} and Nsun5^{-/-} mice is shown.* **E** *Schematic representation of single-molecule sequencing by ONT sequencing. RNA molecules are driven through nanopores inducing changes in the electric current. Changes in the electric current are interpreted and decoded to RNA bases.* **F** *Results of the nanopore sequencing of 28S rRNA from in Nsun5^{+/+} and Nsun5^{-/-} mice. Data was analyzed using NanoConsesus algorithm, which compares pairs of samples to detect differentially methylated residues, retrieving a NanoConsensus Score. Higher scores indicate higher differences between samples. n = 2 mice.*

Nsun5 depletion has no effect on prostate tumor formation

Given that *NSUN5* was found to be overexpressed in several cancers and that the loss of *NSUN5* expression resulted in decreased proliferation capacity and cell cycle arrest *in vitro*, we hypothesized that NSUN5 could serve as a therapeutic target in cancer. To evaluate the potential of NSUN5 as a therapeutic target in prostate cancer, $Nsun5^{-/-}$ mice were crossed with the *Pten*-KO mouse model, to obtain a prostate cancer mouse model lacking *Nsun5* expression. Surprisingly, despite multiple breeding attempts, it was not possible to obtain any mice with homozygous deletion of *Nsun5*. This was surprising since *Nsun5* can be independently knocked out, although certain grade of embryonic lethality was observed (Figure 39C). Importantly, although *Nsun5* is globally deleted, *Pten* deletion only occurs in the prostate and upon activation of Cre recombinase during puberty, making unlikely the occurrence of lethality due to direct dependency between Nsun5 and Pten. Given the challenge in obtaining $Nsun5^{-/-}$ mice, we opted to evaluate the role of Nsun5 in prostate cancer development using heterozygous mice ($Pten^{flox/flox}$; $PB\text{-}Cre^{+/-}$; $Nsun5^{+/-}$ or *Pten*-KO; $Nsun5^{+/-}$). As controls, mice that develop prostate cancer but have a WT *Nsun5* gene ($Pten^{flox/flox}$; $PB\text{-}Cre^{+/-}$; $Nsun5^{+/+}$ or *Pten*-KO; $Nsun5^{+/+}$) were used. *Nsun5* mRNA expression analysis in prostatic tissues by RT-qPCR demonstrated that *Pten*-KO; $Nsun5^{+/+}$ mice express significantly lower levels of *Nsun5* mRNA than the *Pten*-KO; $Nsun5^{+/+}$, making them a suitable model to evaluate the role of Nsun5 in prostate cancer development (Figure 40A).

Unlike the human prostate, which is formed by a single structure, mouse prostate is divided into three pairs of lobes known as anterior prostate (AP), ventral prostate (VP) and dorsolateral prostate (DLP). All prostate lobes from five months-old *Pten*-WT (which do not develop prostate cancer), *Pten*-KO; $Nsun5^{+/+}$ and *Pten*-KO; $Nsun5^{+/-}$ mice were microdissected, weighted and measured. The results showed that both *Pten*-KO; $Nsun5^{+/+}$ and *Pten*-KO; $Nsun5^{+/-}$ mice developed prostate tumors, showing a significative increase in weight and volume compared to *Pten*-WT mice (Figure 40C, D). However, no differences in volume (Figure 40B, C) or weight (Figure 40D) between the $Nsun5^{+/+}$ and $Nsun5^{+/-}$ mice were observed, suggesting that *Nsun5* expression is not essential for prostate tumor formation.

As previously stated, the mouse prostate (like the human prostate) is composed of luminal, basal, and neuroendocrine cells that arrange constituting the prostatic epithelium. It has been reported that, upon tumor development, the number of cells expressing basal markers significantly increases due to the massive proliferation of this compartment [441]. To evaluate whether reduced *Nsun5* expression altered the cell distribution within the prostate tumor, DLP lobes from five months-old *Pten*-KO; $Nsun5^{+/+}$ and *Pten*-KO; $Nsun5^{+/-}$ mice were microdissected, digested, labelled and sorted as previously explained. Sca1-CD49f representation allowed the identification of the stromal, basal and luminal cell populations (Figure 40E). Quantification of the percentage of cells within each

compartment showed no difference between *Pten*-KO; *Nsun5*^{+/+} and *Pten*-KO; *Nsun5*^{+/-} mice, indicating that Nsun5 has no effect in the proliferation of specific subsets of cells within the prostate tumor either.

Altogether, these results indicated that NSUN5 does not play a role the initiation and growth of prostate primary tumors in mice.
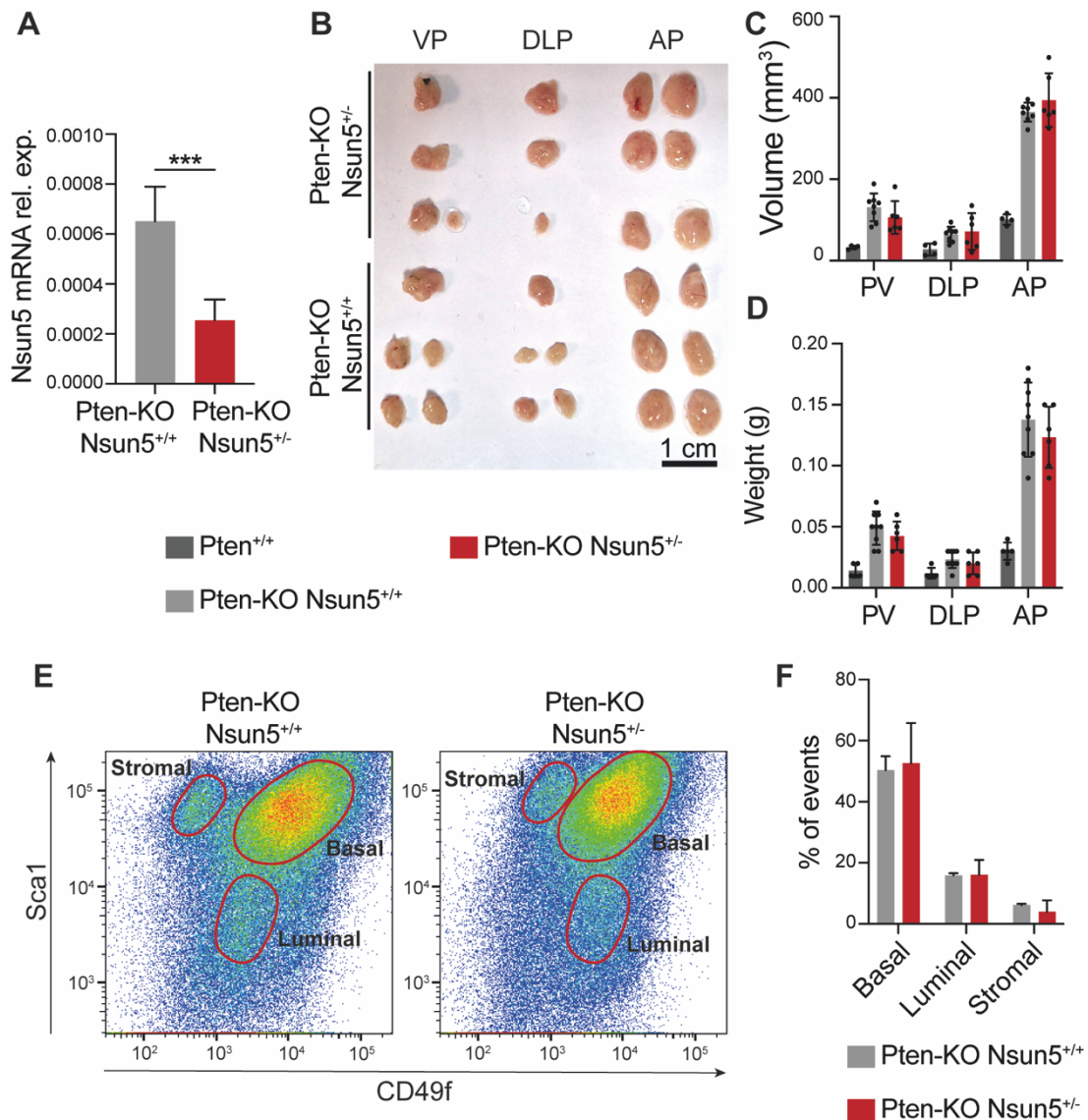
Figure 40. *Role of Nsun5 in prostate tumor formation.* ***A*** *Nsun5 mRNA levels analyzed by RT-qPCR.* ***B*** *Representative images of the three prostate lobes extracted from Pten-KO; Nsun5*^{+/+} *and Pten-KO; Nsun5*^{+/-}*mice.* ***C*** *Weight of the ventral (VP), dorsolateral (DLP) and anterior (AP) prostate lobes extracted from Pten*^{+/+}*, Pten-KO; Nsun5*^{+/+} *and Pten-KO; Nsun5*^{+/-} *mice. n = 4 Pten*^{+/+}*, 9 Pten-KO; Nsun5*^{+/+} *and 6 Pten-KO; Nsun5*^{+/-}*.* ***D*** *Volume of the prostate lobes extracted from Pten*^{+/+}*, Pten-KO; Nsun5*^{+/+} *and Pten-KO; Nsun5*^{+/-}*mice. n = 5 Pten*^{+/+}*, 9 Pten-KO; Nsun5*^{+/+} *and 6 Pten-KO; Nsun5*^{+/-}*.* ***E*** *Luminal (Sca1*^{low}*, CD49f* [low]*), basal (Sca1*^{high}*, CD49f* [high]*) and stromal (Sca1*^{high}*, CD49f* [-]*) composition of Pten-KO; Nsun5*^{+/+} *and Pten-KO; Nsun5*^{+/-} *mice. Tumor cells were separated depending on their expression of Sca1 and CD49f.* ***F*** *Percentage of stromal, luminal and basal cells in prostates dissected from Pten-KO; Nsun5*^{+/+} *and Pten-KO; Nsun5*^{+/-}*mice.*

Nsun5 depletion impairs the metastasis of prostate tumors

 In silico analysis of *NSUN5* mRNA expression in several prostate cancer expression databases showed that *NSUN5* is especially upregulated during the metastatic phase of the disease (Figure 32A). Moreover, *NSUN5* was also found overexpressed in liver tumors with adrenal metastasis compared to non-metastatic tumors (Figure 35C) and in tumors showing microinvasions (Figure 36B). These results suggest that NSUN5 upregulation could be an important event during the transition to a metastatic disease.
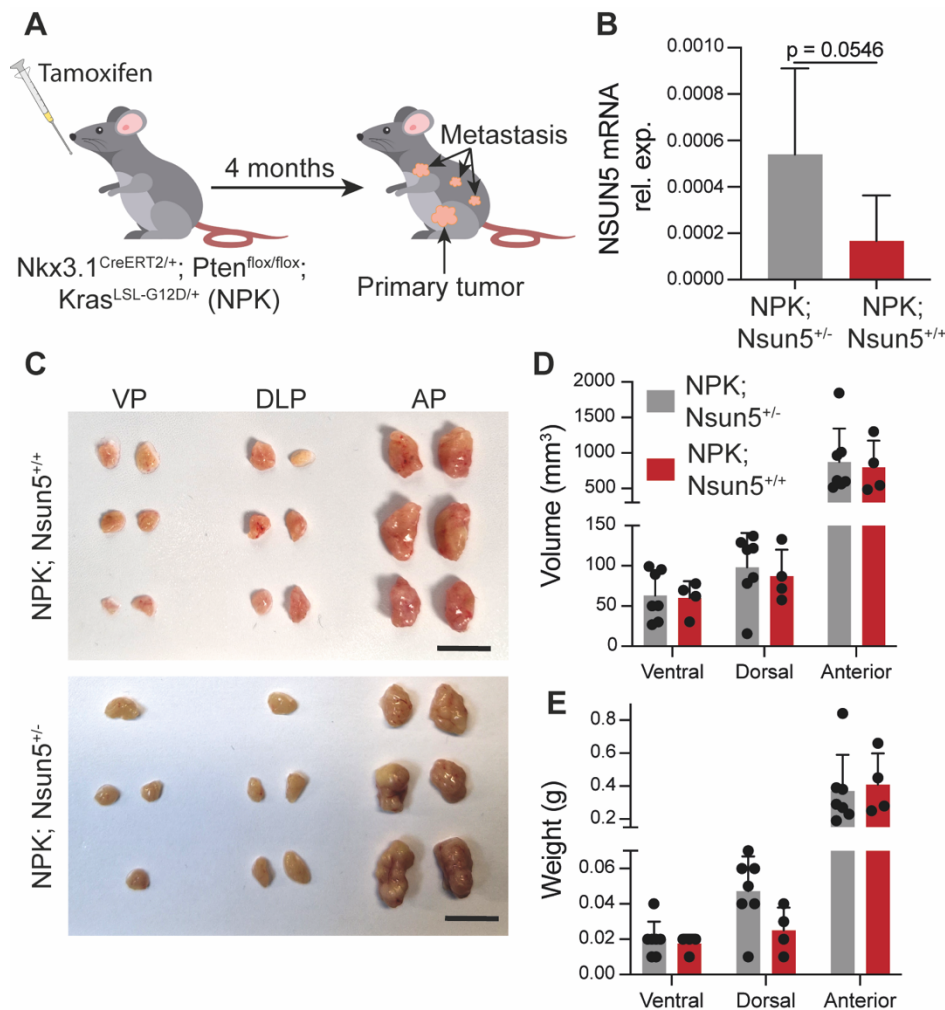

Figure 41. *Role of NSUN5 in advanced and metastatic prostate tumors.* ***A*** *Nkx3.1^CreERT2; Pten^{flox/flox}; Kras^{LSL-G12D/+} (NPK) metastatic prostate cancer mouse model. In this model, both Pten alleles are floxed and a tamoxifen-inducible Cre recombinase is expressed under the promoter of Nkx3.1, which is expressed in the prostatic epithelium. Thus, upon tamoxifen induction, Pten is deleted specifically in the prostatic epithelium. Moreover, tamoxifen induction also leads to the expression of a mutant Kras-G12D allele, which increases the aggressiveness and metastatic capacity of cancer cells, resulting in metastases in lungs, liver and lymph nodes.* ***B*** *Nsun5 mRNA levels analyzed by RT-qPCR in NPK; Nsun5^{+/+} and NPK; Nsun5^{+/-} mice.* ***C*** *Representative images of the three prostate lobes extracted from NPK; Nsun5^{+/+} and NPK; Nsun5^{+/-} mice.* ***D*** *Volume of the ventral (VP), dorsolateral (DLP) and anterior (AP) prostate lobes extracted from NPK; Nsun5^{+/+} and NPK; Nsun5^{+/-} mice. n = 7 NPK; Nsun5^{+/+} and 8 PNK; Nsun5^{+/-}.* ***E*** *Weight of the prostate lobes extracted from PNK; Nsun5^{+/+} and PNK; Nsun5^{+/-} mice. n = 7 PNK; Nsun5^{+/+} and 8 PNK; Nsun5^{+/-}.*

Metastatic prostate cancer has been successfully modeled in mice by Professor Abate Shen laboratory (Columbia University, USA) [442]. This model is based in the concomitant mutation of *Kras* (G12D mutation) and the deletion of *Pten,* which not only leads to the development of prostate tumors but also enables the migration of tumor cells towards lymph nodes, lungs, liver, pancreas and kidney [442]. Importantly, the deletion of *Pten* and expression of the mutant *Kras* occurs upon recombination by a tamoxifen-inducible Cre recombinase that is expressed under the promoter of *Nkx3.1*, a gene exclusively expressed in prostatic epithelium. This *Nkx3.1*[CreERT2]; *Pten*[flox/flox]; *Kras*[LSL-G12D/+] metastatic prostate cancer mouse model (hereafter referred to as "NPK") starts developing aggressive prostate tumors that later metastasize to different organs after tamoxifen induction at 8 weeks-old (Figure 41A). Finally, 16 weeks after induction, mice are sacrificed and prostate tumors, lungs, liver, kidneys, and lymph nodes collected for further analysis.

To evaluate the role of Nsun5 in the development of metastatic prostate cancer, NPK mice were crossed with the previously described *Nsun5*^{-/-} mouse model. As in the *Pten*[flox/flox]; *PB-Cre*^{+/-} model, no *Nsun5*^{-/-} mice were obtained after crossing with the NPK model. Consequently, the role of Nsun5 in metastatic prostate cancer development was evaluated using *Nsun5*^{+/-} mice. The expression of *Nsun5* mRNA in control NPK and NPK; *Nsun5*^{+/-} mice was evaluated by RT-qPCR. Results showed an overall reduction in *Nsun5* mRNA levels that nearly reached statistical significance and was sufficient to evaluate the role of Nsun5 in the development of metastatic prostate cancer (Figure 41B).
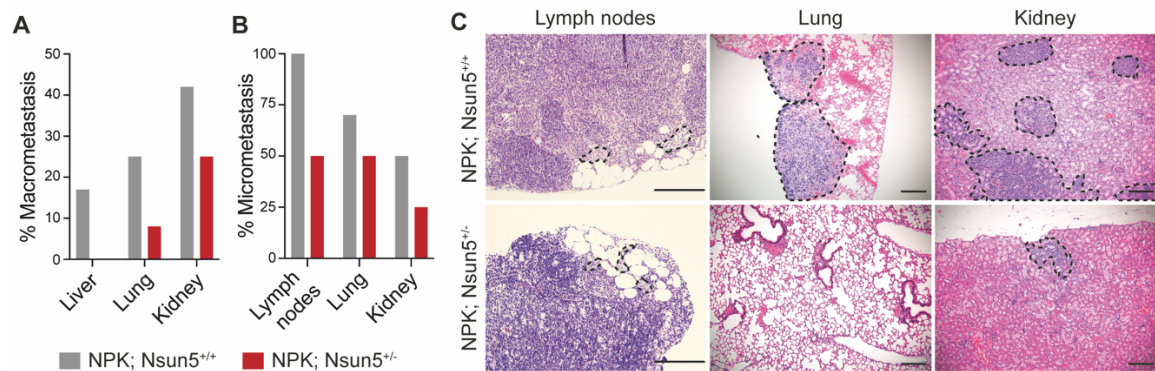
Figure 42. *Percentage of organs with macrometastasis (**A**) micrometastasis (**B**) in NPK; Nsun5*^{+/+} *and NPK; Nsun5*^{+/-} *mice. **C** Representative images of hematoxylin-eosin staining of lymph nodes, lungs and kidneys of NPK; Nsun5*^{+/+} *and NPK; Nsun5*^{+/-}. *Micrometastasis are indicated with a black dashed line. Scale bar represents 100 μm.*

Despite the depletion of *Nsun5* caused no effect on the development of primary prostate tumors in the *Pten*-KO model, we assessed the weight and volume of the primary prostate tumors in the NPK model with reduced *Nsun5* expression. Similarly to the *Pten*-KO model, lower *Nsun5* expression had no impact on the development of primary tumors in the NPK model, as evidenced by the similar weight and volume observed between the NPK; *Nsun5*^{+/+} and NPK; *Nsun5*^{+/-} mice (Figure 41C-E). Importantly, *Nsun5* reduced expression significantly impaired the production of macrometastasis

in liver, lungs and kidney (Figure 42A) and micrometastasis in lymph nodes, lungs and kidneys of NPK mice (Figure 42B, C).

Altogether, these results indicate that a high *Nsun5* expression is not essential for cell and tumor growth in the initial tumor stages but is crucial for cancer cells in advanced stages.

NSUN5 is crucial for cell migration

The results obtained in our metastatic prostate cancer *in vivo* model strongly suggest that NSUN5 might play essential roles in metastasis. To investigate the role of NSUN5 in cell migration, a crucial process in the development of metastasis, we took advantage of different *in vitro* techniques. Firstly, time-lapse movies were recorded to directly evaluate cell migration in our *NSUN5*-KD PC3 cells (Figure 43A). Manual tracking of individual cells and calculation of cell velocity and travelled distance using Fiji revealed that *NSUN5*-KD cells migrate significantly slower (Figure 43B) and cover much shorter distances (Figure 43C) compared to the control cells.
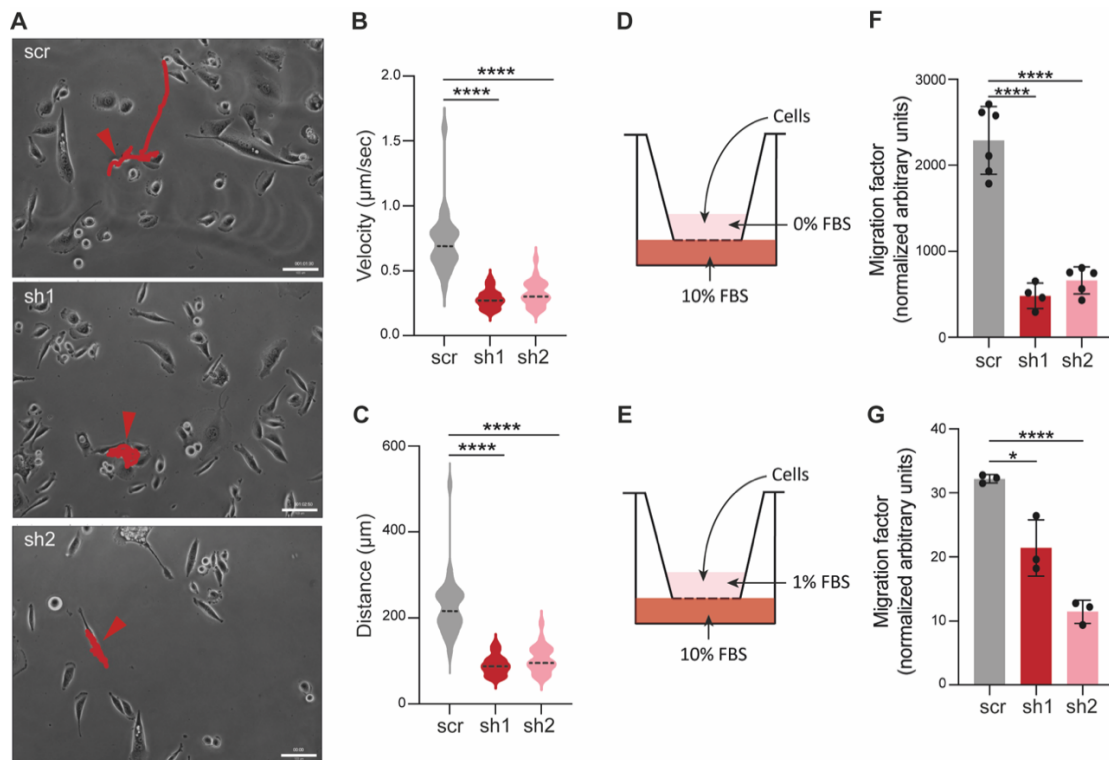

*Figure 43. Role of NSUN5 in cell migration. **A** Representative end-point images of the time-lapse movies recorded. Red lines represent the tracks of single cells. Arrowhead indicates the cells analyzed. **B, C** Velocity (**B**) and distance (**C**) travelled by the cells measured by manual tracking using Fiji. Data is represented as means ± SD, n = 30 cells. Statistical analysis was performed using one-way ANOVA (**** p < 0.0001). **D, E** Schematic representation of the experimental set up Boyden chamber assays performed. Cells migrated from an upper chamber containing serum-free medium (**D**) or medium containing 1% of FBS (**E**) to lower chambers containing medium supplemented with 10% of FBS. **F** Normalized number of cells that migrated from the upper chamber containing serum-free medium to the lower chamber. Data is represented as means ± SD, n = 6 replicates. Statistical analysis was performed using one-way ANOVA (**** p < 0.0001). **G** Normalized number of cells that migrated from the upper chamber containing medium supplemented with 1% of FBS to the lower chamber. Data is represented as means ± SD, n = 6 replicates. Statistical analysis was performed using one-way ANOVA (* p < 0.05, **** p < 0.0001).*

Next, migration capacity was assessed using Boyden chamber assays. In these assays, cells are seeded in an upper chamber with a minimal nutrient supply, such as serum-free medium (Figure 43D) or medium containing 1% of FBS (Figure 43E). This upper chamber is connected by a porous membrane to a lower chamber, in which a chemoattractant is located. In our approach, medium containing 10% of FBS served as chemoattractant to facilitate cell migration in both conditions. Results of the Boyden chamber assays demonstrated that *NSUN5*-KD cells migrate significantly less than the control cells under both conditions (Figure 43F, G).

In summary, *NSUN5* depletion leads to a significant impartment of cell migration. This correlate with the results observed *in vivo* and indicate that NSUN5 expression is essential for facilitating tumor metastasis.

Discussion

Discussion

Proper ribosome function is essential to maintain the cellular demands for protein synthesis. Increased ribosome biogenesis and protein synthesis have been traditionally considered to be essential and sufficient to sustain tumor growth [72, 443, 444]. However, dozens of studies in the past decade have stablished that both quantitative and qualitative changes in ribosomes can result in variations in the translation process, potentially leading to cancer development [72, 152, 445]. Such is the case of the heterozygous loss or mutations of ribosomal proteins, which produce aberrant ribosomes [446, 447]. These aberrant ribosomes are able to bypass quality control mechanisms leading to altered protein synthesis and translational infidelity, eventually supporting cancer progression [447]. rRNA chemical modifications are also known to affect cell proliferation and tumorigenesis by impacting both ribosome biogenesis and function, favoring the translation of oncogenes or impairing the translation of tumor suppressors [149, 152, 158, 162]. Herein we describe the role of NSUN5, the m^5C methyltransferase responsible for methylating position m^5C3782 of human ribosomes, in regulating protein synthesis, cell proliferation and cell cycle progression, as well as its potential role as therapeutic target in cancer.

In our model, NSUN5 is expressed in the nucleolus as previously reported [181]. Moreover, rRNA transcription inhibition, which leads to the reorganization of nucleoli and the formation of the nucleolar caps, does not result in the translocation of NSUN5 protein to the nucleolar caps. This indicates that NSUN5 is located in the granular component of the nucleolus and suggest that its activity takes place during the later phases of ribosome biogenesis. This observation aligns with other studies proposing that, while most 2'-O-me and Ψ occur co-transcriptionally to allow the binding of the guide snoRNAs, stand-alone enzymes responsible for depositing base modifications act in later stages, although exact timing remains elusive in most cases. For instance, WBSCR22-mediated m^7G methylation occurs in the nucleoplasm, during very late steps of ribosome biogenesis [29, 92]. Similarly, DIMTL1, which deposits m^6_2A1850 and m^6_2A1851, also methylates the SSU in the nucleoplasm after WBSCR22-mediated methylation and just before pre-18S rRNA is exported to the cytoplasm [29].

Through loss-of-function approaches using shRNA-mediated knockdown and CRISPR/Cas9-mediated knockout, we show that ribosome biogenesis remains unaffected when NSUN5 expression is depleted. This finding is consistent with previous reports in yeast and human cells demonstrating that NSUN5 loss does not alter ribosome biogenesis [6, 88, 181]. Notably, this is not a unique characteristic of NSUN5, as other rRNA methyltransferases and their methylations, such as ZCCHC4 and the m^6A4220 on 28S rRNA, have also been reported to be dispensable for ribosome biogenesis but essential for other ribosomal functions [135].

Interestingly, our *NSUN5*-depleted cells exhibit a significant deregulation of protein synthesis, resulting in an increased rate of bulk protein synthesis that is independent of the cell cycle phase. Conversely, previous studies in *NSUN5*-KO HeLa cells and mouse embryonic fibroblast (MEFs) indicated a tendency towards reduced global protein synthesis upon *NSUN5* loss, although no changes were observed *in vivo* in different organs from *Nsun5*$^{-/-}$ mice [181]. Additionally, our *NSUN5*-depleted cells recover normal protein synthesis rates much faster than control cells after treatment with NaAsO$_2$, suggesting that they are more resistant to oxidative stress. These findings are consistent with previous reports in *S. cerevisiae*, *D. melanogaster* and *C. elegans* demonstrating that the depletion of their respective *NSUN5* homologs leads to increase resistance to oxidative stress and heat shock, demonstrating that *NSUN5* loss confers stress resistance in a conserved manner [191]. However, these results differ from those observed in glioblastoma cell lines, where oxidative stress induced by exposure to hydrogen peroxide (H$_2$O$_2$) leads to a more pronounced decline in global protein synthesis rates in cells with epigenetic silencing of *NSUN5* compared to those cells that normally express *NSUN5* [6]. These differences could indicate that NSUN5 function is cell type- or tumor-dependent. This is not uncommon as other methyltransferases, such as the m^{6}A methyltransferases METTL3 and METTL14, have shown to play different roles depending on the tumor type [351, 448-451]. For instance, METTL14 promotes metastasis in pancreatic cancer but suppress the same process in hepatocellular carcinoma [351, 451]. Furthermore, differences may also arise from the different source of oxidative stress. In fact, studies in yeast suggest that NaAsO$_2$ and H$_2$O$_2$ activate different protein sensors and elicit different biological responses [452]. Although this effect has not been studied in mammals, we cannot rule out that some of the variability might be caused by the different stressor applied.

Through the analysis of the nascent proteome, we find that *NSUN5*-depleted cells exhibit enhanced synthesis of a specific pool of proteins. Remarkably, this process is regulated at translational level, suggesting that m^{5}C-deficient ribosomes selectively translate specific mRNAs, primarily related to ribosome biogenesis, mitotic regulation and catabolic processes.

Within the ribosome biogenesis category, upregulated proteins included ribosome biogenesis factors and RPs related to both LSU (60%) and SSU (40%). Although no significant differences in ribosome biogenesis were observed by northern blot, it is possible that cells are favoring the synthesis of RPs and ribosome biogenesis factors in an attempt to increase the number of ribosomes to support the elevated protein synthesis rates or to compensate for the presence of defective ribosomes.

Another significant pathway affected in *NSUN5*-depleted cells is mitosis. Terms such as "negative regulation of chromosome organization", "negative regulation of cell population proliferation" and "regulation of mitotic nuclear division" were significantly enriched among the proteins

preferentially translated by the *NSUN5*-KD cells. We validated the overexpression of GCP2 and ZNF207, which are cell cycle-related, through both proteomic analysis and Western blot in at least one of the *NSUN5*-KD cell lines. GCP2 is necessary for microtubule nucleation at the centrosome and mitotic spindle assembly and its deregulation might indicate alterations in mitotic spindle formation [415]. ZNF207, also known as BuGZ, presents several splicing variants with diverse functions. The longer isoform (isoform C) has been reported as dominant in stem cells, where it interacts with master transcription factors to control the transcription of key genes necessary to maintain self-renewal. In contrast, the shorter isoform (isoform B) interacts with Bub3 [416] and facilitates its loading into the kinetochore to regulate proper chromosome alignment [417]. Intriguingly, Western blot analysis reveals that isoform B is more expressed in *NSUN5*-KD cells while isoform C predominates in control cells, suggesting that *NSUN5*-KD cells may show misaligned chromosomes and mitotic exit delay.

Furthermore, cyclin B1 was also found overexpressed in *NSUN5*-KD cells. Continuous expression of Cyclin B can lead to cell cycle arrest, as its degradation is essential for mitotic exit [274, 453], and has also been linked to increased cell death [454]. Moreover, many other cell cycle-related proteins, particularly those related with mitotic spindle, showed expression deregulation in the nascent proteome of *NSUN5*-KD cells. For instance, the A-Kinase Anchoring Protein 9 (AKAP9), required for the association of centrosomes with the poles of the mitotic spindle [455], was downregulated in *NSUN5*-KD cells. Conversely, kinetochore-related proteins like Regulator of chromosome condensation (RCC1), Centromere-kinetochore protein zw10 homolog (ZW10) and Small kinetochore-associated protein (KNSTRN) were upregulated. Additionally, Peptidyl-prolyl cis-trans isomerase NIMA-interacting 1 (PIN1) was significatively upregulated. PIN1 is known to regulate CDK2 activity by promoting the degradation of Cyclin E and the stabilization of the inhibitor p27 [456, 457]. PIN1 also regulates G2/M phase transition by modulating CDC25C and Wee1 activity [458]. Consistently, ribosome profiling analysis in GBM cells have reported a significant increase in the translation efficiency of cell cycle-related genes in *NSUN5*-deficient cells [6], further underscoring the essential role of NSUN5 regulation in the synthesis of cell cycle regulators.

Therefore, this data demonstrates that both negative and positive cell cycle regulators are upregulated in NSUN5-depleated cells. Although this might seem counterintuitive, it probably indicates a profound deregulation in the control of the expression of cell cycle-related proteins in the absence of NSUN5, and thus a deregulation of the cell cycle progression, especially at G2/M.

Notably, other terms significantly enriched among the overexpressed proteins in *NSUN5*-KD are related to the negative regulation of proteasomal catabolic processes. Proteasomal function is essential for cell cycle progression as it is necessary to maintain the cyclic expression of cell cycle

regulators [274, 294]. Thus, abnormal functioning of this crucial process might also contribute to a deregulated cell cycle progression. Both proteomic analysis and Western blot showed altered expression of the subunit beta 7 of proteasome 20S (PSMB7), suggesting a deregulation of the proteasome. Furthermore, other proteins related with protein degradation, such as the E3 ubiquitin ligase MARH7 and the proteasome regulatory particle UBXN1, were also significantly altered in *NSUN5*-KD cells, further indicating the disruption of this essential pathway.

Consistent with the results from the analysis of the nascent proteome, *NSUN5*-KD and *NSUN5*-KO cells exhibit lower proliferation rates and decreased colony formation capacity, indicating that these cells are less proliferative than control cells. As expected, due to the deregulated expression of mitotic regulators, we found that the decreased proliferation rate is, at least in part, attributed to an altered progression through the cell cycle, resulting in a delayed progression of *NSUN5*-depleted cells through S and G2/M phases. Similar reductions in proliferation rates upon *NSUN5* depletion have been observed in ccRCC, LIHC, CRC and GC *in vitro* and in xenograft models [224-226, 459]. Notably, *NSUN5* loss has been reported to impair CRC tumor growth by triggering cell cycle arrest due to a reduced Rb phosphorylation and expression of CDK4, CDK6 and cyclin E [226]. Conversely, *NSUN5* depletion in our model alters expression of proteins mainly related with mitosis, which might indicate that NSUN5 regulation of cell cycle is tumor- or context-dependent.

Other studies have found that *NSUN5* downregulation leads to reduced tumor growth through p53 pathway activation [224]. However, we do not observe p53 activation upon *NSUN5* depletion in several cell lines, suggesting *NSUN5* loss does not activate the p53 response caused by ribosome biogenesis alterations that ultimately lead to cell cycle arrest [270, 271], but rather regulates cell cycle through other mechanisms.

Consistent with the role of NSUN5 in cell cycle control, we describe a phosphorylation occurring in NSUN5 during M phase, which is mediated by CDK1/Cyclin B complex. Importantly, this phosphorylation leads to NSUN5 degradation, which could be a mechanism for NSUN5 regulation during this phase. Ribosome biogenesis is maximal in the S and G2 phases, but it is inhibited during mitosis due to the CDK1-mediated phosphorylation of Pol [460, 461]. Accordingly, NSUN5 expression is increased during S phase, which could be necessary to methylate an increasing number of ribosomes. Then, NSUN5 is phosphorylated during M phase by CDK1, destabilizing the enzyme. It is possible that the phosphorylation of Pol I and NSUN5 co-occur in time leading to the inactivation of both enzymes, which might open a small window of time during which ribosomes being assembled at the onset of mitosis might lack NSUN5-mediated m^{5}C methylation.

Protein synthesis during M phase has traditionally been thought to be strongly repressed. However, recent studies suggest that high levels of protein synthesis are maintained, especially during early

stages of mitosis, which might be crucial for sustaining the expression of regulators that are essential for mitosis completion, especially those with short half-lives [285]. Therefore, phosphorylation could be a physiological mechanism to reduce NSUN5 expression during M phase, allowing the assembly of non-methylated ribosomes, that would help mitotic cells to maintain high levels of protein synthesis and to specifically promote the synthesis of mitotic regulators. The precise mechanism by which m^5C3782-deficient ribosomes might specifically select these mRNAs remains to be elucidated. Mitotic regulators and RPs often exhibit IRES and 5' terminal oligopyrimidine tract (5'TOP) in their mRNAs, respectively [291, 462], which could be a potential method for m^5C3782-deficient ribosomes to select these mRNAs. Future translation analysis, such as ribosome profiling, may shed light on these selection mechanisms.

While S327 phosphorylation does not reside in the catalytic pocket of NSUN5, it is possible that it may inhibit its catalytic activity or RNA binding capacity. NSUN5 protein is normally confined to the nucleoli and nucleus of the cell. However, at the onset of mitosis, the nuclear membrane is disrupted, and nucleoli disassemble, releasing NSUN5 into the nucleoplasm and making other potential targets accessible. Thus, this phosphorylation could prevent unspecific activity of NSUN5 during this phase. Additionally, this phosphorylation could also act as modulator of protein-protein interactions. For instance, NSUN2 phosphorylation by Aurora-B inhibits NSUN2 catalytic activity, leading to its release from NMP1 and binding to the mitotic spindle [244]. Although NSUN5 has not been observed to bind the mitotic spindle, other possible interactions might occur, especially during M phase, when NSUN5 is free in the cytoplasm. These potential functions remain to be explored but could also play a role in NSUN5-mediated cell cycle regulation.

It is conceivable that NSUN5 might have other RNA targets that could play a significant role in the NSUN5-mediated cellular response. Despite being located in the subunit interface, m^5C3782 might not be easily accessible for further modification after LSU subunit maturation. Additionally, NSUN5 regulation at nucleolar level might yield ribosomes with varying degrees of methylation, but the effects of such changes would be slower, likely related to long-term cellular responses. On the contrary, the methylation of less structured RNAs such as mRNAs or lncRNAs would likely be more accessible for NSUN5-mediated methylation, potentially leading to faster cellular responses. Although this potential methylation of other RNAs can occur in the nucleus, the disruption of nucleoli and nucleus during the M phase could facilitate NSUN5 access to an even broader range of substrates. To date, NSUN5 has only been reported to methylate rRNAs. However, there has been no comprehensive analysis to elucidate whether NSUN5 has other RNA targets. Exploring this possibility could provide valuable insights into how the loss of *NSUN5* alters the cell cycle progression more broadly.

The observed changes in protein synthesis leading to specific translation of mitotic regulators and ribosomal proteins in m^5C3782-deficient ribosomes are consistent with recent studies describing ribosomes as heterogeneous entities. Traditionally, ribosomes have been seen as mere machines in charge of protein synthesis, all of them having identical composition and structures. However, a growing body of evidence suggest that ribosomes play an active role in regulation of translation. Thus, ribosomes exhibiting variations in their RPs, the post-translational modifications in their RPs and the post-transcriptional modifications on their rRNAs have been found [99, 100, 162, 292]. Importantly, these ribosomes, known as "heterogeneous ribosomes" or "specialized ribosomes", have shown the ability to selectively translate different pools of mRNAs, thereby contributing to creation of distinct translational programs within cells [97].

While position C3782 of 28S rRNA has been largely though to be 100% methylated, this perception may have been influenced by the extensive use of highly proliferative cell lines, typically cancer cells and immortalized MEFs, in the study of ribosome methylation. Similarly, tumors, characterized by an aberrant proliferation, often exhibit high NSUN5 expression [224-226, 240] and potentially high levels of methylation. However, in healthy tissues, NSUN5 expression varies depending on their proliferative potential, meaning that the rRNA methylation could vary between different tissues. For example, organs with low proliferative potential, like the liver, which in turn express lower levels of NSUN5, exhibit substoichiometric m^5C3782 methylation in mice [181]. In such tissues, non-methylated ribosomes could potentially behave differently, possibly modulating the translational program to adapt it to a less proliferative state. However, further research is needed to fully understand how NSUN5 levels are regulated in healthy tissues and whether this contributes to expression regulation.

Notably, NSUN5-mediated methylation is located in a very important functional area of the ribosome: the subunit interface. Moreover, m^5C3782 directly interacts with the ribosomal protein eL41, a small protein that forms the eukaryotic-specific bridge eB14 [61]. eB14 is the only eukaryotic-specific bridge located in the center of the subunit interface and acts as a pivot for SSU rotation during translation [239]. Our structural study indicates that m^5C3782 methylation is crucial to maintain 80S ribosome stability, probably by interacting with the bridge eB14. Loss of this bridge in yeast results in decreased peptidyl transferase activity but increased ribosome translocation [69], highlighting its importance for ribosome function. Importantly, this bridge is also contacted by other three base methylations in the SSU: ac^4C1337, m^6_2A1850 and m^6_2A1851, which lay in the proximity of the DCC [61]. It has been proposed that these four modifications, together with the eB14 bridge, may be involved in the transmission of allosteric information between subunits [25]. Thus, alterations of these modifications could be sensed by the ribosome, contributing to the regulation of translation efficiency.

However, it is essential to consider that due to the ribosome purification method used in our study, 80S particles lose the mRNA and most of the tRNAs, except for the E-site tRNA, which could also affect the stability. Structural studies of more "native" ribosomes purified with other methods such as gel filtration, known to preserve tRNAs and mRNAs, would provide a better assessment of ribosomal stability in the absence of m^{5}C3782. Moreover, other approaches, such as dissociation studies in varying Mg^{2+} concentrations or bimolecular fluorescence complementation (BiFC) as a reporter of subunit joining [463], may offer additional insights into ribosomal behavior upon m^{5}C3782 loss.

Furthermore, we show that NSUN5 is also overexpressed in hepatocellular carcinoma and cholangiocarcinoma and can be used as prognostic marker for prostate cancer and hepatocellular carcinoma. Importantly, our *in vitro* and *in vivo* findings suggest that NSUN5 could serve as therapeutic target. On one hand, inhibiting NSUN5 alone might prevent tumors from progressing to a metastatic state by inhibiting the migratory capacity of the cells. On the other hand, our results indicate that NSUN5 loss results in delayed mitosis and aberrant expression of components of the mitotic spindle, potentially leading to impaired chromosomal alignment and segregation. Consequently, combining NSUN5 inhibition with mitotic checkpoint inhibitors could induce premature chromosome segregation resulting in mitotic catastrophe and cell death [464]. Moreover, further alteration of cell cycle progression might also produce a cumulative effect. Importantly, CDK4/6 inhibitors have been demonstrated to improve the survival of breast cancer patients, although most of them eventually develop resistance [331, 334]. These inhibitors have demonstrated to produce accumulation of genomic instability and aberrant chromosome segregation [465, 466]. Therefore, further manipulation of the mitotic process, particularly mitotic spindle formation, as observed upon NSUN5 inhibition, might increase cell death.

Notably, while no specific inhibitor of NSUN5 or other m^{5}C RNA methyltransferase has been developed to date, significant efforts are underway to develop RNA methyltransferase inhibitors. This is exemplified by the recent development of a small molecule inhibitor of METTL3, which has shown promising preclinical results, and has advanced to clinical trials [167]. Hopefully, this will pave the way for the development of specific inhibitors targeting other RNA methyltransferases.

Despite our findings that NSUN5 is overexpressed in cancer and that it regulates cell cycle progression *in vitro*, loss of *Nsun5* does not result in a reduction in the tumorigenic capacity of prostate cancer cells *in vivo*. This discrepancy might be attributed to the much more complex environment encountered *in vivo*, where tumor cells interact with the tumor microenvironment and grow in less favorable conditions. Additionally, it is important to note that we could not evaluate the tumor growth in the complete absence of *Nsun5*. Despite observing nearly a 50% reduction in

Nsun5 expression, it is possible that the residual levels of Nsun5 are sufficient to carry out its critical functions, preventing the emergence of a visible phenotype.

However, a noteworthy finding is that *Nsun5* depletion leads to a reduced metastatic potential of the prostate cancer tumors *in vivo*. This is in accordance with *NSUN5* expression in prostate cancer patients, which is particularly high in those patients with metastatic disease, and suggests that NSUN5 overexpression may be pivotal in conferring metastatic capacity to tumor cells. Accordingly, cell migration is impaired in *NSUN5*-depleted cells *in vitro*. Similarly, loss m^{5}C methylation on mt-tRNAs, which is mediated by NSUN3, impairs metastasis but does not affect cell viability or primary tumor growth [189].

Importantly, the cell cycle, ribosome biogenesis, protein synthesis and metastasis have been demonstrated to be highly interconnected. The EMT process is characterized by a cell cycle arrest in G1/S phase and increased rDNA transcription [467]. Importantly, during this cell cycle arrest in G1/S, global protein synthesis is inhibited while the translation of specific mesenchymal markers is promoted, contributing to migration and invasion. These findings support the idea that "specialized ribosomes" may exist during each cell cycle phase, which would favor different cellular processes. NSUN5 may participate in this regulatory mechanism by modulating protein synthesis rates while favoring selective translation, and by modulating the cell cycle progression. For instance, loss of *NSUN5* produces a different subset of ribosomes that are specialized in translating mitotic regulators but inefficiently translate proteins related with cell adhesion and polarized cell movement, such as AKAP9 [468], desmocollin 1 (DSC1) [469] and the Alpha-2-Glycoprotein 1, Zinc-Binding (ZAG2) [470], which were found downregulated in the nascent proteome of *NSUN5*-KD cells. Suggesting that high NSUN5 expression may be necessary during EMT process to allow the translation shift to a more migratory phenotype. However, how NSUN5 expression is regulated during EMT and its exact contribution to this process remains largely unknown and needs further investigation.

In summary, we have unveiled that NSUN5 regulates cell proliferation by modulating the cell cycle progression. Mechanistically, loss of NSUN5-mediated methylation activates a translational program that promotes the synthesis of mitotic regulators, leading to cell cycle arrest in G2/M phase. Additionally, we have identified NSUN5 as a novel CDK1 target. CDK1-mediated phosphorylation destabilizes NSUN5, potentially allowing the assembly of non-methylated ribosomes and activating a mitotic-specific translational program. Our *in silico* analysis of expression databases reveals that *NSUN5* is overexpressed in prostate cancer, hepatocellular carcinoma and cholangiocarcinoma patients and can be used as a marker for poor prognosis. Interestingly, *Nsun5* loss in vivo did not reduce tumorigenic capacity but impaired the metastatic

potential of prostate cancer cells, suggesting that targeting NSUN5 could inhibit the spread of prostate cancer cells.
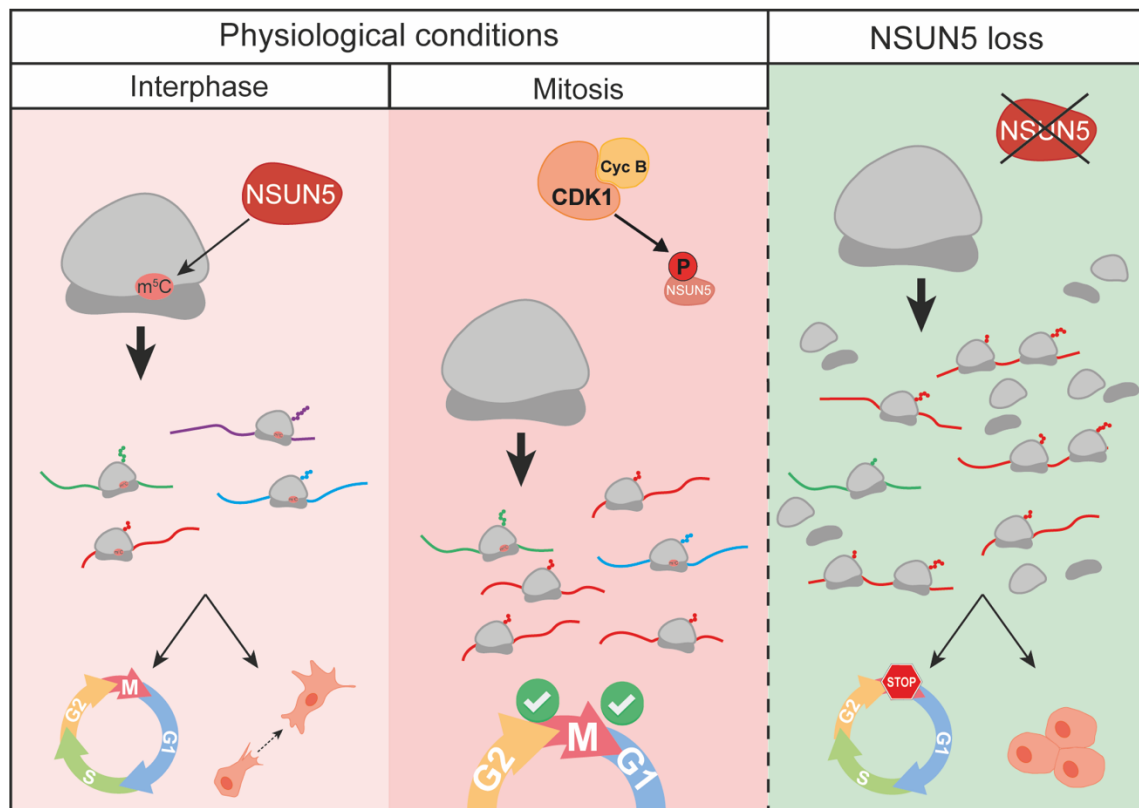
Graphical summary

Figure 44. Schematic representations of the molecular mechanism driving NSUN5-mediated regulation of protein synthesis, cell cycle and migration. In control conditions, NSUN5 methylates the ribosome during interphase, allowing normal protein synthesis, which ensures proper cell cycle progression and migration. Then, during mitosis, CDK1 phosphorylates NSUN5, destabilizing it and avoiding ribosome methylation. This induces the translation of mitotic regulators and allows the completion of the mitosis. In the absence of NSUN5, ribosomes are not methylated. This lack of methylation makes ribosome association less stable, but increases the processivity of those ribosomes that engage in translation. Moreover, these ribosomes specifically select mRNAs encoding for cell cycle regulators, leading to their aberrant expression, which results in cell cycle arrest and impaired migrations of cancer cells.

Conclusions

Conclusions

In conclusion, our study reveals critical insights into the role of NSUN5 and NSUN5-mediated methylation in maintaining ribosome structure, association, or binding, and in regulating protein synthesis, ultimately supporting normal cell function. These findings contribute to our understanding on how rRNA modifications and ribosomal functions are regulated along cell cycle and point to NSUN5 as a potential therapeutic target in advanced metastatic cancers.

Thus, the data obtained in this study lead to the following conclusions:

I. Loss of the m^5C rRNA methyltransferase NSUN5 does not alter rDNA transcription or the processing of the rRNAs.

II. Loss of m^5C3782 destabilizes the 80S ribosomes, leading to increased ribosome dissociation. Moreover, lack of this methylation alters the structure of the ribosome producing a shift in the position of the helix H70 at the subunit interface.

III. *NSUN5* depletion enhances global protein synthesis rates of cancer cells and facilitates the recovery of protein synthesis rates from stress-induced translation inhibition.

IV. *NSUN5* depletion specifically promotes the translation of mRNAs encoding ribosomal proteins and mitotic regulators.

V. Reduced *NSUN5* expression impairs cancer cell proliferation by causing G2/M cell cycle arrest in a p53-independent manner *in vitro*.

VI. CDK1 phosphorylates NSUN5 during mitosis, leading to the destabilization of the methyltransferase.

VII. *NSUN5* is ubiquitously expressed in healthy tissues, with expression levels positively correlating with the proliferative potential of the tissue.

VIII. *NSUN5* is overexpressed in tumors derived from both highly proliferative tissues, such as prostate adenocarcinoma, and tissues with low proliferation rates, such as hepatocellular carcinoma and cholangiocarcinoma, especially in advanced stages, and its upregulation correlates with a higher risk of recurrence.

IX. *Nsun5* depletion does not impair the formation and growth of primary tumors in a prostate cancer murine model but negatively impacts the metastatic capacity of prostate cancer cells.

X. *NSUN5* depletion impairs the migratory capacity of metastatic prostate cancer cells *in vitro*.

Material and methods

Material and methods

Cell culture and treatments

PC3, DU145, 22Rv1, BPH-1 and 293FT cells were provided by Prof A Carracedo (CIC bioGUNE, Spain). A549 cells were provided by Prof P. A. Lazo (CIC, Spain). 293FT, PC3, DU145 and A549 cells were maintained in DMEM (Gibco) supplemented with 10% FBS (Gibco) and 100 U/ml of penicillin and 100 µg/ml of streptomycin (Gibco). 22Rv1 and BPH-1 cells were cultured in RPMI medium (Gibco) supplemented with 10% FBS, 100 U/ml of penicillin and 100 µg/ml of streptomycin. All cells were kept in a humidified atmosphere at 37ºC and 5% CO_2. Cells were tested monthly for mycoplasma by PCR and maintained mycoplasma-free. To perform passages, cells were dissociated using 0.25% Trypsin-EDTA (Gibco).

When CDK1 inhibition was needed, cells were treated with 10 µM of the CDK1-specific inhibitor RO-3306 (Sigma) for 16 hours. To analyze protein stability, cells were treated with 60 µg/ml of cycloheximide (Santa Cruz Biotechnology) for up to 36 hours.

Cloning and site-directed mutagenesis

NSUN5 cDNA was cloned into the puromycin-resistant pTRIPZ vector modified by Dr James D. Sutherland (CIC bioGUNE, Spain) in order to express cDNA. *NSUN5* cDNA encoding for a wild-type or catalytically inactive version of NSUN5 was obtained from pCMV6-Entry plasmids kindly provided by Prof Michaela Frye (DKFZ, Germany). Both *NSUN5* cDNAs were amplified using specific primers (Table 3) and Q5 high-fidelity DNA polymerase (New England Biolabs) following manufacturer's instructions. In addition, Rv primers contained the sequence encoding for a Flag tag (Protein sequence: DYKDDDDK; DNA sequence: GACTACAAAGACGATGACGACAAG). PCR product was gel-purified, digested with EcoRI and AgeI and ligated using T4 DNA ligase (Thermo Fisher Scientific) into a pTRIPZ vector that was previously linearized by using the same restriction enzymes. The resulting plasmids were used to transform DH5-α *E. coli* bacteria. Colonies were picked and grown in LB medium containing 100 µg/ml of ampicilin (Sigma). Plasmidic DNA was isolated using GeneJET Plasmid Maxiprep Kit (Thermo Fisher Scientific) and sequenced by Sanger method to confirm proper insertion.

NSUN5 phosphorylation site was mutated using the Q5 site-directed mutagenesis kit (New England Biolabs) in the pCMV6-NSUN5-Myc-DDK plasmid. Both phosphomimic (S327D) and a phosphonull (S327A) forms of NSUN5 were generated. To achieve this, the codon encoding for serine 327 was identified and primers containing the desired base changes were designed using NEBaseChanger tool (Table 3).

PCR amplification was set up using 10 ng of pCMV6-NSUN5-Myc-DDK plasmid as template, 500 nM of each primer and 1X Q5 Hot Start High-Fidelity MasterMix. PCR reaction was carried out in a C1000 Touch thermal cycler (Bio-Rad). The cycling conditions were as follows: 98ºC for 30 s followed by 25 cycles of 98ºC for 10 s, 60ºC for 20 s and 72ºC for 1 min. A final elongation step was performed at 72ºC for 2 min. Then, kinase, ligase and DpnI (KDL) treatment included in the Q5 site-directed mutagenesis kit was performed for 5 min following manufacturer's instructions. 5 µl of KDL reaction product was used to transform chemically-competent NEB 5-alpha *E. coli* bacteria (New England Biolabs). Colonies were picked and grown in LB medium containing 50 µg/ml of kanamycin (Santa Cruz Biotechnology). Plasmidic DNA was isolated using GeneJET Plasmid Maxiprep Kit and sequenced to confirm mutation by Sanger method.

Table 3. *Primers used for site-directed mutagenesis and conventional PCR.*

Primer	Forward primer sequence (5'-3')	Reverse primer sequence (5'-3')	Use
NSUN5-Flag	TCCACCGGTACCATGGGGCTGTATGCTGCAG	TCCACGCGTTCACTTGTCGTCATCGTCTTTGTAGTCTGTGCAAGGCGGTGTGCAA	NSUN5-Flag cloning
NSUN5-S327A	GGCAGGCACACCTGCCCCGGTGCGTCTGCATGCCC	GGGCATGCAGACGCACCGGGGCAGGTGTGCCTGCC	Site-directed mutagenesis
NSUN5-S327D	GGCAGGCACACCTGACCCGGTGCGTCTGCATGCCC	GGGCATGCAGACGCACCGGGTCAGGTGTGCCTGCC	Site-directed mutagenesis
NSUN5-KO	CTGGCGTCTCTTGCTGTGA	TTCTGCTGCAGCGCATCTC	NSUN5-KO screening
m^{5}C3782	AATGAAGTGTGGGTAAATGG	AAATAAAAACAATAAAAATCTCAT	Bisulfite-PCR

Generation of stable cell lines expressing shRNAs or doxycycline-inducible NSUN5

To generate constitutively silenced cells using *NSUN5*-specific short-hairpin RNAs, constitutively shRNAs-expressing and puromycin-resistant pLKO.1 lentiviral plasmids were obtained from MISSION shRNA library (Sigma). A pLKO.1 plasmid containing a scramble sequence was used as control [471].

To generate stable cell lines expressing a doxycycline-inducible version of NSUN5, a doxycycline-inducible and puromycin-resistant pTRIPZ lentiviral vector was used. 293FT cells were used as lentiviral particles packaging cell line. Specific third- (pRRE, pREV and pVSV-G) or second-generation (pTAT, psPAX2 and pVSV-G) packaging plasmids were transfected along with the pLKO.1 or pTRIPZ vectors into the 293FT cells using JetPEI transfection reagent (Polyplus) according to manufacturer's instructions. Lentiviral particles were collected after 48 and 72 hours from the cell medium and concentrated using Lenti-X concentrator (Takara Bio) according to the

manufacturer's protocol. Concentrated virus were then resuspended in 300 µl of DMEM and conserved at -80ºC. Concentrated virus were added to the target cells together with 8 µg/ml of protamine sulfate (Sigma) as transduction enhancer. After a 24-hour incubation, cells were selected using 2 µg/ml of puromycin (Sigma) for 48 hours. Expression of the flag-tagged version of NSUN5 was induced with 0.25 µg/ml of doxycycline for at least 48 hours. The overexpression and silencing of NSUN5 were tested by RT-qPCR and western blot.

Generation of NSUN5-KO cells by CRISPR/Cas9 technology

To generate PC3 NSUN5-KO cells, crRNAs specifically targeting the chromosomal regions encoding for NSUN5 catalytic residues were generated using CRISPOR [472]. Two crRNAs were selected according to their specificity (sg1: 5'-rCrArTrCrTrTrCrArCrCrCrGrArGrGrCrCrArCrTrGrC - 3'; sg2: 5'-rCrTrCrCrTrGrGrCrArGrArGrGrGrGrArGrCrArCrG-3') (IDT). In addition, crRNAs were selected to also produce the disruption of the recognition site of different restriction enzymes to facilitate screening of positive clones. To obtain the sgRNAs, crRNAs were mixed with Alt-R CRISPR-Cas9 tracrRNAs (IDT), heated for 5 min at 95ºC and then allowed to naturally cool down to room temperature for 30 min. sgRNAs were then incubated with Alt-R S.p. HiFi Cas9 nuclease (IDT) to form the ribonucleoprotein (RNP) complex. The RNP complex was transduced by electroporation using Cell Line Nucleofector Kit V (Lonza) and Nucleofector 2b Device (Lonza) according to manufacturer's instructions. 48 hours after electroporation, single cell clones were generated by serial dilution and individual clones were selected by microscope visualization. In order to genotype the genetic alterations edited by CRISPR/Cas9, genomic DNA (gDNA) of each clone was isolated using QuickExtract DNA Extraction Solution (Lucigen). Briefly, 1×10^6 cells were centrifuged and resuspended in 50 µl of QuickExtract DNA Extraction Solution. Lysate was then incubated for 5 min at room temperature, 15 min at 65ºC and 10 min at 95ºC. 2 µl of lysate was used as template for PCR amplification using NZYTaq II 2x Green Master Mix and 200 nM of each primer (Table 3). Then, PCR products were digested using restriction enzymes to validate the genomic alteration. Clones generated using sg1 were tested using Pst1 restriction enzyme (New England Biolabs) while clones generated with sg2 were tested using BsmBI restriction enzyme (New England Biolabs). In both cases, insertion-deletion (indel) mutations created by reparation pathways after Cas9 cleavage produced the loss of the restriction site of the aforementioned enzymes (PstI: CTGCAG, BsaAI: YACGTR). In both cases, digestion of 10 µl of PCR product was performed according to manufacturer's instructions. PCR and digestion products were resolved in 2% Agarose-TAE (Tris-acetate-EDTA buffer: 40 mM Tris, 20 mM acetate and 1 mM EDTA). gDNA of positive clones was then sequenced to confirm the genomic alteration. Briefly, PCR products were purified using Nucleo-spin Gel and PCR Clean-up kit (Macherey-Nagel). Then, 50 ng of purified PCR products were mixed with 3 pmol of primers and sequenced by Sanger

sequencing. Both Fw and Rv primer used in the PCR (Table 3) were used for sequencing in order to fully cover *NSUN5* sequence. Clones that showed genomic alterations by Sanger sequencing were tested for *NSUN5* expression loss by RT-qPCR and western blot.

Transient transfection of siRNAs and expression plasmids

NSUN5 expression was transiently silenced using two siRNAs (si2: 5'-rCrUrCrCrGrArUrG rArUrGrUrArGrUrUrGrArUrA-3' (Qiagen #SI00661906); si8: 5'-rArCrGrCrUrArCrCrArU rGrArGrGrUrCrCrArCrUrA-3' (Qiagen #SI04189178)). AllStars Negative Control siRNA was used as control (Qiagen #1027280). siRNAs were transfected into the cells using INTERFERin (Polyplus) at a final concentration of 25 nM according to the manufacturer's instructions. When an extended experimental time was required, a second transfection was performed 60 hours after the initial transfection to maintain an optimal silencing of NSUN5. NSUN5 silencing efficiency was confirmed by RT-qPCR or western blot.

Wild-type or mutant forms of NSUN5 cloned into pCMV6-Entry plasmids were transiently transfected using JetPEI transfection reagent according to manufacturer's protocol. Medium was changed 24 hours post transfection to reduce toxicity. Expression was validated by RT-qPCR or western blot.

Growth curves.

Cell growth was assessed through growth curves. Six replicates per condition were seeded in 96-well plates and collected at specific time points. Cells were washed with PBS and then fixed in 4% PFA (Panreac Applichem) for at least 30 min at 4ºC. Then, plates were rinsed with PBS and stained using 0.1% crystal violet (Sigma) in 20% methanol for 45 min at room temperature. After staining, residual crystal violet was washed away using distilled water and plates were air-dried. Finally, crystal violet was resuspended in 10% acetic acid and the optical density at 595 nm was measured using Infinite 200 microplate reader (Tecan). Optical density at each experimental time point was normalized to the optical density of a seeding control collected 8 hours after seeding.

Soft agar colony formation assay

Anchorage-independent growth was evaluated by soft agar colony formation assay. Bottom layers were prepared with 0.6% low melting agarose (Sigma) in DMEM supplemented with 10% FBS, 100 U/ml of penicillin and 100 µg/ml of streptomycin. Bottom layers were poured into 6-well plates and allowed to polymerize for 1 hour at 4ºC. Then, an upper layer containing 1600 cells/ml and

0.3% low melting agarose in medium was poured onto the bottom layer and allowed to polymerize for 15 min at 4ºC. Six replicates were seeded per condition. Colonies were allowed to grow for three weeks. A seeding control was performed for each cell line in 12-well plates for normalization purposes. Seeding control was fixed 16 hours after seeding, stained with crystal violet and optical density was measured as explained for the growth curves. Soft-agar plates were stained with 0.005% crystal violet in 1% methanol and scanned using PowerLook 1000 scanner (UMAX). The number of colonies was unbiased counted using "analyze particle" plug-in of ImageJ. Particles measuring between 2 and 100 pixels were considered. The number of particles measured for each cell line was normalized with the absorbance of the corresponding seeding control.

Migration assays in Boyden Chamber

The migration capacity of the cells was analyzed by Boyden Chamber assay using BD Falcon Cell Culture inserts (Falcon) with 0.4 µm of pore size. Two different assays were conducted. In the first assay, 10000 cells were seeded in the upper chamber in serum-free medium, while medium supplemented with 10% FBS was placed under the transwell inserts as chemoattractant. In the second assay, 10000 cells were seeded in the upper chamber in serum-free medium or medium supplemented with 1% FBS. Medium supplemented with 10% FBS were placed under the transwell inserts. In both cases, 4 replicates per condition were performed. Cells were allowed to migrate for 20 hours. After that, the inserts were washed with PBS, fixed with 4% PFA for 10 min and stained with crystal violet as previously described. Cells from the upper part of the insert were scraped off using a cotton bud and washed with PBS. The inserts were then mounted with Mowiol (4.8% Mowiol 4-88 (Sigma), 12% Glycerol (VWR), 0.05M Tris (Sigma)) and photographed with Olympus BX-51 light microscope coupled to Olympus DP70 digital camera. 6 representative photos were taken of each insert, and the cells were counted manually. The number of cells of each insert was normalized with a seeding control as described in soft-agar colony formation assay. additionally, the number of cells in each insert of the 1% FBS assay was normalized with the number of cells in the non-treated control.

Time lapse

Cells were seeded in triplicates into 12-well plates in DMEM containing 10% FBS, 100 U/ml penicillin and 100 µg/ml streptomycin. In each well, two positions were selected for monitoring and recording using Eclipse TE200-E microscope (Nikon). Bright images were captured every 10 min. Plates were kept at 37ºC and 5% CO_2 by using a cage incubator system (OKOLab). Cell migration was analyzed by using Manual Tracking plug-in of Fiji [473]. For each recording

position, five cells were tracked. The migration velocity and distance were determined for each tracked cell.

Cell synchronization

Cell progression through the cell cycle was analyzed by synchronization and release from G0/G1 and G2/M phases. Synchronization of cells in G0/G1 was achieved by subjecting the cells to serum starvation for 48-60 hours. Then, cells were released from this blockade and allowed to progress through the S phase by adding 10% of FBS to the culture medium. After 16 hours, 50 μg/ml of nocodazole (Santa Cruz Biotechnology) was added to the medium for 16 hours to arrest the cells in G2/M phase. Finally, nocodazole was washed out from the culture medium, allowing the cells to proceed through mitosis. Cells were collected at desired time points based on experimental requirements.

Cell cycle analysis by flow cytometry

To determine the cell cycle profiles, DNA content was measured by flow cytometry. Cells were detached using trypsin, washed with PBS and fixed by gently vortexing in ice-cold 70% ethanol. Cells were allowed to fix and permeabilized for at least 30 min at 4ºC. DNA was then stained either with 2 μg/ml of propidium iodide (Sigma) or 0.1 μg/ml of 4',6-diamidino-2-fenilindol (DAPI, Sigma) for 30 min at room temperature, and RNA was removed using 0.5 μg/ml of RNase A (Sigma). Stained cells were acquired using Accuri C6 Flow Cytometer (BD Biosciences), Accuri C6 Plus Flow Cytometer (BD Biosciences) or FACSAria Cell Sorter (BD Biosciences). DNA content of cells was analyzed using FlowJo software (BD Biosciences). During analysis, cell debris were excluded using FSC-A vs SSC-A gating, and doublets were eliminated using FSC-A vs FSC-H gating. Then, DNA content was represented in histograms and cell cycle phases were manually gated. Three replicates per condition were performed in all cell cycle assays.

Annexin V assay

Cell apoptosis was measured by Annexin V staining. Cells were seeded in triplicates and dethatched using trypsin at 80% confluence. Cells were washed twice with PBS and resuspended in 100 μl of Annexin V binding buffer (10 mM Hepes pH 7.4, 140 mM NaCl, 2.5 mM CaCl$_2$). Then 5 μl of Annexin V-FITC (Immunostep) and 2 μg/μl of propidium iodide were added and incubated for 15 minutes at room temperature in the dark. Stained cells were acquired using Accuri C6 Flow Cytometer. Annexin V staining and DNA content were analyzed using FlowJo.

Table 4. Primers used qPCR analysis using SYBRgreen and UPL probes.

Gene	Specie	Forward primer sequence (5'-3')	Reverse primer sequence (5'-3')	Use
NSUN5	Human	TGCTCCGATGATGTAGTTGATT	CCTTGAGGGCTCGTAAGTCA	UPL
Cyclin A	Human	ATGGCATTTGAGGATGTGTATGAA	CTGTGTTGAAATCCAGCAGGAA	SYBR
Cyclin B1	Human	TCCATTATTGATCGGTTCATGC	TCAGTCACAAAAGCAAAGTCACC	SYBR
Cyclin D1	Human	CTTCCTCTCCAAAATGCCAG	AGAGATGGAAGGGGGAAAGA	SYBR
Cyclin E	Human	CCTCGGATTATTGCACCATC	CATGATTTTCCAGACTTCCTCTC	UPL
GAPDH	Human	GAGTCCACTGGCGTCTTCAC	GTTCACACCCATGACGAACA	UPL
Vim	Mouse	CCAACCTTTTCTTCCCTGAAC	TTGAGTGGGTGTCAACCAGA	UPL
Sca1	Mouse	CCCCTACCCTGATGGAGTCT	TGTTCTTTACTTTCCTTGTTTGAGAA	UPL
Krt5	Mouse	CAGAGCTGAGGAACATGCAG	CATTCTCAGCCGTGGTACG	UPL
Krt8	Mouse	AGTTCGCCTCCTTCATTGAC	GCTGCAACAGGCTCCACT	UPL

Table 5. TaqMan probes and UPL probes for qPCR analysis.

Gene	Specie	Probe number and catalog number
NSUN5	Human	UPL probe #11. Cat. no. 04685105001
GAPDH	Human	UPL probe #45. Cat. no. 04688058001
Cyclin E	Human	UPL probe #61. Cat. no. 04688597001
Vim	Mouse	UPL probe #109. Cat. no. 04688597001
Sca1	Mouse	UPL probe #16. Cat. no. 04692284001
Krt5	Mouse	UPL probe #22. Cat. no. 04686969001
Krt8	Mouse	UPL probe #67. Cat. no. 04688660001
Nsun5	Mouse	TaqMan Probe Mm00520549_m1. Cat. no. 4351372
Gapdh	Mouse	TaqMan Probe Mm99999915_g1. Cat. no. 4331182
Cd49f	Mouse	TaqMan Probe Mm01333831_m1. Cat. no. 4351372

RNA isolation, reverse transcription and qPCR

For expression analysis, RNA was isolated using NZY total RNA isolation kit (Nzytech) following manufacturer's instructions. RNA was quantified using ND-1000 Nanodrop spectrophotometer (Isogen Lifescience). Then, 1 µg of RNA was used as template for cDNA synthesis using NZY First-strand cDNA synthesis kit (Nzytech) according to manufacturer's recommendations. qPCR analyses were performed using either SYBRgreen (Vazyme), TaqMan probes (Applied Biosystems) or UPL probes (Roche). qPCR reactions were set up in MicroAmp Optical 96-well plates (Applied Biosystems) using 1 µl of cDNA as template. For reactions with SYBR green, 5 µl

of 2X AceQ Universal SYBR green mix (Vazyme) and 300 nM of each primer (Table 4) were added to the reaction mixture. When using TaqMan or UPL probes, reactions were carried out using 5 µl of 2X TaqMan Universal master mix (Applied Biosystems). In these cases, either 1X TaqMan probes or 1 µM of specific primers (Table 4) and 80 nM of UPL probes were used. Probes used can be found on Table 5. qPCR data acquisition was conducted using QuantStudio 3 or QuantStudio 5 Real-Time PCR System (Applied Biosystems). GAPDH gene was used for normalization using ΔCt method. For each sample, three technical replicates were performed.

Detection of cytosine-5 methylation on ribosomal RNA using bisulfite-PCR

Total RNA was isolated using QIAzol lysis reagent (Qiagen) following a regular phenol-chloroform extraction protocol. Briefly, 0.2 ml of chloroform (Thermo Fisher Scientific) was added per milliliter of QIAzol and samples were vigorously mixed by vortexing and incubated for 10 min at room temperature. After centrifugation at 13000 rpm and 4ºC for 30 min, the aqueous phase was collected and mixed with an equal volume of isopropanol and 0.3 M sodium acetate pH 5.2. Samples were thoroughly mixed and RNA was allowed to precipitate for at least 2 hours at -80ºC. Precipitated RNA was recovered by centrifugation and washed with 70% ethanol. RNA pellet was resuspended in nuclease-free water (Ambion) and quantified by Nanodrop.

To eliminate possible genomic DNA contamination, RNA samples were treated with TURBO DNAse (Invitrogen) for 30 min at 37ºC. DNase-treated RNA was isolated by adding equal volumes of acid phenol-chloroform-isoamyl alcohol (125:24:1, pH 4.5; Invitrogen) and centrifuging for 5 min at 13000 rpm and 4ºC. The aqueous phase was collected, and RNA was precipitated by adding 3 volumes of 100% ethanol, 0.3 M sodium acetate pH 5.2 and 0.75 µl of Glycoblue co-precipitant (Invitrogen). RNA was allowed to precipitate for at least 2 hours at -80ºC and recovered by centrifugation as previously. DNase-treated RNA was resuspended in nuclease-free water and quantified by Nanodrop.

3 µg of DNase-treated RNA were treated with sodium bisulfite using Methylamp RNA Bisulfite Conversion Kit (Epigentek) following manufacturer's instructions. Bisulfite treatment was carried out in a C1000 Touch thermal cycler. Cycling conditions were 5 min at 65ºC followed by 90 min at 60ºC. Bisulfite-treated RNA was in-column desalted and deaminated and was eluted in nuclease-free water and quantified by Nanodrop.

In the case of the RNA treated with EpiTect Bisulfite kit (Qiagen), 5 µg of DNase-treated RNA were mixed with 42.5 µl of 5 M sodium bisulfite and 17.5 µl of DNA protection buffer and incubated for 6 cycles of 5 min at 70ºC followed by 1 hour at 60ºC. The reaction mixture was then desalted using Micro Bio-spin 6 chromatography colums (Bio-Rad) and desulfonated by adding 1

volume of 1 M Tris-HCl pH 9.0 and incubating the mixture for 1 hour at 37ºC. After desulfonation, 3 volumes of 100% ethanol, sodium acetate 0.06 M and 0,75 µl of GlycoBlue Coprecipitant were added and RNA was precipitated overnight at -80ºC. RNA precipitate was recovered by centrifugation, resuspended in nuclease-free water and quantified by Nanodrop.

In both cases, 300 ng were used as template for cDNA synthesis using Maxima H-minus cDNA synthesis MasterMix (Thermo Fisher Scientific) following manufacturer's recomendations. Reverse transcription product was then used as template for PCR amplification using primers flanking C3782 position in 28S rRNA. Primers were designed to align to the deaminated sequence of 28S rRNA (Table 3). The PCR reaction was performed using DreamTaq Green PCR MasterMix (Thermo Fisher Scientific) and 200 nM of each primer. Once amplification was verified by resolving half of the PCR product on a 2% agarose-TAE gel, the remaining fresh PCR products were ligated into the pCR 2.1 TOPO vector (Invitrogen) following manufacturer's instructions. Ligated vector was used to transform chemically-competent DH5α *E. coli* bacteria. Colonies were tested to verify the proper insertion of the PCR product into individual clones by PCR using M13 Fw and Rv primers (available in the TOPO cloning kit). Plasmid DNA from ten positive clones was isolated using genJET plasmid Miniprep kit (Thermo Fisher Scientific) and sequenced by Sanger sequencing using M13 Fw primer. Sequences were aligned using MEGA11 software and compared to human reference 28S rRNA (NR_003287.4).

Methylation detection by Nanopore direct RNA sequencing

Total RNA from *NSUN5*-KO cells and mice was isolated in duplicates using Qiazol and DNAse-treated as previously stated. RNA integrity was analyzed using 2100 Bioanalyzer and RNA 6000 Nano chip (Agilent). Direct RNA sequencing was performed using Oxford Nanopore Technology (ONT) by Dr Eva Novoa at the Centre for Genomic Regulation (Barcelona, Spain). For the direct RNA sequencing library preparation, the ONT Direct RNA Sequencing protocol version DRS_9080_v2_revI_14Aug2019 was followed. In each reaction, 250 ng of total RNA was ligated to pre-annealed custom RT adaptors (IDT) using concentrated T4 DNA Ligase (New England Biolabs). The RNA was then reverse transcribed using Maxima H Minus RT (Thermo Fisher Scientific) without the heat inactivation step. The resulting products were purified using 1.8x Agencourt RNAClean XP beads (Thermo Fisher Scientific) and washed with 70% ethanol. Next, 50 ng of reverse-transcribed RNA were ligated to the RMX adapter, which consist of sequencing adapters and a motor protein. The mixture was then purified using 1x Agencourt RNAClean XP beads. Sample was eluted and mixed with RNA running buffer before loading onto a primed R9.4.1 flowcell. The sequencing was performed on a MinION sequencer with MinKNOW acquisition software version v.3.5.5.

Base-calling of the raw sequencing data was carried out using the Guppy base-caller developed by Oxford Nanopore Technologies. The base-called reads were then mapped to reference FASTA sequences using minimap2 [474]. Datasets from control and knocked-out mice were compared using Nanoconsensus algorithm developed by Dr Eva Novoa's Laboratory (not published yet).

Ribosome biogenesis analysis by Northern Blot

To analyze rRNA processing, 4 μg of total RNA were mixed with RNA loading buffer (50% formamide, 6% formaldehyde, 20 mM MOPS pH 7, 0.5 mM EDTA, 100 μg/ml ethidium bromide, 0.0025% xylene cyanol, 0.025% bromophenol blue and 10% glycerol) and heated at 65ºC for 12 min. RNAs were resolved on agarose denaturing gels (6.6% formaldehyde, 1.5% agarose, 20 mM MOPS pH 7) for 5.5 hours at 50 V in 20 mM MOPS buffer, pH 7. Then, gels were washed twice in water for 20 min, once in 75 mM NaOH for 20 min, twice in 0.5 M Tris 1.5 M NaCl pH 7 for 15 min and once in 10X sodium citrate buffer (SSC; 150 mM sodium citrate 1.5 M NaCl, pH 7) for 20 min. Then, RNAs were transferred by capillarity for 24 hours in 10X SSC to Hybond-N$^+$ nylon membranes (Amersham). RNAs were crosslinked to the membranes with 120 mJ/cm^2 in UV Stratalinker 2400 (Stratagene). Membranes were then pre-hybridized for 20 min at 52ºC in Church and Gilbert's hybridization buffer (1% BSA fraction V (Nzytech), 1 mM EDTA, 0.5 M NaHPO$_4$, 7% SDS). Probes against ITS1 (5'- CCTCGCCCTCCGGGCTCCG GGCTCCGTTAATGATC-3') and ITS2 (5- CTGCGAGGGAACCCCCAGCCGCGCA-3') were ^{32}P-labelled using T4 PNK (New England Biolabs) following manufacturer's instructions. Probes were boiled 5 min at 95ºC, mixed with pre-hybridization buffer and incubated with the membrane overnight at 52ºC. Membranes were washed for 30 min with 2X SSC, 0.5% SDS and 20 min with 0.5X SSC, 0.05% SDS at 37ºC. Finally, membranes were dried and exposed to X-ray films (Fujifilm) for 24 to 72 hours at -80ºC. In between successive hybridizations, probes were stripped off by introducing the membrane in 1% boiling SDS for 2 hours. Band densitometry was quantified using Fiji. 18S rRNA and 28S rRNA stained with ethidium bromide (Sigma) were used as loading control. Three replicates per condition were performed.

Transcriptomic analysis

RNA from NSUN5-silenced and control cells was extracted in triplicates using NZY Total RNA isolation kit as described previously. RNA integrity was analyzed using 2100 Bioanalyzer and RNA 6000 Nano chip. Microarray analysis was conducted by the Genomics Unit at CIC using Clariom S Assay Human (Affymetrix). Labeling and hybridizations were performed according to the manufacturer's instructions. Briefly, 100 ng of total RNA was amplified and labeled using GeneChip WT Plus reagent kit (Affymetrix, 902280) and then hybridized to Clariom S human

Array (Affymetrix, 902927). Washing and scanning were carried out using GeneChip System of Affymetrix (GeneChip Hybridization Oven 645, GeneChip Fluidics Station 450 and GeneChip Scanner 7G).

For the analysis, raw data was normalized using robust multiarray analysis (RMA) via the oligo package344 and subsequently analyzed to detect genes differentially expressed genes using the limma package345. Differentially expressed genes with Benjamini–Hochberg corrected p-values < 0.05 were considered significant.

Polysome profiling

To obtain polysome profiles, cells were treated with 100 µg/ml of cycloheximide for 5 min at 37ºC and washed with PBS supplemented with 100 µg/ml of CHX. Cells were then scraped and lysed in a lysis buffer containing 20 mM Tris pH 7.5, 100 mM KCl, 5 mM MgCl$_2$, 0.3% Igepal, 100 µg/ml CHX, 1 mM sodium orthovanadate, 1 mM sodium fluoride and 1 mM β-glycerophosphate. The RNA content was measured using Smart-Spec Plus spectrophotometer (Bio-Rad). Equal amounts of extracts were loaded into 7-50% sucrose gradients. Sucrose gradients were prepared in a gradient buffer containing 20 mM Tris pH 7.5, 100 mM KCl, 5 mM MgCl$_2$ and 100 µg/ml CHX. Samples were ultracentrifuged for 165 min at 39000 rpm and 4ºC with the brake off. Gradients were then fractionated using BR-186 Density Gradient Fractionator (Brandel) coupled to a Spectra/Chrom 280 UV Monitor and Chart Recorder (Repligen Corporation).

Protein extraction and Western Blotting

For protein expression analysis, cells were lysed using Pierce RIPA buffer (Thermo Fisher Scientific) supplemented with cOmplete protease inhibitors (Roche) and 1 mM sodium orthovanadate, 1 mM sodium fluoride and 1 mM β-glycerophosphate. Cell lysates were incubated 20 min at 4ºC under rotation followed by 20 min of centrifugation at 13000 rpm and 4ºC. Protein-containing supernatants were collected and quantified using Pierce BCA protein assay (Thermo Fisher Scientific) following manufacturer's instructions.

30 µg of proteins were mixed with Laemmli sample buffer (50 mM Tris pH 6.8, 10% SDS, 10% glycerol, 1% β-mercaptoethanol, 10 mM DTT, 0.2 mg/ml bromophenol blue) and loaded into homemade tris-glycine polyacrylamide gels. Gels were resolved in tris-glycine-SDS buffer (25 mM Tris, 200 mM glycine, 0.05% SDS) and transferred to nitrocellulose membranes (Amersham) at 100V for 2 hours using tris-glycine buffer with 10% of methanol (Honeywell). Proper transference to nitrocellulose membranes was confirmed by Ponceau S Staining (0.04 g Ponceau (Sigma), 10 %

glacial acetic acid (Millipore)). Membranes were washed in Tris-buffered saline supplemented with Tween-20 (TBS-T; 25 mM Tris, 50 mM NaCl, 2.5 mM KCl, 0.001% Tween-20 (Panreac Applichem)) and blocked with 5% skim milk in TBS-T. Primary antibodies were prepared in blocking buffer and incubated overnight at 4ºC. HRP-conjugated secondary antibodies were diluted 1:4000 in TBS-T and incubated for 1 hour at room temperature. Primary and secondary antibodies and their working dilutions can be found on Table 6. Western blots were developed using enhanced chemiluminescence reagent (ECL, 0.2 mM p-coumaric acid (Sigma), 1.25 mM 3-aminophtalhydrazide (Sigma) and 100 mM Tris pH 8.5) and either X-ray films or iBright system (Thermo Fisher Scientific). Band densitometry was quantified using Fiji.

Table 6. *Primary and secondary antibodies used for western blot (WB), immunofluorescence (IF), immunoprecipitation (IP), immunohistochemistry (IHC).*

Antibody	Manufacturer	Catalog number	Dilution
NSUN5	Abcam	ab121633	1:1000 (WB), 1:250 (IHC)
NSUN5	Santa Cruz Biotechnology	sc-376147	1:250 (IF)
GAPDH	Cell signaling	2118S	1:1000 (WB)
HSP90	Santa Cruz Biotechnology	sc-515081	1:1000 (WB)
Flag	Cell Signaling	14793S	1:1000 (WB), 1:400 (IF), 0.75 µg/ml (IP)
p-Serine	Millipore	05-1000	1:500 (WB)
p53	Santa Cruz Biotechnology	sc-126	1:1000 (WB)
uL5	Cohesion biosciences	CPA2018	1:1000 (WB)
Fibrillarin	Santa Cruz Biotechnology	sc-166021	1:250 (IF)
5.8S rRNA	Santa Cruz Biotechnology	sc-33678	1:250 (IF)
PSMB7	Santa Cruz Biotechnology	sc-365725	1:1000 (WB)
GCP2	Santa Cruz Biotechnology	sc-377117	1:1000 (WB)
ZNF207	Santa Cruz Biotechnology	sc-271943	1:1000 (WB)
EIF4H	Santa Cruz Biotechnology	sc-515265	1:750 (WB)
Cdc2 p34	Santa Cruz Biotechnology	sc-54	1:1000 (WB)
Mouse IgG HRP	Cytiva	NXA931V	1:3000 (WB)
Rabbit IgG HRP	Cytiva	NA934V	1:4000 (WB)
Mouse IgG AF594	Invitrogen	A-11032	1:800 (IF)
Rabbit IgG AF488	Invitrogen	A-11008	1:800 (IF)

Cell immunofluorescence

To perform cell immunofluorescences, cells were grown in tissue culture-treated glass coverslips (Knittel glass). For actinomycin-treated cells, once the desired confluence was reached, cells treated

with 100 ng/ml of actinomycin-D (Sigma) for 2 hours. Treated or untreated cells were fixed using 4% PFA for 10 min at room temperature. Then, cells were permeabilized with 0.2% Triton X-100 (Panreac Applichem) for 10 min at room temperature and blocked with 5% normal goat serum (Gibco) or horse serum (Sigma) for 1 hour at room temperature. Primary antibodies were prepared in blocking buffer and incubated overnight at 4ºC in a humid chamber. Primary and secondary antibodies and their working concentration can be found on Table 6. Fluorophore-labelled secondary antibodies, prepared in blocking buffer at 1:800 concentration, were incubated for 1 hour at room temperature, protected from light. Finally, nuclei were counterstained with 0.5 µg/ml of DAPI (Sigma) for 10 min at room temperature and coverslips were mounted on glass slides using Mowiol. Images were acquired using Thunder wide field fluorescence microscope (Leica) or the spectral confocal microscope TCS SP5 (Leica) and analyzed using Fiji. Contrast of images was adjusted using Adobe Photoshop 2022 software.

Tissue immunohistochemistry

Mouse dissected tissues were fixed overnight in 4% PFA at room temperature and then transferred to 70% EtOH. Then, tissues were embedded in paraffin and sectioned with a thickness of 5 µm. Sections were deparaffinized in xylene (Panreac Applichem) and rehydrated through graded ethanol series to distilled water. Antigen retrieval was performed in citrate buffer (pH 6) for 20 min in a microwave and endogenous peroxidase activity was blocked by incubating with 3% hydrogen peroxide (Emsure) for 30 min at room temperature. Tissues were permeabilized with 0.1% Triton X-100 and non-specific binding sites were then blocked with 2.5% normal goat serum (Vector Labs). Sections were incubated with primary antibodies in 2.5% normal goat serum overnight at 4ºC. Primary antibodies and their working dilution can be found on Table 6. Secondary antibody incubation was performed using ImmPRESS® HRP Goat Anti-Rabbit IgG Polymer Detection Kit (Vector Labs). Detection was carried out incubating with ImmPACT DAB Substrate (Vector Labs) for 5 min. Slides were counterstained with hematoxylin (Millipore) for 30 seconds, dehydrated through graded ethanol series to xylene and mounted using DPX (Sigma). Image acquisition was performed using Olympus BX-51 light microscope coupled to Olympus DP70 digital camera. Quantification of NSUN5 intensity was performed using "Colour deconvolution" plug-in of Fiji.

NSUN5 structural analysis.

NSUN5 predicted structure was obtained from AlphaFold (AF-Q98P11-F1). Structure visualization and residue location was performed by Dr. José María de Pereda (Cancer Research Institure, Salamanca, Spain) using PyMOL.

NSUN5 immunoprecipitation

To immunoprecipitate Flag-NSUN5, cells expressing a Flag-tagged version of NSUN5 under a doxycycline-inducible promoter were used. Flag-NSUN5 expression was induced for 72 hours with 0.25 μg/ml of doxycycline. At 80% confluence, cells were collected by trypsinization and lysed using IP lysis buffer (50 mM Tris-HCl pH 8, 1 mM EDTA, 150 mM NaCl, 1% Triton X-100, cOmplete protease inhibitors 1 mM sodium orthovanadate, 1 mM sodium fluoride and 1 mM β-glycerophosphate. Protein concentration was measured by Pierce BCA protein assay kit as previously stated. 80 μg of proteins were saved as input samples. When required for the experiment, proteins were dephosphorylated using calf intestinal alkaline phosphatase (Promega) for 30 min at 30°C. Then, 1 mg of proteins were incubated with 0.75 μg of anti-Flag antibody (Cell signaling, 14793S) overnight at 4°C. Afterwards, protein-antibody complexes were captured using Dynabeads protein A magnetic beads (Invitrogen) for 2 hours at 4°C. Following the incubation, beads were washed with TBS supplemented with 0.05% Tween-20 twice, resuspended in 1X Laemmli sample buffer, boiled and loaded into an 8% polyacrylamide gel. Proteins were transferred to nitrocellulose membranes as described previously for regular western blotting. Membranes were incubated with p-Serine and NSUN5 antibodies. Immunoprecipitations were developed using ECL and iBright system. Band densitometry was quantified using Fiji.

NSUN5 phosphorylation detection by phosphoproteomics

To analyze NSUN5 phosphorylation by mass spectrometry, expression of a flag-tagged version of NSUN5 was induced as described previously and cells were synchronized in G2/M by adding 50 ng/ml of nocodazole to the medium 16 hours prior to collection. When required, CDK1 activity was inhibited with 10 μM of RO-3306. Cells were collected and lysed as described for regular immunoprecipitation and 5 mg of protein lysate were mixed with 2 μg of anti-Flag antibody (Cell Signaling). Immunoprecipitated proteins were resolved into an 8% polyacrylamide gel. Gel was stained with colloidal Coomasie (0.1% Coomasie G-250 (Millipore), 100 μM citric acid (Sigma), 5% ethanol (Sigma)) for 10 min at room temperature. Then, the gel was destained for 20 min with destaining solution (50% methanol and 10% acetic acid) and further destained with MilliQ water for 90 min. Bands corresponding to Flag-NSUN5 were excised. Peptides were analyzed by liquid chromatography coupled to mass spectrometry (LC-MS/MS) by the Proteomics Unit at CIC bioGUNE (Bilbao). Briefly, proteins were in-gel digested using trypsin, concentrated using a speed-vac (Thermo Fisher Scientific), and purified by retention on C12 hydrophobic reverse phase porous resin packed into previously activated and washed small columns. Peptide separation was performed on a nanoACQUITY UPLC System (Waters Corporation) connected online to an LTQ Orbitrap XL mass spectrometer (Thermo Fisher Scientific).

126

In vitro **kinase assays**

To validate NSUN5 as a CDK1 target, *in vitro* kinase assays were performed. 1 µg of NSUN5 recombinant protein (Origene) was incubated with 0.05 µg of CDK1/CyclinB1 complex (Thermo Fisher Scientific), 5 µCi of γ^{32}P-ATP (Perkin Elmer) and 10 µM of cold ATP (Thermo Fisher Scientific) in kinase buffer (50 mM Tris pH 7.5, 10 mM $MgCl_2$, 2 mM DTT and 0.1 mM EDTA). As a negative control, 10 µM of RO-3306 was added to inhibit CDK1 kinase activity. As positive control, 1 µg of the well-known CDK1 substrate Histone H1 was used. Kinase reaction was incubated for 30 min at 30ºC. Reaction was stopped by addition of Laemmli sample buffer and boiling for 5 min. Samples were then loaded into 8% polyacrylamide gels and run as explained for regular western blotting. Proteins were transferred to PVDF membranes for 1 hour at 100V. Membranes were exposed for autoradiography using X-ray films at -80ºC for 4 to 24 hours. For normalization purposes, the same membrane was probed using anti-NSUN5 antibody (Table 6).

Quantification of global protein synthesis rate

To assess the global protein synthesis rate, cells untreated or treated with 200 µM sodium arsenite ($NaAsO_2$) were incubated with 20 µM of O-propargyl-puromycin (or OP-puro) (Medchem Source LLP) for 1 hour at 37ºC. As negative control, cells treated with 100 µg/ml of cyclohexamide (CHX, Sigma) were used. Cells were then trypsinized and fixed using 1% PFA in PBS for 15 min on ice. After fixation, cells were permeabilized in 0.1% saponin (Santa Cruz Biotechnology) for 5 min at room temperature. Detection of OP-puro labelled proteins was performed using CuAAC Cell Reaction Buffer Kit (BTTAA based) (Jena Bioscience). Briefly, 0.1 µM pycolyl azide-conjugated AF488 fluorophore (Jena Bioscience) was bound to the OP-puro through Cu(I)-catalyzed azide-alkyne cycloaddition in the presence of 2 mM $CuSO_4$, 10 mM BTTAA and 100 mM sodium ascorbate. DNA was counterstained with propidium iodide as previously explained for cell cycle monitoring. OP-puro incorporation into nascent peptides and DNA content were measured by flow cytometry and analyzed using FlowJo software. Three replicates were performed by condition.

Nascent proteome

To analyze nascent peptides, cells were treated with 20 µM of OP-puro for 1 hour at 37ºC. Four replicates were performed per condition. OP-puro-tagged proteins were captured using a picolyl azide agarose resin through Cu(I)-catalyzed azide-alkyne cycloaddition using Click-&-Go Plus Protein Enrichment Kit (Click Chemistry tools) following manufacturer's instructions. Proteins were subsequently reduced and alkylated with 40 mM iodoacetamide (Sigma). The captured proteins were then thoroughly washed with 8M urea (Thermo Fisher Scientific) and 20%

acetonitrile (Honeywell) and trypsin digested. Digested proteins were concentrated using speed-vac and desalted using C18 stage tips (Millipore). For mass spectrometry analysis, samples were analyzed using a hybrid trapped ion mobility spectrometry-quadrupole time-of-flight mass spectrometer (timsTOF Pro with PASEF, Bruker Daltonics) coupled online to a nano Elute (Bruker). Protein identification and quantification were performed using MaxQuant software using default settings except for an LFQ min. ratio count of 1. Searches were carried out against a database consisting of human protein entries from Uniprot/Swissprot, with precursor and fragment tolerances of 20 ppm and 0.05 Da, respectively. Only proteins identified with at least two peptides at FDR <1% were considered for further analysis. Data (LFQ intensities) was loaded onto Perseus platform and further processed.

Gene Ontology enrichment analysis.

The "enrichplot" package of R was used for ontology analysis of a list of differentially expressed proteins while the "org.Hs.eg.db" package was used as genome-wide annotation for humans. This list, which consisted of 197 proteins that exhibited significant differential expression (Log2 (sh1/scr) > 2, p-value < 0.05), was used to query gene ontology database for biological process (GO, Biological Process, EBI, UniProt-GOA-ACAP-ARAP, 08.05.2020). Resulting biological terms were represented as a functionally grouped network. In this network, color of each node corresponds to the Bonferroni-adjusted p-value while the size of the node represents number of genes in the GO term. Color of the links indicates a specific functional group.

Structural analysis of 80S ribosomes.

Cells in exponential grow were trypsinized and snap froze in liquid nitrogen. Cell pellet was lysed in 30 mM HEPES pH 7.5, 7.5 mM $MgCl_2$, 125 mM KCl, 0.5 mM EDTA, 2mM DTT and 0.5 % NP-40. Lysate was cleared by centrifugation for 10 min at 21000 g and 4ºC and loaded into 10-40% sucrose gradients prepared in 30 mM HEPES pH 7.5, 7.5 mM $MgCl_2$, 125 mM KCl and 0.5 mM EDTA. Gradients were centrifuged for 3 hours at 40000 rpm and 4ºC in a Beckman Optima XPN ultracentrifuge using SW40 Ti rotor. Fractions containing 80S ribosomes were further centrifuged for 30 min at 80000 rpm and 4ºC in a Beckman Optima MAX-TL ultracentrifuge. Ribosome pellet was resuspended in 30 mM HEPES pH 7.5, 6 mM $MgCl_2$ and 100 mM KCl and snap froze in liquid nitrogen.

Graphene-coated R2/4 grids (Graphenea) were soaked for 1 min in 50 mM 1-pyrenemethylamine (PMA, Sigma) in DMSO. Then, grids were washed in isopropanol and absolute ethanol. Grids were allowed to air-dry at room temperature for 30 min. Purified 80S ribosomes were deposited into

PMA-functionalized grids within the chamber of a Vitrobot Mark IV (Thermo Fisher Scientific) set at 100% humidity and 4ºC. Then, grids were blotted using the following parameters: wait time 30 s, blot time 1 s, blot force -7. Blotted grids were immediately vitrified in liquid ethane and stored in liquid nitrogen.

Datasets were collected using Titan Krios operating at an acceleration voltage of 300 keV at the Department of Biochemistry of Cambridge University (Cambridge, United Kingdom). Micrographs were recorded using a Gatan K3 direct detector (Gatan) through the EPU software. A dose of 40 e$^-$/A^2 was achieved by a 0.8 s exposure time. Defocus was set between -1.8 and -0.8. 10 shots were taken per specimen hole. 7000 micrographs movies were recorded incorporating 30 fractions. Data analysis was performed using CryoSPARC.

Mouse models

The mice used in this study were housed at Animal Research Facility at University of Salamanca, where they were maintained in ventilated racks under specific pathogen-free conditions. Water and food were provided *ad libitum*. All experiments conducted followed the ethical guidelines established by the Bioethics committee at the University of Salamanca (under protocols #506, #595 and #269) and by the Competent Authority of Junta de Castilla y León.

Nsun5$^{tm2b(EUCOMM)Wtsi}$ mice generated by the Knockout Mouse Phenotyping Program (KOMP2) were purchased from The Jackson Laboratory. For genotyping purposes, the tail tip was cut, and DNA was extracted using alkaline lysis method in a final volume of 50 µl. Mouse genotyping was performed by PCR amplification using primers 23412, 23413, 24413 and OIMR7202 (Table 7) simultaneously in a reaction containing 5 µl of NZYTaq II 2x Green Master Mix, 1 µl of template and 500 nM of each primer. The cycling conditions were as follows: 94ºC for 2 min followed by 10 cycles of 94ºC for 20 s, 65ºC for 15 s (with 0.5 ºC decrease per cycle) and 68ºC for 1 min, followed by 28 cycles of 94ºC for 15 s, 60ºC for 15 s and 72ºC for 10 s. PCR products were then resolved in a 1.5% Agarose-TAE gel. *Nsun5*$^{+/+}$ mice yielded a single band of 240 bp and *Nsun5*$^{-/-}$ mice yield a single band of 428 bp, while both bands are detected in *Nsun5*$^{+/-}$ mice. The successful knockout of *Nsun5* in these mice was validated by RT-qPCR from RNA extracted from limbs.

As prostate cancer model, the previously described *Pten*$^{flox/flox}$; *Pb-Cre4* mouse model [390] was provided by Prof Pier Paolo Pandolfi. These mice, which suffer prostatic-specific deletion of *Pten*, were then crossed with Nsun5$^{tm2b(EUCOMM)Wtsi}$ mice. For mice genotyping, DNA was extracted from tail tip as previously explained and genotyping of *Pten* and *Cre* was performed by PCR amplification using Pten-Fw, Pten-Rv, Cre-Fw and Cre-Rv primers (Table 7). Pten was genotyped using 1 µl of template in a reaction containing 5 µl of NZYTaq II 2x Green Master Mix and 500

nM of each primer. The cycling conditions were as follows: 94ºC for 3 min followed by 35 cycles of 94ºC for 30 s, 59ºC for 1 min and 72ºC for 1 min. For Cre genotyping, reaction was set as for *Pten* genotyping and cycling conditions were as follows: 94ºC for 3 min followed by 35 cycles of 94ºC for 30 s, 62ºC for 1 min and 72ºC for 1 min. PCR products were resolved in a 1.5 % Agarose-TAE gel. Mice harboring floxed *Pten* allele, yielded a band of 480 bp, while WT *Pten* alleles yielded a band of 350 bp. Cre recombinase expression was evidenced by the detection of a band of 850 bp. At 5 months of age, mice were sacrificed and prostate tumors were dissected for further analysis. Prostate tumor length and width was manually measured using a ruler and volume was calculated using the following formula: volume = length x width^2 x 0.526.

As metastatic prostate cancer model, *Pten*$^{\text{flox/flox}}$; *Nkx3.1*$^{\text{CreERT2/+}}$; *Kras*$^{\text{LSL-G12D/+}}$ mouse model was provided by Dr. Alvaro Aytes [442]. In this model, *Pten* gene is specifically deleted in the prostate upon induction with tamoxifen of CreERT2 recombinase, which is expressed under the promoter of prostate-specific gen *Nkx3.1*. Additionally, tamoxifen induction leads to the expression of an oncogenic *Kras* allele (Kras$^{\text{LSL-G12D}}$). These mice were crossed with Nsun5$^{\text{tm2b(EUCOMM)Wtsi}}$ mice.

For mice genotyping, tail tip was cut and DNA was extracted as previously explained. *Cre*, *Pten*, *Kras* and *Nsun5* were separately genotyped by PCR amplification. For *Cre* recombinase genotyping, WT and Cre alleles were separately amplified using AAM1 and AAM2 (Cre allele) or AAM3 and AAM4 (WT allele) (Table 7). PCR reaction in both cases was set up using 5 µl of NZYTaq II 2x Green Master Mix and 500 nM of each plasmid. The cycling conditions for the Cre allele were as follows: 94ºC for 5 min followed by 30 cycles of 94ºC for 30 s, 63ºC for 30 s and 72ºC for 1 min. In the case of the WT allele, cycling conditions were the same, but annealing temperature was adjusted to 60ºC. In both cases, positive PCR product yielded a band of approximately 500 bp. *Pten* was genotyped using AAM5 and AAM6 primers (Table 7). PCR reactions was set up in a total volume of 20 µl containing 10 µl of NZYTaq II 2x Green Master Mix and 500 nM of each primer. The cycling conditions were as follows: 94ºC for 2 min followed by 40 cycles of 94ºC for 30 s, 62ºC for 20 s and 72ºC for 1 min. PCR products were then resolved on a 1% Agarose-TAE gel. Floxed *Pten* allele yielded a band of 1 Kb while WT allele yielded a band of 900 bp. *Kras* was genotyped using primers AAM7 and AAM8 (Table 7). PCR reaction was set in a total volume of 10 µl containing 5 µl of NZYTaq II 2x Green Master Mix and 500 nM of each primer. The cycling conditions were as follows: 94ºC for 2 min followed by 40 cycles of 94ºC for 30 s, 55ºC for 30 s and 72ºC for 1 min. PCR products were resolved on a 1.5% Agarose-TAE gel. *Kras* mutated allele yielded a band of 650 bp. Tamoxifen induction was performed at 8 weeks of age through oral administration of 100 mg/kg of tamoxifen (MedChemExpress) once daily for 4 consecutive days. Mice were closely monitored starting from week 10 after induction. At post-

induction week 16, the mice were sacrificed and their prostate, lymph nodes, lungs, liver and kidney were dissected for further analysis.

Table 7. Primers used for mice genotyping.

Primer	Primer sequence (5'-3')
23412	TGCAGCTCAGCAATAAGCA
23413	GCAGTTCCTAGCACCGTGT
24413	ACACGGGGTTTGCAGATG
OIMR7202	CGGTCGCTACCATTACCAGT
Pten-Fw	TGTTTTTGACCAATTAAAGTAGGCTGTG
Pten-Rv	AAAAGTTCCCCTGCTGATGATTTGT
Cre-Fw	GGTGCAAGTTGAATAACCGGA
Cre-Rv	CGGTATTGAAACTCCAGCGC
AAM1	GACATGGCGCGGCAACACC
AAM2	CGCCGGTCTGGCAGTAAAAAC
AAM3	CTCCGCTACCCTAAGCATCC
AAM4	GACACTGTCATATTACTTGGACC
AAM5	ACTCAAGGCAGGGATGAGC
AAM6	GTCATCTTCACTTAGCCATTGG
AAM7	CCTTTACAAGCGCACGCAGACTGTAGA
AAM8	AGCTAGCCACCATGGCTTGAGTAAGTCTGCA

Analysis of mouse prostate cancer cell population

Prostates from five months-old $Pten^{flox/flox}$; $Pb\text{-}Cre^{+/-}$; $Nsun5^{+/+}$ and $Pten^{flox/flox}$; $Pb\text{-}Cre^{+/-}$; $Nsun5^{+/-}$ male mice were dissected and digested for 4 hours at 37ºC using 1X collagenase and 1X hyaluronidase (Sigma) in DMEM/F12 (1:1) (Gibco) supplemented with 5% FBS (Gibco). Then, samples were washed with PBS and resuspended in 0.25% trypsin-EDTA (Gibco) followed by incubation for 1 hour at 37ºC. Trypsin was inactivated with Hank's balanced salt solution (HBSS; 0.137 M NaCl, 5.4 mM KCl, 0.25 mM Na_2HPO_4, 0.1% glucose, 0.44 mM KH_2PO_4, 1.3 mM $CaCl_2$, 1.0 mM $MgSO_4$, 4.2 mM $NaHCO_3$) supplemented with 2% FBS. Samples were further digested using 5 mg/ml of Dispase II (Sigma) and 100 µg/ml DNase I in DMEM and incubated at 37ºC for 30 min. The resulting cell suspension was filtered through a 70 µm cell strainer (Falcon) and viable cells were counted using a Neubauer chamber.

$1x10^6$ to $3x10^6$ cells were incubated for 30 min at room temperature with primary antibodies diluted in HBSS supplemented with 2% FBS. Primary antibodies and their working dilutions can be found on Table 8. After incubation, cells were washed and incubated with 1:800 streptavidin-efluor710

(eBioscience, 49-4317-82) and 1 µg/ml of DAPI in HBSS supplemented with 2% FBS for 20 min. As compensation control, UltraComp eBeads (Invitrogen) were conjugated with each antibody independently for 30 min at room temperature. For DAPI compensation control, 20000 cells were initially separated and stained with 1 µg/ml of DAPI. After antibody conjugation, samples and compensation controls were resuspended in HBSS supplemented with 2% of FBS and analyzed using FACSAria III Cell sorter. FlowJo software was used for data analysis. Alive cells were selected discarding DAPI$^+$ cells. Then, epithelial and stromal cells were separated from blood and endothelial cells using lineage markers (CD31, CD45 and Ter119), that are only expressed in the latter. Finally, the percentage of luminal (Sca1^{low}, CD49f ^{low}), basal (Sca1^{high}, CD49f ^{high}) and stromal (Sca1^{high}, CD49f $^-$) cells was determined.

Table 8. Primary antibodies used for flow cytometry analysis of mouse prostate tumors.

Antibody	Manufacturer	Catalog number	Dilution
CD31-biotin	eBioscience	13-0311-82	1:250
CD45-biotin	eBioscience	15886978	1:500
Ter119-biotin	eBioscience	13-5921-82	1:100
Sca1-APC	eBioscience	17-59581-82	1:100
CD49f-PE	eBioscience	12-0495-83	1:500

Prostate and liver cancer patient samples

Protein samples from patients with prostate hyperplasia or cancer were obtained in collaboration with Dr. Miguel Unda at Basurto University Hospital (Basque Country, Spain). Samples were obtained upon informed consent and with evaluation and approval from the corresponding ethics committee (CEIC code OHEUN11-12 and OHEUN14-14) and described elsewhere [471].

mRNA samples from liver cancer patients were obtained in collaboration with Dr Manuel Gahete at Reina Sofía University Hospital (Córdoba, Spain). Samples were obtained upon informed consent and with evaluation and approval from the corresponding ethics committee.

Human prostate cancer tissue microarray CA4 was obtained from Super Bio Chips. Tissue microarray contained 49 samples (39 prostate cancer samples and 10 paired normal tissues). Section consisted of 2 mm cores of 4 µm thickness.

In silico **analysis of human cancer databases**

The analysis of NSUN5 expression levels at different diseases statuses in human prostate tumors was performed using the bioinformatic interface CANCERTOOL [428]. CANCERTOOL integrates mRNA expression data available in prostate cancer public datasets [377, 386, 475-478].

Differential expression of NSUN5 was determined by calculating Z-scores, which represent the number of standard deviations of expression in cancerous samples compared to the mean expression in a reference population (Primary Tumor versus Normal and Metastasis versus Normal). For evaluation of statistical differences between the diverse groups, ANOVA test was performed.

The analysis of NSUN5 expression levels in human liver tumors were analyzed in collaboration with Dr Manuel Gahete. Expression data was obtained from publicly available databases [431-437]. Cholangiocarcinoma expression analysis were performed in collaboration with Dr Cedric Coulouarn. Expression data was obtained from publicly available databases [429, 430].

Statistical analysis

The data in this study is expressed and median ± SD, unless stated otherwise in the figure legends. No statistical methods were used to determine sample size, but each *in vitro* experiment included at least 3 replicates per group and condition. The "n" values of figure legends indicate the number of independent replicates or mice specimens in the analysis.

Statistical analyses were performed using Graphpad Prism 9. *In vitro* samples or *in vivo* samples with sample sizes greater than 10 were considered normally distributed. The normal distribution of the data was confirmed either by conducting the Saphiro-Wilk normality test or by assuming normality for sample sizes greater than 10 for *in vivo* samples. For normally distributed samples, unpaired two-tailed Student's t-test was used for two component comparisons and ANOVA for multi-component comparisons. For nor normally distributed samples, Mann-Whitney test was used. Confidence level used for all analysis was 0.95 (alpha value = 0.05).

References

References

1. Johnson, T.B. and R. Coghill, *Researches on pyrimidines. C111. The discovery of 5-methyl-cysosine in tuberculinic acid, the nucleic acid of the tubercle bacillus.* Journal of the American Chemical Society, 1925. **47**(11): p. 2838-2844.

2. Cohn, W.E., *Pseudouridine, a carbon-carbon linked ribonucleoside in ribonucleic acids: isolation, structure, and chemical characteristics.* J Biol Chem, 1960. **235**: p. 1488-98.

3. Blanco, S., et al., *Aberrant methylation of tRNAs links cellular stress to neuro-developmental disorders.* EMBO J, 2014. **33**(18): p. 2020-39.

4. Blanco, S., et al., *Stem cell function and stress response are controlled by protein synthesis.* Nature, 2016. **534**(7607): p. 335-40.

5. Frye, M. and S. Blanco, *Post-transcriptional modifications in development and stem cells.* Development, 2016. **143**(21): p. 3871-3881.

6. Janin, M., et al., *Epigenetic loss of RNA-methyltransferase NSUN5 in glioma targets ribosomes to drive a stress adaptive translational program.* Acta Neuropathol, 2019. **138**(6): p. 1053-1074.

7. Boccaletto, P., et al., *MODOMICS: a database of RNA modification pathways. 2021 update.* Nucleic Acids Res, 2022. **50**(D1): p. D231-D235.

8. Efimov, V.A., et al., *Detection of the 5'-cap structure of messenger RNAs with the use of the cap-jumping approach.* Nucleic Acids Res, 2001. **29**(22): p. 4751-9.

9. Roundtree, I.A., et al., *Dynamic RNA Modifications in Gene Expression Regulation.* Cell, 2017. **169**(7): p. 1187-1200.

10. Li, S. and C.E. Mason, *The pivotal regulatory landscape of RNA modifications.* Annu Rev Genomics Hum Genet, 2014. **15**: p. 127-50.

11. Nicholson, A.L. and A.E. Pasquinelli, *Tales of Detailed Poly(A) Tails.* Trends Cell Biol, 2019. **29**(3): p. 191-200.

12. Tarun, S.Z., Jr. and A.B. Sachs, *A common function for mRNA 5' and 3' ends in translation initiation in yeast.* Genes Dev, 1995. **9**(23): p. 2997-3007.

13. Gallie, D.R., *The cap and poly(A) tail function synergistically to regulate mRNA translational efficiency.* Genes Dev, 1991. **5**(11): p. 2108-16.

14. Alekhina, O.M., et al., *Functional Cyclization of Eukaryotic mRNAs.* Int J Mol Sci, 2020. **21**(5).

15. Bass, B.L. and H. Weintraub, *An unwinding activity that covalently modifies its double-stranded RNA substrate.* Cell, 1988. **55**(6): p. 1089-98.

16. Anantharaman, A., et al., *ADAR2 regulates RNA stability by modifying access of decay-promoting RNA-binding proteins.* Nucleic Acids Res, 2017. **45**(7): p. 4189-4201.

17.   Goncharov, A.O., et al., *Interplay between A-to-I Editing and Splicing of RNA: A Potential Point of Application for Cancer Therapy.* Int J Mol Sci, 2022. **23**(9).

18.   Gerber, A.P. and W. Keller, *RNA editing by base deamination: more enzymes, more targets, new mysteries.* Trends Biochem Sci, 2001. **26**(6): p. 376-84.

19.   Wang, H., et al., *A-to-I RNA Editing in Cancer: From Evaluating the Editing Level to Exploring the Editing Effects.* Front Oncol, 2020. **10**: p. 632187.

20.   Christofi, T. and A. Zaravinos, *RNA editing in the forefront of epitranscriptomics and human health.* J Transl Med, 2019. **17**(1): p. 319.

21.   Powell, L.M., et al., *A novel form of tissue-specific RNA processing produces apolipoprotein-B48 in intestine.* Cell, 1987. **50**(6): p. 831-40.

22.   Pan, T., *Modifications and functional genomics of human transfer RNA.* Cell Res, 2018. **28**(4): p. 395-404.

23.   Jackman, J.E. and J.D. Alfonzo, *Transfer RNA modifications: nature's combinatorial chemistry playground.* Wiley Interdiscip Rev RNA, 2013. **4**(1): p. 35-48.

24.   Natchiar, S.K., et al., *Visualization of chemical modifications in the human 80S ribosome structure.* Nature, 2017. **551**(7681): p. 472-477.

25.   Sharma, S. and D.L.J. Lafontaine, *'View From A Bridge': A New Perspective on Eukaryotic rRNA Base Modification.* Trends Biochem Sci, 2015. **40**(10): p. 560-575.

26.   Nombela, P., B. Miguel-Lopez, and S. Blanco, *The role of m(6)A, m(5)C and Psi RNA modifications in cancer: Novel therapeutic opportunities.* Mol Cancer, 2021. **20**(1): p. 18.

27.   Alexandrov, A., M.R. Martzen, and E.M. Phizicky, *Two proteins that form a complex are required for 7-methylguanosine modification of yeast tRNA.* RNA, 2002. **8**(10): p. 1253-66.

28.   Batista, P.J., et al., *m(6)A RNA modification controls cell fate transition in mammalian embryonic stem cells.* Cell Stem Cell, 2014. **15**(6): p. 707-19.

29.   Zorbas, C., et al., *The human 18S rRNA base methyltransferases DIMT1L and WBSCR22-TRMT112 but not rRNA modification are required for ribosome biogenesis.* Mol Biol Cell, 2015. **26**(11): p. 2080-95.

30.   Ishitani, R., S. Yokoyama, and O. Nureki, *Structure, dynamics, and function of RNA modification enzymes.* Curr Opin Struct Biol, 2008. **18**(3): p. 330-9.

31.   Jia, G., et al., *N6-methyladenosine in nuclear RNA is a major substrate of the obesity-associated FTO.* Nat Chem Biol, 2011. **7**(12): p. 885-7.

32.   Aik, W., et al., *Structure of human RNA N(6)-methyladenine demethylase ALKBH5 provides insights into its mechanisms of nucleic acid recognition and demethylation.* Nucleic Acids Res, 2014. **42**(7): p. 4741-54.

33.   Ueda, Y., et al., *AlkB homolog 3-mediated tRNA demethylation promotes protein synthesis in cancer cells.* Sci Rep, 2017. **7**: p. 42271.

34. Mauer, J., et al., *Reversible methylation of m(6)A(m) in the 5' cap controls mRNA stability.* Nature, 2017. **541**(7637): p. 371-375.

35. Wang, X., et al., *N6-methyladenosine-dependent regulation of messenger RNA stability.* Nature, 2014. **505**(7481): p. 117-20.

36. Shi, H., et al., *YTHDF3 facilitates translation and decay of N(6)-methyladenosine-modified RNA.* Cell Res, 2017. **27**(3): p. 315-328.

37. Wang, X., et al., *N(6)-methyladenosine Modulates Messenger RNA Translation Efficiency.* Cell, 2015. **161**(6): p. 1388-99.

38. Xiao, W., et al., *Nuclear m(6)A Reader YTHDC1 Regulates mRNA Splicing.* Mol Cell, 2016. **61**(4): p. 507-519.

39. Liao, S., H. Sun, and C. Xu, *YTH Domain: A Family of N(6)-methyladenosine (m(6)A) Readers.* Genomics Proteomics Bioinformatics, 2018. **16**(2): p. 99-107.

40. Alarcon, C.R., et al., *HNRNPA2B1 Is a Mediator of m(6)A-Dependent Nuclear RNA Processing Events.* Cell, 2015. **162**(6): p. 1299-308.

41. Liu, N., et al., *N(6)-methyladenosine-dependent RNA structural switches regulate RNA-protein interactions.* Nature, 2015. **518**(7540): p. 560-4.

42. Zhou, K.I., et al., *Regulation of Co-transcriptional Pre-mRNA Splicing by m(6)A through the Low-Complexity Protein hnRNPG.* Mol Cell, 2019. **76**(1): p. 70-81 e9.

43. Huang, H., et al., *Recognition of RNA N(6)-methyladenosine by IGF2BP proteins enhances mRNA stability and translation.* Nat Cell Biol, 2018. **20**(3): p. 285-295.

44. Wu, R., et al., *A novel m(6)A reader Prrc2a controls oligodendroglial specification and myelination.* Cell Res, 2019. **29**(1): p. 23-41.

45. Zhang, F., et al., *Fragile X mental retardation protein modulates the stability of its m6A-marked messenger RNA targets.* Hum Mol Genet, 2018. **27**(22): p. 3936-3950.

46. Yang, X., et al., *5-methylcytosine promotes mRNA export - NSUN2 as the methyltransferase and ALYREF as an m(5)C reader.* Cell Res, 2017. **27**(5): p. 606-625.

47. Bird, A.P., *CpG-rich islands and the function of DNA methylation.* Nature, 1986. **321**(6067): p. 209-13.

48. Ivanov, P., et al., *Angiogenin-induced tRNA fragments inhibit translation initiation.* Mol Cell, 2011. **43**(4): p. 613-23.

49. Rosace, D., J. Lopez, and S. Blanco, *Emerging roles of novel small non-coding regulatory RNAs in immunity and cancer.* RNA Biol, 2020. **17**(8): p. 1196-1213.

50. Kirchner, S. and Z. Ignatova, *Emerging roles of tRNA in adaptive translation, signalling dynamics and disease.* Nat Rev Genet, 2015. **16**(2): p. 98-112.

51. Guzzi, N., et al., *Pseudouridylation of tRNA-Derived Fragments Steers Translational Control in Stem Cells.* Cell, 2018. **173**(5): p. 1204-1216 e26.

52. Dominissini, D., et al., *The dynamic N(1)-methyladenosine methylome in eukaryotic messenger RNA.* Nature, 2016. **530**(7591): p. 441-6.

53. Bassler, J. and E. Hurt, *Eukaryotic Ribosome Assembly.* Annu Rev Biochem, 2019. **88**: p. 281-306.

54. Yusupova, G. and M. Yusupov, *High-resolution structure of the eukaryotic 80S ribosome.* Annu Rev Biochem, 2014. **83**: p. 467-86.

55. Bowman, J.C., et al., *Root of the Tree: The Significance, Evolution, and Origins of the Ribosome.* Chem Rev, 2020. **120**(11): p. 4848-4878.

56. Anger, A.M., et al., *Structures of the human and Drosophila 80S ribosome.* Nature, 2013. **497**(7447): p. 80-5.

57. Rodnina, M.V., *The ribosome as a versatile catalyst: reactions at the peptidyl transferase center.* Curr Opin Struct Biol, 2013. **23**(4): p. 595-602.

58. Sonenberg, N. and A.G. Hinnebusch, *Regulation of translation initiation in eukaryotes: mechanisms and biological targets.* Cell, 2009. **136**(4): p. 731-45.

59. Jackson, R.J., C.U. Hellen, and T.V. Pestova, *The mechanism of eukaryotic translation initiation and principles of its regulation.* Nat Rev Mol Cell Biol, 2010. **11**(2): p. 113-27.

60. Melnikov, S., et al., *One core, two shells: bacterial and eukaryotic ribosomes.* Nat Struct Mol Biol, 2012. **19**(6): p. 560-7.

61. Ben-Shem, A., et al., *The structure of the eukaryotic ribosome at 3.0 A resolution.* Science, 2011. **334**(6062): p. 1524-9.

62. Klinge, S., et al., *Atomic structures of the eukaryotic ribosome.* Trends Biochem Sci, 2012. **37**(5): p. 189-98.

63. Fujii, K., et al., *Decoding the Function of Expansion Segments in Ribosomes.* Mol Cell, 2018. **72**(6): p. 1013-1020 e6.

64. Genuth, N.R. and M. Barna, *The Discovery of Ribosome Heterogeneity and Its Implications for Gene Regulation and Organismal Life.* Mol Cell, 2018. **71**(3): p. 364-374.

65. Sulima, S.O. and J.D. Dinman, *The Expanding Riboverse.* Cells, 2019. **8**(10).

66. Parker, M.S., et al., *The Expansion Segments of 28S Ribosomal RNA Extensively Match Human Messenger RNAs.* Front Genet, 2018. **9**: p. 66.

67. Leppek, K., et al., *Gene- and Species-Specific Hox mRNA Translation by Ribosome Expansion Segments.* Mol Cell, 2020. **80**(6): p. 980-995 e13.

68. Gao, N., et al., *Mechanism for the disassembly of the posttermination complex inferred from cryo-EM studies.* Mol Cell, 2005. **18**(6): p. 663-74.

69. Tamm, T., I. Kisly, and J. Remme, *Functional Interactions of Ribosomal Intersubunit Bridges in Saccharomyces cerevisiae.* Genetics, 2019. **213**(4): p. 1329-1339.

70. Little, R.D. and D.C. Braaten, *Genomic organization of human 5 S rDNA and sequence of one tandem repeat.* Genomics, 1989. **4**(3): p. 376-83.

71. Dorner, K., et al., *Ribosome biogenesis factors-from names to functions.* EMBO J, 2023. **42**(7): p. e112699.

72. Pelletier, J., G. Thomas, and S. Volarevic, *Ribosome biogenesis in cancer: new players and therapeutic avenues.* Nat Rev Cancer, 2018. **18**(1): p. 51-63.

73. Ritossa, F.M. and S. Spiegelman, *Localization of DNA Complementary to Ribosomal Rna in the Nucleolus Organizer Region of Drosophila Melanogaster.* Proc Natl Acad Sci U S A, 1965. **53**(4): p. 737-45.

74. McStay, B., *Nucleolar organizer regions: genomic 'dark matter' requiring illumination.* Genes Dev, 2016. **30**(14): p. 1598-610.

75. Henderson, A.S., D. Warburton, and K.C. Atwood, *Location of ribosomal DNA in the human chromosome complement.* Proc Natl Acad Sci U S A, 1972. **69**(11): p. 3394-8.

76. Goodfellow, S.J. and J.C. Zomerdijk, *Basic mechanisms in RNA polymerase I transcription of the ribosomal RNA genes.* Subcell Biochem, 2013. **61**: p. 211-36.

77. Koberna, K., et al., *Ribosomal genes in focus: new transcripts label the dense fibrillar components and form clusters indicative of "Christmas trees" in situ.* J Cell Biol, 2002. **157**(5): p. 743-8.

78. Haeusler, R.A. and D.R. Engelke, *Spatial organization of transcription by RNA polymerase III.* Nucleic Acids Res, 2006. **34**(17): p. 4826-36.

79. Henras, A.K., et al., *An overview of pre-ribosomal RNA processing in eukaryotes.* Wiley Interdiscip Rev RNA, 2015. **6**(2): p. 225-42.

80. Tomecki, R., P.J. Sikorski, and M. Zakrzewska-Placzek, *Comparison of preribosomal RNA processing pathways in yeast, plant and human cells - focus on coordinated action of endo- and exoribonucleases.* FEBS Lett, 2017. **591**(13): p. 1801-1850.

81. Warner, J.R., *The economics of ribosome biosynthesis in yeast.* Trends Biochem Sci, 1999. **24**(11): p. 437-40.

82. Grandi, P., et al., *90S pre-ribosomes include the 35S pre-rRNA, the U3 snoRNP, and 40S subunit processing factors but predominantly lack 60S synthesis factors.* Mol Cell, 2002. **10**(1): p. 105-15.

83. Vanden Broeck, A. and S. Klinge, *An emerging mechanism for the maturation of the Small Subunit Processome.* Curr Opin Struct Biol, 2022. **73**: p. 102331.

84. Wu, S., et al., *Diverse roles of assembly factors revealed by structures of late nuclear pre-60S ribosomes.* Nature, 2016. **534**(7605): p. 133-7.

85. Sloan, K.E., et al., *Tuning the ribosome: The influence of rRNA modification on eukaryotic ribosome biogenesis and function.* RNA Biol, 2017. **14**(9): p. 1138-1152.

86. Sloan, K.E., et al., *The association of late-acting snoRNPs with human pre-ribosomal complexes requires the RNA helicase DDX21.* Nucleic Acids Res, 2015. **43**(1): p. 553-64.

87. Yelland, J.N., et al., *A single 2'-O-methylation of ribosomal RNA gates assembly of a functional ribosome.* Nat Struct Mol Biol, 2023. **30**(1): p. 91-98.

88. Sharma, S., et al., *Yeast Nop2 and Rcm1 methylate C2870 and C2278 of the 25S rRNA, respectively.* Nucleic Acids Res, 2013. **41**(19): p. 9062-76.

89. Liao, H., et al., *Human NOP2/NSUN1 regulates ribosome biogenesis through non-catalytic complex formation with box C/D snoRNPs.* Nucleic Acids Res, 2022. **50**(18): p. 10695-10716.

90. Liang, X.H., Q. Liu, and M.J. Fournier, *Loss of rRNA modifications in the decoding center of the ribosome impairs translation and strongly delays pre-rRNA processing.* RNA, 2009. **15**(9): p. 1716-28.

91. Khoshnevis, S., et al., *Ribosomal RNA 2'-O-methylations regulate translation by impacting ribosome dynamics.* Proc Natl Acad Sci U S A, 2022. **119**(12): p. e2117334119.

92. Haag, S., J. Kretschmer, and M.T. Bohnsack, *WBSCR22/Merm1 is required for late nuclear pre-ribosomal RNA processing and mediates N7-methylation of G1639 in human 18S rRNA.* RNA, 2015. **21**(2): p. 180-7.

93. Granneman, S., et al., *Cracking pre-40S ribosomal subunit structure by systematic analyses of RNA-protein cross-linking.* EMBO J, 2010. **29**(12): p. 2026-36.

94. Strunk, B.S., et al., *Ribosome assembly factors prevent premature translation initiation by 40S assembly intermediates.* Science, 2011. **333**(6048): p. 1449-53.

95. Crick, F.H., *On protein synthesis.* Symp Soc Exp Biol, 1958. **12**: p. 138-63.

96. Brenner, S., F. Jacob, and M. Meselson, *An unstable intermediate carrying information from genes to ribosomes for protein synthesis.* Nature, 1961. **190**: p. 576-581.

97. Shi, Z., et al., *Heterogeneous Ribosomes Preferentially Translate Distinct Subpools of mRNAs Genome-wide.* Mol Cell, 2017. **67**(1): p. 71-83 e7.

98. Xue, S., et al., *RNA regulons in Hox 5' UTRs confer ribosome specificity to gene regulation.* Nature, 2015. **517**(7532): p. 33-8.

99. Mazumder, B., et al., *Regulated release of L13a from the 60S ribosomal subunit as a mechanism of transcript-specific translational control.* Cell, 2003. **115**(2): p. 187-98.

100. Jha, S., et al., *Trans-kingdom mimicry underlies ribosome customization by a poxvirus kinase.* Nature, 2017. **546**(7660): p. 651-655.

101. Higgins, R., et al., *The Unfolded Protein Response Triggers Site-Specific Regulatory Ubiquitylation of 40S Ribosomal Proteins.* Mol Cell, 2015. **59**(1): p. 35-49.

102. Bohnsack, K.E. and M.T. Bohnsack, *Uncovering the assembly pathway of human ribosomes and its emerging links to disease.* EMBO J, 2019. **38**(13): p. e100278.

103. Kiss-Laszlo, Z., et al., *Site-specific ribose methylation of preribosomal RNA: a novel function for small nucleolar RNAs.* Cell, 1996. **85**(7): p. 1077-88.

104. Tollervey, D., et al., *Temperature-sensitive mutations demonstrate roles for yeast fibrillarin in pre-rRNA processing, pre-rRNA methylation, and ribosome assembly.* Cell, 1993. **72**(3): p. 443-57.

105. Zebarjadian, Y., et al., *Point mutations in yeast CBF5 can abolish in vivo pseudouridylation of rRNA.* Mol Cell Biol, 1999. **19**(11): p. 7461-72.

106. Lafontaine, D.L., et al., *The box H + ACA snoRNAs carry Cbf5p, the putative rRNA pseudouridine synthase.* Genes Dev, 1998. **12**(4): p. 527-37.

107. Watkins, N.J. and M.T. Bohnsack, *The box C/D and H/ACA snoRNPs: key players in the modification, processing and the dynamic folding of ribosomal RNA.* Wiley Interdiscip Rev RNA, 2012. **3**(3): p. 397-414.

108. Lane, B.G. and T. Tamaoki, *Studies of the chain termini and alkali-stable dinucleotide sequences in 16 s and 28 s ribosomal RNA from L cells.* J Mol Biol, 1967. **27**(2): p. 335-48.

109. Bardwell, V.J., et al., *Site-directed ribose methylation identifies 2'-OH groups in polyadenylation substrates critical for AAUAAA recognition and poly(A) addition.* Cell, 1991. **65**(1): p. 125-33.

110. Mishler, D.M., A.B. Christ, and J.A. Steitz, *Flexibility in the site of exon junction complex deposition revealed by functional group and RNA secondary structure alterations in the splicing substrate.* RNA, 2008. **14**(12): p. 2657-70.

111. Andersen, C.B., et al., *Structure of the exon junction core complex with a trapped DEAD-box ATPase bound to RNA.* Science, 2006. **313**(5795): p. 1968-72.

112. Iribe, H., et al., *Chemical Modification of the siRNA Seed Region Suppresses Off-Target Effects by Steric Hindrance to Base-Pairing with Targets.* ACS Omega, 2017. **2**(5): p. 2055-2064.

113. Erales, J., et al., *Evidence for rRNA 2'-O-methylation plasticity: Control of intrinsic translational capabilities of human ribosomes.* Proc Natl Acad Sci U S A, 2017. **114**(49): p. 12934-12939.

114. Wang, K., et al., *SNORD88C guided 2'-O-methylation of 28S rRNA regulates SCD1 translation to inhibit autophagy and promote growth and metastasis in non-small cell lung cancer.* Cell Death Differ, 2023. **30**(2): p. 341-355.

115. Zhou, F., et al., *A Dynamic rRNA Ribomethylome Drives Stemness in Acute Myeloid Leukemia.* Cancer Discov, 2023. **13**(2): p. 332-347.

116. Bakin, A.V. and J. Ofengand, *Mapping of pseudouridine residues in RNA to nucleotide resolution.* Methods Mol Biol, 1998. **77**: p. 297-309.

117. Penzo, M. and L. Montanaro, *Turning Uridines around: Role of rRNA Pseudouridylation in Ribosome Biogenesis and Ribosomal Function.* Biomolecules, 2018. **8**(2).

118. Spenkuch, F., Y. Motorin, and M. Helm, *Pseudouridine: still mysterious, but never a fake (uridine)!* RNA Biol, 2014. **11**(12): p. 1540-54.

119. Hudson, G.A., R.J. Bloomingdale, and B.M. Znosko, *Thermodynamic contribution and nearest-neighbor parameters of pseudouridine-adenosine base pairs in oligoribonucleotides.* RNA, 2013. **19**(11): p. 1474-82.

120. Yoon, A., et al., *Impaired control of IRES-mediated translation in X-linked dyskeratosis congenita.* Science, 2006. **312**(5775): p. 902-6.

121. Montanaro, L., et al., *Novel dyskerin-mediated mechanism of p53 inactivation through defective mRNA translation.* Cancer Res, 2010. **70**(11): p. 4767-77.

122. Ito, S., et al., *Human NAT10 is an ATP-dependent RNA acetyltransferase responsible for N4-acetylcytidine formation in 18 S ribosomal RNA (rRNA).* J Biol Chem, 2014. **289**(52): p. 35724-30.

123. Sharma, S., et al., *Yeast Kre33 and human NAT10 are conserved 18S rRNA cytosine acetyltransferases that modify tRNAs assisted by the adaptor Tan1/THUMPD1.* Nucleic Acids Res, 2015. **43**(4): p. 2242-58.

124. Penzo, M., et al., *The importance of being (slightly) modified: The role of rRNA editing on gene expression control and its connections with cancer.* Biochim Biophys Acta, 2016. **1866**(2): p. 330-338.

125. Sharma, S., et al., *Specialized box C/D snoRNPs act as antisense guides to target RNA base acetylation.* PLoS Genet, 2017. **13**(5): p. e1006804.

126. Bartee, D., K.D. Nance, and J.L. Meier, *Site-Specific Synthesis of N(4)-Acetylcytidine in RNA Reveals Physiological Duplex Stabilization.* J Am Chem Soc, 2022. **144**(8): p. 3487-3496.

127. Sas-Chen, A., et al., *Dynamic RNA acetylation revealed by quantitative cross-evolutionary mapping.* Nature, 2020. **583**(7817): p. 638-643.

128. Piekna-Przybylska, D., W.A. Decatur, and M.J. Fournier, *The 3D rRNA modification maps database: with interactive tools for ribosome analysis.* Nucleic Acids Res, 2008. **36**(Database issue): p. D178-83.

129. Taoka, M., et al., *Landscape of the complete RNA chemical modifications in the human 80S ribosome.* Nucleic Acids Res, 2018. **46**(18): p. 9289-9298.

130. Taoka, M., et al., *The complete chemical structure of Saccharomyces cerevisiae rRNA: partial pseudouridylation of U2345 in 25S rRNA by snoRNA snR9.* Nucleic Acids Res, 2016. **44**(18): p. 8951-8961.

131. Waku, T., et al., *NML-mediated rRNA base methylation links ribosomal subunit formation to cell proliferation in a p53-dependent manner.* J Cell Sci, 2016. **129**(12): p. 2382-93.

132. Sharma, S., et al., *A single N(1)-methyladenosine on the large ribosomal subunit rRNA impacts locally its structure and the translation of key metabolic enzymes.* Sci Rep, 2018. **8**(1): p. 11904.

133. Ignatova, V.V., et al., *The rRNA m(6)A methyltransferase METTL5 is involved in pluripotency and developmental programs.* Genes Dev, 2020. **34**(9-10): p. 715-729.

134. Sepich-Poore, C., et al., *The METTL5-TRMT112 N(6)-methyladenosine methyltransferase complex regulates mRNA translation via 18S rRNA methylation.* J Biol Chem, 2022. **298**(3): p. 101590.

135. Pinto, R., et al., *The human methyltransferase ZCCHC4 catalyses N6-methyladenosine modification of 28S ribosomal RNA.* Nucleic Acids Res, 2020. **48**(2): p. 830-846.

136. Heissenberger, C., et al., *The ribosomal RNA m(5)C methyltransferase NSUN-1 modulates healthspan and oogenesis in Caenorhabditis elegans.* Elife, 2020. **9**.

137. Liang, X.H., Q. Liu, and M.J. Fournier, *rRNA modifications in an intersubunit bridge of the ribosome strongly affect both ribosome biogenesis and activity.* Mol Cell, 2007. **28**(6): p. 965-77.

138. Baxter-Roshek, J.L., A.N. Petrov, and J.D. Dinman, *Optimization of ribosome structure and function by rRNA base modification.* PLoS One, 2007. **2**(1): p. e174.

139. Baudin-Baillieu, A., et al., *Nucleotide modifications in three functionally important regions of the Saccharomyces cerevisiae ribosome affect translation accuracy.* Nucleic Acids Res, 2009. **37**(22): p. 7665-77.

140. Yelick, P.C. and P.A. Trainor, *Ribosomopathies: Global process, tissue specific defects.* Rare Dis, 2015. **3**(1): p. e1025185.

141. Nakhoul, H., et al., *Ribosomopathies: mechanisms of disease.* Clin Med Insights Blood Disord, 2014. **7**: p. 7-16.

142. Horos, R. and M. von Lindern, *Molecular mechanisms of pathology and treatment in Diamond Blackfan Anaemia.* Br J Haematol, 2012. **159**(5): p. 514-27.

143. Gazda, H.T., et al., *RNA and protein evidence for haplo-insufficiency in Diamond-Blackfan anaemia patients with RPS19 mutations.* Br J Haematol, 2004. **127**(1): p. 105-13.

144. Vardiman, J.W., N.L. Harris, and R.D. Brunning, *The World Health Organization (WHO) classification of the myeloid neoplasms.* Blood, 2002. **100**(7): p. 2292-302.

145. Ebert, B.L., et al., *Identification of RPS14 as a 5q- syndrome gene by RNA interference screen.* Nature, 2008. **451**(7176): p. 335-9.

146. Boultwood, J., et al., *Narrowing and genomic annotation of the commonly deleted region of the 5q- syndrome.* Blood, 2002. **99**(12): p. 4638-41.

147. Ruggero, D. and A. Shimamura, *Marrow failure: a window into ribosome biology.* Blood, 2014. **124**(18): p. 2784-92.

148. Heiss, N.S., et al., *X-linked dyskeratosis congenita is caused by mutations in a highly conserved gene with putative nucleolar functions.* Nat Genet, 1998. **19**(1): p. 32-8.

149. Bellodi, C., N. Kopmar, and D. Ruggero, *Deregulation of oncogene-induced senescence and p53 translational control in X-linked dyskeratosis congenita.* EMBO J, 2010. **29**(11): p. 1865-76.

150. Armistead, J., et al., *Growth arrest in the ribosomopathy, Bowen-Conradi syndrome, is due to dramatically reduced cell proliferation and a defect in mitotic progression.* Biochim Biophys Acta, 2015. **1852**(5): p. 1029-37.

151. Warda, A.S., et al., *Effects of the Bowen-Conradi syndrome mutation in EMG1 on its nuclear import, stability and nucleolar recruitment.* Hum Mol Genet, 2016. **25**(24): p. 5353-5364.

152. Bellodi, C., et al., *Loss of function of the tumor suppressor DKC1 perturbs p27 translation control and contributes to pituitary tumorigenesis.* Cancer Res, 2010. **70**(14): p. 6026-35.

153. Kim, M.S., et al., *Expressional analysis of NOLA1, NOLA2, NOLA3 and DKC1, the core proteins in H/ACA riboproteins, in gastric and colorectal cancers.* Pathology, 2012. **44**(6): p. 576-7.

154. Hou, P., et al., *DKC1 enhances angiogenesis by promoting HIF-1alpha transcription and facilitates metastasis in colorectal cancer.* Br J Cancer, 2020. **122**(5): p. 668-679.

155. Liu, B., et al., *Dyskerin overexpression in human hepatocellular carcinoma is associated with advanced clinical stage and poor patient prognosis.* PLoS One, 2012. **7**(8): p. e43147.

156. O'Brien, R., et al., *MYC-Driven Neuroblastomas Are Addicted to a Telomerase-Independent Function of Dyskerin.* Cancer Res, 2016. **76**(12): p. 3604-17.

157. Sieron, P., et al., *DKC1 overexpression associated with prostate cancer progression.* Br J Cancer, 2009. **101**(8): p. 1410-6.

158. Ruggero, D., et al., *Dyskeratosis congenita and cancer in mice deficient in ribosomal RNA modification.* Science, 2003. **299**(5604): p. 259-62.

159. Krogh, N., et al., *Profiling of ribose methylations in ribosomal RNA from diffuse large B-cell lymphoma patients for evaluation of ribosomes as drug targets.* NAR Cancer, 2020. **2**(4): p. zcaa035.

160. Marcel, V., et al., *Ribosomal RNA 2'O-methylation as a novel layer of inter-tumour heterogeneity in breast cancer.* NAR Cancer, 2020. **2**(4): p. zcaa036.

146

161. Marcel, V., et al., *p53 acts as a safeguard of translational control by regulating fibrillarin and rRNA methylation in cancer.* Cancer Cell, 2013. **24**(3): p. 318-30.

162. Babaian, A., et al., *Loss of m(1)acp(3)Psi Ribosomal RNA Modification Is a Major Feature of Cancer.* Cell Rep, 2020. **31**(5): p. 107611.

163. Jhiang, S.M., M. Yaneva, and H. Busch, *Expression of human proliferation-associated nucleolar antigen p120.* Cell Growth Differ, 1990. **1**(7): p. 319-24.

164. Huang, H., et al., *Ribosome 18S m(6)A methyltransferase METTL5 promotes pancreatic cancer progression by modulating c-Myc translation.* Int J Oncol, 2022. **60**(1).

165. Peng, H., et al., *N(6)-methyladenosine (m(6)A) in 18S rRNA promotes fatty acid metabolism and oncogenic transformation.* Nat Metab, 2022. **4**(8): p. 1041-1054.

166. Rong, B., et al., *Ribosome 18S m(6)A Methyltransferase METTL5 Promotes Translation Initiation and Breast Cancer Cell Growth.* Cell Rep, 2020. **33**(12): p. 108544.

167. Yankova, E., et al., *Small-molecule inhibition of METTL3 as a strategy against myeloid leukaemia.* Nature, 2021. **593**(7860): p. 597-601.

168. Squires, J.E., et al., *Widespread occurrence of 5-methylcytosine in human coding and non-coding RNA.* Nucleic Acids Res, 2012. **40**(11): p. 5023-33.

169. Garcia-Vilchez, R., A. Sevilla, and S. Blanco, *Post-transcriptional regulation by cytosine-5 methylation of RNA.* Biochim Biophys Acta Gene Regul Mech, 2019. **1862**(3): p. 240-252.

170. Hussain, S., et al., *Characterizing 5-methylcytosine in the mammalian epitranscriptome.* Genome Biol, 2013. **14**(11): p. 215.

171. Tuorto, F., et al., *The tRNA methyltransferase Dnmt2 is required for accurate polypeptide synthesis during haematopoiesis.* EMBO J, 2015. **34**(18): p. 2350-62.

172. Goll, M.G., et al., *Methylation of tRNAAsp by the DNA methyltransferase homolog Dnmt2.* Science, 2006. **311**(5759): p. 395-8.

173. Li, H., et al., *New substrates and determinants for tRNA recognition of RNA methyltransferase DNMT2/TRDMT1.* RNA Biol, 2021. **18**(12): p. 2531-2545.

174. Tuorto, F., et al., *RNA cytosine methylation by Dnmt2 and NSun2 promotes tRNA stability and protein synthesis.* Nat Struct Mol Biol, 2012. **19**(9): p. 900-5.

175. Haag, S., et al., *NSUN6 is a human RNA methyltransferase that catalyzes formation of m5C72 in specific tRNAs.* RNA, 2015. **21**(9): p. 1532-43.

176. Hussain, S., et al., *NSun2-mediated cytosine-5 methylation of vault noncoding RNA determines its processing into regulatory small RNAs.* Cell Rep, 2013. **4**(2): p. 255-61.

177. Li, Y., et al., *Novel long noncoding RNA NMR promotes tumor progression via NSUN2 and BPTF in esophageal squamous cell carcinoma.* Cancer Lett, 2018. **430**: p. 57-66.

178. Sun, Z., et al., *Aberrant NSUN2-mediated m(5)C modification of H19 lncRNA is associated with poor differentiation of hepatocellular carcinoma.* Oncogene, 2020. **39**(45): p. 6906-6919.

179. Selmi, T., et al., *Sequence- and structure-specific cytosine-5 mRNA methylation by NSUN6.* Nucleic Acids Res, 2021. **49**(2): p. 1006-1022.

180. Haag, S., et al., *NSUN3 and ABH1 modify the wobble position of mt-tRNAMet to expand codon recognition in mitochondrial translation.* EMBO J, 2016. **35**(19): p. 2104-2119.

181. Heissenberger, C., et al., *Loss of the ribosomal RNA methyltransferase NSUN5 impairs global protein synthesis and normal growth.* Nucleic Acids Res, 2019. **47**(22): p. 11807-11825.

182. Metodiev, M.D., et al., *NSUN4 is a dual function mitochondrial protein required for both methylation of 12S rRNA and coordination of mitoribosomal assembly.* PLoS Genet, 2014. **10**(2): p. e1004110.

183. Aguilo, F., et al., *Deposition of 5-Methylcytosine on Enhancer RNAs Enables the Coactivator Function of PGC-1alpha.* Cell Rep, 2016. **14**(3): p. 479-492.

184. Ortiz-Barahona, V., et al., *Epigenetic inactivation of the 5-methylcytosine RNA methyltransferase NSUN7 is associated with clinical outcome and therapeutic vulnerability in liver cancer.* Mol Cancer, 2023. **22**(1): p. 83.

185. Motorin, Y. and H. Grosjean, *Multisite-specific tRNA:m5C-methyltransferase (Trm4) in yeast Saccharomyces cerevisiae: identification of the gene and substrate specificity of the enzyme.* RNA, 1999. **5**(8): p. 1105-18.

186. Fu, L., et al., *Tet-mediated formation of 5-hydroxymethylcytosine in RNA.* J Am Chem Soc, 2014. **136**(33): p. 11582-5.

187. Sobala, A. and G. Hutvagner, *Small RNAs derived from the 5' end of tRNA can inhibit protein translation in human cells.* RNA Biol, 2013. **10**(4): p. 553-63.

188. Schaefer, M., et al., *RNA methylation by Dnmt2 protects transfer RNAs against stress-induced cleavage.* Genes Dev, 2010. **24**(15): p. 1590-5.

189. Delaunay, S., et al., *Mitochondrial RNA modifications shape metabolic plasticity in metastasis.* Nature, 2022. **607**(7919): p. 593-603.

190. Trixl, L., et al., *RNA cytosine methyltransferase Nsun3 regulates embryonic stem cell differentiation by promoting mitochondrial activity.* Cell Mol Life Sci, 2018. **75**(8): p. 1483-1497.

191. Schosserer, M., et al., *Methylation of ribosomal RNA by NSUN5 is a conserved mechanism modulating organismal lifespan.* Nat Commun, 2015. **6**: p. 6158.

192. Shen, Q., et al., *Tet2 promotes pathogen infection-induced myelopoiesis through mRNA oxidation.* Nature, 2018. **554**(7690): p. 123-127.

193. Basanta-Sanchez, M., et al., *TET1-Mediated Oxidation of 5-Formylcytosine (5fC) to 5-Carboxycytosine (5caC) in RNA.* Chembiochem, 2017. **18**(1): p. 72-76.

194. Khan, M.A., et al., *Mutation in NSUN2, which encodes an RNA methyltransferase, causes autosomal-recessive intellectual disability.* Am J Hum Genet, 2012. **90**(5): p. 856-63.

195. Fahiminiya, S., et al., *Whole exome sequencing unravels disease-causing genes in consanguineous families in Qatar.* Clin Genet, 2014. **86**(2): p. 134-41.

196. Martinez, F.J., et al., *Whole exome sequencing identifies a splicing mutation in NSUN2 as a cause of a Dubowitz-like syndrome.* J Med Genet, 2012. **49**(6): p. 380-5.

197. Flores, J.V., et al., *Cytosine-5 RNA Methylation Regulates Neural Stem Cell Differentiation and Motility.* Stem Cell Reports, 2017. **8**(1): p. 112-124.

198. Frye, M. and F.M. Watt, *The RNA methyltransferase Misu (NSun2) mediates Myc-induced proliferation and is upregulated in tumors.* Curr Biol, 2006. **16**(10): p. 971-81.

199. Mei, L., et al., *RNA methyltransferase NSUN2 promotes gastric cancer cell proliferation by repressing p57(Kip2) by an m(5)C-dependent manner.* Cell Death Dis, 2020. **11**(4): p. 270.

200. Song, D., et al., *NSUN2-mediated mRNA m(5)C Modification Regulates the Progression of Hepatocellular Carcinoma.* Genomics Proteomics Bioinformatics, 2022.

201. Su, J., et al., *NSUN2-mediated RNA 5-methylcytosine promotes esophageal squamous cell carcinoma progression via LIN28B-dependent GRB2 mRNA stabilization.* Oncogene, 2021. **40**(39): p. 5814-5828.

202. Tong, X., et al., *NSUN2 Promotes Tumor Progression and Regulates Immune Infiltration in Nasopharyngeal Carcinoma.* Front Oncol, 2022. **12**: p. 788801.

203. Awah, C.U., et al., *NSUN6, an RNA methyltransferase of 5-mC controls glioblastoma response to temozolomide (TMZ) via NELFB and RPS6KB2 interaction.* Cancer Biol Ther, 2021. **22**(10-12): p. 587-597.

204. Gorczyca, W., et al., *Cell cycle-related expression of p120 nucleolar antigen in normal human lymphocytes and in cells of HL-60 and MOLT-4 leukemic lines: effects of methotrexate, camptothecin, and teniposide.* Cancer Res, 1992. **52**(12): p. 3491-4.

205. McGrath, P.C., et al., *Proliferation-associated nucleolar antigen P120: a prognostic marker in node-negative breast cancer.* Surgery, 1994. **116**(4): p. 616-20; discussion 20-1.

206. Uchiyama, B., et al., *Expression of nucleolar protein p120 in human lung cancer: difference in histological types as a marker for proliferation.* Clin Cancer Res, 1997. **3**(10): p. 1873-7.

207. Feng, J., et al., *Upregulated expression of NOP2 predicts worse prognosis of gastric adenocarcinoma by promoting tumor growth.* Saudi J Gastroenterol, 2022. **28**(5): p. 369-377.

208. Li, H., et al., *Prognostic Value of an m(5)C RNA Methylation Regulator-Related Signature for Clear Cell Renal Cell Carcinoma.* Cancer Manag Res, 2021. **13**: p. 6673-6687.

209. Fonagy, A., et al., *Cell cycle regulated expression of nucleolar antigen P120 in normal and transformed human fibroblasts.* J Cell Physiol, 1993. **154**(1): p. 16-27.

210. He, Y., et al., *Role of m(5)C-related regulatory genes in the diagnosis and prognosis of hepatocellular carcinoma.* Am J Transl Res, 2020. **12**(3): p. 912-922.

211. Pan, J., Z. Huang, and Y. Xu, *m5C RNA Methylation Regulators Predict Prognosis and Regulate the Immune Microenvironment in Lung Squamous Cell Carcinoma.* Front Oncol, 2021. **11**: p. 657466.

212. Khosronezhad, N., A.H. Colagar, and S.G. Jorsarayi, *T26248G-transversion mutation in exon7 of the putative methyltransferase Nsun7 gene causes a change in protein folding associated with reduced sperm motility in asthenospermic men.* Reprod Fertil Dev, 2015. **27**(3): p. 471-80.

213. Yan, J., et al., *FOXC2-AS1 stabilizes FOXC2 mRNA via association with NSUN2 in gastric cancer cells.* Hum Cell, 2021. **34**(6): p. 1755-1764.

214. Li, Y., et al., *TET2-mediated mRNA demethylation regulates leukemia stem cell homing and self-renewal.* Cell Stem Cell, 2023. **30**(8): p. 1072-1090 e10.

215. Gao, Y., et al., *NOP2/Sun RNA methyltransferase 2 promotes tumor progression via its interacting partner RPL6 in gallbladder carcinoma.* Cancer Sci, 2019. **110**(11): p. 3510-3519.

216. Zhu, W., et al., *Positive epigenetic regulation loop between AR and NSUN2 promotes prostate cancer progression.* Clin Transl Med, 2022. **12**(9): p. e1028.

217. Yang, J.C., et al., *Association of tRNA methyltransferase NSUN2/IGF-II molecular signature with ovarian cancer survival.* Future Oncol, 2017. **13**(22): p. 1981-1990.

218. Paramasivam, A., et al., *Novel Biallelic NSUN3 Variants Cause Early-Onset Mitochondrial Encephalomyopathy and Seizures.* J Mol Neurosci, 2020. **70**(12): p. 1962-1965.

219. Van Haute, L., et al., *Deficient methylation and formylation of mt-tRNA(Met) wobble cytosine in a patient carrying mutations in NSUN3.* Nat Commun, 2016. **7**: p. 12039.

220. Chen, P., et al., *Expression of the RNA methyltransferase Nsun5 is essential for developing cerebral cortex.* Mol Brain, 2019. **12**(1): p. 74.

221. Francke, U., *Williams-Beuren syndrome: genes and mechanisms.* Hum Mol Genet, 1999. **8**(10): p. 1947-54.

222. Yuan, Z., et al., *Agenesis and Hypomyelination of Corpus Callosum in Mice Lacking Nsun5, an RNA Methyltransferase.* Cells, 2019. **8**(6).

223. Zhang, T., et al., *Cognitive deficits in mice lacking Nsun5, a cytosine-5 RNA methyltransferase, with impairment of oligodendrocyte precursor cells.* Glia, 2019. **67**(4): p. 688-702.

224. Li, L., et al., *Knocking down NSUN5 inhibits the development of clear cell renal cell carcinoma by inhibiting the p53 pathway.* Aging (Albany NY), 2023. **15**(11): p. 4757-4773.

225. Zhang, X.W., et al., *NSUN5 promotes progression and predicts poor prognosis in hepatocellular carcinoma.* Oncol Lett, 2022. **24**(6): p. 439.

226. Jiang, Z., et al., *High expression of NSUN5 promotes cell proliferation via cell cycle regulation in colorectal cancer.* Am J Transl Res, 2020. **12**(7): p. 3858-3870.

227. Yang, R., et al., *The RNA methyltransferase NSUN6 suppresses pancreatic cancer development by regulating cell proliferation.* EBioMedicine, 2021. **63**: p. 103195.

228. Tate, J.G., et al., *COSMIC: the Catalogue Of Somatic Mutations In Cancer.* Nucleic Acids Res, 2019. **47**(D1): p. D941-D947.

229. Elhardt, W., et al., *Somatic cancer mutations in the DNMT2 tRNA methyltransferase alter its catalytic properties.* Biochimie, 2015. **112**: p. 66-72.

230. Towns, W.L. and T.J. Begley, *Transfer RNA methytransferases and their corresponding modifications in budding yeast and humans: activities, predications, and potential roles in human health.* DNA Cell Biol, 2012. **31**(4): p. 434-54.

231. Gailhouste, L., et al., *Epigenetic reprogramming using 5-azacytidine promotes an anti-cancer response in pancreatic adenocarcinoma cells.* Cell Death Dis, 2018. **9**(5): p. 468.

232. Ivanoff, S., et al., *5-Azacytidine treatment for relapsed or refractory acute myeloid leukemia after intensive chemotherapy.* Am J Hematol, 2013. **88**(7): p. 601-5.

233. Schaefer, M., et al., *Azacytidine inhibits RNA methylation at DNMT2 target sites in human cancer cell lines.* Cancer Res, 2009. **69**(20): p. 8127-32.

234. Cheng, J.X., et al., *RNA cytosine methylation and methyltransferases mediate chromatin organization and 5-azacytidine response and resistance in leukaemia.* Nat Commun, 2018. **9**(1): p. 1163.

235. Guan, Y., et al., *A Therapeutic Strategy for Preferential Targeting of TET2 Mutant and TET-dioxygenase Deficient Cells in Myeloid Neoplasms.* Blood Cancer Discov, 2021. **2**(2): p. 146-161.

236. Chua, G.N.L., et al., *Cytosine-Based TET Enzyme Inhibitors.* ACS Med Chem Lett, 2019. **10**(2): p. 180-185.

237. Chen, L.L., et al., *Itaconate inhibits TET DNA dioxygenases to dampen inflammatory responses.* Nat Cell Biol, 2022. **24**(3): p. 353-363.

238. Gigova, A., et al., *A cluster of methylations in the domain IV of 25S rRNA is required for ribosome stability.* RNA, 2014. **20**(10): p. 1632-44.

239. Behrmann, E., et al., *Structural snapshots of actively translating human ribosomes.* Cell, 2015. **161**(4): p. 845-57.

240. Zhou, J., et al., *RNA cytosine methyltransferase NSUN5 promotes protein synthesis and tumorigenic phenotypes in glioblastoma.* Mol Oncol, 2023.

241. Pober, B.R., *Williams-Beuren syndrome.* N Engl J Med, 2010. **362**(3): p. 239-52.

242. Tassabehji, M., *Williams-Beuren syndrome: a challenge for genotype-phenotype correlations.* Hum Mol Genet, 2003. **12 Spec No 2**: p. R229-37.

243. Wang, Y.C., S.E. Peterson, and J.F. Loring, *Protein post-translational modifications and regulation of pluripotency in human stem cells.* Cell Res, 2014. **24**(2): p. 143-60.

244. Sakita-Suto, S., et al., *Aurora-B regulates RNA methyltransferase NSUN2.* Mol Biol Cell, 2007. **18**(3): p. 1107-17.

245. Hussain, S., et al., *The nucleolar RNA methyltransferase Misu (NSun2) is required for mitotic spindle stability.* J Cell Biol, 2009. **186**(1): p. 27-40.

246. Muller, M., et al., *Dynamic modulation of Dnmt2-dependent tRNA methylation by the micronutrient queuine.* Nucleic Acids Res, 2015. **43**(22): p. 10952-62.

247. Tuorto, F., et al., *Queuosine-modified tRNAs confer nutritional control of protein translation.* EMBO J, 2018. **37**(18).

248. Manning, M., et al., *Pan-cancer analysis of RNA methyltransferases identifies FTSJ3 as a potential regulator of breast cancer progression.* RNA Biol, 2020. **17**(4): p. 474-486.

249. Wang, Z., *Cell Cycle Progression and Synchronization: An Overview.* Methods Mol Biol, 2022. **2579**: p. 3-23.

250. Pardee, A.B., *G1 events and regulation of cell proliferation.* Science, 1989. **246**(4930): p. 603-8.

251. Morgan, D.O., *Cyclin-dependent kinases: engines, clocks, and microprocessors.* Annu Rev Cell Dev Biol, 1997. **13**: p. 261-91.

252. Nigg, E.A., *Cyclin-dependent protein kinases: key regulators of the eukaryotic cell cycle.* Bioessays, 1995. **17**(6): p. 471-80.

253. Cross, F.R., et al., *Specialization and targeting of B-type cyclins.* Mol Cell, 1999. **4**(1): p. 11-9.

254. Fassl, A., Y. Geng, and P. Sicinski, *CDK4 and CDK6 kinases: From basic science to cancer therapy.* Science, 2022. **375**(6577): p. eabc1495.

255. De Bondt, H.L., et al., *Crystal structure of cyclin-dependent kinase 2.* Nature, 1993. **363**(6430): p. 595-602.

256. Jeffrey, P.D., et al., *Mechanism of CDK activation revealed by the structure of a cyclinA-CDK2 complex.* Nature, 1995. **376**(6538): p. 313-20.

257. Santamaria, D., et al., *Cdk1 is sufficient to drive the mammalian cell cycle.* Nature, 2007. **448**(7155): p. 811-5.

258. Canepa, E.T., et al., *INK4 proteins, a family of mammalian CDK inhibitors with novel biological functions.* IUBMB Life, 2007. **59**(7): p. 419-26.

259. Ortega, S., M. Malumbres, and M. Barbacid, *Cyclin D-dependent kinases, INK4 inhibitors and cancer.* Biochim Biophys Acta, 2002. **1602**(1): p. 73-87.

260. Denicourt, C. and S.F. Dowdy, *Cip/Kip proteins: more than just CDKs inhibitors.* Genes Dev, 2004. **18**(8): p. 851-5.

261. Malumbres, M. and M. Barbacid, *Mammalian cyclin-dependent kinases.* Trends Biochem Sci, 2005. **30**(11): p. 630-41.

262. Barnum, K.J. and M.J. O'Connell, *Cell cycle regulation by checkpoints.* Methods Mol Biol, 2014. **1170**: p. 29-40.

263. Musacchio, A. and E.D. Salmon, *The spindle-assembly checkpoint in space and time.* Nat Rev Mol Cell Biol, 2007. **8**(5): p. 379-93.

264. Visconti, R., R. Della Monica, and D. Grieco, *Cell cycle checkpoint in cancer: a therapeutically targetable double-edged sword.* J Exp Clin Cancer Res, 2016. **35**(1): p. 153.

265. Li, H., et al., *METTL3 promotes cell cycle progression via m(6)A/YTHDF1-dependent regulation of CDC25B translation.* Int J Biol Sci, 2022. **18**(8): p. 3223-3236.

266. Kim, Y., et al., *METTL3 regulates alternative splicing of cell cycle-related genes via crosstalk between mRNA m(6)A modifications and splicing factors.* Am J Cancer Res, 2023. **13**(4): p. 1443-1456.

267. Hirayama, M., et al., *FTO Demethylates Cyclin D1 mRNA and Controls Cell-Cycle Progression.* Cell Rep, 2020. **31**(1): p. 107464.

268. Schaefer, M., J.P. Steringer, and F. Lyko, *The Drosophila cytosine-5 methyltransferase Dnmt2 is associated with the nuclear matrix and can access DNA during mitosis.* PLoS One, 2008. **3**(1): p. e1414.

269. Wilson, A. and J.W. Freeman, *Regulation of P120 mRNA levels during lymphocyte stimulation: evidence that the P120 gene shares properties with early and late genes.* J Cell Biochem, 1996. **60**(4): p. 458-68.

270. Bursac, S., et al., *Activation of the tumor suppressor p53 upon impairment of ribosome biogenesis.* Biochim Biophys Acta, 2014. **1842**(6): p. 817-30.

271. Miliani de Marval, P.L. and Y. Zhang, *The RP-Mdm2-p53 pathway and tumorigenesis.* Oncotarget, 2011. **2**(3): p. 234-8.

272. Zhang, Y. and H. Lu, *Signaling to p53: ribosomal proteins find their way.* Cancer Cell, 2009. **16**(5): p. 369-77.

273. Polymenis, M. and R. Aramayo, *Translate to divide: control of the cell cycle by protein synthesis.* Microb Cell, 2015. **2**(4): p. 94-104.

274. Alber, A.B. and D.M. Suter, *Dynamics of protein synthesis and degradation through the cell cycle.* Cell Cycle, 2019. **18**(8): p. 784-794.

275. Martinez-Salas, E., et al., *Functional interactions in internal translation initiation directed by viral and cellular IRES elements.* J Gen Virol, 2001. **82**(Pt 5): p. 973-984.

276. Fan, H. and S. Penman, *Regulation of protein synthesis in mammalian cells. II. Inhibition of protein synthesis at the level of initiation during mitosis.* J Mol Biol, 1970. **50**(3): p. 655-70.

277. Stumpf, C.R., et al., *The translational landscape of the mammalian cell cycle.* Mol Cell, 2013. **52**(4): p. 574-82.

278. Cornelis, S., et al., *Identification and characterization of a novel cell cycle-regulated internal ribosome entry site.* Mol Cell, 2000. **5**(4): p. 597-605.

279. Qin, X. and P. Sarnow, *Preferential translation of internal ribosome entry site-containing mRNAs during the mitotic cycle in mammalian cells.* J Biol Chem, 2004. **279**(14): p. 13721-8.

280. Ramirez-Valle, F., et al., *Mitotic raptor promotes mTORC1 activity, G(2)/M cell cycle progression, and internal ribosome entry site-mediated mRNA translation.* Mol Cell Biol, 2010. **30**(13): p. 3151-64.

281. Shuda, M., et al., *CDK1 substitutes for mTOR kinase to activate mitotic cap-dependent protein translation.* Proc Natl Acad Sci U S A, 2015. **112**(19): p. 5875-82.

282. Sun, R., et al., *Mitosis-related phosphorylation of the eukaryotic translation suppressor 4E-BP1 and its interaction with eukaryotic translation initiation factor 4E (eIF4E).* J Biol Chem, 2019. **294**(31): p. 11840-11852.

283. Coldwell, M.J., et al., *Phosphorylation of eIF4GII and 4E-BP1 in response to nocodazole treatment: a reappraisal of translation initiation during mitosis.* Cell Cycle, 2013. **12**(23): p. 3615-28.

284. Tanenbaum, M.E., et al., *Regulation of mRNA translation during mitosis.* Elife, 2015. **4**.

285. Miettinen, T.P., et al., *Mammalian cell growth dynamics in mitosis.* Elife, 2019. **8**.

286. Papst, P.J., et al., *Cdc2-cyclin B phosphorylates p70 S6 kinase on Ser411 at mitosis.* J Biol Chem, 1998. **273**(24): p. 15077-84.

287. Belle, R., et al., *Phosphorylation of elongation factor-1 (EF-1) by cdc2 kinase.* Prog Cell Cycle Res, 1995. **1**: p. 265-70.

288. Smith, E.M. and C.G. Proud, *cdc2-cyclin B regulates eEF2 kinase activity in a cell cycle- and amino acid-dependent manner.* EMBO J, 2008. **27**(7): p. 1005-16.

289. Dobrikov, M.I., et al., *Mitotic phosphorylation of eukaryotic initiation factor 4G1 (eIF4G1) at Ser1232 by Cdk1:cyclin B inhibits eIF4A helicase complex binding with RNA.* Mol Cell Biol, 2014. **34**(3): p. 439-51.

154

290. Clemm von Hohenberg, K., et al., *Cyclin B/CDK1 and Cyclin A/CDK2 phosphorylate DENR to promote mitotic protein translation and faithful cell division.* Nat Commun, 2022. **13**(1): p. 668.

291. Haneke, K., et al., *CDK1 couples proliferation with protein synthesis.* J Cell Biol, 2020. **219**(3).

292. Imami, K., et al., *Phosphorylation of the Ribosomal Protein RPL12/uL11 Affects Translation during Mitosis.* Mol Cell, 2018. **72**(1): p. 84-98 e9.

293. Dang, F., L. Nie, and W. Wei, *Ubiquitin signaling in cell cycle control and tumorigenesis.* Cell Death Differ, 2021. **28**(2): p. 427-438.

294. Koepp, D.M., *Cell cycle regulation by protein degradation.* Methods Mol Biol, 2014. **1170**: p. 61-73.

295. Malumbres, M. and M. Barbacid, *To cycle or not to cycle: a critical decision in cancer.* Nat Rev Cancer, 2001. **1**(3): p. 222-31.

296. Malumbres, M. and M. Barbacid, *Cell cycle, CDKs and cancer: a changing paradigm.* Nat Rev Cancer, 2009. **9**(3): p. 153-66.

297. Abukhdeir, A.M. and B.H. Park, *P21 and p27: roles in carcinogenesis and drug resistance.* Expert Rev Mol Med, 2008. **10**: p. e19.

298. Puhalla, H., et al., *Expression of p21(Wafl/Cip1), p57(Kip2) and HER2/neu in patients with gallbladder cancer.* Anticancer Res, 2007. **27**(3B): p. 1679-84.

299. Villwock Mde, M., et al., *Prevalence of p21 immunohistochemical expression in esophageal adenocarcinoma.* Arq Gastroenterol, 2006. **43**(3): p. 212-8.

300. Porter, P.L., et al., *Expression of cell-cycle regulators p27Kip1 and cyclin E, alone and in combination, correlate with survival in young breast cancer patients.* Nat Med, 1997. **3**(2): p. 222-5.

301. Ortiz, A.B., et al., *Prognostic significance of cyclin D1 protein expression and gene amplification in invasive breast carcinoma.* PLoS One, 2017. **12**(11): p. e0188068.

302. Puntervoll, H.E., et al., *Melanoma prone families with CDK4 germline mutation: phenotypic profile and associations with MC1R variants.* J Med Genet, 2013. **50**(4): p. 264-70.

303. Schraml, P., et al., *Cyclin E overexpression and amplification in human tumours.* J Pathol, 2003. **200**(3): p. 375-82.

304. Caruso, J.A., et al., *Low-Molecular-Weight Cyclin E in Human Cancer: Cellular Consequences and Opportunities for Targeted Therapies.* Cancer Res, 2018. **78**(19): p. 5481-5491.

305. Wingate, H., et al., *The tumor-specific hyperactive forms of cyclin E are resistant to inhibition by p21 and p27.* J Biol Chem, 2005. **280**(15): p. 15148-57.

306. Porter, D.C., et al., *Tumor-specific proteolytic processing of cyclin E generates hyperactive lower-molecular-weight forms.* Mol Cell Biol, 2001. **21**(18): p. 6254-69.

307. Yang, Y., et al., *Systematic Pan-Cancer Analysis Identifies CDK1 as an Immunological and Prognostic Biomarker.* J Oncol, 2022. **2022**: p. 8115474.

308. Consortium, A.P.G., *AACR Project GENIE: Powering Precision Medicine through an International Consortium.* Cancer Discov, 2017. **7**(8): p. 818-831.

309. Yasmeen, A., et al., *E- and A-type cyclins as markers for cancer diagnosis and prognosis.* Expert Rev Mol Diagn, 2003. **3**(5): p. 617-33.

310. Consortium, I.T.P.-C.A.o.W.G., *Pan-cancer analysis of whole genomes.* Nature, 2020. **578**(7793): p. 82-93.

311. Jardim, D.L., et al., *Cyclin Pathway Genomic Alterations Across 190,247 Solid Tumors: Leveraging Large-Scale Data to Inform Therapeutic Directions.* Oncologist, 2021. **26**(1): p. e78-e89.

312. Au-Yeung, G., et al., *Selective Targeting of Cyclin E1-Amplified High-Grade Serous Ovarian Cancer by Cyclin-Dependent Kinase 2 and AKT Inhibition.* Clin Cancer Res, 2017. **23**(7): p. 1862-1874.

313. Huber, A.R., et al., *High expression of carbonic anhydrase IX is significantly associated with glandular lesions in gastroesophageal junction and with tumorigenesis markers BMI1, MCM4 and MCM7.* BMC Gastroenterol, 2015. **15**: p. 80.

314. DeLair, D.F., et al., *The genetic landscape of endometrial clear cell carcinomas.* J Pathol, 2017. **243**(2): p. 230-241.

315. Milne, A.N., et al., *Cyclin E low molecular weight isoforms occur commonly in early-onset gastric cancer and independently predict survival.* J Clin Pathol, 2008. **61**(3): p. 311-6.

316. Shamloo, B. and S. Usluer, *p21 in Cancer Research.* Cancers (Basel), 2019. **11**(8).

317. Korkolopoulou, P., et al., *Expression of retinoblastoma gene product and p21 (WAF1/Cip 1) protein in gliomas: correlations with proliferation markers, p53 expression and survival.* Acta Neuropathol, 1998. **95**(6): p. 617-24.

318. Zhang, W., et al., *High levels of constitutive WAF1/Cip1 protein are associated with chemoresistance in acute myelogenous leukemia.* Clin Cancer Res, 1995. **1**(9): p. 1051-7.

319. de Bruijn, I., et al., *Analysis and Visualization of Longitudinal Genomic and Clinical Data from the AACR Project GENIE Biopharma Collaborative in cBioPortal.* Cancer Res, 2023.

320. Gao, J., et al., *Integrative analysis of complex cancer genomics and clinical profiles using the cBioPortal.* Sci Signal, 2013. **6**(269): p. pl1.

321. Bencivenga, D., et al., *A cancer-associated CDKN1B mutation induces p27 phosphorylation on a novel residue: a new mechanism for tumor suppressor loss-of-function.* Mol Oncol, 2021. **15**(4): p. 915-941.

322. Olivier, M., M. Hollstein, and P. Hainaut, *TP53 mutations in human cancers: origins, consequences, and clinical use.* Cold Spring Harb Perspect Biol, 2010. **2**(1): p. a001008.

323. Linn, P., et al., *Targeting RB1 Loss in Cancers.* Cancers (Basel), 2021. **13**(15).

324. Sofi, S., et al., *Targeting cyclin-dependent kinase 1 (CDK1) in cancer: molecular docking and dynamic simulations of potential CDK1 inhibitors.* Med Oncol, 2022. **39**(9): p. 133.

325. Li, J., et al., *CDK1 and CDC20 overexpression in patients with colorectal cancer are associated with poor prognosis: evidence from integrated bioinformatics analysis.* World J Surg Oncol, 2020. **18**(1): p. 50.

326. Liu, X., H. Wu, and Z. Liu, *An Integrative Human Pan-Cancer Analysis of Cyclin-Dependent Kinase 1 (CDK1).* Cancers (Basel), 2022. **14**(11).

327. Yu, M., Q. Zhan, and O.J. Finn, *Immune recognition of cyclin B1 as a tumor antigen is a result of its overexpression in human tumors that is caused by non-functional p53.* Mol Immunol, 2002. **38**(12-13): p. 981-7.

328. Yamasaki, L., *Role of the RB tumor suppressor in cancer.* Cancer Treat Res, 2003. **115**: p. 209-39.

329. Burkhart, D.L. and J. Sage, *Cellular mechanisms of tumour suppression by the retinoblastoma gene.* Nat Rev Cancer, 2008. **8**(9): p. 671-82.

330. Friend, S.H., et al., *A human DNA segment with properties of the gene that predisposes to retinoblastoma and osteosarcoma.* Nature, 1986. **323**(6089): p. 643-6.

331. Braal, C.L., et al., *Inhibiting CDK4/6 in Breast Cancer with Palbociclib, Ribociclib, and Abemaciclib: Similarities and Differences.* Drugs, 2021. **81**(3): p. 317-331.

332. Hortobagyi, G.N., et al., *Overall Survival with Ribociclib plus Letrozole in Advanced Breast Cancer.* N Engl J Med, 2022. **386**(10): p. 942-950.

333. Suski, J.M., et al., *Targeting cell-cycle machinery in cancer.* Cancer Cell, 2021. **39**(6): p. 759-778.

334. Xu, X.Q., et al., *Intrinsic and acquired resistance to CDK4/6 inhibitors and potential overcoming strategies.* Acta Pharmacol Sin, 2021. **42**(2): p. 171-178.

335. Olson, C.M., et al., *Development of a Selective CDK7 Covalent Inhibitor Reveals Predominant Cell-Cycle Phenotype.* Cell Chem Biol, 2019. **26**(6): p. 792-803 e10.

336. Patel, H., et al., *ICEC0942, an Orally Bioavailable Selective Inhibitor of CDK7 for Cancer Treatment.* Mol Cancer Ther, 2018. **17**(6): p. 1156-1166.

337. Liu, S., et al., *Optimization of non-ATP competitive CDK/cyclin groove inhibitors through REPLACE-mediated fragment assembly.* J Med Chem, 2013. **56**(4): p. 1573-82.

338. Sandig, V., et al., *Adenovirally transferred p16INK4/CDKN2 and p53 genes cooperate to induce apoptotic tumor cell death.* Nat Med, 1997. **3**(3): p. 313-9.

339. Chen, S. and L. Li, *Degradation strategy of cyclin D1 in cancer cells and the potential clinical application.* Front Oncol, 2022. **12**: p. 949688.

340. Saini, S.S. and M.A. Klein, *Targeting cyclin D1 in non-small cell lung cancer and mesothelioma cells by antisense oligonucleotides.* Anticancer Res, 2011. **31**(11): p. 3683-90.

341. Llovet, J.M., et al., *Molecular pathogenesis and systemic therapies for hepatocellular carcinoma.* Nat Cancer, 2022. **3**(4): p. 386-401.

342. Suresh, D., A.N. Srinivas, and D.P. Kumar, *Etiology of Hepatocellular Carcinoma: Special Focus on Fatty Liver Disease.* Front Oncol, 2020. **10**: p. 601710.

343. Anwanwan, D., et al., *Challenges in liver cancer and possible treatment approaches.* Biochim Biophys Acta Rev Cancer, 2020. **1873**(1): p. 188314.

344. Llovet, J.M., et al., *Sorafenib in advanced hepatocellular carcinoma.* N Engl J Med, 2008. **359**(4): p. 378-90.

345. Llovet, J.M., et al., *Hepatocellular carcinoma.* Nat Rev Dis Primers, 2021. **7**(1): p. 6.

346. Schulze, K., et al., *Exome sequencing of hepatocellular carcinomas identifies new mutational signatures and potential therapeutic targets.* Nat Genet, 2015. **47**(5): p. 505-511.

347. Torrecilla, S., et al., *Trunk mutational events present minimal intra- and inter-tumoral heterogeneity in hepatocellular carcinoma.* J Hepatol, 2017. **67**(6): p. 1222-1231.

348. Sun, T., et al., *ZNRF3 and RNF43 cooperate to safeguard metabolic liver zonation and hepatocyte proliferation.* Cell Stem Cell, 2021. **28**(10): p. 1822-1837 e10.

349. Hernandez-Meza, G., et al., *DNA Methylation Profiling of Human Hepatocarcinogenesis.* Hepatology, 2021. **74**(1): p. 183-199.

350. Um, T.H., et al., *Aberrant CpG island hypermethylation in dysplastic nodules and early HCC of hepatitis B virus-related human multistep hepatocarcinogenesis.* J Hepatol, 2011. **54**(5): p. 939-47.

351. Ma, J.Z., et al., *METTL14 suppresses the metastatic potential of hepatocellular carcinoma by modulating N(6) -methyladenosine-dependent primary MicroRNA processing.* Hepatology, 2017. **65**(2): p. 529-543.

352. McMahon, M., et al., *A single H/ACA small nucleolar RNA mediates tumor suppression downstream of oncogenic RAS.* Elife, 2019. **8**.

353. Tamura, S., et al., *Urinary pseudouridine as a biochemical marker in the diagnosis and monitoring of primary hepatocellular carcinoma.* Am J Gastroenterol, 1988. **83**(8): p. 841-5.

354. Amuro, Y., et al., *Serum pseudouridine as a biochemical marker in patients with hepatocellular carcinoma.* Clin Chim Acta, 1988. **178**(2): p. 151-8.

355. Zhang, X., et al., *Deletions of chromosome 13q, mutations in Retinoblastoma 1, and retinoblastoma protein state in human hepatocellular carcinoma.* Cancer Res, 1994. **54**(15): p. 4177-82.

356. Seki, S., et al., *Expression of the retinoblastoma gene product in human hepatocellular carcinoma.* Hum Pathol, 1995. **26**(4): p. 366-74.

357. Liew, C.T., et al., *High frequency of p16INK4A gene alterations in hepatocellular carcinoma.* Oncogene, 1999. **18**(3): p. 789-95.

358. Suh, S.I., et al., *5-Aza-2'-deoxycytidine leads to down-regulation of aberrant p16INK4A RNA transcripts and restores the functional retinoblastoma protein pathway in hepatocellular carcinoma cell lines.* Cancer Lett, 2000. **160**(1): p. 81-8.

359. Zhu, Y.Z., et al., *Hepatitis B virus X protein promotes hypermethylation of p16(INK4A) promoter through upregulation of DNA methyltransferases in hepatocarcinogenesis.* Exp Mol Pathol, 2010. **89**(3): p. 268-75.

360. Kaneto, H., et al., *Detection of hypermethylation of the p16(INK4A) gene promoter in chronic hepatitis and cirrhosis associated with hepatitis B or C virus.* Gut, 2001. **48**(3): p. 372-7.

361. Shim, Y.H., et al., *p16 Hypermethylation in the early stage of hepatitis B virus-associated hepatocarcinogenesis.* Cancer Lett, 2003. **190**(2): p. 213-9.

362. Zhu, R., et al., *Association of p16INK4A hypermethylation with hepatitis B virus X protein expression in the early stage of HBV-associated hepatocarcinogenesis.* Pathol Int, 2007. **57**(6): p. 328-36.

363. Wang, K., et al., *Genomic landscape of copy number aberrations enables the identification of oncogenic drivers in hepatocellular carcinoma.* Hepatology, 2013. **58**(2): p. 706-17.

364. Nishida, N., et al., *Amplification and overexpression of the cyclin D1 gene in aggressive human hepatocellular carcinoma.* Cancer Res, 1994. **54**(12): p. 3107-10.

365. Diril, M.K., et al., *Cyclin-dependent kinase 1 (Cdk1) is essential for cell division and suppression of DNA re-replication but not for liver regeneration.* Proc Natl Acad Sci U S A, 2012. **109**(10): p. 3826-31.

366. Bisteau, X., M.J. Caldez, and P. Kaldis, *The Complex Relationship between Liver Cancer and the Cell Cycle: A Story of Multiple Regulations.* Cancers (Basel), 2014. **6**(1): p. 79-111.

367. Bollard, J., et al., *Palbociclib (PD-0332991), a selective CDK4/6 inhibitor, restricts tumour growth in preclinical models of hepatocellular carcinoma.* Gut, 2017. **66**(7): p. 1286-1296.

368. Rivadeneira, D.B., et al., *Proliferative suppression by CDK4/6 inhibition: complex function of the retinoblastoma pathway in liver tissue and hepatoma cells.* Gastroenterology, 2010. **138**(5): p. 1920-30.

369. Pernar, C.H., et al., *The Epidemiology of Prostate Cancer.* Cold Spring Harb Perspect Med, 2018. **8**(12).

370. Rawla, P., *Epidemiology of Prostate Cancer.* World J Oncol, 2019. **10**(2): p. 63-89.

371. Attard, G., et al., *Prostate cancer.* Lancet, 2016. **387**(10013): p. 70-82.

372. Sekhoacha, M., et al., *Prostate Cancer Review: Genetics, Diagnosis, Treatment Options, and Alternative Approaches.* Molecules, 2022. **27**(17).

373. Francini, E. and M.E. Taplin, *Prostate cancer: Developing novel approaches to castration-sensitive disease.* Cancer, 2017. **123**(1): p. 29-42.

374. Mansinho, A., et al., *Castration-Resistant Prostate Cancer: Mechanisms, Targets and Treatment.* Adv Exp Med Biol, 2018. **1096**: p. 117-133.

375. Fan, L., et al., *Comparative Analysis of Genomic Alterations across Castration Sensitive and Castration Resistant Prostate Cancer via Circulating Tumor DNA Sequencing.* J Urol, 2021. **205**(2): p. 461-469.

376. Robinson, D., et al., *Integrative clinical genomics of advanced prostate cancer.* Cell, 2015. **161**(5): p. 1215-1228.

377. Grasso, C.S., et al., *The mutational landscape of lethal castration-resistant prostate cancer.* Nature, 2012. **487**(7406): p. 239-43.

378. Trewartha, D. and K. Carter, *Advances in prostate cancer treatment.* Nat Rev Drug Discov, 2013. **12**(11): p. 823-4.

379. Beer, T.M., et al., *Enzalutamide in metastatic prostate cancer before chemotherapy.* N Engl J Med, 2014. **371**(5): p. 424-33.

380. de Bono, J.S., et al., *Abiraterone and increased survival in metastatic prostate cancer.* N Engl J Med, 2011. **364**(21): p. 1995-2005.

381. Ryan, C.J., et al., *Abiraterone in metastatic prostate cancer without previous chemotherapy.* N Engl J Med, 2013. **368**(2): p. 138-48.

382. Wang, G., et al., *Genetics and biology of prostate cancer.* Genes Dev, 2018. **32**(17-18): p. 1105-1140.

383. Zhang, D., et al., *Prostate Luminal Progenitor Cells in Development and Cancer.* Trends Cancer, 2018. **4**(11): p. 769-783.

384. Shen, M.M. and C. Abate-Shen, *Molecular genetics of prostate cancer: new prospects for old challenges.* Genes Dev, 2010. **24**(18): p. 1967-2000.

385. Khemlina, G., S. Ikeda, and R. Kurzrock, *Molecular landscape of prostate cancer: implications for current clinical trials.* Cancer Treat Rev, 2015. **41**(9): p. 761-6.

386. Taylor, B.S., et al., *Integrative genomic profiling of human prostate cancer.* Cancer Cell, 2010. **18**(1): p. 11-22.

387. Jamaspishvili, T., et al., *Clinical implications of PTEN loss in prostate cancer.* Nat Rev Urol, 2018. **15**(4): p. 222-234.

388. Pourmand, G., et al., *Role of PTEN gene in progression of prostate cancer.* Urol J, 2007. **4**(2): p. 95-100.

389. Song, M.S., L. Salmena, and P.P. Pandolfi, *The functions and regulation of the PTEN tumour suppressor.* Nat Rev Mol Cell Biol, 2012. **13**(5): p. 283-96.

390. Trotman, L.C., et al., *Pten dose dictates cancer progression in the prostate.* PLoS Biol, 2003. **1**(3): p. E59.

391. Engelman, J.A., J. Luo, and L.C. Cantley, *The evolution of phosphatidylinositol 3-kinases as regulators of growth and metabolism.* Nat Rev Genet, 2006. **7**(8): p. 606-19.

392. Armenia, J., et al., *The long tail of oncogenic drivers in prostate cancer.* Nat Genet, 2018. **50**(5): p. 645-651.

393. Ben-Salem, S., V.B. Venkadakrishnan, and H.V. Heemers, *Novel insights in cell cycle dysregulation during prostate cancer progression.* Endocr Relat Cancer, 2021. **28**(6): p. R141-R155.

394. Jarrard, D.F., et al., *Deletional, mutational, and methylation analyses of CDKN2 (p16/MTS1) in primary and metastatic prostate cancer.* Genes Chromosomes Cancer, 1997. **19**(2): p. 90-6.

395. Friedlander, T.W., et al., *Common structural and epigenetic changes in the genome of castration-resistant prostate cancer.* Cancer Res, 2012. **72**(3): p. 616-25.

396. Martignano, F., et al., *GSTP1 Methylation and Protein Expression in Prostate Cancer: Diagnostic Implications.* Dis Markers, 2016. **2016**: p. 4358292.

397. Lin, P.C., et al., *Epigenomic alterations in localized and advanced prostate cancer.* Neoplasia, 2013. **15**(4): p. 373-83.

398. Suzuki, H., et al., *Androgen receptor involvement in the progression of prostate cancer.* Endocr Relat Cancer, 2003. **10**(2): p. 209-16.

399. Bantis, A., et al., *Expression of p120, Ki-67 and PCNA as proliferation biomarkers in imprint smears of prostate carcinoma and their prognostic value.* Cytopathology, 2004. **15**(1): p. 25-31.

400. Kallakury, B.V., et al., *The prognostic significance of proliferation-associated nucleolar protein p120 expression in prostate adenocarcinoma: a comparison with cyclins A and B1, Ki-67, proliferating cell nuclear antigen, and p34cdc2.* Cancer, 1999. **85**(7): p. 1569-76.

401. Stockert, J.A., et al., *Predictive value of pseudouridine in prostate cancer.* Am J Clin Exp Urol, 2019. **7**(4): p. 262-272.

402. Katunaric, M. and G. Zamolo, *Modulating telomerase activity in tumor patients by targeting dyskerin binding site for hTR.* Med Hypotheses, 2012. **79**(3): p. 319-20.

403. Perez-Rambla, C., et al., *Non-invasive urinary metabolomic profiling discriminates prostate cancer from benign prostatic hyperplasia.* Metabolomics, 2017. **13**(5): p. 52.

404. Yi, Y., et al., *A PRC2-independent function for EZH2 in regulating rRNA 2'-O methylation and IRES-dependent translation.* Nat Cell Biol, 2021. **23**(4): p. 341-354.

405. Lopez, J., et al., *Epigenetic and Epitranscriptomic Control in Prostate Cancer.* Genes (Basel), 2022. **13**(2).

406. Schaefer, M., et al., *RNA cytosine methylation analysis by bisulfite sequencing.* Nucleic Acids Res, 2009. **37**(2): p. e12.

407. Warnecke, P.M., et al., *Identification and resolution of artifacts in bisulfite sequencing.* Methods, 2002. **27**(2): p. 101-7.

408. Gundry, M.C., et al., *Technical considerations for the use of CRISPR/Cas9 in hematology research.* Exp Hematol, 2017. **54**: p. 4-11.

409. Ran, F.A., et al., *Double nicking by RNA-guided CRISPR Cas9 for enhanced genome editing specificity.* Cell, 2013. **154**(6): p. 1380-9.

410. Vakulskas, C.A., et al., *A high-fidelity Cas9 mutant delivered as a ribonucleoprotein complex enables efficient gene editing in human hematopoietic stem and progenitor cells.* Nat Med, 2018. **24**(8): p. 1216-1224.

411. Nieto, B., et al., *Efficient fractionation and analysis of ribosome assembly intermediates in human cells.* RNA Biol, 2021. **18**(sup1): p. 182-197.

412. Tafforeau, L., et al., *The complexity of human ribosome biogenesis revealed by systematic nucleolar screening of Pre-rRNA processing factors.* Mol Cell, 2013. **51**(4): p. 539-51.

413. McCloy, R.A., et al., *Partial inhibition of Cdk1 in G 2 phase overrides the SAC and decouples mitotic events.* Cell Cycle, 2014. **13**(9): p. 1400-12.

414. Liu, J., et al., *Imaging protein synthesis in cells and tissues with an alkyne analog of puromycin.* Proc Natl Acad Sci U S A, 2012. **109**(2): p. 413-8.

415. Zimmerman, W.C., et al., *Mitosis-specific anchoring of gamma tubulin complexes by pericentrin controls spindle organization and mitotic entry.* Mol Biol Cell, 2004. **15**(8): p. 3642-57.

416. Jiang, H., et al., *A microtubule-associated zinc finger protein, BuGZ, regulates mitotic chromosome alignment by ensuring Bub3 stability and kinetochore targeting.* Dev Cell, 2014. **28**(3): p. 268-81.

417. Fang, F., et al., *A distinct isoform of ZNF207 controls self-renewal and pluripotency of human embryonic stem cells.* Nat Commun, 2018. **9**(1): p. 4384.

418. Carroll, A.G., et al., *p53 oncogene mutations in three human prostate cancer cell lines.* Prostate, 1993. **23**(2): p. 123-34.

419. Hayward, S.W., et al., *Establishment and characterization of an immortalized but non-transformed human prostate epithelial cell line: BPH-1.* In Vitro Cell Dev Biol Anim, 1995. **31**(1): p. 14-24.

420. Leroy, B., et al., *Analysis of TP53 mutation status in human cancer cell lines: a reassessment.* Hum Mutat, 2014. **35**(6): p. 756-65.

421. Hornbeck, P.V., et al., *PhosphoSitePlus, 2014: mutations, PTMs and recalibrations.* Nucleic Acids Res, 2015. **43**(Database issue): p. D512-20.

422. Nigg, E.A., *Cellular substrates of p34(cdc2) and its companion cyclin-dependent kinases.* Trends Cell Biol, 1993. **3**(9): p. 296-301.

423. Moreno, S. and P. Nurse, *Substrates for p34cdc2: in vivo veritas?* Cell, 1990. **61**(4): p. 549-51.

424. Suzuki, K., et al., *Identification of non-Ser/Thr-Pro consensus motifs for Cdk1 and their roles in mitotic regulation of C2H2 zinc finger proteins and Ect2.* Sci Rep, 2015. **5**: p. 7929.

425. Vassilev, L.T., et al., *Selective small-molecule inhibitor reveals critical mitotic functions of human CDK1.* Proc Natl Acad Sci U S A, 2006. **103**(28): p. 10660-5.

426. Garcia-Garcia, T., et al., *Role of Protein Phosphorylation in the Regulation of Cell Cycle and DNA-Related Processes in Bacteria.* Front Microbiol, 2016. **7**: p. 184.

427. Jumper, J., et al., *Highly accurate protein structure prediction with AlphaFold.* Nature, 2021. **596**(7873): p. 583-589.

428. Cortazar, A.R., et al., *CANCERTOOL: A Visualization and Representation Interface to Exploit Cancer Datasets.* Cancer Res, 2018. **78**(21): p. 6320-6328.

429. Sia, D., et al., *Integrative molecular analysis of intrahepatic cholangiocarcinoma reveals 2 classes that have different outcomes.* Gastroenterology, 2013. **144**(4): p. 829-40.

430. Montal, R., et al., *Molecular classification and therapeutic targets in extrahepatic cholangiocarcinoma.* J Hepatol, 2020. **73**(2): p. 315-327.

431. Roessler, S., et al., *A unique metastasis gene signature enables prediction of tumor relapse in early-stage hepatocellular carcinoma patients.* Cancer Res, 2010. **70**(24): p. 10202-12.

432. Roessler, S., et al., *Integrative genomic identification of genes on 8p associated with hepatocellular carcinoma progression and patient survival.* Gastroenterology, 2012. **142**(4): p. 957-966 e12.

433. Mas, V.R., et al., *Genes involved in viral carcinogenesis and tumor initiation in hepatitis C virus-induced hepatocellular carcinoma.* Mol Med, 2009. **15**(3-4): p. 85-94.

434. Wurmbach, E., et al., *Genome-wide molecular profiles of HCV-induced dysplasia and hepatocellular carcinoma.* Hepatology, 2007. **45**(4): p. 938-47.

REFERENCES

435. Pinyol, R., et al., *Molecular characterisation of hepatocellular carcinoma in patients with non-alcoholic steatohepatitis.* J Hepatol, 2021. **75**(4): p. 865-878.

436. Zhu, H., et al., *Proteomics of adjacent-to-tumor samples uncovers clinically relevant biological events in hepatocellular carcinoma.* Natl Sci Rev, 2023. **10**(8): p. nwad167.

437. Roessler, S., et al., *Integrative genomic and transcriptomic characterization of matched primary and metastatic liver and colorectal carcinoma.* Int J Biol Sci, 2015. **11**(1): p. 88-98.

438. Arriaga, J.M. and C. Abate-Shen, *Genetically Engineered Mouse Models of Prostate Cancer in the Postgenomic Era.* Cold Spring Harb Perspect Med, 2019. **9**(2).

439. Ittmann, M., *Anatomy and Histology of the Human and Murine Prostate.* Cold Spring Harb Perspect Med, 2018. **8**(5).

440. Skarnes, W.C., et al., *A conditional knockout resource for the genome-wide study of mouse gene function.* Nature, 2011. **474**(7351): p. 337-42.

441. Mulholland, D.J., et al., *Lin-Sca-1+CD49fhigh stem/progenitors are tumor-initiating cells in the Pten-null prostate cancer model.* Cancer Res, 2009. **69**(22): p. 8555-62.

442. Aytes, A., et al., *ETV4 promotes metastasis in response to activation of PI3-kinase and Ras signaling in a mouse model of advanced prostate cancer.* Proc Natl Acad Sci U S A, 2013. **110**(37): p. E3506-15.

443. Sharifi, S. and H. Bierhoff, *Regulation of RNA Polymerase I Transcription in Development, Disease, and Aging.* Annu Rev Biochem, 2018. **87**: p. 51-73.

444. Arabi, A., et al., *c-Myc associates with ribosomal DNA and activates RNA polymerase I transcription.* Nat Cell Biol, 2005. **7**(3): p. 303-10.

445. Ajore, R., et al., *Deletion of ribosomal protein genes is a common vulnerability in human cancer, especially in concert with TP53 mutations.* EMBO Mol Med, 2017. **9**(4): p. 498-507.

446. Rao, S., et al., *Inactivation of ribosomal protein L22 promotes transformation by induction of the stemness factor, Lin28B.* Blood, 2012. **120**(18): p. 3764-73.

447. Sulima, S.O., et al., *Bypass of the pre-60S ribosomal quality control as a pathway to oncogenesis.* Proc Natl Acad Sci U S A, 2014. **111**(15): p. 5640-5.

448. Orsolic, I., A. Carrier, and M. Esteller, *Genetic and epigenetic defects of the RNA modification machinery in cancer.* Trends Genet, 2023. **39**(1): p. 74-88.

449. Yuan, Y., et al., *The M6A methyltransferase METTL3 promotes the development and progression of prostate carcinoma via mediating MYC methylation.* J Cancer, 2020. **11**(12): p. 3588-3595.

450. Liu, J., et al., *m(6)A mRNA methylation regulates AKT activity to promote the proliferation and tumorigenicity of endometrial cancer.* Nat Cell Biol, 2018. **20**(9): p. 1074-1083.

451. Lu, J., et al., *METTL14 Facilitates the Metastasis of Pancreatic Carcinoma by Stabilizing LINC00941 in an m6A-IGF2BP2-Dependent Manner.* J Cancer, 2023. **14**(7): p. 1117-1131.

452. Rodriguez-Gabriel, M.A. and P. Russell, *Distinct signaling pathways respond to arsenite and reactive oxygen species in Schizosaccharomyces pombe.* Eukaryot Cell, 2005. **4**(8): p. 1396-402.

453. Murray, A., *Cyclin ubiquitination: the destructive end of mitosis.* Cell, 1995. **81**(2): p. 149-52.

454. Eichhorn, J.M., A. Kothari, and T.C. Chambers, *Cyclin B1 overexpression induces cell death independent of mitotic arrest.* PLoS One, 2014. **9**(11): p. e113283.

455. Ohta, S., et al., *CENP-32 is required to maintain centrosomal dominance in bipolar spindle assembly.* Mol Biol Cell, 2015. **26**(7): p. 1225-37.

456. Yeh, E.S., B.O. Lew, and A.R. Means, *The loss of PIN1 deregulates cyclin E and sensitizes mouse embryo fibroblasts to genomic instability.* J Biol Chem, 2006. **281**(1): p. 241-51.

457. Zhou, W., et al., *Pin1 catalyzes conformational changes of Thr-187 in p27Kip1 and mediates its stability through a polyubiquitination process.* J Biol Chem, 2009. **284**(36): p. 23980-8.

458. Zhou, X.Z., et al., *Pin1-dependent prolyl isomerization regulates dephosphorylation of Cdc25C and tau proteins.* Mol Cell, 2000. **6**(4): p. 873-83.

459. Su, Y., et al., *NSUN5-FTH1 Axis Inhibits Ferroptosis to Promote the Growth of Gastric Cancer Cells.* Cell Biochem Biophys, 2023. **81**(3): p. 553-560.

460. Kuhn, A., et al., *Mitotic phosphorylation of the TBP-containing factor SL1 represses ribosomal gene transcription.* J Mol Biol, 1998. **284**(1): p. 1-5.

461. Heix, J., et al., *Mitotic silencing of human rRNA synthesis: inactivation of the promoter selectivity factor SL1 by cdc2/cyclin B-mediated phosphorylation.* EMBO J, 1998. **17**(24): p. 7373-81.

462. Fitzgerald, K.D. and B.L. Semler, *Bridging IRES elements in mRNAs to the eukaryotic translation apparatus.* Biochim Biophys Acta, 2009. **1789**(9-10): p. 518-28.

463. Al-Jubran, K., et al., *Visualization of the joining of ribosomal subunits reveals the presence of 80S ribosomes in the nucleus.* RNA, 2013. **19**(12): p. 1669-83.

464. Soria-Bretones, I., et al., *The spindle assembly checkpoint is a therapeutic vulnerability of CDK4/6 inhibitor-resistant ER(+) breast cancer with mitotic aberrations.* Sci Adv, 2022. **8**(36): p. eabq4293.

465. Kettner, N.M., et al., *Combined Inhibition of STAT3 and DNA Repair in Palbociclib-Resistant ER-Positive Breast Cancer.* Clin Cancer Res, 2019. **25**(13): p. 3996-4013.

466. Park, Y.H., et al., *Prospective longitudinal multi-omics study of palbociclib resistance in hormone receptor+/HER2- metastatic breast cancer.* Journal of Clinical Oncology, 2021. **39**(15_suppl): p. 1013-1013.

467. Prakash, V., et al., *Ribosome biogenesis during cell cycle arrest fuels EMT in development and disease.* Nat Commun, 2019. **10**(1): p. 2110.

468. Yang, C., et al., *EB1 and EB3 regulate microtubule minus end organization and Golgi morphology.* J Cell Biol, 2017. **216**(10): p. 3179-3198.

469. Lapcik, P., et al., *Desmocollin-1 is associated with pro-metastatic phenotype of luminal A breast cancer cells and is modulated by parthenolide.* Cell Mol Biol Lett, 2023. **28**(1): p. 68.

470. Lei, G., et al., *Characterization of zinc-alpha(2)-glycoprotein as a cell adhesion molecule that inhibits the proliferation of an oral tumor cell line.* J Cell Biochem, 1999. **75**(1): p. 160-9.

471. Zabala-Letona, A., et al., *mTORC1-dependent AMD1 regulation sustains polyamine metabolism in prostate cancer.* Nature, 2017. **547**(7661): p. 109-113.

472. Concordet, J.P. and M. Haeussler, *CRISPOR: intuitive guide selection for CRISPR/Cas9 genome editing experiments and screens.* Nucleic Acids Res, 2018. **46**(W1): p. W242-W245.

473. Schindelin, J., et al., *Fiji: an open-source platform for biological-image analysis.* Nat Methods, 2012. **9**(7): p. 676-82.

474. Li, H., *Minimap2: pairwise alignment for nucleotide sequences.* Bioinformatics, 2018. **34**(18): p. 3094-3100.

475. Tomlins, S.A., et al., *Integrative molecular concept modeling of prostate cancer progression.* Nat Genet, 2007. **39**(1): p. 41-51.

476. Lapointe, J., et al., *Gene expression profiling identifies clinically relevant subtypes of prostate cancer.* Proc Natl Acad Sci U S A, 2004. **101**(3): p. 811-6.

477. Varambally, S., et al., *Integrative genomic and proteomic analysis of prostate cancer reveals signatures of metastatic progression.* Cancer Cell, 2005. **8**(5): p. 393-406.

478. Cancer Genome Atlas Research, N., *The Molecular Taxonomy of Primary Prostate Cancer.* Cell, 2015. **163**(4): p. 1011-25.

Funding

Funding

- Post-transcriptionally modified RNAs as survival and growth mediators in cancer cells (LABAE19040BLAN).

    Principal investigator: Sandra Blanco.

    Financial entity/program: Scientific Foundation of Spanish Association Against Cancer.

    Duration: 01/01/2020 – 31/12/2022 (3 years)

    Amount: €300.000

- Papel de la epitranscriptómica y su implicación en la metástasis y la respuesta inmune en cáncer (PID2019-111692RB-I00).

    Principal investigator: Sandra Blanco.

    Financial entity/program: Proyectos Retos i+D+i, Spanish Research Agency.

    Duration: 01/06/2020 – 31/05/2023 (3 years)

    Amount: €237.000

Resumen en Castellano

Resumen en Castellano

Título

La metilación del ARN ribosómico controla el ciclo celular a través de la síntesis de proteínas.

Índice

Introducción

<u>La epitranscriptómica</u>

De manera similar a cómo el DNA y las proteínas son modificados sin alterar su secuencia, el RNA también puede sufrir docenas de modificaciones post-transcripcionales diferentes. Al conjunto de estas modificaciones se le conoce como el epitranscriptoma. El epitranscriptoma engloba una gran cantidad de modificaciones diferentes, desde la colocación de la caperuza 5' del ARN mensajero (ARNm) a la edición del ARN, pasando por las modificaciones químicas. La mayor diversidad en modificaciones post-transcripcionales la encontramos en este último grupo, donde se han descrito más de 170 modificaciones químicas diferentes que ocurren en todos los tipos de ARN y en prácticamente todas las especies. Estas modificaciones pueden ocurrir tanto en las bases nitrogenadas como en el anillo de ribosa y tienen el potencial de regular las funciones y las propiedades químicas del ARN. De entre todos los tipos de ARN, el ARN de transferencia (ARNt) es el que se encuentra más modificado, encontrándose aproximadamente el 17% de sus nucleótidos modificados. El ARNt puede sufrir modificaciones muy diversas. De hecho, se han encontrado hasta 25 modificaciones diferentes en estas moléculas. Tras este, el ARN ribosómico (ARNr) es el segundo más modificado, con un total de aproximadamente 201 modificaciones por ribosoma. La modificación más común en el ARNr son la metilación de la ribosa en la posición 2'-OH (2'-O-me) y la isomerización de la uridina a pseudouridina (Ψ). En el caso del ARNm, la modificación interna más común es la 6-metiladenosina (m^{6}A), que constituye aproximadamente entre el 0.1% y el 0.4% de todas las adenosinas encontradas en estas moléculas.

Las modificaciones post-transcripcionales del ARN son colocadas por un grupo de enzimas generalmente conocidas como "writers", que pueden pertenecer a diferentes familias como la familia METTL, NSUN o TRMT. Por otro lado, existe otro grupo de enzimas denominadas "erasers" que se encargan de eliminar las modificaciones del ARN. El descubrimiento de estas enzimas fue un hito importante en la epitranscriptómica, pues supuso demostrar que las modificaciones de ARN pueden ser reversibles. A pesar de que los primeros "erasers" que se descubrieron se encargaban de eliminar la m^{6}A, también se han descrito "erasers" de otras modificaciones como la 5-metilcitosina (m^{5}C). Este es el caso de las enzimas de la familia TET, que se encargan de eliminar la m^{5}C mediante su hidroxilación y oxidación, lo que ha demostrado jugar un importante papel en la regulación de algunos procesos biológicos. Finalmente, existe otro grupo de proteínas, conocidas como "readers" que se encargan de reconocer de forma específica las modificaciones y desencadenar diferentes funciones como la degradación, la traducción o el splicing de ese RNA.

Así, mientras que se ha visto que las modificaciones del ADN principalmente actúan regulando la expresión génica, las modificaciones de ARN tienen funciones mucho más diversas que incluyen, mantenimiento de la estabilidad, regulación de la transcripción, splicing, degradación o traducción.

<u>El ribosoma.</u>

Los ribosomas son grandes complejos macromoleculares que se encargan de catalizar la síntesis de proteínas en un complejo proceso altamente regulado llamado traducción. Los ribosomas tienen un alto grado de conservación y, en todas las especies, están formados por dos partes: la subunidad grande (LSU por sus siglas en inglés) y la subunidad pequeña (SSU por sus siglas en inglés). En los organismos eucariotas, la LSU está formada por tres ARNr (28S/25S, 5.8S y 5S) y 47 proteínas ribosomales (PRs) mientras que la SSU está constituida por el rRNA 18S y 33 PRs.

Todos los ribosomas están constituidos sobre la misma estructura basal, que se conoce como el centro universal o conservado del ribosoma. Este centro conservado contiene las partes funcionales esenciales del ribosoma como son: en la LSU el centro peptidil transferasa y el túnel de salida; y en la SSU el centro decodificador. Dentro del centro conservado y constituido por las dos subunidades encontramos los sitios de unión para los ARNt y la interfaz entre subunidades. Además de esto, a lo largo de la evolución, los ribosomas de los distintos reinos y especies han ido divergiendo tanto en estructura como en función, adquiriendo nuevas características y complejidad.

Los ribosomas se forman mediante un proceso altamente regulado y complejo conocido como biogénesis del ribosoma. Este proceso implica la actuación de las tres ARN polimerasas, de más de 200 factores y de numerosos complejos ribonucleoproteicos pequeños nucleolares (snoRNPs por sus siglas en inglés). Este proceso se inicia en el nucleolo, donde el ADN ribosómico (rDNA) se transcribe dando lugar al pre-ARNr 47S, que contiene los ARNr 28S, 5.8S y 18S. El procesamiento del pre-ARNr 47S implica complejos cortes endonucleolíticos y exonucleolíticos, el plegamiento del ARNr, la formación de partículas pre-ribosomales y la modificación del ARNr. A lo largo de este proceso, las partículas pre-ribosomales viajan desde el nucleolo al núcleo y luego al citoplasma, donde experimentan los últimos pasos de maduración para convertirse en subunidades ribosomales funcionales.

<u>Las modificaciones post-transcripcionales del ARN ribosómico</u>

Las modificaciones de ARN juegan un papel esencial durante la biogénesis del ribosoma, ya que afectan al procesamiento del ARNr, el plegamiento y la compactación. Estas modificaciones, que pueden estar catalizadas por enzimas que usan ARN nucleolares pequeños (snoARNs) o enzimas

independientes, ocurren durante varias etapas de la maduración del ARNr. Algunas de estas modificaciones son esenciales para una correcta biogénesis del ribosoma como la 2'-O-me en G2922 y la metilación m^5C mediada por Nop2 para la biogénesis de la subunidad pre-60S en levaduras o la hipermodificación de Ψ1248, que influye en la maduración del ARNr 18S. También existen casos de algunas enzimas modificadoras, como DIMT1L y WBSCR22, tienen funciones esenciales durante la biogénesis pero que son independientes de su actividad catalítica.

El 95% de las modificaciones encontradas en el ARNr son 2'-O-me y Ψ, guiadas por Fibrilarina y Diskerina, respectivamente. Estas modificaciones juegan un papel crucial en el ribosoma, afectando a su estabilidad y a la traducción. El 5% restante de las modificaciones incluye las modificaciones de las bases nitrogenadas y aminocarboxipropilaciones. Muchas de estas modificaciones están conservadas desde levaduras hasta humanos y se agrupan en áreas críticas del ribosoma, como el centro decodificador (DCC), el centro peptidil transferasa (PTC) y la interfaz entre subunidades. Es importante destacar que la pérdida de algunas de estas modificaciones en específico es capaz de alterar la función del ribosoma y los programas de traducción, como es el caso de la pérdida de la metilación m^1A por NML o m^6A por ZCCHC4.

La metilación en citosina-5

La metilación m^5C es una modificación del ARN altamente frecuente que se encuentra en todos los dominios de la vida, con una mayor abundancia en los ARNt y ARNr. También se encuentra en ARNm, ARN largos no codificantes (lncARNs), vault RNAs (vtARNs) y snoARNs, aunque con menor frecuencia. Esta modificación es catalizada por metiltransferasas que pertenecen a las familias DNMT2 y NSUN. DNMT2, originalmente considerada una metiltransferasa de ADN, ha demostrado metilar varios ARNt. Por otro lado, la familia NSUN consta de 7 miembros, cada uno con especificidad por un tipo de ARN o posición. NSUN2 metila ARNt, ARNm, vtARN y lncARN. NSUN6 también es capaz de metilar ARNt y ARNm. NSUN3 metila los ARNt mitocondriales mientras que NSUN4 metila los ARNr mitocondriales. NOP2 y NSUN5 metilan el ARNr citoplasmático. Finalmente, NSUN7 interacciona con "ARNs enhancer" (eARN) y recientemente ha demostrado metilar ARNm.

En general, la modificación m5C en ARN y sus reguladores tienen diversas funciones fisiológicas en los diferentes tipos de ARN, influyendo en procesos como la traducción, las respuestas al estrés y la regulación de la expresión génica. Un mejor estudio de estas funciones es esencial para desentrañar la complejidad del epitranscriptoma y sus implicaciones en la salud y la enfermedad.

<u>La metiltransferasa de citosina-5 NSUN5</u>

NSUN5 es una metiltransferasa altamente conservada que metila la posición C3782 del ARNr 28S. Esta posición se encuentra en el hélix 70 del dominio IV de este ARNr, que compone parte de la interfaz entre las subunidades ribosomales y es una de las modificaciones más conservadas a lo largo de la evolución, lo que indica que podría tener una función importante.

Aunque la mayoría de los estudios de esta metilación se han llevado a cabo en levaduras, el alto nivel de conservación sugiere que podría realizar funciones similares en humano. En levaduras, el homólogo de NSUN5, Rcm1, metila la posición C2278 del ARNr 25S. Aunque la pérdida de esta metilación no altera la biogénesis del ribosoma, produce una mayor sensibilidad al antibiótico anisomicina y altera la supervivencia a estrés y la vida media de levaduras, *Caenorhabditis elegans* y *Drosophila melanogaster*. Esto se debe a una alteración en el programa traduccional de las células que lleva a una síntesis más eficiente de proteínas relacionadas con la respuesta a estrés. De manera similar, en humanos la pérdida de NSUN5 también produce un aumento de la síntesis de estas proteínas.

NSUN5 en humanos se encuentra en la región cromosómica delecionada en el síndrome de Williams-Beuren, un síndrome que afecta al neurodesarrollo, aunque su implicación real en la enfermedad no está muy estudiada aún. Además, NSUN5 también está implicado en cáncer. Esta enzima se encuentra sobre-expresada en cáncer colorrectal (CRC), hepatocarcinoma (LIHC) y carcinoma renal de células claras (ccRCC), produciendo un aumento de la proliferación de las células tumorales. Por otro lado, NSUN5 también se encuentra implicado en glioblastoma (GBM), aunque su papel en este cáncer aún es controvertido. Por un lado, en algunos estudios ha demostrado comportarse como un gen supresor de tumores mientras que en otros actúa como un oncogén. Por tanto, aún es necesario estudiar la función NSUN5 en estos y en otros tipos de cáncer para conocer mejor su implicación en la formación de dichos tumores y su posible uso como diana terapéutica.

Objetivos

La metilación de la citosina-5 es una modificación post-transcripcional común en el ARN. Esta modificación se encuentra principalmente en los ARNt y ARNr, y, con menor frecuencia, en los ARNm, ARNlnc y ARNvt. Estudios a gran escala de esta modificación han demostrado que juega un papel crítico en los ARNt, afectando a su estabilidad y controlando la función de las células madre y la respuesta a estrés. Sin embargo, nuestro conocimiento sobre m^{5}C en el ARNr sigue siendo escaso.

Los ribosomas contienen dos residuos de m^{5}C en su rRNA 28S, en la subunidad grande. Uno de estos residuos es depositado por NOP2 en el centro peptidil transferasa. NOP2 es una metiltransferasa regulada por el ciclo celular que desempeña un papel esencial en la biogénesis de los ribosomas y la regulación de la traducción. Además, NOP2 está altamente expresado en muchos tumores, y se usa como marcador de mal pronóstico en la práctica clínica. El otro residuo de m^{5}C que podemos encontrar en el rRNA 28S es depositado por una enzima altamente conservada, NSUN5, en la interfaz entre la subunidad grande y la pequeña. Esta enzima juega un papel importante en la síntesis de proteínas y la resistencia al estrés en varios organismos modelo. Además, NSUN5 se ha asociado recientemente con varios tipos de cáncer, donde regula la proliferación de células tumorales. Sin embargo, el mecanismo subyacente a su contribución a la tumorigénesis aún se desconoce en gran medida.

Dada la alta conservación y la ubicación tan importante de la modificación m^{5}C mediada por NSUN5, hipotetizamos que contribuye a la regulación de procesos celulares clave, como el ciclo celular y la proliferación, al modular la función ribosómica. Para probar esta hipótesis, proponemos los siguientes objetivos específicos:

1. Investigar el impacto de la metilación del rRNA mediada por NSUN5 en la biogénesis de los ribosomas y el control de la síntesis de proteínas.
2. Explorar los factores que modulan los cambios dinámicos en la metilación de m^{5}C en el RNA.
3. Evaluar los patrones de expresión de NSUN5 en varios tipos de cáncer.
4. Determinar el potencial tumorigénico de NSUN5 en células tumorales tanto *in vivo* como *in vitro*.

Resultados

La metilación m^{5}C en el ARNr es una de las más conservadas en todas las especies. Sin embargo, se sabe relativamente poco sobre las funciones de esta metilación, en especial sobre la catalizada por NSUN5 en la interfaz entre subunidades ribosómicas. Para investigar el papel de NSUN5, en este estudio silenciamos NSUN5 en una línea celular humana de cáncer de próstata metastásico mediante el uso de ARNs de horquilla corta (shRNAs por sus siglas en inglés). Mediante este método, se alcanzó un silenciamiento considerable tanto del ARNm como de la proteína de NSUN5. Sin embargo, el análisis de la metilación del ARNr indicó que la bajada en la metilación era de tan solo un 20%, probablemente debido a limitaciones de la técnica.

Para un mejor estudio de las funciones de NSUN5, se generaron células con pérdida completa de su expresión (*NSUN5*-KO) mediante tecnología CRISPR/Cas9. Los análisis de expresión indicaron que tres clones obtenidos mediante esta técnica (C15, C16 y C22) tenían una bajada casi completa de expresión de la enzima. Los estudios de metilación del ARNr indicaron que, mientras que el C22 y el C16 tenían una bajada total de la metilación, el C15 no presentaba ninguna diferencia con respecto al control, probablemente porque aún poseía una versión activa de NSUN5. Estos datos indican que el C22 y el C16 podrían ser usados para el estudio de las funciones de NSUN5.

Dado que NSUN5 es una metiltransferasa de ARNr, hipotetizamos que podría tener una función en la biogénesis del ribosoma. Sin embargo, el estudio del procesamiento del ARNr mediante Northern blot indicó que no existía acumulación o reducción de ningún intermediario del procesamiento, sugiriendo que NSUN5 no es esencial en la biogénesis del ribosoma.

Dado que las modificaciones de ARNr también pueden jugar un papel importante en el mantenimiento de la estructura del ribosoma, realizamos un análisis estructural de los ribosomas 80S mediante criomicroscopía electrónica (Cryo-EM). Los resultados demostraron que los ribosomas carentes de metilación son menos estables, produciéndose una mayor disociación de las subunidades. Además, observamos que existe una alteración estructural en la zona en la que se encuentra la metilación depositada por NSUN5, indicando que esta metilación es necesaria para mantener una correcta estructura del ribosoma.

A continuación, estudiamos si esta falta de metilación podría afectar a la síntesis de proteína. Nuestros resultados indican que, en ausencia de NSUN5, la síntesis de proteína se ve incrementada con respecto al control. Además, observamos que este aumento se debe, principalmente, a una mayor síntesis de reguladores mitóticos y proteínas ribosomales. Esto

indica que la falta de NSUN5 favorece un programa traduccional diferente y sugiere que los procesos mitóticos podrían estar alterados en estas células.

De acuerdo con estas observaciones, las células carentes de NSUN5 presentaron unos menores niveles de proliferación y una alteración del ciclo celular, específicamente en fase G2/M. Además, demostramos que la alteración del ciclo celular es independiente de p53. Esto indica que NSUN5 no activa la típica respuesta de arresto del ciclo celular debido a alteraciones de la biogénesis del ribosoma, sino que este arresto del ciclo se produce por otros mecanismos.

Todos estos resultados indican que NSUN5 juega un papel en la regulación del ciclo celular. Para posicionar la función de NSUN5 en el ciclo celular, analizamos si su actividad o expresión estaban moduladas a lo largo de este proceso. Nuestros resultados sugieren que NSUN5 aumenta ligeramente su expresión en fase S y luego, en fase M, sufre una fosforilación. Esta fosforilación es mediada por CDK1 y conlleva una pérdida de la estabilidad de NSUN5, sin afectar a su localización.

Para estudiar si NSUN5 podría ser usado como diana terapéutica, evaluamos su expresión en tejidos. NSUN5 se expresa en todos los tejidos sanos, aunque su nivel de expresión se correlaciona directamente con el nivel de proliferación de cada tejido. Dado que los niveles de NSUN5 correlacionan con el potencial proliferativo de los tejidos y los tumores se caracterizan por tener unos niveles de proliferación aberrantes, estudiamos si NSUN5 está sobre-expresado en tumores. Nuestros resultados indican que los tumores, tanto aquellos procedentes de tejidos altamente proliferativos como la próstata, como aquellos procedentes de tejidos menos proliferativos como el hígado, presentan unos niveles elevados de NSUN5 tanto en nuestros análisis *in silico* como en muestras de paciente o líneas celulares. Esto nos indica que NSUN5 podría ser usado como diana terapéutica en cáncer.

De manera similar, Nsun5 también se encuentra sobre-expresado en modelos murinos de cáncer de próstata, indicando que podría ser usado como modelo para estudiar el efecto de NSUN5 en este tumor. Este modelo se cruzó con ratones que no expresan Nsun5 para evaluar cómo la pérdida de expresión de esta metiltransferasa afecta al desarrollo de tumores. Nuestros resultados indican que una disminución de la expresión de Nsun5 no tiene efecto en la formación y crecimiento de tumores primarios de próstata, pero si ocasiona una reducción de la formación de metástasis en hígado, pulmón, riñón y nódulos linfáticos. Esto indica que NSUN5 podría ser usado como diana terapéutica para impedir el progreso de los tumores a un estado avanzado y metastásico.

Conclusiones

En resumen, nuestro estudio revela funciones críticas de NSUN5 y la metilación en el ARNr en el mantenimiento de la estructura y estabilidad del ribosoma y en la regulación de la síntesis de proteínas, lo que participa en el mantenimiento del funcionamiento de las células. Estos resultados contribuyen a entender mejor cómo las modificaciones del ARNr y las funciones ribosomales están reguladas a lo largo del ciclo celular y sugieren que NSUN5 podría ser usado como diana terapéutica en tumores avanzados.

Así, los datos obtenidos en este estudio nos llevan a las siguientes conclusiones:

I.   La pérdida de expresión de la metiltransferasa NSUN5 no altera la transcripción del ADNr o el procesamiento del ARNr.

II. La pérdida de la metilación m^5C3782 desestabiliza los ribosomas, lo que lleva a un aumento de su disociación. Además, produce una alteración de la estructura del hélix H70, en la interfaz entre subunidades ribosomales.

III. La disminución de la expresión de *NSUN5* produce un aumento de la síntesis de proteínas y facilita la recuperación de esta tras una inhibición de la síntesis de proteínas inducida por estrés.

IV. La expresión reducida de *NSUN5* promueve la traducción de ARNm que codifican para proteínas ribosomales y reguladores mitóticos.

V.   La disminución de la expresión de *NSUN5* reduce la proliferación causando un arresto de las células en fase G2/M de una forma independiente de p53.

VI. CDK1 fosforila a NSUN5 durante la mitosis, produciendo una desestabilización de la enzima.

VII. *NSUN5* se expresa de forma ubicua en todos los tejidos sanos, y su expresión correlaciona de forma positiva con la proliferación del tejido.

VIII. *NSUN5* se encuentra altamente expresado en tumores derivados tanto de tejidos poco proliferativos, como el hígado, como de tejidos altamente proliferativos, como la próstata. Además, su expresión correlaciona con un aumento en el riesgo de recaídas.

IX. La disminución de la expresión de *Nsun5* no afecta a la formación y el crecimiento del tumor primario de próstata en un modelo de ratón, pero impide la formación de metástasis.

X.   La reducción de la expresión de *NSUN5* afecta negativamente a la migración de las células de cáncer de próstata metastásico *in vitro*.